Anaerobic fluorescent reporters for studying *Pseudomonas aeruginosa*-specific responses in a CF polymicrobial assay

Caetanie Fometeu Tchagang

Thesis submitted to the University of Ottawa
in partial fulfillment of the requirements for the
Doctorate in Philosophy degree in Microbiology and Immunology

Department of Biochemistry, Microbiology, and Immunology
Faculty of Medicine
University of Ottawa

“Life is good when you are happy; but much better when others are happy because of you.”
— Pope Francis

Abstract

Pseudomonas aeruginosa is an opportunistic pathogen that persists in the hypoxic and anaerobic microenvironments characteristic of the cystic fibrosis (CF) airways, where it often exists as part of polymicrobial communities and forms biofilms that contribute to chronic infections. Studying *P. aeruginosa* under these conditions is complicated by the limited availability of tools for monitoring bacterial behaviour and a lack of experimentally validated *in vitro* models that capture relevant interspecies interactions. This thesis addresses these gaps by developing oxygen-independent fluorescent reporters, implementing and validating an anaerobic CF polymicrobial model, and engineering a stable reporter strain that was used to study the spatial distribution of *P. aeruginosa* in multi-species biofilm systems.

In **Chapter 2**, I designed a suite of fluorescent reporters, including phiLOV2.1 and FAST. I demonstrated their functionality in monitoring *P. aeruginosa* under low-oxygen or anaerobic conditions. Furthermore, I showed that phiLOV2.1 and FAST could also be used in dual-culture imaging to monitor *P. aeruginosa* subpopulations. The broad host range of these reporters allows adaptation to diverse Gram-negative bacteria to enable real-time visualization in biofilms and other hypoxic niches.

In **Chapter 3**, I implemented and validated a CF polymicrobial model system incorporating *P. aeruginosa, Staphylococcus aureus, Streptococcus sanguinis,* and *Prevotella melaninogenica*. Using this anaerobic multi-species assay, I assessed the persistence of six *P. aeruginosa* deletion mutant strains. I evaluated their susceptibility to tobramycin across a range of concentrations in the context of complex interspecies interactions. The mutant Δ*tctED* had the strongest phenotype, being the most susceptible strain compared to the wild type. This finding highlights *tctED* as a biofilm-specific antibiotic resistance gene under conditions that closely approximate those present in the CF lung environment. This suggests that *tctED* could be a potential target in combating antibiotic resistance *in vivo*.

In **Chapter 4**, I engineered a stable, antibiotic-independent plasmid, pCFT4.2.1, encoding phiLOV2.1 and the VapBC toxin–antitoxin system. This construct was retained in over 90% of *P. aeruginosa* PA14 WT cells for at least three days without antibiotic pressure, maintaining detectable fluorescence. Within the CF polymicrobial assay, I have provided evidence that *P. aeruginosa* harbouring pCFT4.2.1 forms both surface-attached and biofilm-like structures resembling floating aggregates.

Collectively, this work provides novel fluorescent tools, validates a relevant CF polymicrobial model system, substantiates *tctED* as a *P. aeruginosa* biofilm-specific antibiotic resistance gene under multiple conditions, establishes a stable reporter strain for tracking *P. aeruginosa* in anaerobic multi-species communities, and offers insights into the nature of *P. aeruginosa* biofilms in this assay. Altogether, these findings advance our ability to study the persistence, antibiotic susceptibility, and biofilm formation ability of *P. aeruginosa* in clinically relevant contexts.

Résumé

Pseudomonas aeruginosa est un pathogène opportuniste qui persiste dans les microenvironnements hypoxiques et anaérobiques caractéristiques des voies respiratoires des patients atteints de fibrose cystique (CF)—une maladie génétique héréditaire marquée par la production de mucus visqueux principalement dans les poumons, ce qui conduit à des infections respiratoires chroniques. Dans le poumon CF, *P. aeruginosa* coexiste souvent au sein de communautés polymicrobiennes et forme des biofilms contribuant à ces infections. L'étude de *P. aeruginosa* dans ces conditions est complexifiée par le nombre limité d'outils permettant de suivre son comportement et par l'absence de modèles *in vitro* capables de reproduire les interactions interespèces pertinentes. Cette thèse vise à combler ces lacunes en développant des rapporteurs fluorescents indépendants de l'oxygène, en mettant en œuvre et en validant un modèle polymicrobien anaérobique de la CF, et en construisant une souche rapporteur stable utilisée pour étudier la distribution spatiale de *P. aeruginosa* dans des systèmes de biofilms multi-espèces.

Au **Chapitre 2,** j'ai conçu une série de rapporteurs fluorescents, incluant phiLOV2.1 et FAST, et démontré leur fonctionnalité pour le suivi de *P. aeruginosa* en conditions hypoxiques ou anaérobiques. J'ai également montré que phiLOV2.1 et FAST pouvaient être employés pour l'imagerie en co-culture pour observer des sous-populations de *P. aeruginosa*. La large gamme d'hôtes compatibles avec ces rapporteurs permet leur adaptation à diverses bactéries à Gram-négatif, ouvrant la voie à une visualisation en temps réel dans les biofilms et autres niches hypoxiques.

Au **Chapitre 3**, j'ai mis en œuvre et validé un système modèle polymicrobien de la CF intégrant *P. aeruginosa*, *Staphylococcus aureus*, *Streptococcus sanguinis* et *Prevotella melaninogenica*. À l'aide de ce système anaérobique multi-espèces, j'ai étudié la persistance de six souches mutantes de *P. aeruginosa* et évalué leur sensibilité à la tobramycine sur une gamme de concentrations, dans ce contexte d'interactions interespèces complexes. Le mutant Δ*tctED* a présenté le phénotype le plus marqué, se révélant la souche la plus sensible par rapport au type sauvage. Cette découverte met en

évidence *tctED* comme un gène de résistance aux antibiotiques spécifique aux biofilms dans des conditions proches de celles de l'environnement pulmonaire de la CF, suggérant que *tctED* pourrait être une cible thérapeutique potentielle pour lutter contre la résistance aux antibiotiques *in vivo*.

Au **Chapitre 4**, j'ai construit un plasmide stable et indépendant des antibiotiques, pCFT4.2.1, codant pour phiLOV2.1 et le système toxine–antitoxine VapBC. Ce plasmide a été maintenu dans plus de 90% des cellules de *P. aeruginosa* PA14 WT pendant au moins trois jours sans pression de sélection antibiotique, tout en conservant une fluorescence détectable. Dans le cadre du modèle polymicrobien CF, l'étude de *P. aeruginosa* porteur du plasmide pCFT4.2.1 a permis de mettre en évidence la capacité de ce pathogène à former des biofilms adhérents à des surfaces ainsi que des agrégats flottants assimilables à des biofilms.

Dans l'ensemble, ce travail fournit de nouveaux outils fluorescents, valide un modèle polymicrobien pertinent pour la CF, confirme *tctED* comme un gène de résistance aux antibiotiques spécifique aux biofilms de *P. aeruginosa* dans diverses conditions, établit une souche rapporteur stable pour étudier *P. aeruginosa* dans des communautés multi-espèces anaérobiques, et révèle des informations sur la nature des biofilms de *P. aeruginosa* dans ce modèle polymicrobien. Collectivement, ces résultats renforcent notre capacité à étudier la persistance, la sensibilité aux antibiotiques et la capacité de formation de biofilms de *P. aeruginosa* dans des contextes cliniques pertinents.

Acknowledgments

First and foremost, I would like to thank God and my Saviour Jesus Christ, who brings meaning to my work and life. To You belongs the glory, and I surrender all my success to You.

Thank you to my thesis supervisor, Dr. Thien-Fah Mah, for your unwavering support, encouragement, and positive outlook, which have motivated me to persevere. From failed experiments to cancelled projects, your positivity kept me going, and giving up was never an option. Thank you for guiding me to become a better scientist, asking critical questions, and helping me improve my writing skills. I also appreciate how you taught me to be more patient with myself and others. You are truly an inspiration in science and beyond. I am leaving your lab as a better scientist, but more importantly, as a better person overall. So, thank you.

Thank you to my thesis co-supervisor, Dr. F-X Campbell-Valois. Your challenging questions pushed my critical thinking far beyond what I expected. You consistently encouraged me to look deeper than the surface and critically evaluate each result. Your dedication and commitment to science are truly inspiring. Thank you for your ongoing support and encouragement throughout this journey. “Je n’ai pas lâché la patate!”

Thanks to all past and current members of the Mah and F-X’s labs. Thank you, Li Zhang, for your constant willingness to help and support me in the lab. Thanks to Navoun Silué for your encouragement and for consistently checking in on me even after leaving the lab. Thanks to Nathaline Haidar-Ahmad, France Manigat, Waad Bajunaid, and Kyle Tomaro for continually cheering me up. Thank you, Olivier Chagnon-St-Amour, for your positive attitude and all your help with this project.

I am grateful for all members of my thesis advisory committee—Dr. Marceline Coté, Dr. Vanessa D’Costa, and Dr. Mathieu Lavallée-Adam—for their time, valuable guidance, and advice throughout my graduate studies.

I am indebted to my first undergraduate project supervisor, Dr. James Tambong. I appreciate the life-changing opportunity to join your lab, which ignited my passion for bacteriology and molecular biology and guided me through my initial steps in these fields.

I express my gratitude to the Department of Biochemistry, Microbiology and Immunology, as well as the Department of Chemistry and Biomolecular Sciences at the University of Ottawa, for the opportunity to complete my doctoral work at such a wonderful training institution.

Thank you to my dear friend Abbé Guy Calvin for your prayers and to my friends Aissata and Julie for the multiple conversations that truly uplifted my spirit.

To my beloved sisters Glawdys and Estève, my aunt Tata Rachel, and cousin Léopoldine, thank you for your prayers, unconditional and constant encouragement. You also made this accomplishment possible.

Thank you to my in-laws, Maman Françoise, Tata Félicité, Arol, Ivael and Maeva for your support throughout this long journey.

I am deeply grateful to my beloved parents, Rose and Pierre Fometeu. I owe you everything. Thank you for your steadfast support, continuous encouragement, and ongoing prayers. You motivated me to pursue this PhD degree and made many sacrifices so that I could succeed. Thank you from the bottom of my heart for everything you have done and continue to do for me.

To my dear husband, Dr. Alain Tchagang, you are truly my hero without a cape. You have sacrificed so much so I could reach this point. Thank you for your love, support, and patience through the thick and thin, as well as the rigour of grad school. I sincerely appreciate that you always prioritize my well-being. Thank you for accompanying me on this long journey, for inspiring me to work hard and never seek the easy way out. Thank you so much.

To my daughters, Abelle and Mileva, and my sons, Gaddiel and Lionel, you are my greatest joy and my legacy. Thank you to each of you for your unique ways of encouraging me. I love you deeply.

To everyone I have not explicitly mentioned here, but who has supported and encouraged me in tangible or intangible ways, you all contributed to shaping who I am today. So, thank you!

Table of Contents

List of figures

List of tables

List of abbreviations

ABC	ATP-Binding Cassette
ABX	Antibiotics
ANOVA	Analysis of Variance
Ap	Ampicillin
ASM	Artificial Sputum Media
ASM+	Artificial Sputum Media with Mucin
bd	below detection
BFP	Blue Fluorescent Protein
BLS	Biofilm-Like Structures
BR	Bilirubin
BV	Biliverdin
Cb	Carbenicillin
CcdAB	Control of Cell Death
C-di-GMP	Cyclic-di-GMP (Cyclic diguanylate)
CF	Cystic Fibrosis
CFTR	Cystic Fibrosis Transmembrane Conductance Regulator
CFU	Colony Forming Units
CLSM	Confocal Laser Scanning Microscopy
CV	Crystal Violet
DIC	Differential Interference Contrast
eGFP	enhanced GFP
EPS	Extracellular Polymeric Substances
EV	Empty Vector
Ex/Em	Excitation and Emission wavelengths
FAD	Flavin Adenine Dinucleotide
FAST	Fluorescence-Activating and Absorption-Shifting Tag
FbFPs	Flavin-based Fluorescent Proteins
FMN	Flavin Mononucleotide
FPs	Fluorescent Proteins
GFPs	Green Fluorescent Proteins
HBR	Synthetic fluorogenic analog of 4-hydroxybenzylidene-rhodamine
HO	Heme Oxygenase
iLOV	improved-LOV
Km	Kanamycin
LB	Lysogeny Broth
LBN	LB media + 100 mM KNO_3
LOV	Light-Oxygen-Voltage
LucY	Lucigen Yellow
M63N	M63 minimal media + 1 mM $MgSO_4$ + 0.4% L-arginine + 100 mM KNO_3

MBC	Minimal Bactericidal Concentration
MBC-B	Minimal Bactericidal Concentration in Biofilms
Mix(B)	Mixed cultures for biofilm cells
Mix(P)	Mixed cultures for planktonic cells
MRSA	Methicillin-Resistant *Staphylococcus aureus*
MSA	Mannitol Salt Agar
NIR-FPs	Near-Infrared Fluorescent Proteins
ns	non significant
NT	Non Treated
OD600	Optical Density at 600 nm
PA14	*Pseudomonas aeruginosa* wild type strain UCBPP-PA14
PBS	Phosphate Buffered Saline
PCR	Polymerase Chain Reaction
PGM	*Prevotella* growth medium
phiLOV2.1	photostable improved-LOV
PIA	*Pseudomonas* Isolation Agar
Pr	*Prevotella melaninogenica*
PSA	*Prevotella* Selective Agar
PSK	Post-Segregational Killing
qPCR	quantitative Polymerase Chain Reaction
QS	Quorum Sensing
RFPs	Red Fluorescent Proteins
Sa	*Staphylococcus aureus*
SD	Standard Deviation
SSA	*Streptococcus* Selective Agar
St	*Streptococcus sanguinis*
T3SS	Type III Secretion System
T6SS	Type VI Secretion System
TA	Toxin-Antitoxin
TCA	Tricarboxylic acid
TCS	Two-Component Systems
THBY	Todd Hewitt Broth + 0.5 % yeast extract
TOB	Tobramycin
TSA	Tryptic Soy Broth + 1.5% agar
TSB	Tryptic Soy Broth
VapBC	Virulence-associated proteins B and C
WT	Wild Type

Chapter 1: General Introduction

1.1. *Pseudomonas aeruginosa*, an opportunistic pathogen

1.1.1. Overview

Pseudomonas aeruginosa is a Gram-negative, rod-shaped bacterium belonging to the *Pseudomonadaceae* family. *P. aeruginosa* is renowned for its ability to colonize various environments, including soil, water, plants and host tissues [1–3]. It is classified as an aerobic organism capable of anaerobic respiration and fermentation. During aerobic respiration, *P. aeruginosa* uses molecular oxygen as the terminal electron acceptor in its respiratory chain. During anaerobic respiration, *P. aeruginosa* primarily uses denitrification—a process where nitrate (NO_3^-) or nitrite (NO_2^-) serves as an alternative terminal electron acceptor [4, 5]. Although *P. aeruginosa* is a nonfermentative organism incapable of sustaining growth through fermentation, it can nevertheless ferment arginine and pyruvate for long-term survival under anaerobic, nitrate-limited conditions [3, 6]. This versatility allows *P. aeruginosa* to thrive in a wide range of nutrients, oxygen availability, temperatures, and pH [3, 7, 8]. In individuals with a healthy immune system, *P. aeruginosa* is generally harmless and is infrequently found in their endogenous microbial flora [9]. However, in individuals with a weakened immune system, unable to control *P. aeruginosa*, this bacterium acts as an opportunistic pathogen [9].

1.1.2. Pathogenicity and Virulence

P. aeruginosa is an opportunistic pathogen able to cause a wide range of human infections. The World Health Organization recognizes it as an emerging threat to public health and classifies it among a group of multidrug-resistant and highly virulent bacteria called ESKAPE—*Enterococcus faecium, Staphylococcus aureus, Klebsiella pneumoniae, Acinetobacter baumannii, P. aeruginosa and Enterobacter* spp. *P. aeruginosa* is particularly detrimental to immunocompromised individuals, including those suffering from cystic fibrosis, burn wounds, or cancer, and is also a major cause of sepsis and ventilator-associated pneumonia, such as in COVID-19 patients [10–15]. *P. aeruginosa* can spread through contact with contaminated surfaces or equipment, or exposure to soil and water.

The ability of *P. aeruginosa* to cause both acute and chronic infections stems from its elaborate repertoire of virulence factors that often interact synergistically. These factors include structural components, secreted factors, secretion systems, and regulatory systems that facilitate adhesion, invasion, tissue damage, immune evasion, and biofilm formation [10, 16, 17]. The structural components, also known as cell-associated virulence factors, are integral to the bacterial surface and play a role in motility, adhesion, and protection against host defences. They include lipopolysaccharides, Type IV pili, flagella, and outer membrane proteins (e.g. OprF, OprH, OprD) [10, 18, 19].

The secreted virulence factors are extracellular molecules that can damage host tissues or disrupt immune functions. They include exopolysaccharides (e.g., alginate, Pel, Psl), proteases (e.g., LasA, LasB elastase), phenazines (e.g., pyocyanin) [10, 18, 19] and siderophores (e.g., pyoverdine, pyochelin), which support bacterial growth and virulence under host-imposed iron restriction [20].

Secretion systems are specialized nanomachines acting as molecular channels to transport effector proteins or toxins into host cells or competing bacterial cells. There are currently six types of secretion systems reported in *P. aeruginosa* (T1SS to T6SS) [10], with the T3SS being the most extensively studied for its considerable role in virulence [21–23]. For example, the T3SS injects the effectors ExoS, ExoT, ExoU, and ExoY, which are exotoxins, into host cells via a syringe-like apparatus, thereby disrupting the cytoskeleton and inducing apoptosis [10, 24, 25].

Lastly, there are regulatory systems that coordinate virulence factor expression in response to environmental cues. These systems include the Quorum Sensing (QS; Las, Rhl, Pqs)—cell-density-dependent signalling mechanism involved in biofilm maturation and adaptation in chronic infection [26, 27] and the Two-Component Systems (TCS)—implicated in virulence gene regulation, including T3SS and alginate production [28–31].

In summary, *P. aeruginosa* is an opportunistic pathogen that particularly affects immunocompromised individuals and represents a recognized threat to public health. Its pathogenicity arises from a multifaceted repertoire of virulence determinants, including

structural components, secreted factors, secretion systems, and regulatory systems such as QS and TCS. These virulence factors act synergistically to promote adhesion, invasion, immune evasion, and tissue damage, underpinning *P. aeruginosa* persistent infections. Furthermore, *P. aeruginosa* pathogenicity culminates in its ability to form surface-attached communities called biofilms.

1.2. Biofilms

1.2.1. Overview

Biofilms are aggregates of microorganisms embedded in a matrix composed of extracellular polymeric substances (EPS), which include exopolysaccharides, proteins, lipids, and DNA. The biofilm matrix provides structure to the community and protects bacteria from stresses such as starvation, desiccation, predation, etc. [32, 33]. Importantly, the matrix also acts as a shield to external threats, such as some antibiotics and the host's immune system [33].

In many instances, biofilms are beneficial to humans. For example, biofilm-forming biocontrol agents can suppress pathogen colonization by adopting a biofilm lifestyle, which enables competitive exclusion and the localized production of antimicrobial compounds on agriculturally important crops such as tomatoes [34]. Biofilms adherent to intestinal mucus surfaces also support gut health by protecting beneficial bacteria, aiding in nutrient utilization and overall maintaining the body's homeostasis [35]. Lastly, biofilms represent an economical and environmentally friendly bioremediation technique for wastewater treatment by effectively removing contaminants such as organic pollutants, heavy metals, nitrates, etc. [36].

However, as discussed above, biofilms also represent a double-edged sword in the context of *P. aeruginosa* pathogenicity. Indeed, biofilms developing on medical devices such as contact lenses, urinary catheters, and implants [37] contribute to persistent infections that remain refractory to antibiotic treatment, thereby fostering the development of antibiotic resistance [38–44].

1.2.2. Biofilm formation

Biofilms are highly organized structures with a cyclic lifestyle that comprises five main stages: adsorption, adhesion, microcolony formation, maturation and dispersal [45] **(Figure 1.1A)**. During adsorption, the planktonic cells, also called free-swimming cells, attach to a surface that could be biotic or abiotic. This initial attachment is reversible as the interaction between cells and the surface is weak, leading to cells that can easily detach and revert to a planktonic state. The adhesion or irreversible attachment in bacteria is generally mediated by the loss of the expression of motility appendages, such as the flagella. At this stage, bacteria also start secreting EPS, which reinforces their adhesion to the surface.

During microcolony formation, bacterial cells divide and multiply, forming microcolony clusters and creating a three-dimensional structure aided by the secreted EPS that fosters strong adhesion between the cells. This stage also involves significant growth and cell-cell communication, such as QS systems. In addition, microcolony formation also occurs through twitching mobility, where cells move along the surface using Type IV pili to join other cells attached to the surface. During maturation, EPS production increases, and the microcolonies evolve into an extensive three-dimensional mushroom-like structure. Lastly, at the dispersal, planktonic cells detach from the biofilm and disperse to new niches to perpetuate the biofilm cycle.

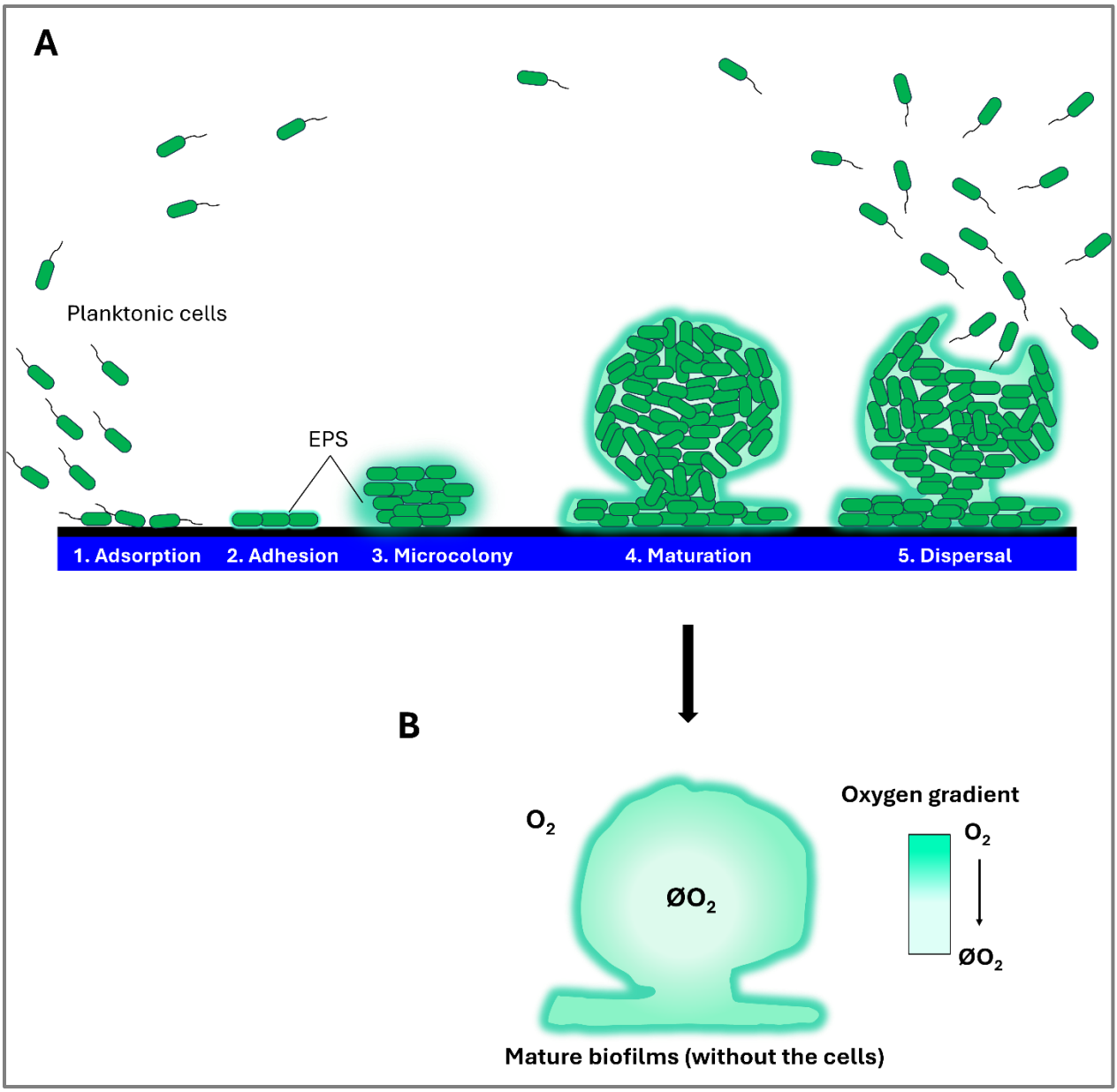

Figure 1.1: Cycle of *P. aeruginosa* biofilm formation. A. The five stages are presented: 1. Adsorption, 2. Adhesion, 3. Microcolony formation, 4. Maturation and 5. Dispersal. The planktonic cells and the development of extracellular polymeric substances (EPS) matrix are also presented. **B.** An emphasis on mature biofilm highlights the oxygen gradient from the outer to inner layers of the matrix. This gradient ranges from aerobic (O_2) to fully anaerobic ($ØO_2$). The cells were removed for better clarity. The figure was created using Microsoft PowerPoint.

1.2.3. Regulation of biofilm formation

Biofilm formation is tightly regulated by interconnected mechanisms responding to environmental cues such as cell density, nutrients, iron, phosphate, and oxygen levels. Regulation ensures adaptive responses, enhancing pathogenicity and antibiotic resistance. Key biofilm regulators include QS systems, Cyclic di-GMP (c-di-GMP), and TCS [46]. QS is a primary density-dependent communication system that coordinates biofilm development through the production and detection of autoinducer signalling molecules [42]. These molecules collectively play a role in promoting biofilm formation, matrix production, mature biofilm maintenance, nutrient sensing and responses to iron limitation and phosphate starvation [42].

C-di-GMP acts as a second messenger, with elevated levels promoting the sessile biofilm lifestyle by enhancing EPS production and adhesion [46, 47]. In contrast, reduced c-di-GMP levels facilitate dispersion and transition to planktonic growth. In addition, c-di-GMP is also crucial for irreversible attachment and maturation [46, 47].

TCS sense environmental signals and regulate biofilm formation through sensor kinases and response regulators. These systems influence attachment and microcolony formation by responding to nutrients and stresses [48, 49]. Taken together, these regulatory mechanisms, along with others not mentioned here, interconnect to allow *P. aeruginosa* to adapt and regulate biofilms for survival in diverse environments.

1.2.4. O_2 gradient in mature biofilms

Another degree of complexity in biofilms is the varying levels of oxygen encountered throughout the different regions of the three-dimensional architecture of mature biofilms **(Figure 1.1B)**. On the one hand, the outer layers are generally oxygen-rich, supporting aerobic microorganisms' growth. On the other hand, the inner layers exhibit a restricted to complete depletion of oxygen, creating conditions that support the growth and survival of anaerobic organisms.

In hypoxic environments, low oxygen levels significantly influence biofilm characteristics by promoting cell elongation [50], reducing growth rates and decreasing metabolic activity

[51], resulting in thicker and denser biofilms that exhibit enhanced resistance to traditional antibiotics [52, 53]. The virulence of *P. aeruginosa* is also modulated by oxygen availability. For instance, hypoxic conditions downregulate acute-phase virulence factors, including alkaline protease and siderophores [54], while activating the anaerobic regulator Anr, which in turn upregulates the T3SS [55].

In summary, O_2 distribution shapes biofilm structure and composition, metabolic activity, resistance to antimicrobials and pathogenicity of the resident microbial population.

1.2.5. Biofilm-like structures (BLS)

Biofilm-like structures (BLS) are a specific sub-category of biofilms. BLS is a term coined by Haley and colleagues in 2012 [56] to refer to *P. aeruginosa* structures that resemble typical biofilms with characteristics such as the composition of the matrix and growth rate [57] while lacking adherence to a surface. BLS were characterized as suspended bacterial aggregates in a viscous artificial mucin-containing medium mimicking the cystic fibrosis airway environment [56]. Additionally, the architecture and quantitative structural characteristics of these *P. aeruginosa* BLS were also influenced by *in vivo* changes, including environmental conditions and QS gene expression [56].

The concept of non-attached biofilms, also referred to as floating or suspended biofilms, or non-surface attached bacterial aggregates, is not recent and has been previously observed in freshwater and marine environments [58–61]. In clinical settings, non-attached biofilms are often found in chronic infections, where they tend to be more resistant to antibiotics and immune responses than surface-attached biofilms [57, 62–65]. The non-attached biofilms form when planktonic cells cluster together and produce EPS to create a protective matrix. These biofilms can display varying growth rates, antibiotic resistance, and metabolic activities compared to their surface-attached counterparts [61, 66].

Although BLS were initially mainly tied to *P. aeruginosa*, there is no clear distinction in the literature between non-attached biofilms formed by *P. aeruginosa* and BLS, as they often refer to the same concept. Nonetheless, the consensus is that these BLS contribute directly

to persistent lung infections, chronic inflammation and progressive lung damage in cystic fibrosis patients [67, 68].

1.3. Antibiotic resistance

1.3.1. Overview

Antibiotic resistance is a phenomenon in which bacteria evolve to withstand antibiotic treatment that would typically kill or inhibit their growth. This makes infections more difficult to eradicate, resulting in more prolonged illnesses, increased medical expenses, and higher mortality rates. The causes of antibiotic resistance are commonly attributed to overuse or misuse of antibiotics, incomplete treatment courses and the spread of resistant strains. In addition, it is also recognized that bacteria collectively possess an antibiotic resistome—the collective pool of genes from both pathogenic and commensal organisms related to antibiotic resistance. The concept of the resistome was initially formalized by D'Costa et al. in 2006 [69], providing a framework to trace the origins of antibiotic resistance genes within environmental reservoirs, including soil and water, as well as in both pathogenic and non-pathogenic microorganisms.

Generally, bacteria exhibit two main types of antibiotic resistance: intrinsic resistance and acquired resistance. Intrinsic resistance is a bacterium's natural and inherent ability to resist antibiotic treatment without prior exposure. This mode of resistance is innately encoded in the bacterial chromosome and could entail membrane impermeability, efflux pumps, lack of target site and enzyme inactivation. Conversely, acquired resistance occurs after antibiotic exposure and is gained by bacteria through genetic mutation or horizontal gene transfer.

1.3.2. Antibiotic resistance in *P. aeruginosa*

P. aeruginosa can exhibit both intrinsic and acquired antibiotic resistance. Its intrinsic resistance is mediated through low outer membrane permeability, which severely restricts the penetration of antibiotics inside the cells [70]. Additionally, intrinsic resistance can arise from enzymatic inactivation, such as AmpC β-lactamase, which hydrolyzes specific β-lactam antibiotics, making them ineffective [70]. Furthermore, four efflux pumps in *P.*

aeruginosa—MexAB-OprM, MexXY, MexCD-OprJ, and MexEF-OprN—actively pump antibiotics out of the cell [70, 71].

P. aeruginosa acquired resistance can occur through upregulation of those efflux pumps due to mutations of their regulators [72, 73] and horizontal gene transfer, through which *P. aeruginosa* acquires resistance genes from other bacteria [74]. This type of resistance contributes to the rise of multidrug-resistant strains.

1.3.2.1. Antibiotic resistance in *P. aeruginosa* biofilms

P. aeruginosa biofilm cells can be up to 1,000 times more resistant to antimicrobial compounds than planktonic cells [75–80]. This finding underlined why the concepts of antibiotic resistance and biofilm formation are intertwined. Several factors explain the increase in resistance noted for biofilm cells. Examples are listed in the following sentences, and **Section 1.3.2.2** emphasizes the identification of biofilm-specific antibiotic resistance genes.

Contrary to planktonic cells, the biofilm extracellular matrix represents a physical barrier restricting the penetration of some antibiotics and inhibiting phagocytosis by immune cells, including neutrophils and macrophages [81–84]. Furthermore, biofilm cells often upregulate efflux pumps [74], exhibit reduced metabolic activity that promotes the persistence of dormant cells, which are inherently less susceptible to antibiotics [74, 85], and exhibit an elevated frequency of horizontal gene transfer, facilitating the dissemination of resistance traits [86]. Collectively, these features confer superior antibiotic resistance to biofilm cells relative to their planktonic counterparts.

1.3.2.2. Biofilm-specific antibiotic resistance genes in *P. aeruginosa*

1.3.2.2.1. Overview

In an effort to thwart antibiotic resistance as it pertains to *P. aeruginosa* biofilms, several studies have identified genetic determinants specifically related to biofilms and studied how these genes contribute to the increased resistance. The efflux pump systems listed above have been reported to confer antibiotic resistance in biofilms, notably MexAB-OprM [72],

MexXY-OprM and MexEF-OprN [87]. One well-characterized regulator that upregulates these efflux pumps in biofilms is BrlR [88].

In addition to these efflux pumps and their regulators, the Mah laboratory has also identified six genetic loci that are important for biofilm-specific antibiotic resistance in *P. aeruginosa*: PA2070, PA5033, *ndvB, PA1874-77, tssC1 and tctED* [40, 76–78, 89]. PA2070 and PA5033 encode putative proteins whose roles remain under investigation [78]. However, the other four loci are currently the best characterized and thus will be the next topic discussed.

1.3.2.2.2. *ndvB*

The *ndvB* gene in *P. aeruginosa* encodes a glucosyltransferase essential for synthesizing cyclic-β-(1,3)-glucans [40]. Cyclic glucans synthesized by the *ndvB* gene product sequester antibiotics, such as the aminoglycoside tobramycin, in the periplasm, preventing them from reaching their cytoplasmic target, which is the ribosome [40, 90]. Furthermore, NdvB plays a crucial role in modulating the expression of biofilm-specific genes associated with ethanol oxidation [91]. Although the precise mechanism linking ethanol-oxidation genes to biofilm-associated antibiotic resistance remains unresolved, current evidence indicates that their activity contributes to enhanced tolerance by modulating intracellular redox balance. In particular, the reduction of reactive oxygen species (ROS)—which are known to damage essential cellular components and potentiate antibiotic lethality—represents a plausible mechanism underlying this association [92, 93].

Work in the Mah laboratory has found that *ndvB* is highly expressed in biofilms and that deletion of this gene did not affect biofilm formation nor antibiotic resistance in planktonic cultures, but increased the susceptibility of biofilm cultures to antibiotics such as tobramycin, gentamycin and ciprofloxacin [40, 76, 90]. Hence, *ndvB* was coined as a biofilm-specific antibiotic resistance gene.

1.3.2.2.3. *PA1874-77*

PA1874-PA1875-PA1876-PA1877 (PA1874-77) is a four-gene operon that codes for a multidrug efflux pump associated with aminoglycoside resistance in biofilms [40, 78, 90]. As mentioned above, efflux pumps contribute to antibiotic resistance by expelling antimicrobial

substances outside of the cell, hampering their interaction with their targets. Similar to *ndvB*, deletion of *PA1874-77* does not affect biofilm formation nor antibiotic resistance in planktonic cultures, but an elevated susceptibility of biofilm cultures to the same subset of antibiotics was observed [40, 76, 90, 94]. Therefore, the *PA1874-77* operon in *P. aeruginosa* plays a role in biofilm-specific antibiotic resistance.

1.3.2.2.4. *tssC1*

The *tssC1* gene encodes the core sheath protein of the Type VI secretion system (T6SS), which is essential for the assembly and contraction of the T6SS apparatus. This system mediates the delivery of toxins and effector proteins into both prokaryotic competitors and eukaryotic host cells, contributing to interbacterial competition and virulence [95]. In addition, *tssC1* expression is upregulated in biofilms, giving *P. aeruginosa* a competitive advantage [77]. Congruent with the biofilm-specific resistance phenotype of the two previous genetic loci, deletion of *tssC1* does not affect biofilm formation or antibiotic susceptibility in planktonic cultures, but its loss results in decreased resistance in biofilm cultures for tobramycin, gentamicin and ciprofloxacin [77]. However, the precise resistance mechanism of *tssC1* remains under investigation.

1.3.2.2.5. *tctED*

The *tctD-tctE (tctED)* operon encodes a TCS essential for the uptake of tricarboxylic acid in *P. aeruginosa,* thereby providing substrates to be used as carbon and energy sources. In line with the previous genetic loci, *deletion* of *tctED* resulted in a significant decrease in biofilm bactericidal concentrations of aminoglycoside antibiotics such as tobramycin and gentamicin [89]. The resistance mechanism of *tctED* also remains a matter of active research.

1.3.3. Other genes of interest related to biofilm antibiotic resistance

1.3.3.1. *PA1759-60*

One of the research pillars in the Mah laboratory is the identification and characterization of transcription regulators (TRs) implicated in biofilm antibiotic resistance in *P. aeruginosa*. In support of that quest, a genetic screen designed to identify TRs involved in biofilm

antibiotic resistance was carried out by Dr. C. Hall (a former PhD student in the Mah laboratory). This screen resulted in the identification of *PA1759* and *PA1760* as TRs potentially involved in biofilm antibiotic resistance. The genes are components of a bicistronic operon, which is predicted to encode two proteins associated with the MalT-type transcription factor [96]. However, their exact functions have yet to be determined. The deletion of *PA1759* and *PA1760* genes in PA14 resulted in a biofilm with enhanced susceptibility to tobramycin compared to the wild type isogenic strain, although the exact mechanism remains unknown (Hall, CW et al.; manuscript in preparation). In addition, the *PA1759-60* operon is essential for persistence in the *C. elegans* slow-killing model (Hall, CW et al.; manuscript in preparation). These findings underscored *PA1759-60* as relevant in antibiotic resistance, which warrants further investigation.

1.3.3.2. *flgK*

The *flgK* gene encodes a flagellar hook-filament junction protein, which is a structural component of the flagellum and plays a crucial role in the assembly and stability of the flagellum. Flagella are essential for bacterial motility and are also involved in biofilm formation [97]. *P. aeruginosa* mutants lacking *flgK* showed impaired motility [98]. The *flgK* mutant also displayed altered biofilm formation because of the non-functional flagellum [97]. Although *flgK* is not directly linked to biofilm-specific antibiotic resistance, its involvement may rather be indirect through mechanisms such as the regulation of QS signalling and efflux pumps [53]. More importantly, this mutant is of interest in this project because of the prevalence of *P. aeruginosa* mutants deficient in flagellar motility in cystic fibrosis lung infections [99].

1.4. Genetically encoded reporters

1.4.1. Overview of tools for studying biofilms

Due to the inherently complex nature of biofilms, an array of methodologies, often used in combination, have been developed to study their formation, structure, and behaviour [100–102]. Some commonly used methods to study biofilms are molecular and genetic techniques, which facilitate the analysis of specific genes related to their formation, development and dynamics [103–105]; biochemical and analytical techniques, which help

in biofilm quantification and viability [106]; mechanical and physical analysis, which provides insights into biofilm formation and stability [107–109]; computational and bioinformatics tools which assess and predict pathways associated with different biofilm phenotypes [110, 111]; and finally, microscopy, which allows imaging and the analysis of their architecture [112, 113]. This latter tool is of interest in this project and will be explored in more detail.

Microscopy techniques to study biofilms encompass scanning electron microscopy, which reveals structural details; atomic force microscopy, which provides the surface properties and mechanical characteristics of biofilms; and confocal laser scanning microscopy (CLSM), which gives 3D imaging of biofilms for analyzing the spatial-temporal distribution of biofilm cells. CLSM uses fluorescence to enable high-resolution visualization of samples under the microscope. For imaging living bacterial cells, fluorescent reporter systems such as dyes (SynaptoRed, CellTrace, etc.) or fluorescent proteins (GFP, mCherry, etc.) have been developed.

In this project's scope, emphasis will be placed on fluorescent proteins applied to the study of *P. aeruginosa*. To address the key question of the oxygen gradient that creates normoxic, hypoxic and even anoxic conditions in biofilms as described in **Section 1.2.4**, the fluorescent reporters used to study biofilms could be oxygen-dependent or oxygen-independent. Their respective advantages and limits are presented in the following sections.

1.4.2. Aerobic fluorescent reporters

1.4.2.1. Green fluorescent proteins (GFPs) and blue-shifted alternatives

The green fluorescent protein (GFP) is the most used fluorescent reporter for cell biology, microbial quantification, bacterial physiology, environmental interactions and protein dynamics in live cells [114–118]. When excited, GFP emits light with a peak near 509 nm, which falls within the green region of the visible spectrum. In *P. aeruginosa*, GFP has been used to study gene expression, biofilm formation, host-pathogen interactions, and the tracking of bacteria in biofilm and host tissues [119–121].

GFP is thermostable and resistant to proteases. Various GFP variants have been re-engineered throughout the years to improve their brightness, photostability or pH sensitivity [122, 123]. For example, the enhanced GFP (eGFP) variant exhibits a 35-fold increase in brightness and greater photostability than the WT GFP [124, 125]. The GFPmut2 variant demonstrates 7-fold faster maturation than WT GFP, coupled with enhanced brightness and photostability, enabling the observation of fast-paced cellular processes [126].

Some GFP variants with shifted spectral characteristics, such as blue-shifted fluorescent proteins which emit at shorter wavelengths than GFPs, have been described to create different colours like blue (emission ~440-460 nm), cyan (emission ~470-495 nm), and violet (emission <440 nm) ranges. These alternatives are useful for dual-imaging applications and to capture intracellular events such as protein-protein interactions [127, 128].

However, despite their broad spectrum of applications, GFP and its variants are pH sensitive (pH < 5), relatively large (~27 kDa) [129, 130], and they are restricted to aerobic systems since the reaction required for the maturation of their chromophore involves O_2 [131]. For instance, Monmeyran et al. found that, in an *E. coli* biofilm model, the fluorescence kinetics of the GFP was inconsistent with the biomass development, and that was strongly correlated to the depleted oxygen environment at the core of a mature biofilm [132]. This restricts the use of GFP and its variants in the context of low-oxygen environments like biofilms. In addition to this drawback, GFPs have relatively short emission wavelengths, which limits deep tissue penetration while also suffering from autofluorescence, which could interfere with proper imaging.

1.4.2.2. Red Fluorescent Proteins

Red fluorescent proteins (RFPs), emitting at longer wavelengths across yellow (~520-550 nm), orange (~550-580 nm), red (~580-620 nm), and far-red (>620 nm) ranges, serve as fitting alternatives to GFPs. This is due to their chromophores' extended N-acylimine group, which enhances electronic conjugation, enabling fluorescence at longer wavelengths [133–135], and mitigating several limitations associated with GFPs.

DsRed was the first RFP discovered, but due to slow maturation and low photostability, engineered variants like mCherry with improved photostability and maturation rate are preferred. For instance, mCherry has successfully been used for labelling *P. aeruginosa* in dual-species biofilms [136]. Despite advancements in improving the maturation kinetics of RFPs, they generally mature more slowly than GFPs due to structural differences in their chromophores [137–139]. Consequently, using RFPs may restrict the temporal accuracy of dynamic processes. Although RFPs and GFPs revolutionized fluorescence imaging, they both belong to the same family and have limited use in hypoxic or anaerobic settings because of their strict O_2 requirement. An emerging category of oxygen-independent fluorescent reporters has been developed to address this limitation.

1.4.3. Anaerobic reporters for studying bacterial species

1.4.3.1. Flavin-based fluorescent proteins

Flavin-based fluorescent proteins (FbFPs) are derived from the light-oxygen-voltage (LOV) domain and are characterized mainly by their independence from environmental O_2 for fluorescence [140]. Examples of FbFPs are iLOV (improved-LOV) [141], phiLOV2.1 (photostable improved-LOV) [131] and evoglow-Bs2 [140]. These proteins are significantly smaller than GFP; they mature fast, and shortly after folding can bind to flavin mononucleotide (FMN), which acts as a chromophore for fluorescence [131, 141]. FMN is abundant in bacteria as an essential enzymatic cofactor involved in metabolic pathways, respiratory chains, etc. [142]. Therefore, no addition of exogenous molecules is required for fluorescence.

One potential disadvantage of using these fluorescent proteins is the lower brightness that they exhibit compared to GFP [143, 144]. Individually, iLOV is reported to be brighter but less photostable than phiLOV2.1, and both were developed for broader applications, including plant and mammalian systems [144, 145]. In contrast, evoglow-Bs2 is part of a commercial kit (evoglow®) optimized for specific bacterial hosts. LucY (Lucigen Yellow) is another FbFP which, instead of FMN, uses flavin adenine dinucleotide (FAD) as a chromophore [129]. LucY possesses the same advantages as the LOV–based fluorescent

proteins, except it is slightly brighter [129]. In addition, Lucy is also bigger (33.2 kDa) than GFP (~27 kDa) [129].

The characteristics of the fluorescent proteins described above are presented in **Chapter 2 – Table 2.1**. While the FbFPs bind endogenous chromophores, another category of fluorescent proteins uses an exogenous ligand as their chromophore.

1.4.3.2. Fluorescent proteins requiring an exogenous chromophore

Analogous to the FbFPs that emit light upon binding to an endogenous chromophore, the proteins in this category become fluorescent when provided with an exogenous chromophore. The chromophore could be a commercially available synthetic dye or probe, or it might be a compound not naturally present in bacteria. Examples of such fluorescent proteins include UnaG, Fluorescence-Activating and Absorption-Shifting Tag (FAST), and $SNAP_f$, which rely respectively on bilirubin, a synthetic fluorogenic analog of 4-hydroxybenzylidene-rhodanine, and a fluorogenic benzylguanine probe for fluorescence [143, 146, 147].

UnaG is small and reported to be extremely bright upon bilirubin binding [143]. FAST has been shown to outcompete GFP in an *E. coli* biofilm model substantially [132]. As could be predicted, one potential drawback of these fluorescent proteins is their dependence on an exogenous molecule not inherently found in bacteria to be used as a chromophore to achieve fluorescence. Moreover, the exogenous molecules may be autofluorescent or have limited permeability to the bacterial cell membrane, resulting in less bioavailability in the cytosol. These factors potentially add some complexity to using these reporters. The characteristics of UnaG and FAST are also presented in **Chapter 2 – Table 2.1**.

1.4.3.3. Near-infrared fluorescent proteins

The emergence of near-infrared fluorescent proteins (NIR-FPs) is attributable to the need for a non-invasive method to image deep tissue, especially in live mammal studies [148]. NIR-FPs typically emit beyond 650 nm and have been engineered using bacterial phytochromes [149]. Phytochromes are photosensory receptors that absorb light in the red (600 – 700 nm) and far-red (700 – 900 nm) ranges [150]. Consequently, NIR-FPs are more

effective at penetrating tissue at wavelengths near the infrared (650–900 nm). An example of an NIR-FP is iRFP670 [151] whose features are also listed in **Chapter 2 – Table 2.1.**

Besides their deep-tissue penetration advantage due to reduced light scattering, NIR-FPs are renowned for minimal autofluorescence [148, 152]. NIR-FPs use biliverdin as their chromophore to generate fluorescence. Although biliverdin is endogenous to mammalian cells as a natural product of heme metabolism, it is not nearly as abundant, if at all present, in bacteria. NIR-FPs are theoretically valuable in studying bacteria and precisely mature biofilms. Indeed, the deep light penetration across the biofilm layers could facilitate imaging and minimize autofluorescence.

1.4.4. Plasmids

1.4.4.1. Overview

Plasmids are self-replicating DNA molecules found in microorganisms that are distinct from chromosomal DNA [153]. They can confer competitive advantages such as antibiotic resistance, virulence factors or metabolic versatility to their host [154]. In addition, some plasmids are mobilizable genetic elements that can be transferred between different organisms [155, 156]. In bacteria, plasmids are often horizontally transferred through conjugation, transduction or transformation. This transfer capability with bacteria has been the workhorse of experimental genetic engineering and biotechnology [155].

For instance, transformation is a central technique in genetic engineering for gene cloning, where a foreign gene—such as one encoding a fluorescent protein—is inserted into a synthetic plasmid, which is then introduced or more accurately "transformed" into competent cells. The plasmid is subsequently replicated during bacterial division, producing multiple copies of the gene and enabling expression of the protein of interest, as evidenced here by cellular fluorescence. This is just one example of how plasmids are used to express fluorescent reporters when studying bacteria.

One challenge in utilizing artificial plasmids as expression vectors in bacteria is to ensure their maintenance and stable segregation during cell division. Traditionally, this challenge is tackled by incorporating a selective marker, such as an antibiotic resistance gene, into the

plasmid, coupled with the addition of the corresponding antibiotic to the culture medium to ensure plasmid retention. Though this is an excellent solution, it is not always appropriate to use antibiotics in certain contexts, such as in multispecies biofilms, where the presence of an antibiotic may adversely affect susceptible species. As an alternative, endogenous plasmid maintenance mechanisms in bacteria are often exploited.

1.4.4.2. Plasmid maintenance tools

Naturally occurring plasmids in bacteria are maintained through three main mechanisms, namely, multimer resolution systems [157], partition systems [158] and post-segregational killing (PSK) systems [159]. In the multimer system, plasmid multimers are generated during the replication and recombination of sister plasmids, thereby improving the availability of plasmid copies for segregation [157]. Partition systems separate sister plasmids between daughter cells via a process akin to chromosome segregation during mitosis [158]. Lastly, daughter cells that lose the plasmid are selectively killed by toxins in PSK systems, ensuring plasmid maintenance in the bacterial population [159]. This last mechanism will be elaborated further as it is important in this thesis.

1.4.4.2.1. Toxin-Antitoxin systems

Toxin-Antitoxin (TA) systems generally consist of a bicistronic operon where one gene encodes a stable toxin and the other gene produces a labile antitoxin that inhibits the toxin, ensuring a specific equilibrium of the two within the bacterial cell [160]. Although the first characterized TA system was associated with plasmid maintenance through PSK of plasmid-free cells [161], subsequent studies have revealed that TA systems also play crucial roles in bacterial physiology, including adaptation to environmental stresses, biofilm formation and virulence [162]. TA systems are categorized into eight types (I–VIII) based on the nature of the antitoxin and its mechanism of action in neutralizing the toxin—whether as RNA, protein, enzyme, adaptor, or post-translational modifier [163], since toxins are invariably proteins [164]. Type II systems are the most extensively studied and feature a proteinaceous antitoxin that directly binds and inhibits the toxin protein.

Regarding plasmid maintenance through PSK, there is a selective pressure for a bacterium to keep the plasmid encoding the TA. Indeed, in plasmid-free cells, the intrinsic instability of the antitoxin leads to its rapid degradation, whereas the more stable toxin persists longer. Consequently, the sustained presence of the toxin induces cell death, thereby enforcing the PSK mechanism. An illustration of this PSK mechanism by Type II TA systems is presented in **Figure 1.2**.

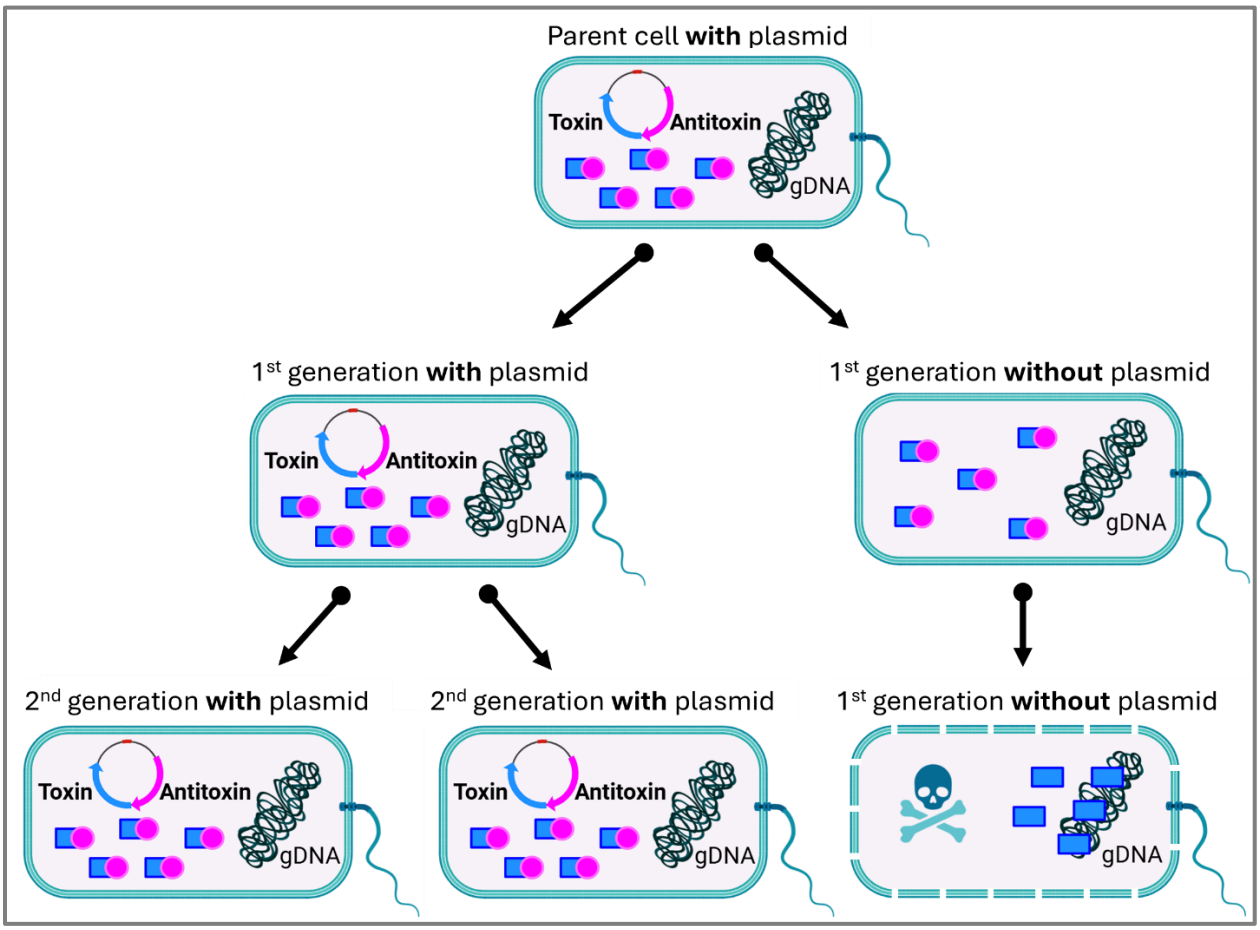

Figure 1.2: Plasmid maintenance of Type II TA systems via post-segregational killing mechanism. The parental cell harbours a plasmid encoding both the toxin (blue rectangle) and its cognate antitoxin (pink circle), with the latter binding to and neutralizing the toxin to prevent cytotoxicity. Upon cell division, the plasmid-bearing daughter cell continues to proliferate, giving rise to subsequent generations. In contrast, the plasmid-free daughter cell rapidly degrades the unstable antitoxin, leaving the stable toxin in this example to bind genomic DNA (gDNA) and induce cell death. The figure was created with Biorender.

Some examples of Type II TA systems with reported evidence of plasmid maintenance include CcdAB, VapBC and PumAB.

CcdAB (Control of Cell Death) was the first Type II TA involved in PSK ever discovered [161] and the best-characterized TA system [165]. It was originally identified on the *E. coli* F-plasmid and is involved in plasmid maintenance [165]. The toxin CcdB targets the DNA gyrase, which proceeds with the formation of a covalent GyrA-DNA complex that prevents DNA replication and leads to cell death, whereas the antitoxin CcdA directly binds to and neutralizes CcdB [166–168].

VapBC (Virulence-associated proteins B and C) is a representative of the largest and most diverse family of Type II TA systems, ubiquitous in both bacterial and archaeal genomes [169–171]. The bicistronic operon encodes VapC, a toxin with a PIN-domain ribonuclease activity that cleaves specific RNA targets such as tRNA, mRNA, or rRNA, thereby inhibiting translation and halting cell growth [172–174]. The VapB antitoxin counteracts VapC activity by functioning as a transcription regulator and binding to VapB, thereby inhibiting its enzymatic function [175, 176]. In *Shigella flexneri*, for example, VapBC is crucial in maintaining its virulence plasmid [177–179].

The PumAB system is encoded on plasmid pUM505 isolated from a clinical strain of *P. aeruginosa* [180]. The toxin PumA possesses an endoribonuclease that cleaves mRNA, thereby inhibiting cell growth and potentially modulating virulence, whereas the antitoxin PumB neutralizes PumA by binding to it and acting as a transcriptional regulator [180, 181]. PumAB has demonstrated plasmid stability in *E. coli* [180].

Although CcdAB, VapBC and PumAB are known for their roles in plasmid stabilization, their functions extend beyond this phenomenon. Indeed, CcdAB also contributes to stress responses, antibiotic tolerance, and persistence [165, 182, 183]; VapBC supports stress adaptation, persistence, and increasing virulence [170, 184, 185], while PumAB is involved in virulence enhancement and stress regulation [180, 181, 186]. Notably, although the TA systems discussed herein have been primarily characterized within bacterial contexts, the CcdAB system has also been adapted as a selectable marker in synthetic plasmids to confer

stability in laboratory strains such as *E. coli* BL21(DE3), an approach commercialized as the Staby® system by Delphi Genetics [187].

1.5. Cystic Fibrosis (CF)

1.5.1. Etiology

Cystic fibrosis (CF), a fatal genetic disease with an incidence of approximately 1 in 3,848 live births in Canada and a median age of survival of 62.3 years as of 2023, manifests as a multi-system disease, with its most severe impacts in the lungs, where pulmonary complications contribute to nearly 80% of mortality among affected individuals [188].

CF is a genetic disorder caused by mutations in the CF transmembrane conductance regulator (CFTR) gene. CFTR protein is a chloride channel, and its dysfunction creates an imbalance in ion and water transport across epithelial cells. This results in a failure to properly hydrate airway secretions and a reduction in mucociliary clearance, particularly in the airways, leading to a thick and sticky mucus build-up in the lungs [189]. The mucus build-up and impaired immune response favour recurrent microbial colonization and airway infections. In addition, CF is punctuated with episodes of pulmonary exacerbations characterized by worsening respiratory symptoms (increased cough and mucus, difficulty breathing, reduced appetite, etc.). The exacerbation events are associated with declining lung function, decreased quality of life, hospitalizations, and lower survival rates [190].

Unfortunately, CF has no cure. Therefore, treatment and management therapies consist of airway clearance by physiotherapy and mucolytics, inhaled antibiotics to target *P. aeruginosa* particularly, and CFTR modulators to improve the function of the malfunctioning CFTR protein [188]. For example, Trikafta is a triple-combination CFTR modulator therapy composed of two correctors, elexacaftor and tezacaftor, and one potentiator, ivacaftor. The correctors facilitate proper processing and trafficking of the defective CFTR protein to the cell surface, while the potentiator enhances the gating activity of the protein once localized at the membrane. This combined mechanism increases both the quantity and functional activity of CFTR at the cell surface, thereby restoring chloride and water transport and alleviating CF symptoms. Trikafta represents a significant therapeutic advancement,

particularly for individuals harbouring the prevalent F508del mutation. As of 2023, 2,761 out of the 4,513 Canadians living with CF, i.e., 61%, were on the Trikafta CFTR modulator [188]. However, as it is not curative, ongoing investigations are directed toward CRISPR-Cas–based approaches that aim to achieve permanent correction of CFTR mutations through targeted gene editing.

Improving CFTR function addresses only one facet of the CF pathology; however, the chronic, polymicrobial infections characteristic of the CF lung, driven by *P. aeruginosa* and other pathogens, also represent a critical challenge. This challenge necessitates targeted investigations into their polymicrobial dynamics to develop novel therapeutic interventions that complement CFTR-focused strategies.

1.5.2. CF lung microbiota

The diversity of microbes inhabiting the thick mucus layers lining the airways of individuals with CF constitutes the CF lung microbiota. This microbiota is composed predominantly of bacteria, but also includes fungi (e.g., *Aspergillus fumigatus, Candida albicans*), viruses (e.g., rhinovirus, adenovirus, influenza), and bacteriophages (e.g., filamentous bacteriophage [Pf phage]) [191–193]. While the bacterial population composition varies considerably among individuals with CF, a core community—comprising taxa consistently detected at high relative abundance across many patients may act as opportunistic pathogens alongside the so-called classical CF pathogens.

In the core community, genera such as *Streptococcus*, *Prevotella* and *Veillonella* are prevalent [194, 195]. Among the classical pathogens, there are species such as *P. aeruginosa, Staphylococcus aureus*, *Stenotrophomonas maltophilia* and species belonging to the *Burkholderia cepacia* complex [195–198]. Although these taxa influence CF disease to varying degrees, a recent report highlights *P. aeruginosa, S. aureus, Streptococcus* spp.*, and Prevotella* spp. as key determinants of health outcomes in CF, as demonstrated by studies employing both culture-dependent and culture-independent approaches [199].

1.5.2.1. *Pseudomonas aeruginosa*

P. aeruginosa is notably the most common pathogen responsible for chronic CF infection, especially in the adult CF population [188, 200, 201]. Chronic lung colonization by *P. aeruginosa* is also associated with worse clinical outcomes, notably the deterioration of lung function, quality of life and premature death [13, 202]. As a result, *P. aeruginosa* is of primary importance in the CF disease. Because *P. aeruginosa* can form biofilm within the mucus layers in the CF lung, CF is considered a biofilm-based infection.

As mentioned in **Section 1.5.1**, the treatment regimen for CF patients is mainly based on a cocktail of antibiotics depending on the disease progression. In acute *P. aeruginosa* infection, the CF Foundation in the USA currently recommends the use of inhaled tobramycin (300 mg twice daily) for 28 days [203]. As infection becomes chronic and eradication is unlikely, therapeutic goals shift toward preserving lung function and reducing pulmonary exacerbations. This long-term management relies on inhaled antibiotics such as tobramycin, colistin, and aztreonam lysine, and may also include fosfomycin, ciprofloxacin, or levofloxacin [204, 205]. Despite these strategies, eradication therapies fail in 10–40% of CF patients [206]. An emerging therapeutic approach uses phage therapy and has demonstrated promising results in the treatment of *P. aeruginosa* infections, particularly of multidrug-resistant strains [207].

1.5.2.2. *Staphylococcus aureus*

S. aureus is a Gram-positive, facultative anaerobe and another prominent member of the CF lung microbiota with a higher prevalence in children [188]. In children with CF, *S. aureus* is linked to heightened inflammatory activity in the airways and poorer nutritional status [208–212].

Currently, the specific role of *S. aureus* in morbidity and mortality remains unclear, potentially since it is often outcompeted by *P. aeruginosa* during the later stages of the disease [211]. However, the ability of *S. aureus* to form biofilms is a significant virulence trait that enables its adaptation to grow in CF airways, as it promotes immune evasion and aids in protecting the pathogen from antibiotic treatment [213, 214]. Furthermore, the extent of

S. aureus pathogenicity is dependent on its related strains, isolates or clones, as some tend to be more virulent than others [215]. Indeed, bearing some exceptions, strains like methicillin-resistant *S. aureus* (MRSA) are associated with more significant lung damage, increased hospitalization and premature death [216, 217]. There is no clear consensus for the treatment of *S. aureus* infections, but a combination of prophylaxis and antibiotics (e.g. tetracycline, ceftaroline) is a common practice [211, 217].

1.5.2.3. Other examples

While *P. aeruginosa* and *S. aureus* are considered classical CF pathogens due to their direct contribution to morbidity and mortality [218], emerging bacteria such as some *Streptococcus* spp. and *Prevotella* spp. have also been identified as relevant members of the CF lung microbiota [218–224]. Members of the *Streptococcus* genus are Gram-positive and facultative anaerobes, whereas *Prevotella* spp are Gram-negative and obligate anaerobes. Contrastingly, both species have been alternatively associated with positive and negative impacts in CF patients [222, 225–229]. Despite these conflicting findings, these bacteria influence health outcomes in CF, according to studies utilizing both culture-dependent and culture-independent methods [221, 230, 231]. However, their specific clinical relevance remains an active area of research.

1.5.3. Model systems to study cystic fibrosis

CF is a multi-system disorder that affects the respiratory, digestive, and reproductive systems; however, its most devastating effects occur in the lungs, where infections are characteristically polymicrobial.

While some models focus on studying and improving CFTR function, others concentrate on lung infections. Although no model is perfect, the pig and ferret CFTR-knockout models most accurately recapitulate the human CF phenotype [232]. However, their widespread use is restricted because they are costly to maintain. Given the microbiology focus of this thesis, emphasis will be placed on CF microbial model systems with *P. aeruginosa* as the focal point. It is a long-standing issue that antimicrobial susceptibility observed in studying a singular bacterium does not lead to better outcomes in the clinic [233–235]. Therefore,

several groups have worked to create a representative model of the CF polymicrobial community, aiming to bridge the gap between *in vitro* antimicrobial susceptibility profiles and clinical outcomes.

For example, in 2020, Vandeplassche and colleagues created a microaerophilic multispecies biofilm model made of six members of the CF microbiota [236]. The authors demonstrated that the impact of antibiotics targeting *P. aeruginosa* within a multispecies biofilm on microbial community evenness—reflected in the relative abundances of community members—varies depending on the specific antibiotic used. Since this model used a rich medium and aerobic conditions, Jean-Pierre and colleagues designed a different CF polymicrobial model to mimic the CF lung environment more closely [199]. In this model, the authors used an artificial sputum CF medium under anaerobic conditions and focused on four members of the CF microbiota.

In summary, while no single model fully captures the complexity of the CF lung disease, advances in animal and *in vitro* systems—particularly those focusing on polymicrobial communities—have improved our ability to study *P. aeruginosa* within the context of the CF microbiota. These models help bridge the gap between traditional antimicrobial susceptibility testing and clinical outcomes, providing more physiologically relevant platforms for investigating microbial interactions and therapeutic strategies.

1.6. Rationale, hypotheses and objectives

1.6.1. Rationale

It has been established that 1) *P. aeruginosa* is a highly resilient pathogen during CF lung infections; 2) The intricate architecture of biofilms, especially mature ones, exhibits spatially heterogeneous oxygen levels; and 3) CF is a biofilm and polymicrobial-based disease. To connect these three aspects and get a better insight into *P. aeruginosa* within the context of CF, specialized tools need to be developed. This development requires that important questions be addressed.

For instance, are there fluorescent tools that are suitable to investigate *P. aeruginosa* under oxygen-limited conditions, such as in biofilms? Or within a multispecies

environment? In this context, what do we understand about the persistence of *P. aeruginosa* and the notable mutants previously linked to biofilm antibiotic resistance, as discussed in **Section 1.3**? Additionally, what is their status regarding antibiotic susceptibility in a polymicrobial environment? And lastly, what about the nature and the spatial distribution of *P. aeruginosa* biofilm in a CF-like environment? These questions are central to the work presented in this thesis.

1.6.2. Hypotheses

With the appropriate tools to study *P. aeruginosa* in an anaerobic and polymicrobial environment, 1) I hypothesize that in this setting, *P. aeruginosa* will exhibit heightened antibiotic resistance, potentially accounting for its persistence observed *in vivo*. This enhanced resistance is likely mediated by biofilm-specific genetic loci, including *ndvB*, *PA1874-77*, *tssC1*, and *tctED*, which are hypothesized to have evolved to confer protection against diverse environmental antimicrobials. 2) I also hypothesize that the deletion mutants Δ*ndvB*, Δ*PA1874-77*, Δ*tssC1*, Δ*tctED*, Δ*PA1759-60*, and Δ*flgK* will exhibit reduced survival in a polymicrobial setting due to the disruption of the protective mechanisms provided by these genes in the wild type strain. 3) Lastly, I hypothesize that, in a polymicrobial setting, *P. aeruginosa* biofilms will exhibit increased biomass and enhanced resilience compared to those formed in a monospecies context, correlating with heightened antibiotic resistance. This observation will be congruent with the persistence of *P. aeruginosa* biofilms in the CF airway environment, reinforcing the protective role of biofilm architecture in antimicrobial resistance.

1.6.3. Objectives

My thesis project has four objectives. 1) Construct fluorescent reporters to study *P. aeruginosa* under anaerobic conditions. 2) Improve the best fluorescent reporter from 1) so that it can be expanded to be used in a multispecies system. 3) Evaluate the persistence of several *P. aeruginosa* strains in a CF polymicrobial assay, as well as assessing their antibiotic susceptibility. 4) Investigate *P. aeruginosa* biofilm spatial distribution in the CF polymicrobial assay.

Together, these four objectives were designed to generate tools and insights for studying *P. aeruginosa* under conditions of increasing biological complexity, ranging from restricted oxygen environments to multispecies communities that mimic more closely the conditions in the CF lung. The fluorescent reporters developed here are intended not only to facilitate investigations of *P. aeruginosa* physiology but also to be adaptable for use in other Gram-negative bacteria that may cause similar infections and colonize comparable environments. In parallel, evaluating the persistence and antibiotic susceptibility of wild type and mutant *P. aeruginosa* strains in a CF polymicrobial assay provides an opportunity to understand how strain-specific traits influence treatment outcomes—knowledge that could ultimately inform clinical decision-making. Finally, characterizing the spatial distribution of *P. aeruginosa* biofilms in both mono- and mixed-culture contexts will shed light on how biofilm architecture may impact antibiotic treatment—a factor that is central to biofilm-associated infections [237–239]. Collectively, this work aims to advance our understanding of *P. aeruginosa* pathogenesis in the CF lung and to contribute to the broader effort of unravelling the complexities of CF disease.

Chapter 2: Construction of anaerobic fluorescent reporters for *P. aeruginosa*

2.1. Preface

The work presented in this chapter has been published in the journal *Frontiers in Microbiology*.

> **Tchagang CF**, Mah T-F and Campbell-Valois F-X (2023). Anaerobic fluorescent reporters for live imaging of *Pseudomonas aeruginosa*. *Front. Microbiol*. 14:1245755. doi: 10.3389/fmicb.2023.1245755

Author contributions

Tchagang CF contributed to the study's design, performed the experiments, analyzed the data, and wrote the manuscript.

Mah T-F and **Campbell-Valois F-X** obtained the funding, designed the study, and critically revised the manuscript.

2.2. Abstract

Pseudomonas aeruginosa thrives in the airways of individuals with cystic fibrosis, in part by forming robust biofilms that are resistant to immune clearance or antibiotic treatment. In the cystic fibrosis lung, the thickened mucus layers create an oxygen gradient, often culminating with the formation of anoxic pockets. In this environment, *P. aeruginosa* can use nitrate instead of oxygen to grow. Current fluorescent reporters for studying *P. aeruginosa* are limited to the GFP and related analogs. However, these reporters require oxygen for the maturation of their chromophore, making them unsuitable for the study of anaerobically

grown *P. aeruginosa*. To overcome this limitation, we evaluated seven alternative fluorescent proteins, including iLOV, phiLOV2.1, evoglow-Bs2, LucY, UnaG, Fluorescence-Activating and Absorption-Shifting Tag (FAST), and iRFP670, which have been reported to emit light under oxygen-limiting conditions. We generated a series of plasmids encoding these proteins and validated their fluorescence using plate reader assays and confocal microscopy. Six of these proteins successfully labelled *P. aeruginosa* in anoxia. In particular, phiLOV2.1 and FAST provided superior fluorescence stability and enabled dual-colour imaging of both planktonic and biofilm cultures. This study provides a set of fluorescent reporters for monitoring *P. aeruginosa* under low-oxygen conditions. These reporters will facilitate studies of *P. aeruginosa* in biofilms or other contexts relevant to its pathogenesis, such as those found in cystic fibrosis airways. Due to the broad host range of our expression vector, the phiLOV2.1 and FAST-based reporters may be applicable to the study of other Gram-negative bacteria that inhabit similar low-oxygen niches.

2.3. Introduction

Pseudomonas aeruginosa is a Gram-negative opportunistic pathogen causing hospital-acquired diseases and infecting the lungs of cystic fibrosis patients. It is the most commonly isolated cystic fibrosis pathogen [200, 201] and is associated with worse clinical outcomes by accelerating the deterioration of pulmonary function [202]. Therapeutic interventions against *P. aeruginosa* are complicated by its high level of resistance to multiple antibiotics and its ability to form biofilms [75, 240].

Biofilms constitute a physical barrier to the host defence system [192]. Moreover, *P. aeruginosa* cells within the biofilm are up to 1,000 times more resistant to antimicrobial compounds than their planktonic counterparts [75, 90]. There is a steep O_2 gradient within the cystic fibrosis airways caused by the accumulation of mucus that restrains O_2 diffusion and the consumption of O_2 by host cells and bacteria [241–243]. Thus, the oxygen concentration ranges from aerobic to anaerobic levels in cystic fibrosis lungs, and *P. aeruginosa* can thrive under all these conditions. In fact, although *P. aeruginosa* is an obligate aerobe, it can also grow anaerobically through denitrification using nitrate instead of O_2 as an electron acceptor in the respiratory chain [4, 5]. Strikingly, the capacity of *P.*

aeruginosa to form biofilms is superior in anoxia than in normoxia [244], but tools to reliably study biofilms under low O_2 are lacking.

Genetically encoded fluorescent reporters have revolutionized the imaging of dynamic processes in living cells, including in bacterial pathogens [245, 246]. The green fluorescent protein (GFP), with its high brightness and robustness to various environmental conditions, was instrumental in this endeavour. In addition, some variants, such as GFPmut2 [126], rapidly mature their chromophore, allowing for the monitoring of fast-paced cellular processes. However, GFP and related variants have drawbacks, notably their strict O_2 requirement [118]. This property has limited their applications in living biofilms where O_2 is low [132].

By contrast, several alternative fluorescent proteins (FPs) are functional under oxygen-limiting conditions. However, to our knowledge, none of these FPs have been tested in *P. aeruginosa*. We thus selected seven FPs that spanned a wide range of excitation and emission spectra **(Table 2.1)**. The first group evaluated was the light, oxygen or voltage proteins (LOV): iLOV [141], phiLOV2.1 [131] and evoglow-Bs2 [140]. These FPs are significantly smaller and mature faster than GFP, and they use flavin mononucleotide (FMN) as their chromophore [131, 141]. One potential disadvantage of using these FPs is their low brightness [143]. In addition, we selected LucY, which is brighter than many LOV and uses flavin adenine dinucleotide (FAD) as its chromophore [129]. It is noteworthy that both FMN and FAD are abundant in the bacterial cytosol; thus, LOV and LucY spontaneously emit light in bacteria.

The Fluorescence-Activating and absorption-Shifting Tag (FAST) emits light when bound to a synthetic fluorogenic analog of 4-hydroxybenzylidene-rhodamine (HBR) [146]. The application of FAST in *P. aeruginosa* is promising because it was shown to outcompete the GFP in *Escherichia coli* biofilms [132]. UnaG and iRFP670 fluoresce when they form a complex with bilirubin [143] and biliverdin [247], respectively. UnaG is characterized by its brightness and wavelengths similar to the GFP. Finally, the red-shifted emission of iRFP670 may address the auto-fluorescence of *P. aeruginosa* at shorter wavelengths, which is

detrimental to the analyses of thick biofilms. It is important to note that bilirubin is not naturally present in *P. aeruginosa* and related bacteria, so it must be added to the growth medium. Similarly, free biliverdin is restricted in bacteria as its production is tightly dependent on iron availability. Therefore, it must be produced endogenously through the co-introduction of a heme oxygenase into the bacterial host [247].

Here, we report a panel of fluorescent proteins that successfully monitor *P. aeruginosa* in planktonic and biofilm cultures under anoxia. We demonstrate that phiLOV2.1 and FAST can be combined to track dual subpopulations of *P. aeruginosa* in microscopy experiments. This study provides tools that will be useful to researchers studying the behaviour of *P. aeruginosa* when the concentration of oxygen is too low to use the GFP. The broad host range plasmid used to develop these reporters suggests that their use could be readily extended to other Gram-negative bacteria.

Table 2.1: Characteristics of the different fluorescent proteins used in this project

FP acronym	Molecular weight (kDa)	Chromophore	Excitation (nm)	Emission (nm)	O_2 depen-dence
GFPmut2	26.9	p-hydroxybenzylidene imidazole	480	511	Yes
iLOV	11.3		450	495	
phiLOV2.1	11.3	*FMN	450	495	No
evoglow-Bs2	19		448	496	
LucY	33.2	**FAD	276, 377, 460	530	No
FAST (green channel)	14	[TF]Amber	499	558	No
FAST (red channel)	14	[TF]Coral	516	600	No
UnaG	15.6	Bilirubin	498	527	No
iRFP670	34.5	Biliverdin	643	670	[‡]No

*FMN, Flavin Mono Nucleotide. **FAD, Flavin Adenine Dinucleotide. [‡]As initially described in *Escherichia coli* [151]. [TF]Amber (HBR-3,5DM). [TF]Coral (HBR-3,5DOM). GFPmut2, iLOV, phiLOV2.1, evoglow-Bs2 and LucY use an endogenous chromophore; FAST, UnaG and iRFP670 use an exogenous chromophore.

2.4. Materials and methods

2.4.1. Construction of plasmids

pSMC21, a derivative of pSMC2 [120], allowing the constitutive expression of the GFPmut2 under the *tacp* promoter, was used to derive several new plasmids. First, GFPmut2 was excised by PCR-mediated deletion mutagenesis with the High fidelity Phusion DNA polymerase (ThermoFisher) and recircularized with the T4 DNA ligase (New England Biolabs) to yield the resulting empty vector control pCFT1. Second, the coding sequences of seven alternative fluorescent proteins were amplified by PCR with the Phusion DNA polymerase and introduced independently into pCFT1 by combining PCR-mediated deletion mutagenesis and isothermal cloning with the NEB Gibson assembly master mix (NEB, #E2611), thus yielding pCFT2 – 8. The coding sequence of the fluorescent proteins iLOV, phiLOV2.1, evoglow-Bs2, LucY, FAST (Bio Basic Markham, ON) and UnaG (Integrated DNA Technologies, IA) was obtained by gene synthesis. iRFP670 and the heme oxygenase (HO) from *Bradyrhizobium* sp. ORS 278 were a kind gift from Vladislav Verkhusha [247]. The HO gene was cloned downstream of iRFP670 to generate a bicistronic gene. Both open reading frames were separated by two stop codons, a Shine-Dalgarno sequence AAUGGAGGAAU [248] and a 5-adenine spacer [249]. The sequence of the cloned fragment in each resulting plasmid was confirmed by Sanger sequencing. The *tacp* (empty vector control), iLOV, phiLOV2.1, FAST and GFPmut2 were inserted by isothermal cloning into pUdO4a [250], as described above, thus yielding pCFT1.2, pCFT3.2, pCFT7.2 and pCFT9.2 (Addgene plasmids #208975, #208806, #208807, #208808 and #208809, respectively). pUdO4a is a small plasmid (~2.8 kbp) that possesses strong transcription terminators L3S2P21, *thrLABC* and *arcA*, an ampicillin resistance gene and a BBR1 origin of replication, which can be maintained in *Pseudomonas* spp. **(**[251]; **Supplementary Figure S2.1 – plasmid maps)**. **Table 2.2** and **Supplementary Table S2.1** list the plasmids and primers used in this study.

Table 2.2: Plasmids used and generated in this study

Plasmid name		Fluorescent protein	Antibiotic resistance	Reference
pSMC21 derivatives	pSMC21	GFP	Ap, Cb, Km	[120]
	pCFT1	Empty Vector (EV)	Ap, Cb, Km	This study
	pCFT2	evoglow-Bs2	Ap, Cb, Km	This study
	pCFT3	iLOV	Ap, Cb, Km	This study
	pCFT4	phiLOV2.1	Ap, Cb, Km	This study
	pCFT5	UnaG	Ap, Cb, Km	This study
	pCFT6	iRFP670	Ap, Cb, Km	This study
	pCFT7	FAST	Ap, Cb, Km	This study
	pCFT8	LucY	Ap, Cb, Km	This study
	pUdO4a	Empty Vector (EV)	Ap, Cb	[250]
pUdO4a derivatives	pCFT9.2	GFP	Ap, Cb	This study
	pCFT3.2	iLOV	Ap, Cb	This study
	pCFT4.2	phiLOV2.1	Ap, Cb	This study
	pCFT7.2	FAST	Ap, Cb	This study

Ap, Ampicillin; Cb, Carbenicillin; Km, Kanamycin.

2.4.2. Bacterial strains and growth conditions

The *Escherichia coli* strain DH10B was used for plasmid propagation. The wild type *Pseudomonas aeruginosa* str. PA14 was used in the fluorescence experiments [252]. Unless otherwise stated, the culture medium was LB supplemented with ampicillin (100 µg/ml) or carbenicillin (100 or 200 µg/ml) for DH10B and PA14 transformants, respectively. Anaerobic culturing of PA14 was performed in LB supplemented with carbenicillin, and 100 mM KNO_3 (LBN) to allow anaerobic respiration. Anaerobic planktonic cultures were incubated in anaerobic Hungate culture tubes with butyl rubber stoppers and screwcaps (Hungate, #CLS-4208). Biofilm anaerobic cultures were incubated in a BactronEZ chamber (Sheldon Manufacturing. Inc, Cornelius, OR) under an anaerobic atmosphere of 5% H_2, 5% CO_2, 90% N_2 that contained fewer than 4.7 parts per million O_2 per the manufacturer specifications. All incubations were performed at 37°C.

2.4.3. Growth curves under anaerobic conditions

PA14 strains harbouring one of the pCFT plasmids were grown on LB agar carbenicillin plates. A single colony from each plate was used to inoculate 5 mL of LB carbenicillin. These cultures were aerobically grown for ~ 18 h with shaking (250 rpm), then subcultured for 5h, and their optical density at 600 nm (OD600) was adjusted to 1. The cultures were next transferred in the anaerobic chamber and diluted 1:100 in 5 mL LBN in anaerobic Hungate culture tubes. These sealed tubes were then incubated at 37°C for ~ 24 h with shaking (250 rpm) in an incubator located in a room with normal oxygen levels. Following this first incubation, the cultures were transferred back into the anaerobic chamber and diluted 1:10 in LBN. Finally, 100 µL of the resulting inoculates were dispensed in a flat black bottom 96-well plate (Greiner bio-one, #655096). The samples were overlaid with Johnson and Johnson ® oil, as described [253]. Subsequently, the plate was sealed with an adhesive film (BioRad, #MSB1001), then wrapped with parafilm to prevent O_2 exposure prior to exiting the anaerobic chamber. The plate was then incubated with medium shaking in a Hybrid Synergy H4 plate reader (BioTeK), where the absorbance at 600 nm was continuously tracked and recorded every hour for 24 h. The fluorescence signal of PA14 cells expressing the GFP (excitation: 480±9.0 nm, emission: 511±9.0 nm) was recorded at 0 and 24 h to ensure anoxia was maintained throughout the experiment. A sample of the 24 h culture was exposed to O_2 for 2 h prior to the measurements to allow for the maturation of the GFP.

2.4.4. Fluorescence plate reader assay

PA14 cultures harbouring pCFT plasmids were grown anaerobically in LBN at 37°C for 24 h in anaerobic Hungate culture tubes as described above. Depending on the fluorescent proteins assayed, the samples were treated as follows. First, PA14 expressing the flavin-binding fluorescent proteins iLOV, phiLOV2.1, evoglow-Bs2 and LucY were processed immediately. Second, PA14 carrying pCFT1 (empty vector) or pCFT5 (UnaG) were grown in LBN ± 10 µM bilirubin (Merck) and processed immediately. Third, after the anaerobic incubation in the regular anaerobic medium, 1.5 mL of PA14 cultures with pCFT1 (empty vector) or pCFT7 (FAST) were transferred to a microfuge tube with their cap tightly wrapped with parafilm inside the anaerobic chamber. These cultures were then centrifuged (2400×g,

10 min) and resuspended in PBS ± 10 µM ^{TF}Amber (4-hydroxy-3,5-dimethyl benzylidene, The Twinkle Factory, Paris, France) [254] as described [255]. As described above, GFP-expressing cells were included in every assayed plate to confirm that anoxia was maintained during the experiment. The light emitted by the GFP-expressing cells exposed (or not) to O_2 was measured along with the assayed FP at their optimal excitation and emission wavelengths **(Table 2.1)** using a Hybrid Synergy H4 Hybrid plate reader (BioTeK). The data were normalized according to the OD600.

2.4.5. Live fluorescence imaging by microscopy

Experiments with PA14 planktonic cultures were carried out using the pSMC21 derivatives, whereas experiments with PA14 biofilm cultures were conducted with the pUdO4a derivatives. Aerobic PA14 cells carrying either phiLOV2.1, FAST or the empty vector were incubated in LB media supplemented with carbenicillin for 16 h to 18 h. These cultures were then diluted to an OD600 of 1 and used as inocula for anaerobic cultures. A 1:1000 dilution of this inoculum was made for planktonic cultures that were subsequently grown anaerobically for 18 h in LBN. A 1:100 dilution of the inoculum was made for biofilm cultures grown anaerobically in a 35 mm glass-bottom dish (Cellvis, #D35-20-1.5H) underneath a 2% agarose pad in the anaerobic chamber. Biofilms were incubated in M63 minimal media supplemented with 1 mM $MgSO_4$, 0.4% L-arginine, 100 mM KNO_3 and carbenicillin (M63N) for 24 h. After the incubation, cells were prepared for imaging as follows. For planktonic cell imaging, the anaerobic cultures were centrifuged (2400×g, 10 min) and resuspended in M63N; for FAST imaging, this medium was supplemented with 5 µM ^{TF}Coral (4-hydroxy-3,5-dimethoxy benzylidene, The Twinkle Factory) [254]. For biofilm imaging, the culture medium was removed, and the attached cells were washed once in PBS before adding a 200 µL solution of M63N ± 10 µM ^{TF}Coral. Both planktonic and biofilm cells were blanketed with a 2% agarose pad in a 35 mm glass-bottom dish (Cellvis, #D35-20-1.5H) for fluorescence imaging. The glass-bottom dish was then covered with a 35 mm glass-top cover (Cellvis, #D35-20-0-TOP) for differential interference contrast (DIC) imaging. To curtail O_2 infiltration during imaging, the edges of the dishes were tightly wrapped in parafilm before exiting the anaerobic chamber for microscopy. It is noteworthy that although cells were incubated

anaerobically and specific measures were taken to minimize O_2 exposure during the imaging setup, the strict control of anoxia could not be warranted throughout the entire imaging process. Micrographs were acquired on a Zeiss LSM 880 AxioObserverZ1 confocal microscope equipped with an EC Plan-Neofluar 100×/1.3 oil M27 objective. Fluorescence was captured using the argon laser at 458 nm for phiLOV2.1 [excitation: 458 nm; emission: 466 – 544 nm (monocultures) and 466 – 522 nm (dual cultures)] and at 514 nm for FAST:^{TF}Coral [excitation: 514 nm; emission: 555 – 722 nm (monocultures) and 586 – 722 (dual cultures)]. The photostability of iLOV and phiLOV2.1 in planktonic PA14 was evaluated by performing time-lapse acquisition every 30 seconds for three minutes under the conditions described above. All micrographs were collected with the ZEN software (Zeiss) and prepared with the ImageJ software [256]. The single cell quantitation of the fluorescence intensity from the planktonic micrographs was performed with ImageJ as previously described [257]. The total number of bacteria measured in these analyses was: 126 (empty vector, EV), 262 (LucY), 111 (UnaG), 218 (phiLOV2.1) and 168 (FAST:^{TF}Coral), and were collected from four biological replicates.

2.4.6. Statistical analysis

For the plate assay experiments, three biological replicates are presented. The micrographs shown are representative of four biological replicates. The single-cell fluorescence intensity analyses were performed on micrographs of four biological replicates. Statistical analyses were computed with GraphPad Prism 8 (GraphPad Software, La Jolla, CA). Plate reader assay data are presented as mean ± standard deviation. The confidence level was set at 95% ($p < 0.05$).

2.5. Results

2.5.1. Construction of plasmid-borne fluorescent reporters

To study *P. aeruginosa* under anaerobic conditions, we picked the FPs iLOV, phiLOV2.1, evoglow-Bs2, LucY, UnaG, FAST and iRFP670 whose fluorescence is in principle independent of O_2 **(Table 2.1)**. The open reading frame of each of these proteins was cloned into the vector pCFT1 to generate pCFT2 – 8 **(Supplementary Figure S2.1** and **Table 2.2)**.

pCFT6 included a bicistronic operon of iRFP670 and HO to produce the biliverdin by heme degradation, a strategy that yielded functional iRFP670 in *E. coli* [247].

2.5.2. Anaerobic growth of *P. aeruginosa* is not impinged by the expression of the fluorescent proteins

To test the effects of the expression of the FPs on the growth of PA14, strains carrying the different plasmid were incubated in LB supplemented with carbenicillin and nitrate (LBN) under anaerobic conditions. Most strains carrying the plasmids containing the FPs grew similarly to the empty vector **(Figure 2.1A)**. A notable exception was the strain carrying pCFT6, which contained iRFP670 and the HO, and appeared to grow at a slower rate. However, the statistical analyses of the growth rate during the exponential phase indicated this change was not significant **(Supplementary Table S2.2**). There was no increase in the fluorescence of the GFP between the beginning and the end of the measurements **(Figure 2.1B),** indicating that anoxia was maintained throughout the experiment. By contrast, exposure of the 24 h sample to O_2 during 2 h increased fluorescence by approximately 20-fold, confirming that immature GFP had indeed accumulated during anaerobic growth **(Figure 2.1B)**. Taken together, these results suggest that when cultured anaerobically, the viability and the growth of PA14 are unaffected by the expression of our collection of FPs, except perhaps for the iRFP670-HO bicistronic gene.

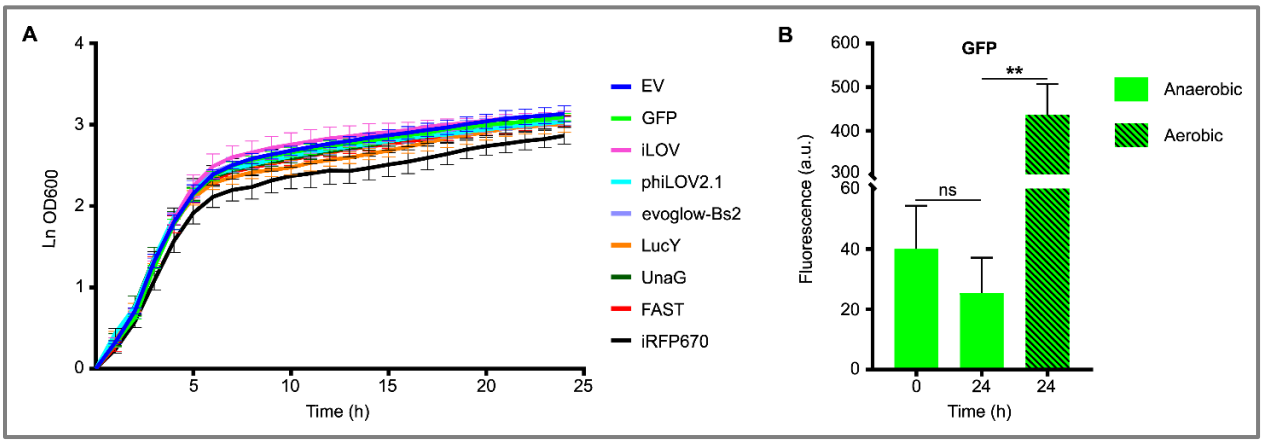

Figure 2.1: Fitness evaluation of *Pseudomonas aeruginosa* PA14 expressing different fluorescent proteins under anoxia. A. Growth curves of PA14 carrying the plasmids pCFT1–8 and pSCM21 **(Table 2.2)** and incubated in LB supplemented with KNO_3 and carbenicillin at

37°C under anaerobic conditions. The growth rate constant for each strain during the exponential phase was calculated and compared to the control empty vector (EV). The statistical significance of the change in exponential growth rate between the control EV and the strains expressing the fluorescent proteins was assessed by a two-tailed unpaired Student's t-test ($p < 0.05$); none of the variations observed were significant. **B.** The fluorescence of PA14 cells expressing GFP was measured at the beginning (0 h, anaerobic) and the end of the experiment (24 h, anaerobic), and after a subsequent exposure to oxygen (24 h, aerobic). Statistical analysis was performed using a paired Student's t-test. Fluorescence was normalized with the OD600, and the means with standard deviations as error bars are shown (ns = nonsignificant; n = 3).

2.5.3. All FPs but iRFP670 are functional under anoxia

Since the fluorescent proteins had little to no impact on growth, we proceeded to compare their signal intensity. We assumed that their fluorescent signal would be representative of their overall behaviour in PA14 and used it as a proxy that integrated their unique critical properties such as their expression level, maturation and brightness. This is a practical solution that circumvented the challenges arising from comparing a diverse set of proteins. Therefore, to evaluate the functionality of the FPs under anoxia, we first measured their fluorescence in PA14 using a plate reader assay.

In this context, we grew planktonic PA14 cultures harbouring the plasmids pCFT1 – 8 under anoxia and distributed them in 96-well plates under the anoxia-preserving conditions described above. PA14 expressing the LOV FPs showed a robust fluorescence signal compared to cells carrying the empty vector **(Figure 2.2A)**, with iLOV showing the highest signal, followed by evoglow-Bs2 and phiLOV2.1. PA14 cells expressing LucY also displayed strong fluorescence relative to those carrying the empty vector (**Figure 2.2B**). Similarly, PA14 cells expressing UnaG **(Figure 2.3A)** and FAST **(Figure 2.3B)** exhibited a substantial fluorescence increase in the presence of 10 µM bilirubin and 10 µM ^{TF}Amber, respectively. In contrast, the fluorescence of cells harbouring the empty vector was negligible.

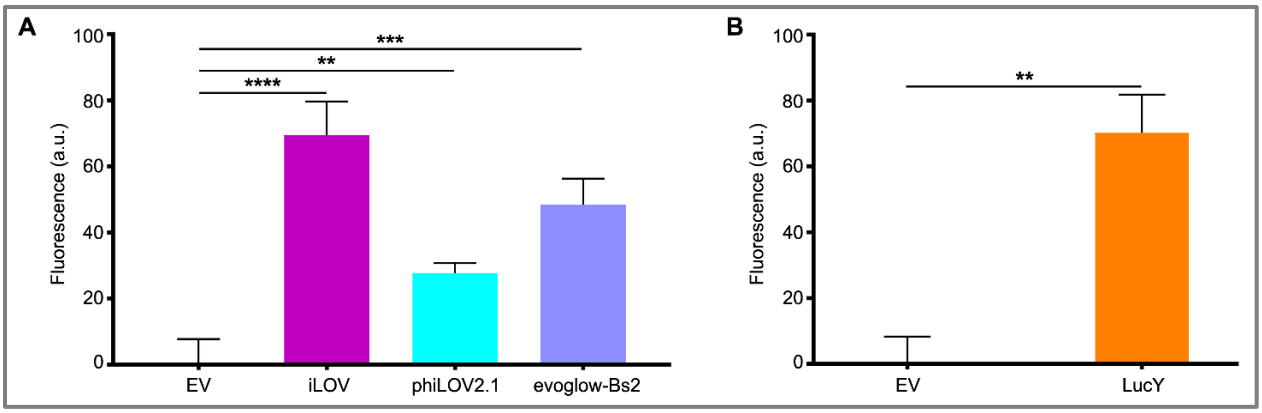

Figure 2.2: Fluorescence of PA14 expressing the flavin-based fluorescent proteins in anoxia. A. Fluorescence of PA14 cells carrying plasmids allowing the expression of iLOV (pCFT3), phiLOV2.1 (pCFT4) and evoglow-Bs2 (pCFT2) compared with those carrying the empty vector (pCFT1). Fluorescence was recorded at excitation 450 nm and emission 495 nm. Statistical analysis was performed using one-way analysis of variance (ANOVA) followed by Bonferroni's multiple comparisons test. **B.** Fluorescence of PA14 cells carrying plasmids allowing the expression of LucY (pCFT8) expressed in PA14 cells compared with those carrying the empty vector (pCFT1). Fluorescence was recorded at excitation 460 nm and emission 530 nm. Statistical analysis was done using an unpaired Student's t-test. Fluorescence was normalized with the OD600, and the means with standard deviations as error bars are shown *(**$p < 0.01$; ***$p < 0.001$; ****$p < 0.001$*; n = 3).

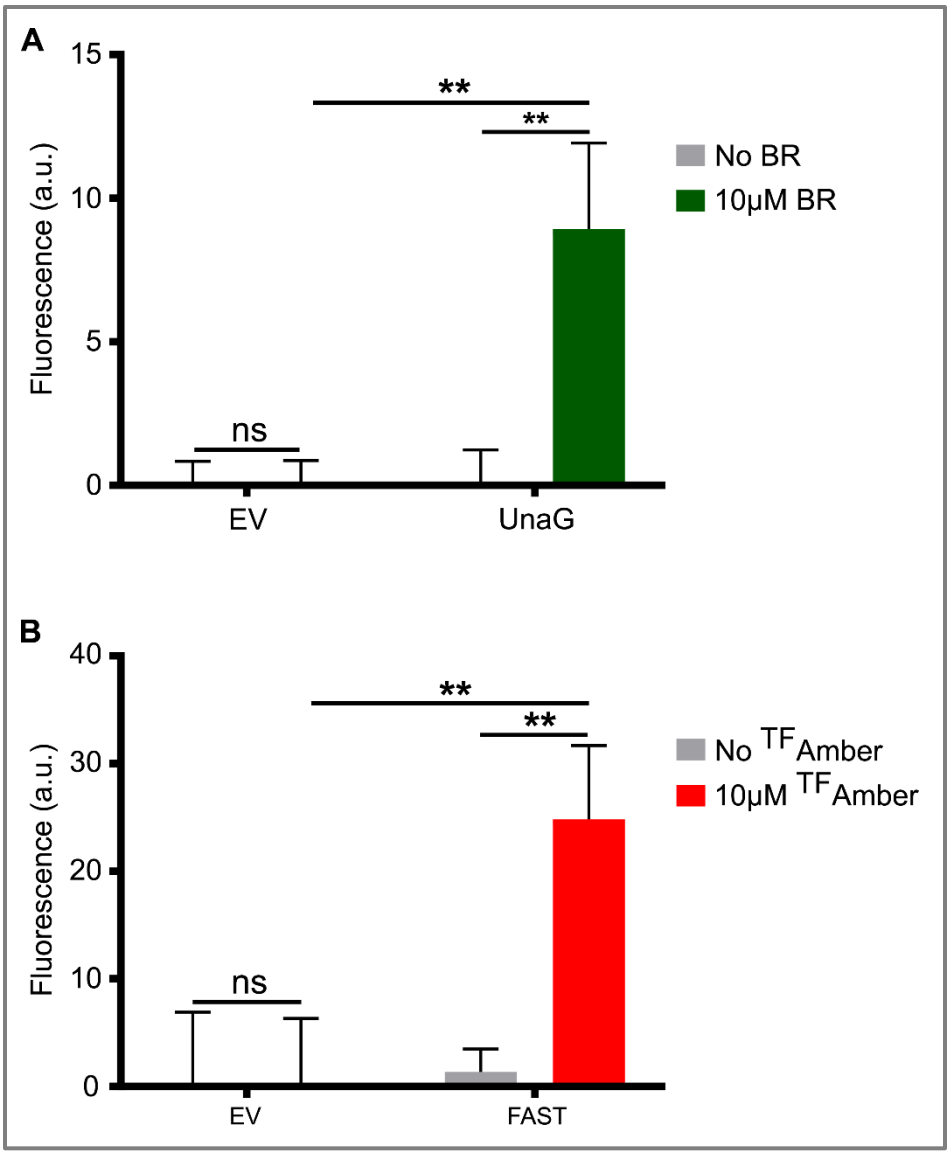

Figure 2.3: Fluorescence of PA14 expressing UnaG and FAST in anoxia. A. Fluorescence of PA14 cells carrying plasmids allowing the expression of UnaG (pCFT5) compared with those carrying the empty vector (pCFT1) in absence and presence of 10 μM bilirubin (BR). Fluorescence was recorded at excitation 498 nm and emission 527 nm. **B.** Fluorescence of PA14 cells carrying plasmids allowing the expression of FAST (pCFT7) compared with those carrying the empty vector (pCFT1) in the presence and the absence of 10 μM ^{TF}Amber. Fluorescence was recorded at excitation 482 nm and emission 536 nm. In both panels, statistical analysis was executed using two-way analysis of variance (ANOVA) followed by Bonferroni's multiple comparisons test. Fluorescence was normalized with the OD600, and the means with standard deviations as error bars are shown (ns, nonsignificant; $^{**}p < 0.01$; n = 3).

iRFP670 did not fluoresce when co-expressed with the HO in PA14 under anoxia **(Supplementary Figure S2.2)**. In order to emit light, iRFP670 must form a complex with its chromophore biliverdin, which can be derived from heme in the presence of HO. Although this enzymatic reaction requires O_2, previous data suggested that fluorescent protein related to iRFP670 can emit light in anaerobically grown *E. coli,* simultaneously expressing the HO [151]. Our data indicated this is not possible in PA14. We reasoned that providing biliverdin, excess hemin or both in the growth medium might rescue the fluorescence. Unfortunately, these additives did not increase iRFP670 emission under anoxia. By contrast, iRFP670 fluoresced when co-expressed with the HO in aerobically incubated PA14, independent of exogenous additives **(Supplementary Figure S2.2).** Altogether, these data suggested that HO and O_2 are required to yield enough biliverdin to produce functional iRFP670 in PA14. Hence, we did not investigate iRFP670 further. On the other hand, we pursued our investigation of the six FPs that emitted light under anoxia according to this plate reader assay.

2.5.4. Live fluorescent confocal microscopy imaging

As previously reported [131], we found phiLOV2.1 to be more photostable than iLOV **(Supplementary Figure S2.3)** and thus selected it for microscopic analyses of PA14. Next, we evaluated the other FPs to identify a suitable co-imaging partner for phiLOV2.1. Bacteria expressing LucY and UnaG were both visible in fluorescent microscopy **(Supplementary Figure S2.4).** The fluorescence of bacteria expressing LucY was bright and homogenous **(Supplementary Figure S2.4A)**. By contrast, the fluorescence of bacteria expressing UnaG was heterogenous, with only a small subpopulation of strongly fluorescent cells. **(Supplementary Figure S2.4B)**. Subsequent single-cell analyses of the fluorescent intensity confirmed these observations **(Supplementary Figure S2.4C)**. Thus, the use of UnaG in PA14 was complicated by the heterogeneity of its signal. Our attempts to resolve this issue failed and led us to discard UnaG.

While the use of LucY seemed promising, it was not ideal for use in combination with phiLOV2.1 because their emission spectra overlap. The emission spectrum of FAST:^{TF}Amber used in the plate reader assay also overlaps with phiLOV2.1. Hence, we turned our attention

to FAST:^{TF}Coral to cover the red region left unoccupied by the exclusion of iRFP670 as we reasoned it would combine well with phiLOV2.1. Indeed, planktonic PA14 cells carrying the empty vector were invisible **(Figure 2.4A)**, whereas those expressing phiLOV2.1 or FAST:^{TF}Coral were fluorescent **(Figure 2.4B**). The single-cell analyses of the fluorescent intensity showed that phiLOV2.1 yielded a homogenous and strong signal. By contrast, FAST:^{TF}Coral resulted in a heterogenous and overall lower signal **(Supplementary Figure S2.5)**. The heterogeneity of the signal observed with FAST:^{TF}Coral is reminiscent of that of UnaG and may be attributable, at least in part, to their use of an exogenous chromophore. This hypothesis is supported by the homogenous signal of LucY and phiLOV2.1 who use an endogenous chromophore. Next, we tested the combined use of phiLOV2.1 and FAST:^{TF}Coral to image dual cultures of *P. aeruginosa*. In brief, the strains used in monocultures were mixed and imaged. To avoid spectral bleed through, the span of wavelengths collected was narrowed for both fluorescent proteins. Once analyzed with these new acquisition parameters, the phiLOV2.1 and FAST:^{TF}Coral subpopulations were distinguishable **(Figure 2.4C)**. However, due to adjusting the acquisition parameters, the signal of both fluorescent proteins was dimmer than under the acquisition parameters used in the monocultures.

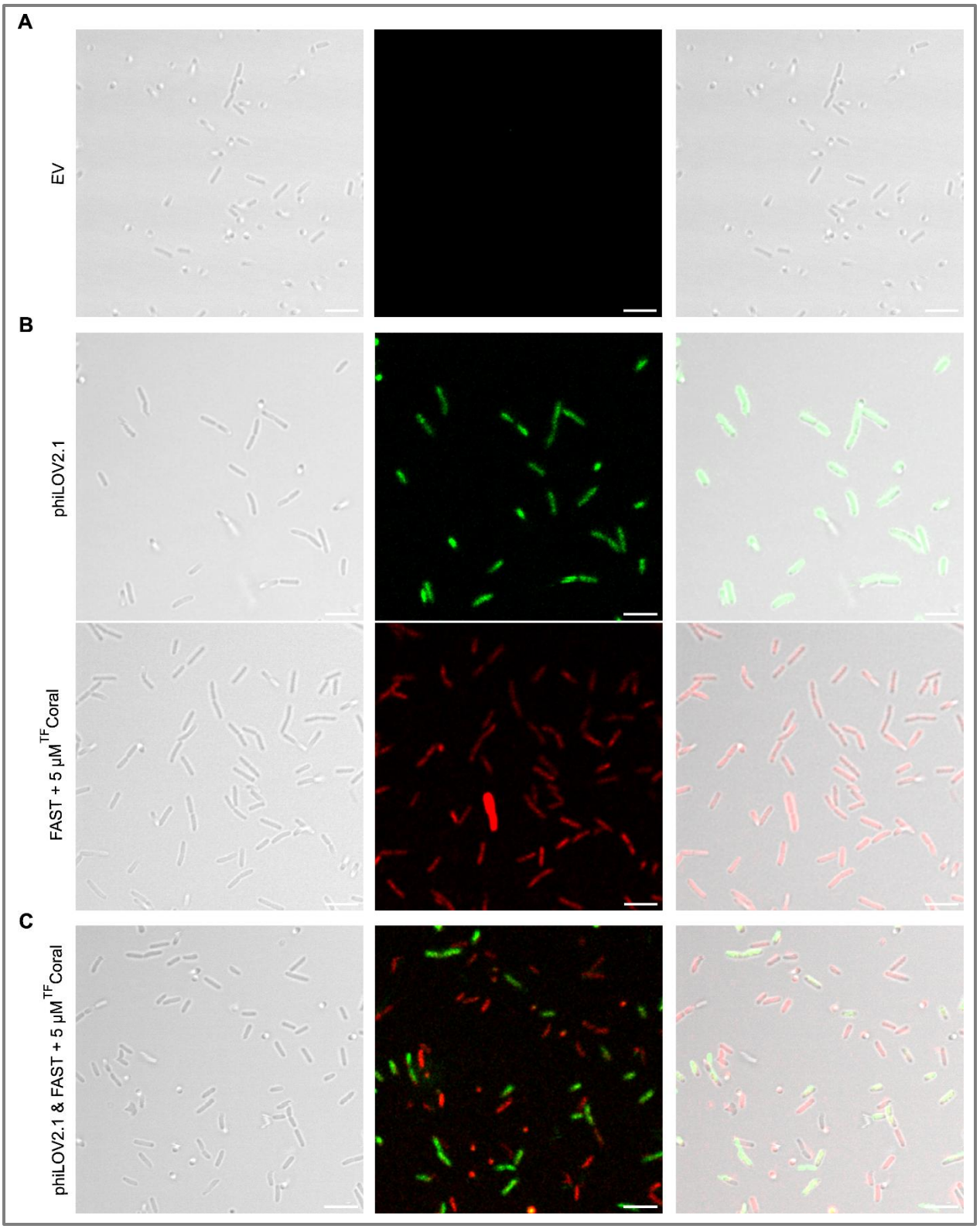

Figure 2.4: Fluorescence imaging of planktonic PA14 with phiLOV2.1 and FAST. A. Micrograph of PA14 harbouring the empty vector (pCFT1). **B.** Micrograph of PA14 expressing

phiLOV2.1 (pCFT4) and FAST:^{TF}Coral (pCFT7) in the top and bottom panel, respectively. **C.** Micrograph of a mix of PA14 cells expressing phiLOV2.1 or FAST:^{TF}Coral (1:1 inoculation ratio). From left to right: differential interference contrast (DIC), single channel fluorescence and overlay (scale bar = 5 µm).

Preliminary microscopy observations indicated that light emitted by phiLOV2.1 and FAST:^{TF}Coral decreased beyond detection limits in PA14 biofilms (data not shown). This decrease may be due to a reduction of the activity of the tac promoter or a reduction in the number of plasmid copies in biofilms. To address this pitfall, we subcloned the original tacp::phiLOV2.1 and tacp::FAST reporters into pUdO4a [250]. This synthetic plasmid harbours a broad host range BBR1 origin, which is functional in *Pseudomonas* spp. and differs from that used in pSMC21 **(Supplementary Figure S2.1B)** [251]. In addition, the strong transcriptional terminators flanking the multiple cloning sites of pUdO4a may contribute to increasing gene expression [250]. Indeed, we found that the pUdO4a derivative pCFT4.2 expressing phiLOV2.1 produced higher fluorescence levels in planktonic PA14 than its pSMC21-derived counterpart pCFT4 **(Supplementary Figure S2.6).**

Fortunately, the increased fluorescent signal of the FPs from the pUdO4a derivatives allowed the imaging of PA14 biofilms **(Figure 2.5)**. Biofilm cultures carrying the empty vector were included as negative control **(Figure 2.5A).** In comparison with this control, biofilm monocultures of PA14 cells expressing phiLOV2.1 and FAST:^{TF}Coral emitted light upon excitation at the expected wavelength **(Figure 2.5B).** Akin to the mixed planktonic cultures described above **(Figure 2.4C),** PA14 subpopulations expressing either of the two FPs were distinguishable in biofilm micrographs **(Figure 2.5C)**. However, the signal distribution in the dual cultures appeared more scattered, with the appearance of a higher proportion of weakly non-fluorescent cells than in the monoculture. This could result from the adjustment of the acquisition parameters required for dual imaging, as described above. It is noteworthy that the optimal concentration of the ^{TF}Coral chromophore was higher in biofilm than in planktonic cultures. This is likely due to the higher cell density in biofilms.

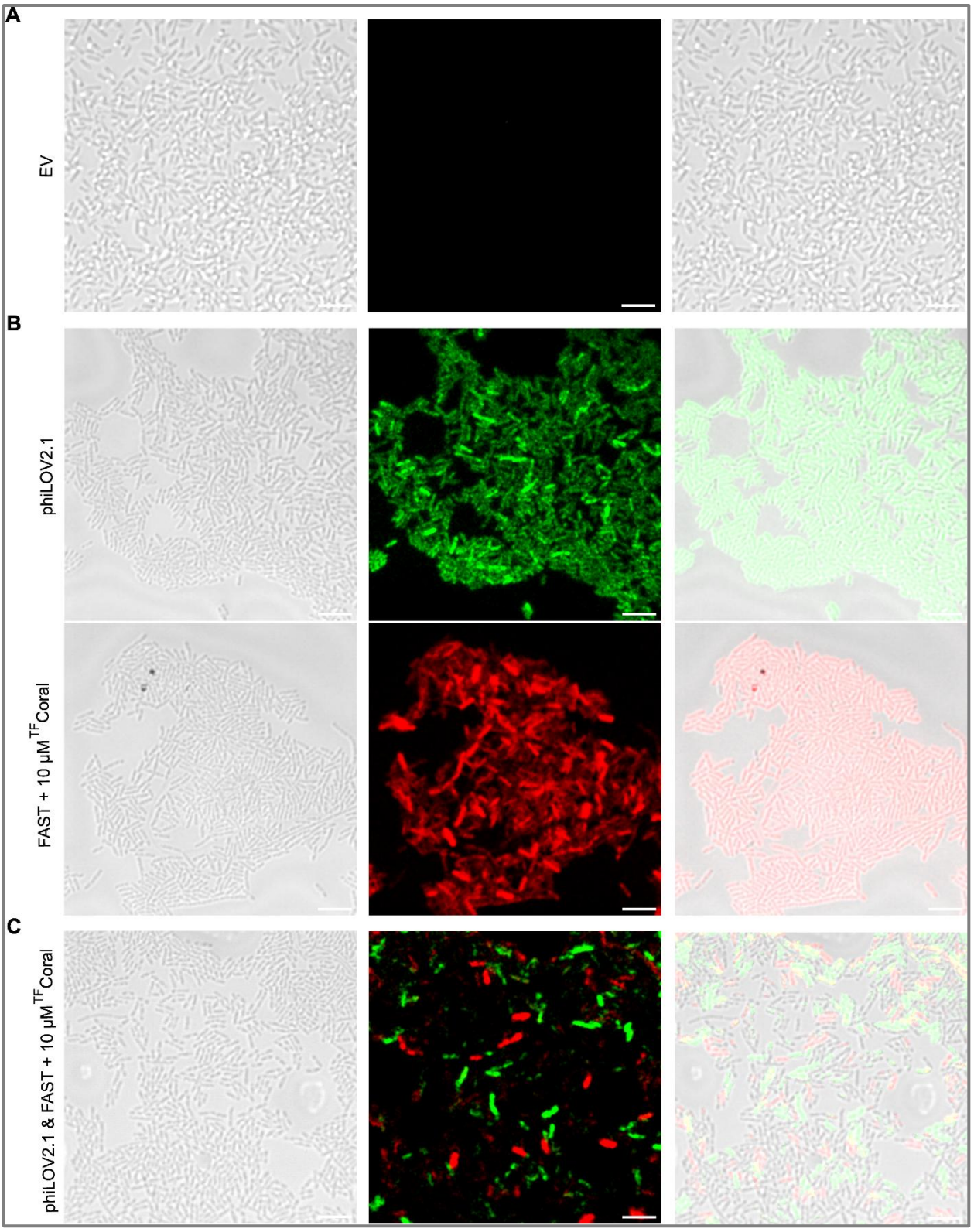

Figure 2.5: A new expression system allows fluorescence imaging of PA14 biofilms with phiLOV2.1 and FAST. A. Micrograph of PA14 harbouring the empty vector (pUdO4a). **B.**

Micrograph of PA14 expressing phiLOV2.1 (pCFT4.2) and PA14 expressing FAST:^{TF}Coral (pCFT7.2) in the top and bottom panel, respectively. **C.** Micrograph of co-cultured PA14 cells expressing phiLOV2.1 or FAST:^{TF}Coral (1:1 mix ratio). From left to right: differential interference contrast (DIC), single channel fluorescence and overlay (scale bar = 5 µm).

2.6. Discussion

In this study, we demonstrated that the fluorescent proteins iLOV, phiLOV2.1, evoglow-Bs2, LucY, UnaG and FAST allowed for the monitoring of live *P. aeruginosa* in plate reader assays under anaerobic conditions. In addition, we showed that phiLOV2.1, LucY and FAST:^{TF}Coral are practical solutions for confocal microscopy. We characterized further the use of phiLOV2.1 and FAST:^{TF}Coral and showed that they allowed for co-monitoring of dual subpopulations of *P. aeruginosa* by fluorescence microscopy. In summary, this study identified alternative fluorescent proteins for plate reader and microscopy assays when O_2 levels are insufficient for the maturation of the GFP chromophore.

Our initial analyses included iRFP670. However, co-expressing this fluorescent protein and the heme oxygenase required to produce its biliverdin chromophore yielded no fluorescence under anaerobic growth. In mammalian tissue culture cells, biliverdin-binding fluorescent proteins such as iRFP670 could work under low oxygen conditions by scavenging biliverdin, which is ubiquitous in their cytosol [247, 258]. In several pathogenic bacteria, including *P. aeruginosa*, heme oxygenases are expressed under iron starvation conditions [259–264], limiting the natural production of biliverdin in the growth conditions used here. Therefore, a *Bradyrhizobium* heme oxygenase was introduced to increase the endogenous production of biliverdin [247]. However, in anaerobically grown *P. aeruginosa*, these heme oxygenases did not yield sufficient biliverdin to produce a detectable iRFP670 signal. This issue was not resolved by exogenous biliverdin, probably because of its lack of membrane permeability or accumulation in the cytosol. Conversely, the same strain grown in normoxia fluoresced. This suggests that cytosolic iRFP670 can function in *P. aeruginosa*, but the paucity of intracellular biliverdin precludes its use under anoxia.

UnaG has been used under aerobic and anaerobic conditions in *Bacteroides thetaiotaomicron, Bacteroides ovatus* and *E. coli* by adding bilirubin in the growth media

[265, 266]. Here, we observed that *P. aeruginosa* expressing UnaG was also fluorescent when grown in the presence of bilirubin. Nevertheless, the signal was heterogeneous, with only a small fraction of the population emitting a high fluorescent signal. When averaged over the whole population in the plate reader assay, the signal of UnaG seemed inferior to the LOV proteins. Poor membrane permeability [267] and efflux pumps, such as MexAB-OprM [268, 269], may contribute to limiting the amount of bilirubin available to UnaG in the cytosol of *P. aeruginosa*.

Regarding the LOV fluorescent proteins, our data were congruent with previous studies. The signal of iLOV was the strongest, whereas the signal of phiLOV2.1 was the weakest, and the signal of evoglow-Bs2 was intermediate [145, 270, 271]. However, the photostability of phiLOV2.1 [131] likely explains its superior performance in fluorescence microscopy of *P. aeruginosa*, which has also been observed in *Clostridium* species [272]. Although the fluorescence intensity of LucY was similar to iLOV as reported [129, 140], we did not investigate LucY in depth because phiLOV2.1 was a more practical option to use in combination with FAST. Indeed, the efficiency of FAST:HBR as fluorescent reporters has been previously described in several microorganisms, including *E. coli* [132, 255], *Clostridium acetobutylicum* [255], *Listeria monocytogenes* [273] and in the archaea *Methanococcus maripaludis* [274]. Likewise, we showed that FAST:HBR is suitable for monitoring *P. aeruginosa* in plate reader assays (^{TF}Amber) and by confocal light microscopy (^{TF}Coral). Taken together, these data suggest that phiLOV2.1 and FAST:HBR are currently the best candidates for imaging dual cultures of *P. aeruginosa* under anaerobic conditions.

The dual imaging of *P. aeruginosa* subpopulations with phiLOV2.1 and FAST:^{TF}Coral was straightforward in planktonic cells. Upon switching to biofilms, we observed a substantial reduction in the fluorescence signal that was detrimental to imaging. We hypothesized that this phenomenon could stem from the downregulation of the promoter or a reduction of the number of copies of the plasmid when *P. aeruginosa* formed biofilms. This first generation of reporters was derived from pSMC21, a historical *P. aeruginosa* expression plasmid [120, 275]. It previously worked to monitor biofilm in aerobic conditions with the bright GFPmut2 [276]. The low brightness of phiLOV2.1 and FAST:^{TF}Coral revealed previously hidden

suboptimal performance of pSMC21 as an expression vector. We, thus, switched these reporter genes to a novel plasmid called pUdO4a. This plasmid is maintained by a BBR1 origin, its sequence is fully known, much smaller than that of pSMC21, and its multiple cloning site is flanked by strong transcription terminators that may contribute to increasing the expression levels of a gene of interest. Indeed, the brightness of *P. aeruginosa* harbouring the pUdO4a derivatives pCFT4.2 (phiLOV2.1) and pCFT7.2 (FAST:^{TF}Coral) allowed the imaging of individual cells in the biofilms. Moreover, it also distinguished the two subpopulations in dual-culture biofilms. It is noteworthy that during co-imaging, the span of wavelengths collected was narrowed to avert signal overlap. This put some cells under the threshold of detection, thereby unveiling the limitation in the compatibility of phiLOV2.1 and FAST:^{TF}Coral. Fluorescent proteins with brighter emission and more widely separated emission peaks would likely improve the imaging performance. Nevertheless, this study paves the way to monitoring dual *P. aeruginosa* populations in a variety of genetic background and environmental conditions. The broad host range of the BBR1 origin suggests that the second generation of pCFT reporters derived from pUdO4a could be seamlessly transferred to several other Gram-negative bacteria.

This study identified six fluorescent proteins that are functional under anoxia in *P. aeruginosa*. However, their brightness is only a small fraction of that of the GFP under aerobic conditions. Therefore, discovering brighter and complementary O_2-independent fluorescent proteins will drive future development by improving our capacity to monitor multiple *P. aeruginosa* subpopulations. For example, three brighter variants of phiLOV2.1 were recently described – phiLOV3, mini-GFP1 and mini-GFP2 [277, 278]. Secondly, FAST derivatives such as FAST2 and tdFAST2 have improved brightness in their HBR-bound state [279]. Moreover, frFAST bound a different chromophore that extended the fluorescence emission palette toward the far-red [280]. Alternative self-labeling proteins not tested here, such as $SNAP_f$, $CLIP_f$ and Halo-tag, yielded excellent anaerobic reporters [147, 281]. Finally, pUdO4a and its derivatives described above provide an excellent platform to expand the fluorescent tools for studying microbes under oxygen-limited conditions in a variety of environmental and physiological settings.

2.7. Supplementary Materials

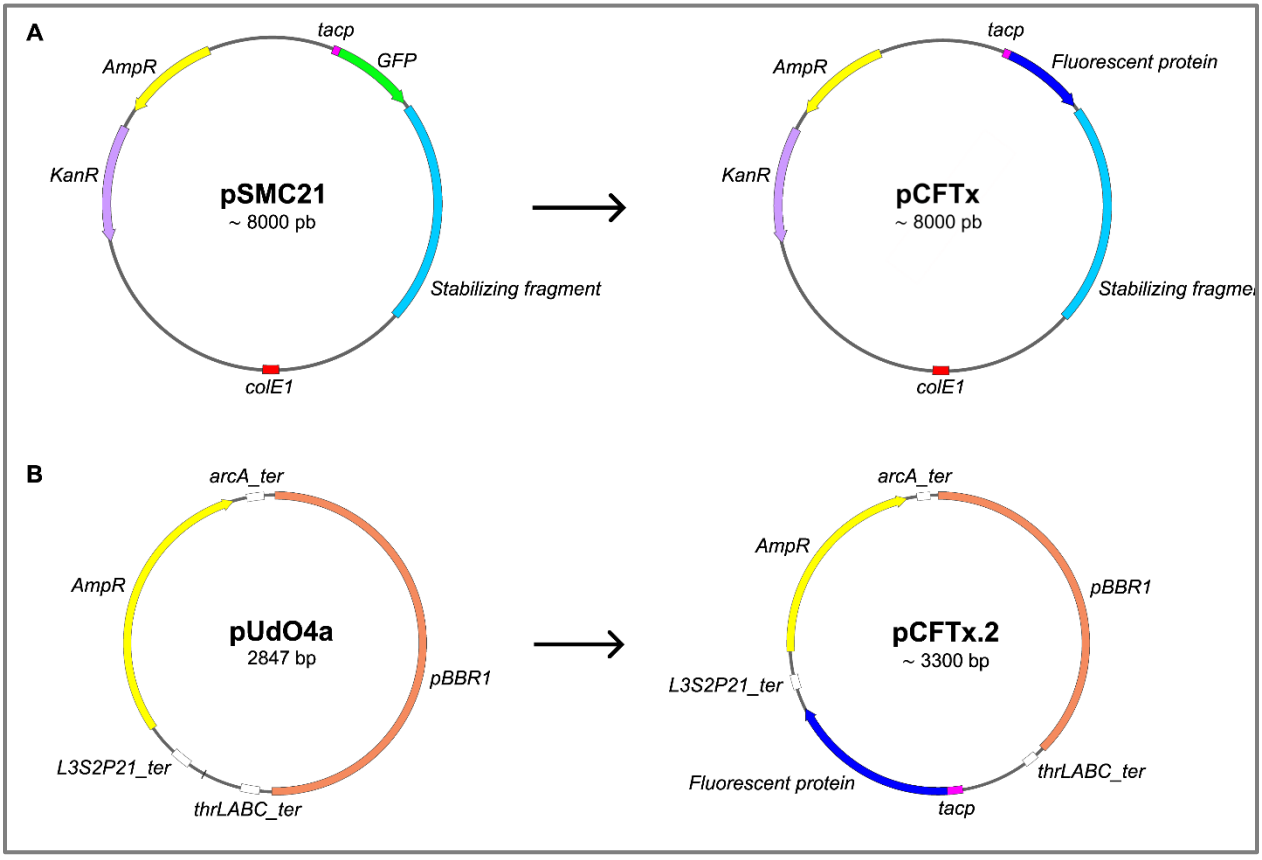

Figure S2.1: Plasmid maps of pCFTx and pCFTx.2. A. pCFTx derived from pSMC21, where the GFP has been removed or replaced by the fluorescent proteins listed in Table 1. **B.** pCFTx.2 derived from pUdO4a where tacp::GFPmut2, tacp::iLOV, tacp::phiLOV2.1 and tacp::FAST were subcloned. The maps are not to scale and were prepared using SnapGene Viewer v.6.2.2.

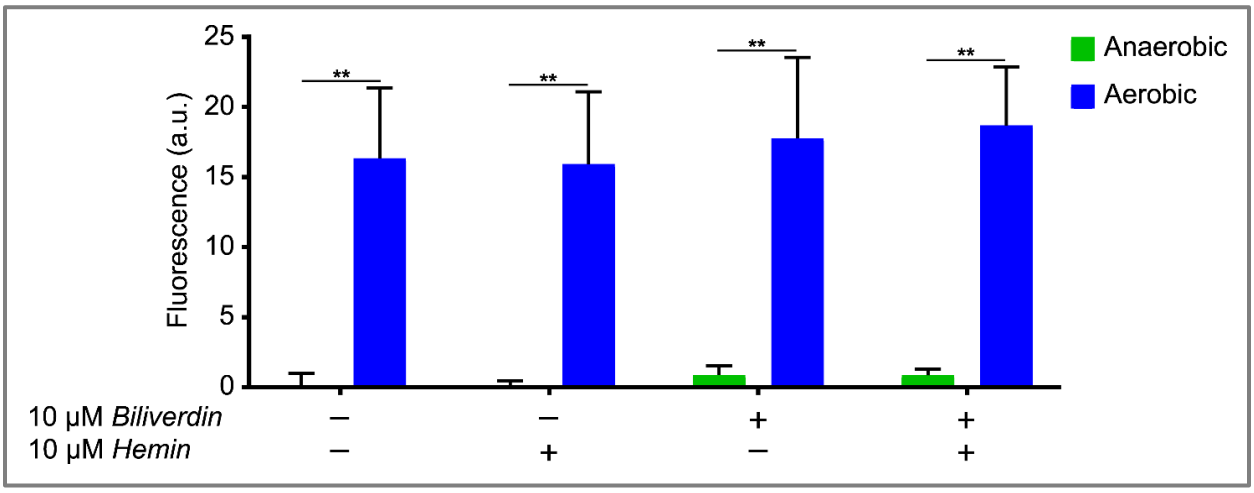

Figure S2.2: Comparison of fluorescence level of *P. aeruginosa* PA14 expressing iRFP670 in normoxia versus anoxia. Fluorescence of PA14 cells expressing iRFP670 was recorded at 643 nm excitation and 670 nm emission wavelengths in the presence or absence of 10 µM biliverdin and 10 µM hemin. Fluorescence was normalized to OD600. Statistical analysis was computed using two-way analysis of variance (ANOVA) followed by Bonferroni's multiple comparisons test. The means with standard deviations as error bars are shown (**, $p < 0.01$; n = 3).

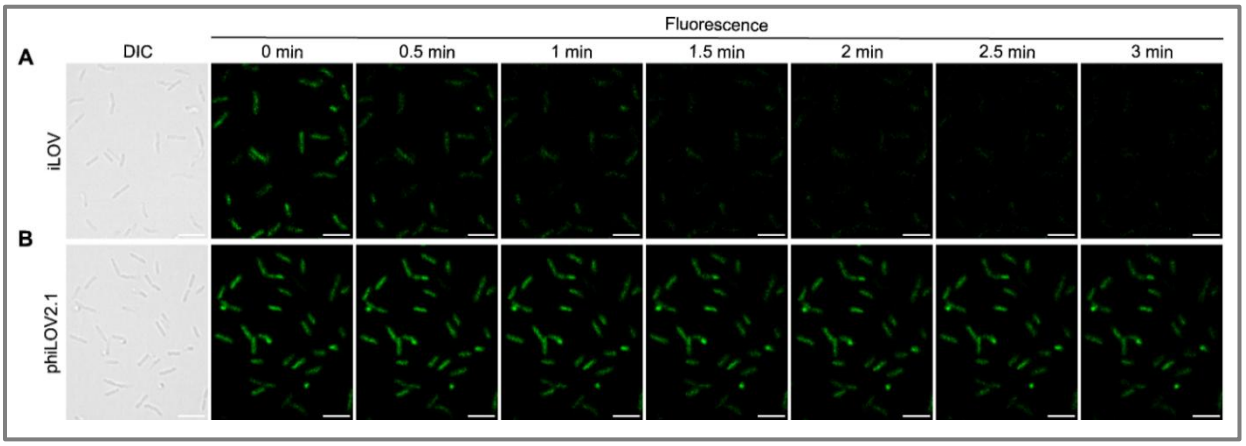

Figure S2.3: Comparison of photostability between iLOV (pCFT3) and phiLOV2.1 (pCFT4) using time-lapse imaging of *P. aeruginosa* PA14 cells. Micrographs were acquired every 30 seconds for 3 minutes at excitation 458 nm and emission 505 nm. Far-left panels are differential interference contrast (DIC), and the others are single channel fluorescence (scale bar = 5µm).

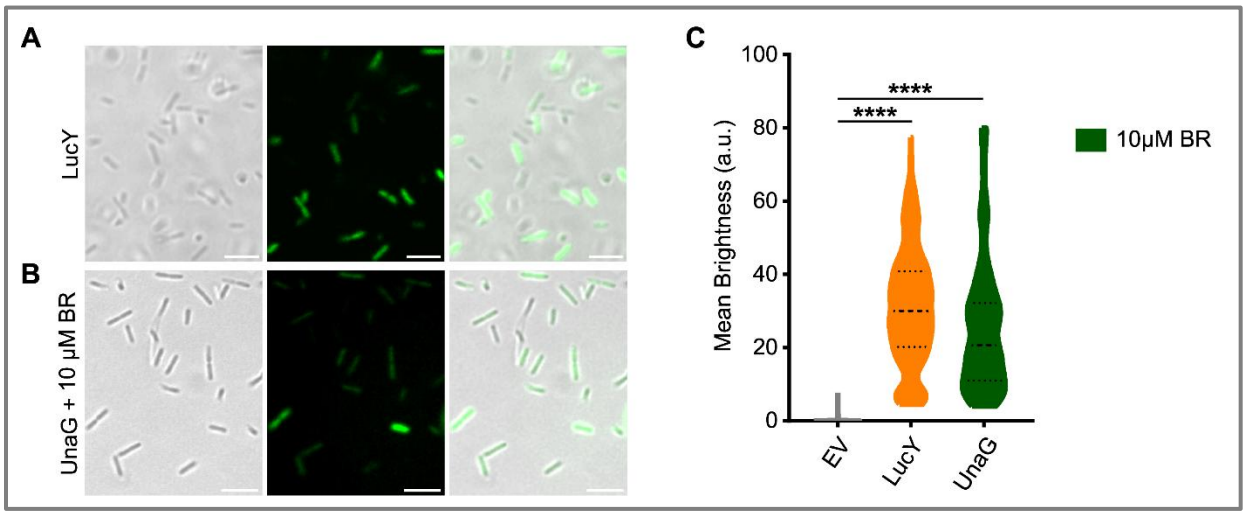

Figure S2.4: Fluorescence of LucY and UnaG in anaerobic planktonic cultures of *P. aeruginosa* PA14 cells. **A.** Micrograph of PA14 expressing LucY (pCFT8) recorded at excitation 488 nm and emission 558 nm. **B**. Micrograph of PA14 expressing UnaG (pCFT5) in the presence of 10 µM bilirubin (BR) recorded at excitation 488 nm and emission 539 nm. From left to right: differential interference contrast (DIC), single channel fluorescence and overlay (scale bar = 5µm). **C.** Single-cell fluorescence quantification of LucY and UnaG compared to EV, the empty vector (pCFT1) used as the control for background fluorescence. Mean brightness intensities were measured with ImageJ and statistical analysis was performed using an unpaired T-test (****, $p < 0.0001$; n = 4).

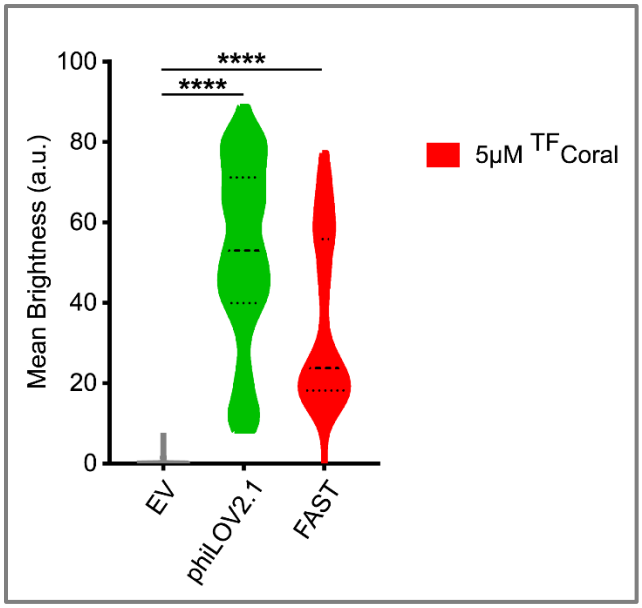

Figure S2.5: Single-cell fluorescence quantification of phiLOV2.1 (pCFT4) and FAST (pCFT7) compared to EV, the empty vector (pCFT1) used as the control for background fluorescence. Mean brightness intensities were measured with ImageJ and statistical analysis was assessed using an unpaired T-test (****, $p < 0.0001$; n = 4).

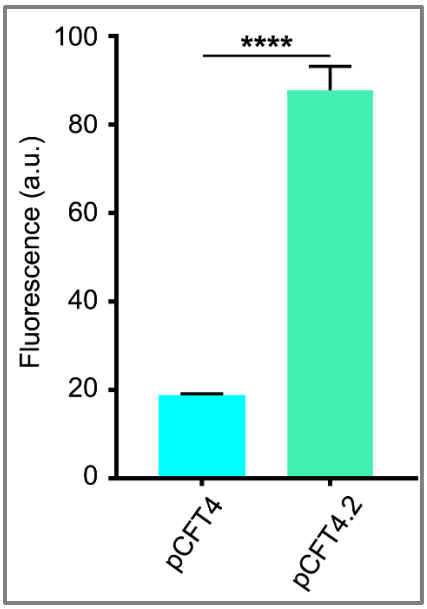

Figure S2.6: PA14 carrying pCFT4.2 produced higher phiLOV2.1 fluorescence than pCFT4. Fluorescence of PA14 expressing phiLOV2.1 in two different plasmids background. Fluorescence was recorded at excitation 450 nm and emission 495 nm and normalized to OD600. Statistical analysis was performed using an unpaired T-test. The means with standard deviations as error bars are shown (****, $p < 0.0001$; n = 3).

Table S2.1: List of primers used in this study

Long name	Primers sequences
pSMC21_rev_ctr	GTCTGGACATATGTATATCTCCTTCTTAAATCTAGAG
pSMC21_fwd_ctr	AGATATACATATGTCCAGACCTGCAGCAATG
pSMC21_rev	ATGTATATCTCCTTCTTAAATCTAGAG
evoglowBS2_fwd	TTTAAGAAGGAGATATACATATGAAAGCATCTTTCCAG
evoglowBS2_rev	ATTGCTGCAGGTCTGGACATTCAGTTACTCGAGCAGCTTTTC
pSMC21_fwd	CTGAATGTCCAGACCTGCAGCAATG
phiLOV2.1_fwd	TTTAAGAAGGAGATATACATATGAAAATCGAGAAATCGTTC
phiLOV2.1_rev	ATTGCTGCAGGTCTGGACATTCAGTTACACGTGATCAGACCC
iLOV_fwd	TTTAAGAAGGAGATATACATATGAAAATCGAGAAGAACTTC
iLOV_rev	ATTGCTGCAGGTCTGGACATTCAGTTACACATGATCCGAACC
UnaG_fwd	TTTAAGAAGGAGATATACATATGGTGGAAAAATTCGTCGGCAC
UnaG_rev	ATTGCTGCAGGTCTGGACATTCAGTTATTCGGTGGCGCGCCG
iRFP670_fwd	TTTAAGAAGGAGATATACATATGGCGCGTAAGGTCGATC
iRFP670_rev	TTTTATTCCTCCATTTCAGTTAGCGTTGGTGGTGGGC

heme_fwd_670	CCAACGCTAACTGAAATGGAGGAATAAAAAATGTTGGACCGAGTTGATTC CAATCACGTC
heme_rev	ATTGCTGCAGGTCTGGACATTTAGTCAGCGGCCGAGCCCCGC
pSMC21_fwd_heme	CTAAATGTCCAGACCTGCAGCAATG
pUdO4a_noMCS_fwd	CGACACGGTCTCTGAGAG
pUdO4a_noMCS_rev	CGAAGACACTCGGCTCTTC
pUdO4a_FP_orf_revseq_fwd	CGAAGAGCCGAGTGTCTTCGCGGTAACGACGTCCAGAC
pUdO4a_FP_orf_revseq_rev	TTCTCTCAGAGACCGTGTCGCACTTAACATTATGCTGAGTGATATC

Table S2.2: Comparison of growth rates of *P. aeruginosa* PA14 expressing different fluorescent proteins in anoxia with EV (empty vector) as the control.

	EV	GFP	iLOV	phiLOV2.1	evoglow-Bs2	LucY	UnaG	FAST	iRFP 670
Slopes	0.43	0.43	0.45	0.42	0.44	0.4	0.42	0.42	0.38
P values	-	1.00	0.52	0.86	0.73	0.48	0.8	0.87	0.16

Chapter 3: Characterization of *P. aeruginosa* strains in a CF polymicrobial assay

3.1. Preface

All experiments, data collection, and analyses presented in this chapter were performed by me. This work was carried out in collaboration with Dr. George O'Toole (Dartmouth College, Hanover, NH, USA) and Dr. Fabrice Jean-Pierre (Université de Sherbrooke, Sherbrooke, QC, Canada). At the outset of the collaboration, Dr. Jean-Pierre was a postdoctoral fellow in Dr. O'Toole's laboratory, where I spent a week learning the polymicrobial model system under his guidance. Following this training, I independently established and implemented the system in Ottawa, where I conducted the entirety of the experimental work described in this chapter.

3.2. Introduction

Advances in culture-targeted and culture-independent approaches have revealed tremendous diversity in the microbial population of the cystic fibrosis (CF) airway. In that environment, *P. aeruginosa* is significantly less susceptible to antibiotics than when it exists in traditional *in vitro* monocultures [233, 235, 282]. To reduce the gap between *in vitro* antimicrobial susceptibility and clinical responses, a recent report employed computational approaches to develop an *in vitro* CF polymicrobial assay comprising four important CF pathogens: *P. aeruginosa, Staphylococcus aureus, Streptococcus sanguinis*, and *Prevotella melaninogenica* [199]. In their report, the authors employed 16S rRNA sequencing libraries, clinical metadata, and metabolic modelling to define a prevalent bacterial community found in about 34% of airway infections among individuals with CF [199]. Furthermore, stemming from numerous previous studies [230, 231, 283–288], the authors also argued that these four bacteria significantly influence the health outcomes in CF patients [199]. Consequently, these four bacteria represent an *in vitro* CF polymicrobial model system that is implemented under anaerobic conditions. This model proved valuable in improving the understanding of microbial interactions and responsiveness to antimicrobial treatment.

In **Chapter 1 – Section 1.3**, I introduced six genetic loci of *P. aeruginosa*, five of which have been directly linked to antibiotic resistance. The six isogenic *P. aeruginosa* deletion mutants derived from these genetic loci were divided into two groups. The first group

comprises Δ*ndvB,* Δ*PA1874-77,* Δ*tssC1* and Δ*tctED,* which have been characterized in the Mah laboratory as biofilm-specific antibiotic resistance genes [40, 76–78]. That is, each of these mutants can form a biofilm and displays equal susceptibility to antibiotics as the wild type strain when grown as planktonic cultures [40, 76–78]. However, these mutants exhibit a heightened susceptibility to antibiotics when cultivated as biofilms [40, 76–78].

The second group of *P. aeruginosa* mutants includes Δ*PA1759-60* and Δ*flgK*. Δ*PA1759-60* association with antibiotic resistance is currently under active research. For instance, the two-gene operon *PA1759-60* is being investigated in the Mah laboratory as a potential transcriptional regulator implicated in biofilm antibiotic resistance. Indeed, deleting *PA1759* and *PA1760* genes in PA14 produced a biofilm with increased susceptibility to tobramycin when compared to the wild type isogenic strain (Hall, CW et al.; manuscript in preparation). In addition, Δ*PA1759-60* exhibits a significantly slower growth under anaerobic conditions compared to the wild type [96]. The Δ*flgK* mutant, on the other hand, forms altered biofilms due to its flagellum deficiency [97, 98]. *P. aeruginosa* mutants with this deficiency are prevalent in the CF microbiota, having evolved as an adaptation mechanism [98, 99]. Therefore, it is of interest to characterize Δ*flgK* in CF-like conditions within the polymicrobial assay.

Notably, the importance of these genetic loci regarding *P. aeruginosa* antibiotic resistance has been elucidated in *in vitro* aerobic mono-species biofilm models. However, I alluded earlier to the disconnect between *P. aeruginosa in vitro* antimicrobial susceptibility and clinical responses. Therefore, I aimed to 1) Characterize *P. aeruginosa* strains harbouring mutations on these loci by assessing their ability to persist in a CF polymicrobial assay, and 2) Evaluate their responses to tobramycin, an antibiotic generally used to treat CF infections.

I hypothesized that these genes would be essential for *P. aeruginosa* survival in this more complex system. As a widespread environmental bacterium, *P. aeruginosa* encounters numerous antimicrobial compounds in the soil [289–292], and these genes likely provide some form of protection against these compounds, thus allowing for persistence in the environment. Therefore, deleting them would impact *P. aeruginosa* ability to thrive in a

polymicrobial setting. Thus, the findings presented in this chapter aim to deepen our understanding of *P. aeruginosa* responses to antibiotic treatment and may help inform the development of new strategies for managing CF infections.

3.3. Materials and Methods

3.3.1. Bacterial strains and growth conditions

In this chapter, all the strains are listed in **Table 3.1**, and the culture media are listed in **Table 3.2**. PA14 WT, *S. aureus* Newman and *S. sanguinis* SK36 were obtained from the O'Toole laboratory. *P. melaninogenica* strain ATCC25845 was purchased from ATCC. All mutant strains are from our laboratory. The growth conditions were prepared as described in [199] with minor exceptions. Briefly, each bacterium frozen stock was routinely streaked on its respective agar medium **(**see **Table 3.2)**. *P. aeruginosa* and *S. aureus* solid cultures were incubated aerobically for 16 – 18 h at 37°C. Plates with *S. sanguinis* and *P. melaninogenica* were incubated for 24 – 48 h at 37°C in a BactronEZ chamber (Sheldon Manufacturing. Inc., Cornelius, OR) under an anaerobic atmosphere of 5% H_2, 5% CO_2, 90% N_2 that contained fewer than 4.7 parts per million O_2 per the manufacturer's specifications. A single axenic colony of each bacterium was used to inoculate its respective liquid media **(**see **Table 3.2)** and was incubated under the same conditions as mentioned above, except that aerobic cultures were placed in a shaking incubator (250 rpm). These cultures were then used as inocula for subsequent assays. In those assays, the culture media was the Artificial Sputum Media (ASM), which mimics the nutritional content of the CF lung [293, 294] and was prepared as described in [199]. In this chapter, ASM media without the addition of mucin (5 mg/mL) will be referred to as ASM. ASM media supplemented with mucin (5 mg/mL) will be referred to as ASM+. All anaerobic incubations were carried out in the aforementioned BactronEZ chamber.

Table 3.1: Bacterial strains used in this chapter.

Species	Strains	Phenotype/Genotype	Reference
P. aeruginosa	PA14 WT	Laboratory reference strain	[252]
	PA14::Δ*ndvB*	In-frame deletion of *ndvB* gene	[40]
	PA14::Δ*PA1874-77*	In-frame deletion of *PA1874-77* genes	[76]
	PA14::Δ*tssC1*	In-frame deletion of *tssC1* gene	[77]
	PA14::Δ*tctED*	In-frame deletion of *tctED* gene	[89]
	PA14::Δ*PA1759-60*	In-frame deletion of *PA1759-60* genes	Hall, CW et *al.*; manuscript in preparation
	PA14::Δ*flgK*	In-frame deletion of *flgK* gene	[97]
S. aureus	Newman	Methicillin-susceptible *Staphylococcus aureus*	[295]
S. sanguinis	Strain SK36	-	[296]
P. melaninogenica	ATCC25845	-	[297]

Table 3.2: Culture media used in this chapter.

	Bacterial strains	Solid media	Liquid media
Routine culture	*P. aeruginosa* strains *S. aureus*	Tryptic Soy Broth - TSB + 1.5% agar (TSA)	Tryptic Soy Broth (TSB)
	S. sanguinis *P. melaninogenica*	TSA + 5% sheep blood (BA)	Todd Hewitt Broth + 0.5 % yeast extract (THBY) *Prevotella* growth medium (PGM)*
Selective culture	*P. aeruginosa* strains	*Pseudomonas* Isolation Agar (PIA)	
	S. aureus	Mannitol Salt Agar (MSA)	
	S. sanguinis	*Streptococcus* Selective Agar (SSA)**	
	P. melaninogenica	*Prevotella* Selective Agar (PSA)***	

***** PGM = TSB + 0.5% yeast extract + 5 µg/mL hemin + 2.85 mM L-cysteine hydrochloride + 1 µg/mL menadione.
****** SSA = BA + 10 µg/mL polymyxin B + 10 µg/mL oxolinic acid.
******* PSA = PGM + 1.5% agar + 100 µg/mL kanamycin + 7.5 µg/mL vancomycin + 5 µg/mL polymyxin B.

3.3.2. Colony forming units assay to assess the ability of *P. aeruginosa* to persist in a multi-species setting

The colony forming units (CFU) assay was performed as previously reported in [199]. In brief, using the overnight liquid cultures described in **Section 3.3.1**, *P. aeruginosa, S. aureus,* and *P. melaninogenica* were washed twice in sterile 1 mL PBS by centrifugation at 10,000 × *g* for 2 min, while *S. sanguinis* was washed once. Cell pellets were resuspended in ASM and diluted to a concentration equivalent to an optical density (OD600) of 0.2 in ASM+. Mono- and mixed-cultures were adjusted to a final concentration of 0.01 in ASM+ using cell suspensions with a starting concentration of 0.2. The mixed cultures consist of equal ratios of each bacterial suspension, initially at a concentration of 0.2. The average starting CFU of each bacterial suspension corresponding to an OD600 of 0.01 is presented in **Table 3.3**. A volume of 100 µL of each bacterial suspension was dispensed in a polystyrene flat-bottom 96-well plate, and each sample was assayed in triplicate. The plate was then incubated anaerobically for 24 h at 37°C.

After the first 24 h incubation period, the spent supernatant containing planktonic cells was removed, and 100 µL of ASM+ media were loaded onto each well. The incubation was pursued for another 24 h. After 48 h of incubation, the planktonic fraction was collected, 10-fold serially diluted and plated on selective plates **(**see **Table 3.2)**. The attached cells were washed in PBS to remove residual planktonic cells and then resuspended in 50 µL PBS using a multiprong device. This resuspension was transferred to a clean 96-well plate, then 10-fold serially diluted and finally plated on selective media **(**see **Table 3.2)**.

Pseudomonas Isolation Agar (PIA), Mannitol Salt Agar (MSA), *Streptococcus* Selective Agar (SSA), and *Prevotella* Selective Agar (PSA) are solid media selective for *P. aeruginosa, S. aureus, S. sanguinis* and *P. melaninogenica,* respectively. PIA and MSA plates were incubated aerobically for 16 – 18 h, while SSA and PSA plates were incubated anaerobically for 24 – 48 h. All incubations were conducted at 37°C, followed by colony counting. For each bacterial strain, the CFU/mL was determined by averaging counts from a technical triplicate. Each experiment was performed with at least three independent biological replicates. The results were tabulated and plotted, and statistical analyses were computed with GraphPad

Prism 8 (GraphPad Software, La Jolla, CA). Data are presented as mean ± standard deviation, with a 95% confidence level ($p < 0.05$).

Table 3.3: Average starting bacterial concentration at an OD600 of 0.01

Bacterial strains	Average starting CFU*
PA14 WT	6.7×10^6 CFU/mL
PA14::Δ*ndvB*	5.7×10^6 CFU/mL
PA14::Δ*PA1874-77*	4.5×10^6 CFU/mL
PA14::Δ*tssC1*	5.4×10^6 CFU/mL
PA14::Δ*tctED*	5.2×10^6 CFU/mL
PA14::Δ*PA1759-60*	3.4×10^6 CFU/mL
PA14::Δ*flgK*	5.5×10^6 CFU/mL
S. aureus	7.3×10^6 CFU/mL
S. sanguinis	2.6×10^6 CFU/mL
P. melaninogenica	2.5×10^6 CFU/mL

*The standard deviation for all the CFU was ± 1.

3.3.3. Minimal bactericidal concentration assay

To determine the minimal bactericidal concentration (MBC), the assay was prepared as follows: overnight cultures of all *P. aeruginosa strains* **(Table 3.1)** were diluted to a final OD600 of 0.01 in ASM+, and 100 µL of these cell cultures were distributed in triplicate in a 96-well plate. The plate was then incubated anaerobically for 24 h at 37°C. After the first 24 h incubation period, the spent supernatant was removed, and 100 µL of ASM+ media containing or not tobramycin (TOB) at different concentrations ranging from 0 to 250 µg/mL **(Table 3.4)** were loaded onto each well. Anaerobic incubation was continued for an additional 24 h at 37°C. Following this incubation, the cultures containing both planktonic and biofilm cells were disrupted using a multiprong device. Three microliters of these cell suspensions were spotted on TSA plates, which were subsequently incubated aerobically at 37°C for 16 to 18 h. The viability was assessed by the presence or absence of growth.

Table 3.4. Final concentrations of tobramycin (TOB) in each cell suspension

[TOB] (µg/mL)	0	0.24	0.49	0.98	1.95	3.91	7.81	15.63	31.25	62.5	125	250

3.3.4. Tobramycin susceptibility assay of *P. aeruginosa* strains in a CF polymicrobial assay

The multi-species system was implemented as described in **Section 3.3.2**. PA14 WT, and the six *P. aeruginosa* deletion mutant strains were assayed as mono- and mixed-cultures. After 24 h of incubation, the spent supernatant was removed and replaced with 100 µL of fresh ASM+, and the incubation was pursued for another 24 h. After 48 h of incubation, the spent supernatant was removed once again and replaced with 100 µL of fresh ASM+ supplemented with TOB 50 µg/mL or TOB 100 µg/mL. Controls with only ASM+ and no TOB were also assayed. The incubation was pursued for another 24 h. After a total of 72 h of incubation, the planktonic portion was transferred to a 96-well plate, 10-fold serially diluted, and plated on selective media **(Table 3.2)**. The biofilm portion or attached cells were washed in PBS and resuspended in 50 µL PBS using a multiprong device. This resuspension was transferred to a clean 96-well plate, 10-fold serially diluted and finally plated on selective media **(Table 3.2)**. Following the incubation, the colony count and data analysis were performed as described in **Section 3.3.2**.

3.4. Results

3.4.1. *P. aeruginosa* strains in the CF polymicrobial model assay

3.4.1.1. PA14 WT is stably maintained in a CF polymicrobial assay

Using PA14 WT, the first goal was to reproduce the CF polymicrobial assay developed by Jean-Pierre et al. [199], specifically Figure 1C in their article. In their assay, the authors modelled an *in vitro* mixed community of *P. aeruginosa, S. aureus, S. sanguinis, and P. melaninogenica* that can be stably maintained for up to two weeks [199]. Overall, the CFU counts for each species presented in **Figure 3.1** are relatively similar to the results in [199] except for the results with *P. melaninogenica*.

The PA14 WT biofilm population exhibited no significant difference in CFU counts when grown as mono- or mixed-culture **(Figure 3.1**, first two green bars**)**. In contrast, the PA14 WT planktonic population showed a slight decrease in the mixed- compared to the mono-culture **(Figure 3.1**, last two green bars**)**. This finding is identical to the one in [199]. For *S. aureus*, biofilm and planktonic populations showed a slight decrease in CFU in the mixed-

compared to mono-culture **(Figure 3.1**, orange bars**)**. The result for the biofilm population **(Figure 3.1**, first two orange bars**)** differs slightly from the one in [199], as the authors described no statistically significant changes in both culture conditions. For *S. sanguinis* **(Figure 3.1**, blue bars**)**, no substantial changes in CFU counts were noted for biofilm or planktonic populations regardless of the mode of culture (mono or mixed). As noted similarly for *S. aureus* biofilm, the result for *S. sanguinis* biofilm also diverges slightly from [199]. Indeed, the authors found a statistically significant difference between mono- and mixed-culture. Lastly, *P. melaninogenica* mixed culture showed a moderate ~ 1 log decrease compared to the monoculture in biofilm and planktonic populations (**Figure 3.1**, grey bars). This result is the most different from [199] as the authors reported no detectable growth of *P. melaninogenica* in monocultures. In the discussion (**Section 3.5**), I will explore plausible reasons for these discrepancies.

Taken together, the data presented in **Figure 3.1** showed that the different bacterial taxa remained relatively stable in specific culture conditions (mono vs. mixed) and growth mode (planktonic vs. biofilm). This also demonstrates that I was able to reproduce the polymicrobial assay developed by Jean-Pierre et al. [199].

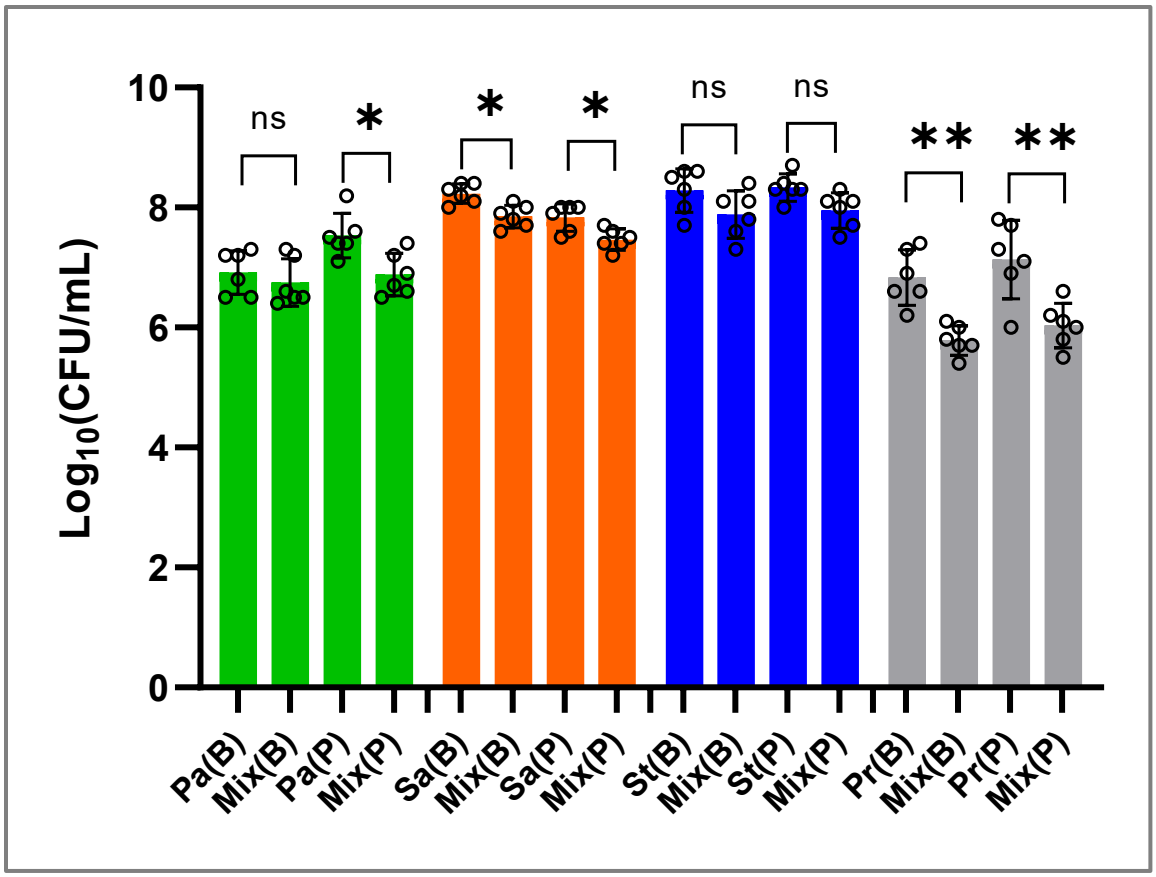

Figure 3.1: Colony forming units (CFU) counts of each bacterial strain grown anaerobically as a monoculture and in a mixed culture (Mix) for biofilm (B) and planktonic (P) fractions. CFU analysis was performed by plating on a medium selective for the growth of each species. The histogram represents the average of six biological replicates (n=6), and each data point represents the average of three technical replicates. Statistical analysis was performed using ordinary one-way ANOVA and Tukey's multiple comparisons post-test *$p<0.05$, **$p < 0.01$ and ns = non-significant. Error bars represent SD. Pa (green bars) = *Pseudomonas aeruginosa*, Sa (orange bars) = *Staphylococcus aureus*, St (blue bars) = *Streptococcus sanguinis*, Pr (grey bars) = *Prevotella melaninogenica*.

3.4.1.2. *P. aeruginosa* mutant strains Δ*ndvB, ΔPA1874-77,* Δ*tssC1* and Δ*tctED* are stably maintained in the CF polymicrobial assay

In the general introduction **(Chapter 1 – Section 1.3.2.2)**, I described *ndvB, PA1874-77, tssC1*, and *tctED* as genetic loci important for biofilm-specific antibiotic resistance in *P. aeruginosa*. These genetic loci have been characterized in mono-species studies under aerobic culture conditions. However, CF is a mixed-species and biofilm-based infection where *P. aeruginosa,* as a major CF pathogen, thrives in various O_2 concentrations. Prior to

evaluating the antibiotic responses of the mutants within the complex CF polymicrobial assay under anaerobic conditions, an initial step involved confirming the ability of these deletion mutants to persist in the assay. This was undertaken to ensure that the targeted gene deletions in PA14 did not compromise the mutant strains competitive fitness against other bacterial species within this model system.

To that end, I replaced PA14 WT in the mixed population (composed of *S. aureus, S. sanguinis* and *P. melaninogenica*) with four isogenic mutants: Δ*ndvB,* Δ*PA1874-77,* Δ*tssC1,* and Δ*tctED*, and assessed whether the CFU counts for each strain mirrored those of the wild type strain or differed. Because of the emphasis on *P. aeruginosa* in this thesis, only the results pertaining to this species are presented here.

The results for this first group of *P. aeruginosa* mutants are presented in **Figure 3.2.** Similar to the wild type strain, Δ*ndvB* biofilm and planktonic populations showed no statistically significant differences in CFU counts when grown either as a mono- or mixed-culture **(Figure 3.2A**, blue bars**)**. This finding also applies to the biofilm populations of Δ*PA1874-44* **(Figure 3.2B**, first two red bars**)**, Δ*tssC1* **(Figure 3.2C**, first two green bars**)** and Δ*tctED* **(Figure 3.2D**, first two pink bars**)**. In contrast, the CFU counts for planktonic cultures exhibited a small but significant 0.5 log decrease in mixed cultures compared to monocultures for Δ*PA1874-44* (**Figure 3.2B**, last two red bars**)**, Δ*tssC1* **(Figure 3.2C**, last two green bars**)** and Δ*tctED* (**Figure 3.2D**, last two pink bars**)**.

Altogether, the deletion of these different genetic loci in PA14 did not impede the mutant strains' ability to persist in a mixed community when grown as biofilms. However, a small but significant 0.5 log decrease was noted in the mixed-species for planktonic cells, except for the Δ*ndvB* strain, which had consistent CFU counts between mono- and mixed-cultures.

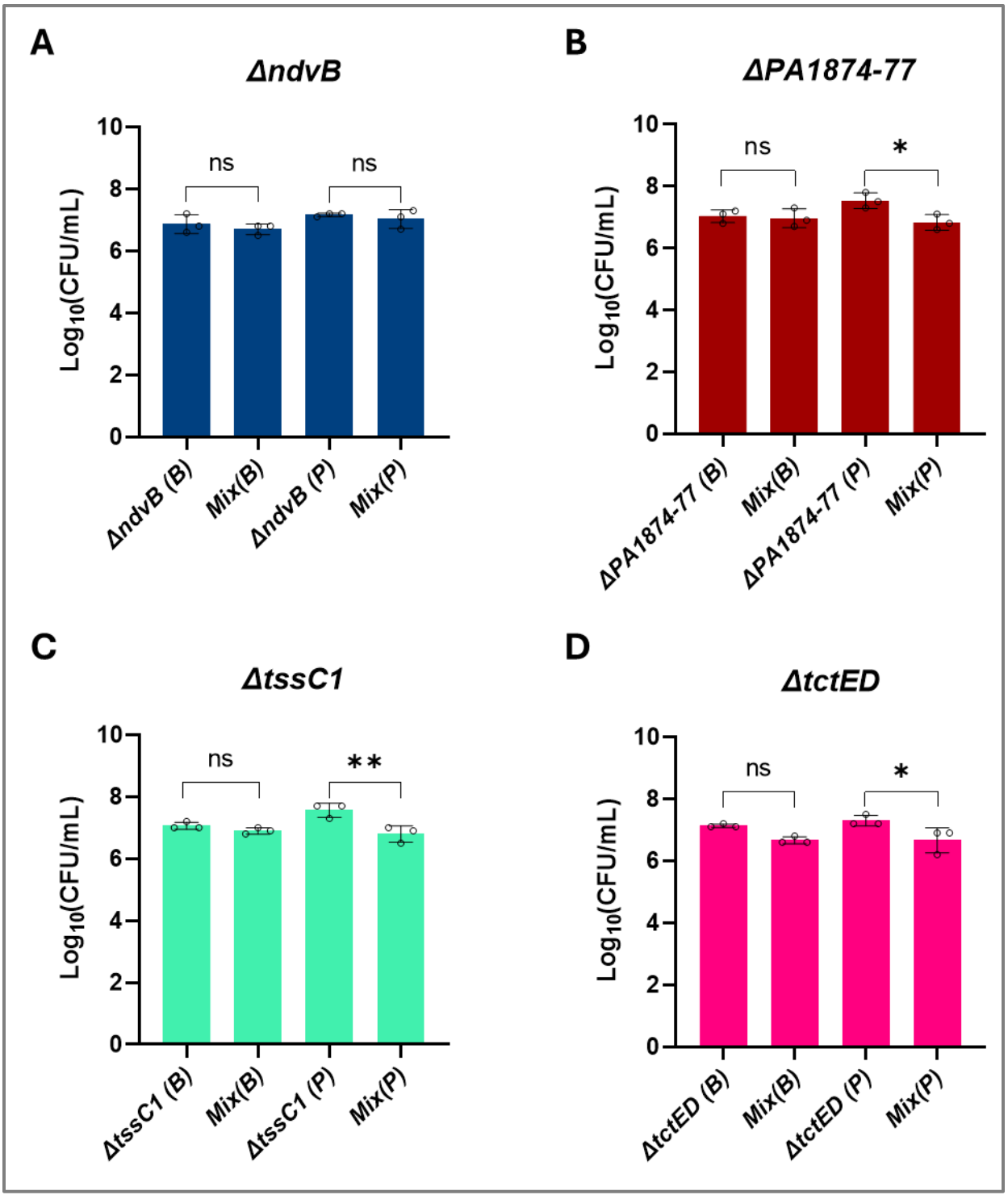

Figure 3.2: Colony forming units (CFU) counts of four *P. aeruginosa* mutant strains grown anaerobically as a monoculture and in a mixed culture (Mix) for biofilm (B) and planktonic (P) fractions. CFU of **(A)** Δ*ndvB* (blue bars), **(B)** Δ*PA1874-77* (red bars), **(C)** Δ*tssC1*(green bars), and **(D)** Δ*tctED* (pink bars)**.** The histogram represents the average of three biological replicates (n=3), and each data point represents the average of three

technical replicates. Statistical analysis was performed using ordinary one-way ANOVA and Tukey's multiple comparisons post-test with *$p<0.05$, **$p < 0.01$ and ns = non-significant. Error bars represent SD.

3.4.1.3. *P. aeruginosa* mutant strains Δ*PA1759-60* and Δ*flgK* are stably maintained in a CF polymicrobial assay

The second group of *P. aeruginosa* mutants assessed included Δ*PA1759-60* and Δ*flgK*. While *PA1759-60* are predicted to encode transcription regulators implicated in antibiotic resistance, Δ*flgK* mutants are flagellar-deficient and commonly found in CF. To evaluate the persistence of both Δ*PA1759-60* and Δ*flgK* mutants in a CF polymicrobial context, I once again performed a CFU assay as described in **Section 3.3.2**. The results are presented in **Figure 3.3**.

The CFU counts of biofilm and planktonic populations of Δ*PA1759-60* were not statistically different regardless of culture setting (mono vs. mixed), as observed in **Figure 3.3A**, purple bars. Although the Δ*flgK* biofilm populations exhibited comparable CFU counts in both mono- and mixed-cultures (**Figure 3.3B**, first two blue bars), a modest reduction (about 1 log) in planktonic populations was noted in the mixed culture when compared to the monocultures **(Figure 3.3B**, last two blue bars**)**. Overall, the ability of Δ*PA1759-60* to persist was not hindered in the polymicrobial assay. This observation also held for Δ*flgK* when the bacteria were cultured as a biofilm. By contrast, planktonic cultures of Δ*flgK* experienced a slight but significant reduction in CFU in the mixed community.

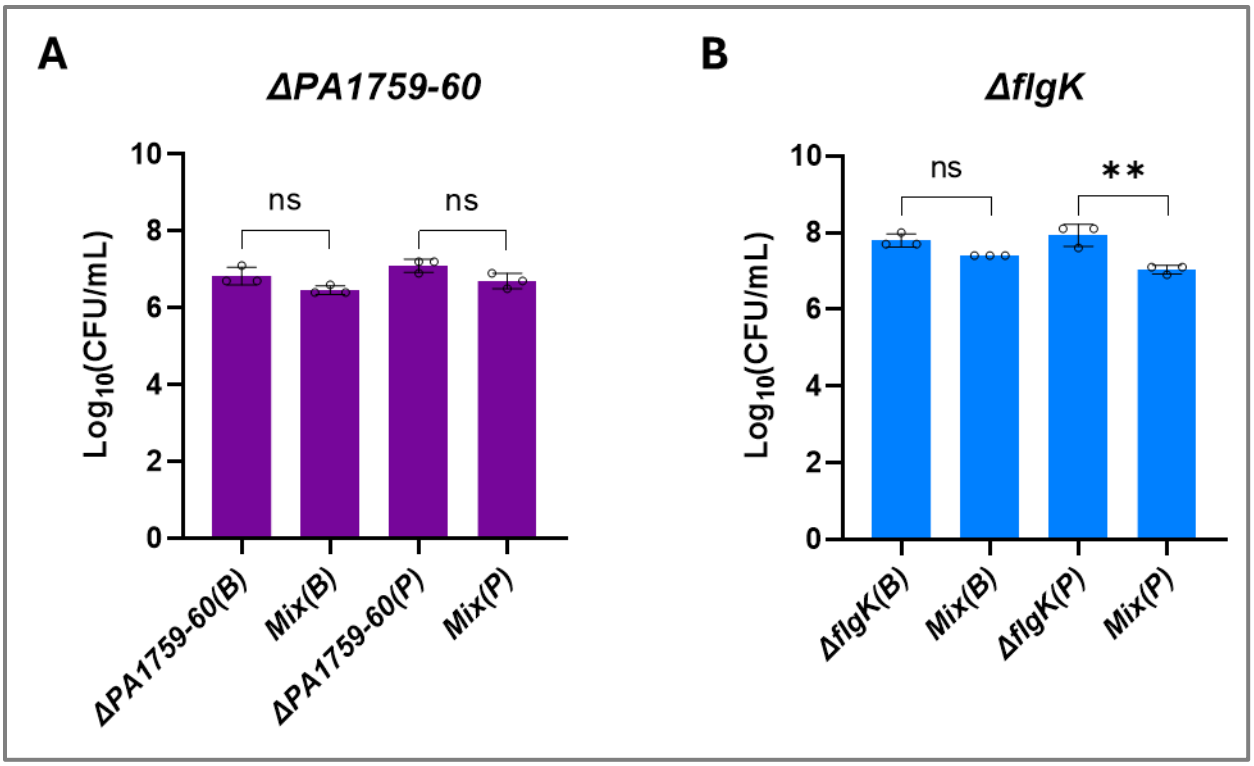

Figure 3.3: Colony forming units (CFU) counts of two *P. aeruginosa* mutant strains grown anaerobically as a monoculture and in a mixed culture (Mix) for biofilm (B) and planktonic (P) fractions. CFU of **(A)** Δ*PA1759-60* and **(B)** Δ*flgK*. The histogram represents the average of three biological replicates (n=3), and each data point represents the average of three technical replicates. Statistical analysis was performed using ordinary one-way ANOVA and Tukey's multiple comparisons post-test with $**p < 0.01$ and ns = non-significant. Error bars represent SD.

In conclusion, only Δ*ndvB* and Δ*PA1759-60* unequivocally persisted in the mixed community, suggesting that *ndvB* and *PA1759-60* are unlikely to play critical roles in the ability of *P. aeruginosa* to persist in this specific environment. The other mutants persisted only in biofilm conditions with reduced planktonic populations in the mixed community, highlighting the context-specific role of these genes. These results offer insights into the differing genetic needs for survival in a microbial context like CF. These findings establish a basis for future studies on the molecular mechanisms of community persistence.

3.4.2. Minimal bactericidal concentration assay

All the PA14 deletion mutant strains studied in this chapter have been linked to biofilm antibiotic resistance. For instance, *ndvB* encodes a glucosyltransferase essential for the synthesis of cyclic-β-(1,3)-glucans, which in turn prevents tobramycin from reaching the ribosome, by sequestering it in the bacterial periplasm [40, 90]. *PA1874-77* is a four-gene operon that codes for an ABC (ATP-binding cassette) multidrug efflux pump associated with aminoglycoside resistance in biofilms [40, 78, 90]. While the molecular mechanisms governing the antibiotic resistance characteristics related to the other genetic loci, namely *tssC1, tctED, PA1759-60,* and *flgK*, remain elusive, studies probing those genes have reported or implied increased biofilm antibiotic susceptibility when those genes were deleted [77, 78, 298, 299].

Tobramycin is an antibiotic routinely prescribed for treating infections in CF [188]. It was also one of the antibiotics previously used to characterise these deletion mutants under monoculture aerobic conditions. Therefore, tobramycin was the antibiotic of choice to assess the susceptibility of these mutants in a CF polymicrobial context. I started with the classic minimal bactericidal concentration (MBC) assay [300] with a few modifications. This was to evaluate the MBC values for all the *P. aeruginosa* strains in anaerobic ASM+ compared to the previous values reported in aerobic studies [40, 77, 78, 90]. The results revealed that, except for Δ*PA1874-77* and Δ*tctED*, with an MBC of 125 μg/mL, the WT and the other four mutant strains obtained an MBC value of 62.5 μg/mL **(Table 3.5)**. Therefore, these data indicate that, under anaerobic conditions in ASM+, the MBC of the mutants is comparable to that of the WT, which contrasts with previously reported data obtained under aerobic conditions.

Table 3.5: Minimal Bactericidal Concentration (MBC) values for the different PA14 strains following 24 h of tobramycin (TOB) treatment in ASM+ media under anaerobic conditions (n = 3).

PA 14 strains	MBC TOB (µg/ml)
WT	62.5
Δ*ndvB*	62.5
Δ*PA1874-77*	125
Δ*tssC1*	62.5
Δ*tctED*	125
Δ*PA1759-60*	62.5
Δ*flgK*	62.5

3.4.3. Susceptibility of different *P. aeruginosa* strains to tobramycin in a CF polymicrobial assay

As outlined in the previous section, the *P. aeruginosa* strains examined to this point have been associated with antibiotic resistance. However, none of the reports about the antibiotic susceptibility of these strains have encompassed the complexity of a mixed community in an anaerobic environment, which is characteristic of typical CF lung infections. I began by demonstrating in **Section 3.4.1** that all these strains can persist in the CF polymicrobial assay **(Figures 3.1 – 3)**. Next, based on the MBC values calculated in **Table 3.5** and clinically relevant concentration of tobramycin used in CF infections [301, 302], I aimed to evaluate the susceptibility responses of the *P. aeruginosa* strains in the CF polymicrobial assay. To achieve this goal, each *P. aeruginosa* strain was challenged with tobramycin at 50 µg/mL and 100 µg/mL in a CF polymicrobial assay, and their response profiles were analyzed.

3.4.3.1. PA14 WT susceptibility to tobramycin is unaltered in the CF polymicrobial assay

The data for PA14 WT are presented in **Figure 3.4**. In the presence of tobramycin, a reduction of CFU was observed in biofilm and planktonic populations. The reduction was greater in planktonic cultures compared to biofilms, as previously reported [39, 90, 303]. The presence or absence of other bacteria did not affect the antibiotic susceptibility of PA14 WT, as the same results were observed in both mono- and mixed-culture conditions.

Additionally, there was no significant difference between tobramycin at 50 or 100 µg/mL in biofilm cells, highlighting the ability of the bacteria to tolerate both concentrations of the antibiotic equally. As expected, at a concentration of 100 µg/mL, tobramycin completely eradicated planktonic cells, demonstrating substantial susceptibility compared to biofilm cells.

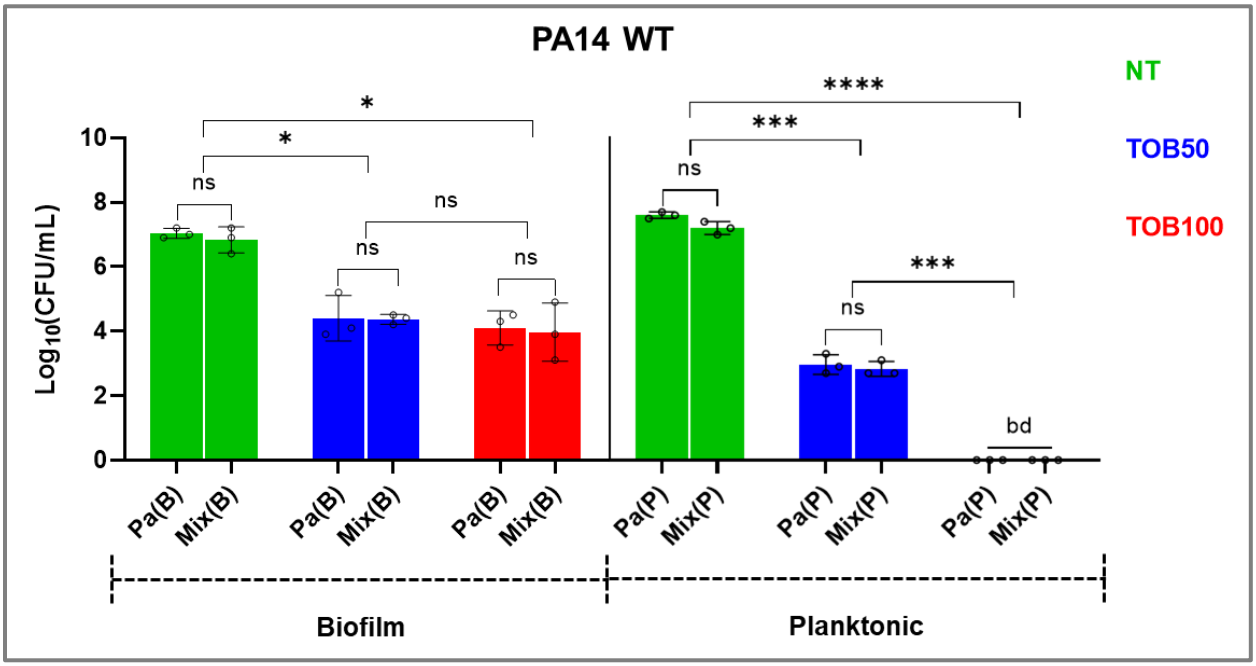

Figure 3.4: PA14 WT responses to tobramycin when grown anaerobically in a monoculture and in a mixed culture (Mix) for biofilm (B) and planktonic (P) fractions. Colony forming units (CFU) of the non-treated sample (NT, green bars); sample treated with 50 µg/mL of tobramycin (TOB50, blue bars) and sample treated with 100 µg/mL of tobramycin (TOB100, red bars). The histogram represents the average of three biological replicates (n=3), and each data point represents the average of three technical replicates. Statistical analysis was performed using ordinary two-way ANOVA and Tukey's multiple comparisons post-test with *$p<0.05$, ***$p < 0.001$, ****$p < 0.0001$, ns = non-significant and bd = below detection. Error bars represent SD. Pa = *Pseudomonas aeruginosa* str. PA14 WT.

3.4.3.2. *P. aeruginosa* mutant strains Δ*ndvB*, Δ*1874-77*, Δ*tssC1* and Δ*tctED* are differentially susceptible to tobramycin in the CF polymicrobial assay

In the presence of tobramycin, the mutant Δ*ndvB* exhibited a similar pattern to that of PA14 WT for biofilm cells but was noticeably different for planktonic cells, where it was more

susceptible than the wild type cells **(Figure 3.5)**. Indeed, at tobramycin 50 µg/mL, Δ*ndvB* planktonic cells in the mixed culture were not detectable as opposed to their monoculture counterpart. This reveals Δ*ndvB* heightened susceptibility to tobramycin, particularly for planktonic cells in a mixed-species environment. With tobramycin 100 µg/mL, both the wild type **(Figure 3.4)** and Δ*nvdB* planktonic cells yielded no detectable counts, which was indicative of the increased killing at that tobramycin concentration.

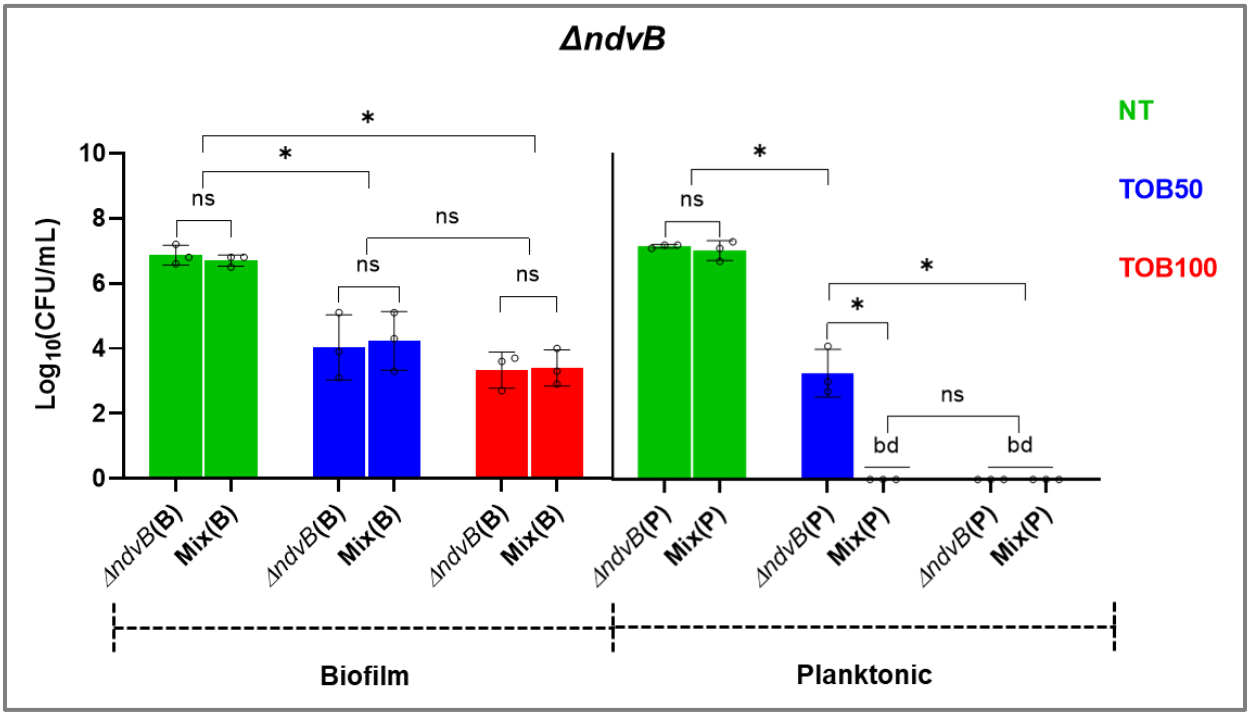

Figure 3.5: Δ*ndvB* responses to tobramycin when grown anaerobically in a monoculture and in a mixed culture (Mix) for biofilm (B) and planktonic (P) fractions. Colony forming units (CFU) of the non-treated sample (NT, green bars); sample treated with 50 µg/mL of tobramycin (TOB50, blue bars) and sample treated with 100 µg/mL of tobramycin (TOB100, red bars). The histogram represents the average of three biological replicates (n=3), and each data point represents the average of three technical replicates. Statistical analysis was performed using ordinary two-way ANOVA and Tukey's multiple comparisons post-test with *$p<0.05$, ns = non-significant and bd = below detection. Error bars represent SD.

For Δ*PA1874-77*, the tobramycin response was comparable to that of PA14 WT and Δ*ndvB,* specifically concerning biofilm cells. However, a striking susceptibility was observed for Δ*PA1874-77* planktonic cells, where there were no detectable counts at 50 and 100

μg/mL of tobramycin **(Figure 3.6)**. In line with PA14 WT and Δ*ndvB, ΔPA1874-77* showed a decrease in CFU when tobramycin was present, but with the complete eradication of its planktonic cells, demonstrating their higher sensitivity. The polymicrobial context did not affect its susceptibility.

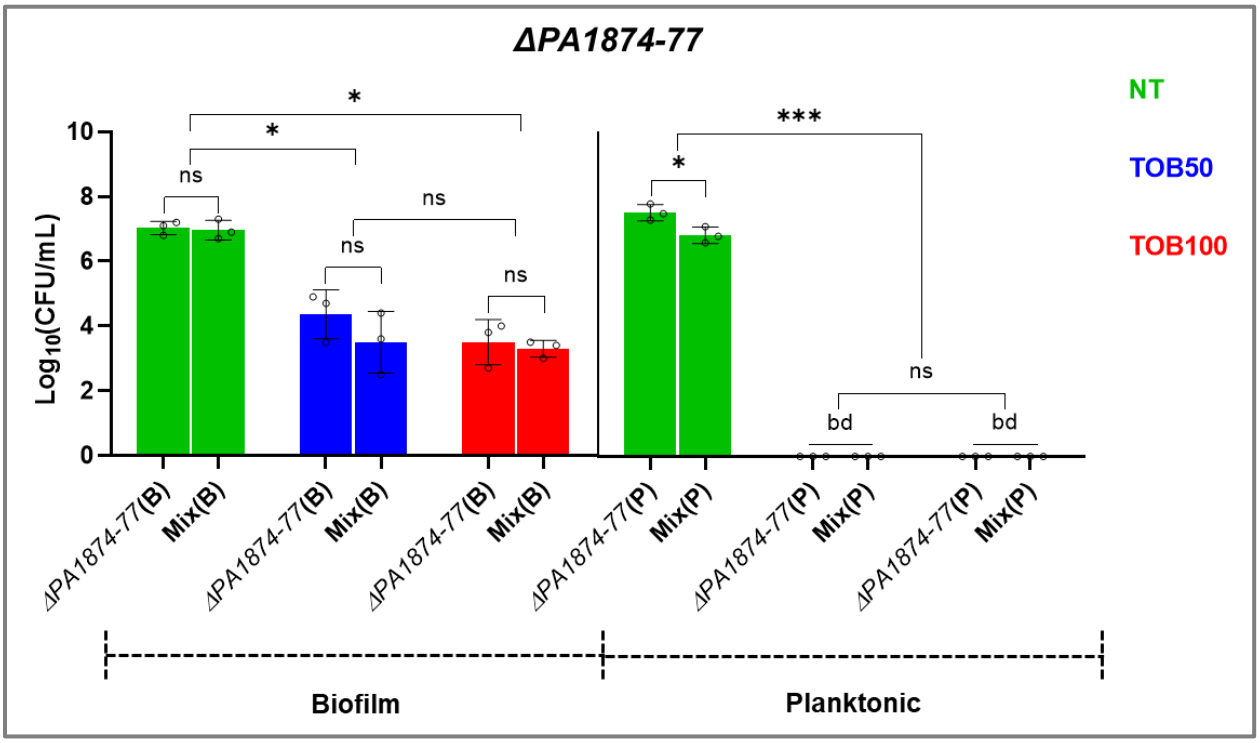

Figure 3.6: Δ*PA1874-77* responses to tobramycin when grown anaerobically in a monoculture and in a mixed culture (Mix) for biofilm (B) and planktonic (P) fractions. Colony forming units (CFU) of the non-treated sample (NT, green bars); sample treated with 50 μg/mL of tobramycin (TOB50, blue bars) and sample treated with 100 μg/mL of tobramycin (TOB100, red bars). The histogram represents the average of three biological replicates (n=3), and each data point represents the average of three technical replicates. Statistical analysis was performed using ordinary two-way ANOVA and Tukey's multiple comparisons post-test with *$p<0.05$, ***$p < 0.001$, ns = non-significant and bd = below detection. Error bars represent SD.

The response of the Δ*tssC1* deletion mutant to tobramycin was similar to that of PA14 WT. There was an increased susceptibility to tobramycin at 50 μg/mL, with an even greater susceptibility observed at the highest concentration of 100 μg/mL, where complete

eradication of planktonic cells was achieved **(Figure 3.7).** Furthermore, the polymicrobial context did not appear to affect the observed outcomes.

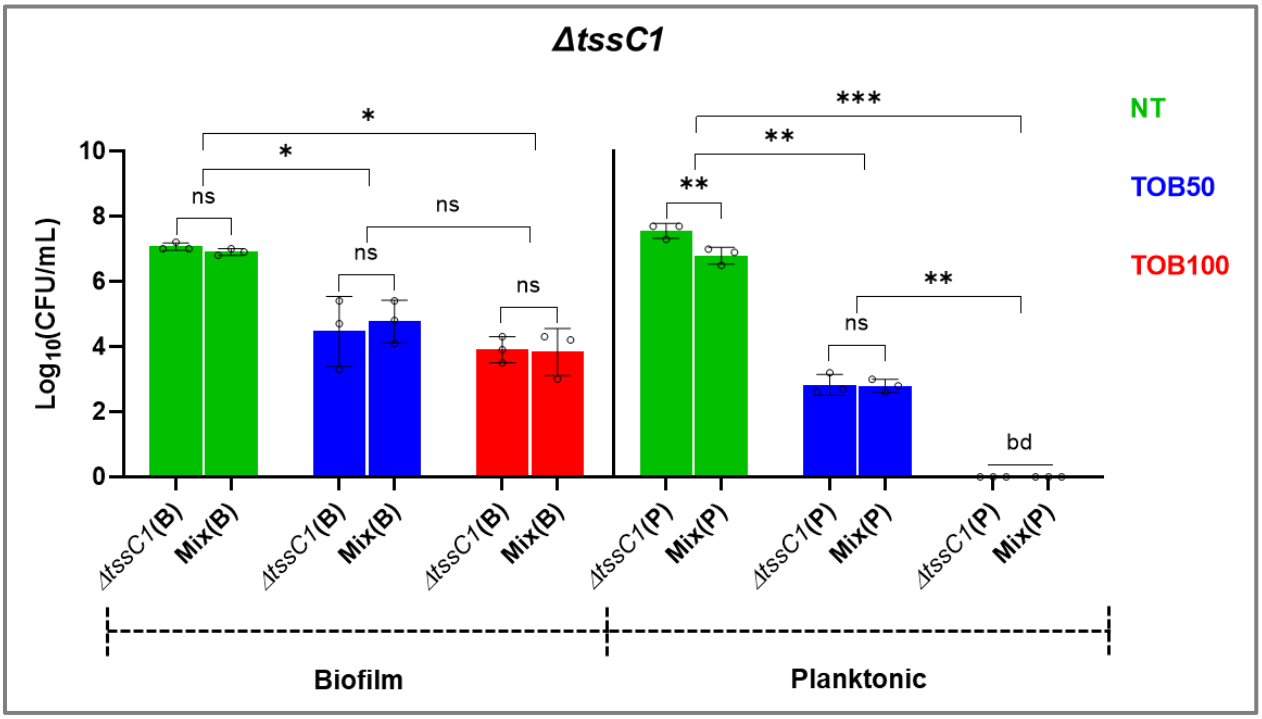

Figure 3.7: Δ*tssC1* responses to tobramycin when grown anaerobically in a monoculture and in a mixed culture (Mix) for biofilm (B) and planktonic (P) fractions. Colony forming units (CFU) of the non-treated sample (NT, green bars); sample treated with 50 µg/mL of tobramycin (TOB50, blue bars) and sample treated with 100 µg/mL of tobramycin (TOB100, red bars). The histogram represents the average of three biological replicates (n=3), and each data point represents the average of three technical replicates. Statistical analysis was performed using ordinary two-way ANOVA and Tukey's multiple comparisons post-test with *$p<0.05$, **$p < 0.01$, ***$p < 0.001$, ns = non-significant and bd = below detection. Error bars represent SD.

The Δ*tctED* mutant exhibited the most divergent results compared to the wild type strain. Interestingly, there were no detectable viable counts for Δ*tctED* biofilm cells in either a mono- or mixed-culture in the presence of 100 µg/mL of tobramycin **(Figure 3.8)**, which contrasted with the counts noted with the wild type. This observation extended to planktonic cells that all vanished in the presence of tobramycin at 50 or 100 µg/mL **(Figure 3.8)**. The Δ*tctED* mutant demonstrated the greatest susceptibility to tobramycin treatment, and the

polymicrobial environment did not influence this result. Moreover, the difference in biofilm susceptibility at 100 µg/mL tobramycin between Δ*tctED* and PA14 WT was statistically significant **(Supplementary Figure S3.1)**. A similar trend was observed for the other mutant tested **(Supplementary Figure S3.1)**, further confirming Δ*tctED* as the most susceptible strain among those examined.

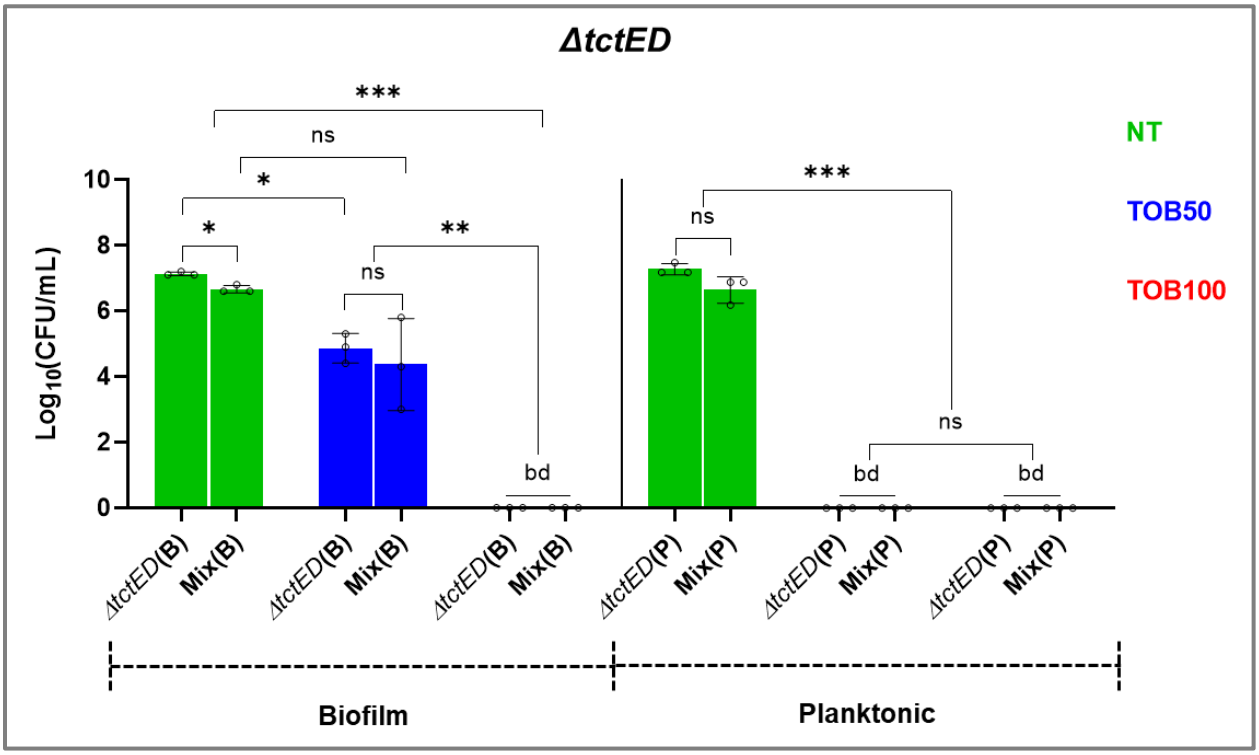

Figure 3.8: Δ*tctED* responses to tobramycin when grown anaerobically in a monoculture and in a mixed culture (Mix) for biofilm (B) and planktonic (P) fractions. Colony forming units (CFU) of the non-treated sample (NT, green bars); sample treated with 50 µg/mL of tobramycin (TOB50, blue bars) and sample treated with 100 µg/mL of tobramycin (TOB100, red bars). The histogram represents the average of three biological replicates (n=3), and each data point represents the average of three technical replicates. Statistical analysis was performed using ordinary two-way ANOVA and Tukey's multiple comparisons post-test with *$p<0.05$, **$p < 0.01$, ***$p < 0.001$, ns = non-significant and bd = below detection. Error bars represent SD.

3.4.3.3. *P. aeruginosa* mutant strains Δ*PA1759-60* and Δ*flgK* have different responses to tobramycin in the CF polymicrobial assay

The susceptibility responses to tobramycin of the Δ*PA1759-60* and Δ*flgK* were evaluated in the same polymicrobial context as the set of experiments described above. For Δ*PA1759-60*, the results showed a statistically significant decrease in viable cells in the presence of tobramycin for biofilm and planktonic populations **(Figure 3.9A)**. Moreover, while there was no difference between the CFU counts for tobramycin 50 and 100 µg/mL in biofilm cells, there was a substantial killing of planktonic cells precisely in the mixed cultures at 100 µg/mL **(Figure 3.9A)**. This indicates that at this concentration of tobramycin, Δ*PA1759-60* were considerably more susceptible within the mixed community. In comparison to the wild type, this strain exhibited the same susceptibility profile for biofilm cultures. However, for planktonic cells, tobramycin at 100 µg/mL was detrimental to the wild type in both mono- and mixed-cultures, with no CFU counts recorded. In contrast, *ΔPA1759-60* monocultures showed some tolerance, with a detectable number of CFU counts.

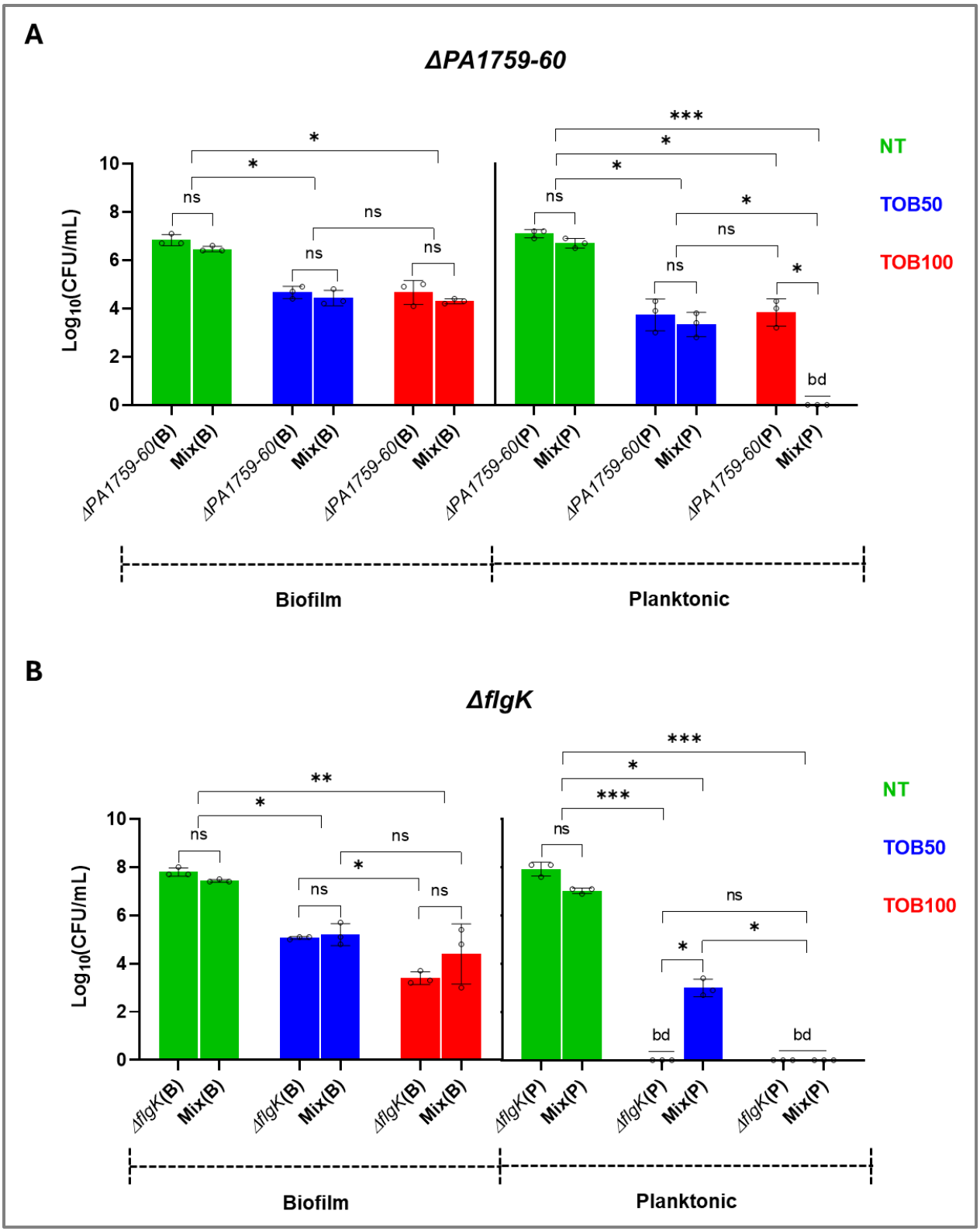

Figure 3.9: Δ*PA1759-60 and* Δ*flgK* responses to tobramycin when grown anaerobically in a monoculture and in a mixed culture (Mix) for biofilm (B) and planktonic (P) fractions.

Colony forming units (CFU) of **(A)** Δ*PA1759-60* and **(B)** Δ*flgK*. CFU of the non-treated sample (NT, green bars); sample treated with 50 μμμg/mL of tobramycin (TOB50, blue bars) and sample treated with 100 μg/mL of tobramycin (TOB100, red bars). The histogram represents the average of three biological replicates (n=3), and each data point represents the average of three technical replicates. Statistical analysis was performed using ordinary two-way ANOVA and Tukey's multiple comparisons post-test with *$p<0.05$, **$p < 0.01$, ***$p < 0.001$, ns = non-significant and bd = below detection. Error bars represent SD.

Lastly, Δ*flgK* biofilm cells showed increased susceptibility to tobramycin, as demonstrated by a decreased CFU count compared to tobramycin absence **(Figure 3.9B)**. This susceptibility was even more pronounced for planktonic cells, where no detectable counts were observed in the presence of tobramycin except for the mixed population at tobramycin 50 μg/mL (**Figure 3.9B**). This points to an advantage for planktonic Δ*flgK* cells to withstand the tobramycin treatment when other members of the community are present. This advantage, however, seems to vanish at a higher concentration of tobramycin. Compared to the wild type strain, Δ*flgK* exhibited similar responses to tobramycin when grown as a biofilm, although its planktonic cells showed slight differences from the wild type. Indeed, planktonic cells of both strains have identical responses when exposed to tobramycin 100 μg/mL. However, the wild type seemed to tolerate tobramycin 50 μg/mL better, as some counts were observed, whereas Δ*flgK* appeared more susceptible at that concentration of tobramycin, especially in the monocultures, as previously mentioned.

3.5. Discussion

In this chapter, I implemented the CF polymicrobial assay composed of *P. aeruginosa, S. aureus, S. sanguinis, and P. melaninogenica* developed by Jean-Pierre et al. [199] in order to 1) Reproduce and validate the model with PA14 WT strain, 2) Assess whether six *P. aeruginosa* mutant strains can persist in this multi-species setting under anaerobic conditions, and 3) Evaluate their susceptibility profiles at different tobramycin concentrations, within this same multi-species setting, under anaerobic conditions. While many studies have assessed the contribution of various genes to antibiotic resistance in *P.*

aeruginosa [40, 76–78, 89, 94, 304–306], this is the first study to determine the contribution of these genes to antibiotic resistance under conditions that more closely mimic those encountered *in vivo* in CF infections.

PA14 WT is stably maintained in a CF polymicrobial assay

The initial assessment with PA14 WT in the CF polymicrobial assay, composed of *S. aureus, S. sanguinis*, and *P. melaninogenica,* showed a successful reproduction of the model described by Jean-Pierre et al. [199] with minor differences in CFU counts that will be discussed below. PA14 WT CFU counts exhibited the same trend and identical statistics as reported in the original article, confirming the validity of this implementation for this strain **(Figure 3.1)**.

The CFU counts for *S. aureus* and *S. sanguinis* were relatively similar to those in the original article, though there was a slight difference in biofilm populations. Indeed, for *S. aureus,* I reported a small but statistically significant ~ 0.5 log reduction between mono- and mixed species while the original report showed no differences **(Figure 3.1)**. On the contrary, for *S. sanguinis*, I found no differences between mono- and mixed-species, while the original report showed a small but statistically significant ~ 0.5 log reduction between the two settings **(Figure 3.1)**.

These differences could stem from the inherent variability of the bacterial CFU assay. Indeed, this assay is performed with manual colony counting. Inconsistent colony identification from high cell densities causes colony overlap, complicating enumeration, while low cell densities result in sampling errors (e.g., uneven distribution of bacteria in the cell suspension and inaccurate sample volume). Furthermore, inconsistent dilution techniques and pipetting errors also add to the variability in bacterial counts. Numerous studies have highlighted these drawbacks and limitations, and various solutions have emerged to address the variability, such as automating the CFU counting through image acquisition and analysis [307–309]. Unfortunately, none of these solutions were utilized here due to time, financial, and expertise limitations. Despite the differences noted between my data and the original report for *S. sanguinis* and *S. aureus*, they remain modest. With the

focus on *P. aeruginosa*, these differences were acknowledged but not intensively investigated.

Lastly, the most considerable discrepancy was observed with *P. melaninogenica*. While I obtained a similar number of CFU for planktonic and biofilm in the mixed cultures, as reported in the original study, I also counted some colonies in the monocultures **(Figure 3.1)**. However, this last observation conflicted with other studies that highlighted the inability of *P. melaninogenica* to grow as a monoculture in ASM with or without mucin [199, 310, 311]. I decided to investigate the possible reasons behind this discrepancy between my data and published reports.

I started by ruling out the possibility of contamination of the *P. melaninogenica* culture stock at -80°C. To this end, I inoculated colonies of *P. melaninogenica* in anaerobic ASM without mucin. Indeed, given that 2X ASM and 2X mucin solutions were prepared and stored independently before being freshly combined on the day of the experiment to produce the ASM+ culture media, it was deemed appropriate to investigate each solution separately. After 48 h of incubation, there was no visible growth in the ASM culture tube. Next, I focused on the mucin stock used to prepare ASM+ media. Mucin is a complex glycoprotein with varying glycosylation patterns across sources [312]. Hypothetically, although *P. melaninogenica* is not typically regarded as a mucin degrader, it may produce glycoside hydrolases or other enzymes that enable it to break down specific mucin components, such as sialic acids, N-acetylglucosamine or fucose [312, 313]. Therefore, the differences in mucin composition from various sources could potentially support the growth of *P. melaninogenica* as a monoculture. Testing different mucin stocks from various providers would have been insightful to verify this hypothesis. However, due to time constraints, I did not perform such a comparative analysis. I also considered the possibility of a batch effect in different ASM+ preparations. My reasoning was that since ASM+ contains approximately 20 ingredients, any imbalance in preparation, especially with mucin, could potentially trigger the growth of this bacterium as a monoculture. Nonetheless, all my ASM+ batches resulted in the growth of *P. melaninogenica* in monoculture.

These investigations on the growth of *P. melaninogenica* monoculture in ASM with mucin lead me to conclude that the problem could be the mucin sterilization technique. The sterilization process likely requires re-evaluation and improvement because autoclaving alone may not be as effective. Acknowledging this setback and limitation, I chose to move forward with the experiments, prioritizing the emphasis on *P. aeruginosa* in this study. This decision hinged on the requirement that the growth levels or CFU counts for other species, along with the growth of *P. melaninogenica* in the mixed culture, aligned with published reports.

P. aeruginosa mutant strains in the CF polymicrobial assay and their susceptibility responses to tobramycin

In biofilms, similar levels of CFU counts for all six *P. aeruginosa* deletion mutant strains (Δ*ndvB,* Δ*PA1874-77,* Δ*tssC1,* Δ*tctED,* Δ*PA1759-60 and* Δ*flgK*) were recorded in mono- versus mixed-culture **(Figures 3.2 and 3.3)**. A modest decrease of ~ 0.5 log in the mixed- compared to the mono-culture was recorded for all these strains in the planktonic growth, except for Δ*ndvB* and Δ*PA1759-60*, which showed no reduction **(Figures 3.2 and 3.3)**. Of note, outside of their increased antibiotic sensitivity in biofilm, the mutants Δ*ndvB,* Δ*PA1874-77,* Δ*tssC1* and Δ*tctED* were characterized as behaving identically to the wild type strain [40, 76–78, 89]. These observations are also echoed here in the CF polymicrobial assay. In summary, all six deletion mutants persisted in the CF polymicrobial assay, despite the genetic loss of function incurred by each strain.

The minimal bactericidal concentration (MBC) of tobramycin, calculated for PA14 WT and the six PA14 deletion mutant strains, under anaerobic conditions, revealed that Δ*PA1874-77* and Δ*tctED* had the highest values at 125 µg/mL **(Table 3.5)**. In comparison, the other five mutants had a value of 62.5 µg/mL. The tobramycin MBC value of 62.5 µg/mL observed for PA14 WT aligns with previous findings [199]; however, the one-fold difference across species is insufficient to define a distinct phenotype for any mutant.

Upon treatment with tobramycin 50 and 100 µg/mL, PA14 WT and the six PA14 deletion mutants showed increased susceptibility in the CF polymicrobial assay **(Figures 3.4 – 3.9)**.

Except for Δ*ndvB* and Δ*flgK* planktonic cells, the polymicrobial context does not seem to drive the overall susceptibility responses observed.

Aside from the Δ*tctED* mutant, biofilm cultures of Δ*ndvB*, Δ*PA1874-77,* and Δ*tssC1* exhibited the same susceptibility profile as PA14 WT. It is worth remembering that the genetic loci *ndvB*, *PA1874-77*, and *tssC1* are predominantly expressed in biofilms and have previously been associated with biofilm-specific antibiotic resistance in PA14 WT in mono-species studies using M63 minimal media in an aerobic environment [76–78, 91]. In other words, Δ*ndvB*, Δ*PA1874-77* and Δ*tssC1* showed increased susceptibility to tobramycin compared to PA14 WT only when cultivated as biofilms in aerobic M63 media. These observations were not verified here in the CF polymicrobial assay, which was performed in anaerobic ASM+, which contains mucin. Previous reports indicate that components of the biofilm matrix, such as mucin and extracellular DNA, can bind to tobramycin [98]. This binding reduces the antibiotic's bioavailability, thereby diminishing its effectiveness in killing bacteria [98]. Since ASM+ contains both DNA and mucin, this may explain why tobramycin susceptibility reported in M63 media for Δ*ndvB*, Δ*PA1874-77,* and Δ*tssC1* biofilms was not observed in the CF polymicrobial context assay.

Beyond the composition of the culture media, the oxygen level in the incubation atmosphere, the size of the inoculum and the experimental technique (such as dilution) are known to impact antibiotic susceptibility to varying degrees [314–317]. Therefore, the discrepancy between my findings and previous reports could potentially be explained by differences in culture conditions, which may influence gene expression, impact biofilm formation, and affect the response to tobramycin.

Regarding the gene expression, to my knowledge, no studies have reported the level of expression of *ndvB*, *PA1874-77*, and *tssC1* under anaerobic conditions compared to aerobic conditions. However, alongside the slower bacterial metabolism under anaerobic conditions, numerous studies have highlighted a notable variation in gene expression and regulation that occurs when oxygen levels are low or absent, affecting bacteria broadly and particularly *P. aeruginosa* [6, 318, 318–322]. This begs the questions, are those genes even

expressed under anaerobic conditions? What about their regulation? Indeed, if they are not expressed under anaerobic conditions in the PA14 WT strain, it is unsurprising to observe that the deletion of those genes makes no difference when it comes to antibiotic susceptibility. The same conclusion could be drawn for the deletion mutants Δ*PA1759-60* and Δ*flgK*, which biofilm cultures also have the same phenotype as PA14 WT in response to tobramycin treatment. In light of these observations, several assays, including transcriptomic analysis, RT-qPCR, reporter gene assays and fluorescent protein tagging, among others, could help assess the expression level of these different genes in the experimental conditions outlined here and answer the aforementioned questions.

Another factor affecting the transferability of the susceptibility responses reported for aerobic studies to the results reported in this study is that the oxygen level vastly influences the quality of biofilm formed during incubation and the length of the incubation. Indeed, under anaerobic conditions, the growth is considerably slower with reduced metabolic rates [84, 323]. Arguably, due to this slow growth in a short 24 to 48 h time frame, biofilms formed anaerobically may be less robust and more susceptible to antibiotic treatment compared to aerobic biofilms. In contrast, an extended incubation time results in more robust biofilms under anaerobic conditions due to the production of viscous exopolysaccharides such as alginates [56, 243, 244]. Moreover, other factors like the composition of the culture media or incubation surface could significantly influence the nature or robustness of the biofilm formed. In the specific context of the CF microbial assay, I demonstrate in the next chapter **(Chapter 4)** that biofilms formed in anaerobic ASM+ versus aerobic M63 minimal media are structurally different.

A Focus on the Δ*tctED* Mutant

Among all the mutants, biofilm culture of Δ*tctED* exhibited a heightened 4-fold susceptibility to tobramycin 100 µg/mL compared to the PA14 WT **(Figures 3.4 and 3.8)**. Furthermore, I performed a statistical analysis to substantiate that this difference is significant, not only for PA14 WT but also for all the other mutants in this study **(Supplementary Figure S3.1)**. Previous work from the Mah laboratory conducted under

aerobic conditions in M63 minimal media demonstrated that the deletion mutant Δ*tctED* was also 4-fold more susceptible to tobramycin compared to PA14 WT when cultivated as a biofilm [78]. In other words, despite the difference in culture conditions (aerobic vs. anaerobic, M63 vs. ASM+ media), this mutant consistently proved more susceptible to tobramycin than the wild type strain. These observations reinforce the finding that *tctED* is an antibiotic resistance gene in a wide array of environmental conditions.

The *tctED* operon encodes a two-component system consisting of TctE as the histidine sensor kinase and TctD as the corresponding response regulator, both of which are essential for the uptake of tricarboxylic acid (TCA) in *P. aeruginosa* [89]. The *tctED* system senses and responds to TCA cycle intermediates, such as citrate, which is an important metabolite and preferred carbon source for *P. aeruginosa* [324–327]. In addition, *P. aeruginosa* also secretes citrate [327, 328]. However, previous work in our laboratory found that in the presence of exogenous citric acid (conjugate acid of citrate), Δ*tctED* formed poor biofilms and exhibited an increased susceptibility to tobramycin [89]. Therefore, to justify the increased tobramycin sensitivity of Δ*tctED* noted in my experiments, I speculate that although both PA14 WT and Δ*tctED* can secrete citrate, only the wild type strain can also uptake it as a part of its regulation of extracellular citrate/citric acid.

In contrast, Δ*tctED*, because of its inability to sense or uptake citric acid, would end up with an accumulation of that molecule extracellularly. In this context, the addition of tobramycin would lead to heightened accumulation of tobramycin in the biofilm matrix of the Δ*tctED* mutant, resulting in increased killing, as previously reported [89]. To test this hypothesis, I could start by confirming that both PA14 WT and Δ*tctED* secrete citrate but differ in citrate uptake, and that Δ*tctED* accumulates extracellular citrate due to defective uptake. Mould and colleagues performed a similar experiment [327]. Next, I could show that tobramycin treatment results in greater accumulation in the Δ*tctED* biofilm matrix and enhanced killing, as performed in our laboratory [89].

In the broader context of antibiotic resistance involving adaptive mechanisms, a study published by Bielecki et al. demonstrated that TctED participates in crosstalk with another

two-component system called PhoBR [329]. This system responds to phosphate limitation, with PhoR as the sensor kinase and PhoB as the response regulator. Bielecki et al. demonstrated a crosstalk between TctD and PhoB, which amplifies citrate uptake when phosphate is scarce, allowing *P. aeruginosa* to integrate citrate and phosphate signals. Although the precise molecular mechanism remains underexplored, this regulatory interplay enhances metabolic flexibility in nutrient-limited environments like CF. In my experiments using a CF polymicrobial assay that approximates the conditions *in vivo*, it would be interesting to evaluate the responses of Δ*tctED* in varying conditions of phosphate concentrations and the presence of tobramycin. The goal would be to decipher how phosphate and citrate concurrently affect the tobramycin susceptibility of this mutant in a CF model of infection.

Limits and Future Directions

The tobramycin susceptibility profiles of the *P. aeruginosa* strains reported here in the CF polymicrobial assay are unique and cannot be directly comparable to those reported in previous studies [40, 76–78]. This divergence can be attributed to differences in experimental parameters, including media composition (ASM+ versus M63) and oxygen availability (aerobic versus anaerobic), both of which influence gene expression, biofilm architecture, and antimicrobial responses. Given the physiological relevance of the CF polymicrobial assay to the CF lung environment, it is plausible that the mutant-specific responses to tobramycin reported here may reflect *in vivo* behaviour. Nonetheless, while this model provides a robust framework for studying polymicrobial interactions in a CF-like context, its limitations cannot be overlooked.

I mentioned earlier that the incubation duration of 24 to 48 h may be problematic and does not ensure that mature and robust biofilms are formed under anaerobic conditions. Extending the incubation period over multiple days may offer a more representative model of the chronic infection dynamics, which is characteristic of the CF lung environment, thereby yielding more physiologically relevant data. The nature of the biofilm in the assay appears to consist more of floating BLS than solely surface-attached aggregates. This means

that refreshing the culture media daily by discarding the spent supernatant eliminates a sizeable portion of those BLS. Therefore, the experiment should be adapted and tailored for BLS studies because, as currently performed, it is more suited for surface-attached biofilms. One way to achieve this is to promote the adhesion of those BLS to the surface by coating or priming the bottom of the well with mucin before adding the bacterial suspension in ASM. Indeed, growing biofilm cells tend to attach more easily to a mucin layer at the bottom rather than floating residues in the liquid medium. Landry and colleagues developed such a model of mucin-coated surfaces and showed that specific adhesin–mucin interaction blocked surface motility, resulting in a highly structured, heterogeneous biofilm that had increased tolerance to tobramycin in *P. aeruginosa* [98]. Hence, by uniformizing the experimental model, it would be objectively more accurate to delineate particular phenotypes associated with specific strains.

Lastly, CF infections are notoriously polymicrobial in nature and although Jean-Pierre et al. provided solid evidence of restricting their CF model to four species [199], multiple strains or subpopulations of the same species with various pheno- and genotypic traits can colonize the CF lung at the same time [330–335]. However, the assay as presently constructed does not allow the simultaneous study of strains from the same species. One way to address this for *P. aeruginosa,* is to use the fluorescent reporter tools described in **Chapter 2** of this thesis. Indeed, using fluorescent reporters that are compatible with one another to mark different strains from the same species in the assay would allow the assessment of individual strains and how they co-evolve. This way, the readout would be fluorescence rather than CFU.

In this discussion, I have focused mainly on the biofilm cultures because they are the bottleneck of CF infections and are much more challenging to eradicate. However, the CF polymicrobial assay yielded notable differences in tobramycin susceptibility with regard to the planktonic cultures of the various *P. aeruginosa* strains **(Figures 3.4 – 3.9)**. In those planktonic cultures, for example, the polymicrobial context seemed to have a greater influence on the tobramycin responses on strains like Δ*ndvB* and Δ*flgK*, which might be of interest and could be explored further. While there may be multiple reasons for these

differences in this specific experimental setup, one possibility is that, unlike in biofilm cultures, these genes could be more actively expressed in planktonic cultures, which could then explain the observations noted here.

3.6. Conclusions

In summary, my initial hypothesis stated that *P. aeruginosa* deletion mutants would not be able to persist in a mixed-species environment because the loss of specific genes may impair their competitive fitness against other species. However, this hypothesis was unverified. Indeed, to some degree, all the mutants persisted in the CF polymicrobial assay. Their responses to tobramycin treatment for biofilm cells were equivalent to those of the wild type, with the exception of Δ*tctED*, which was more susceptible. Conversely, their responses to tobramycin for planktonic cells are more divergent from those of the wild type, with different tolerance levels noted, especially at a subinhibitory concentration of the antibiotic. While this study highlighted different responses to the antibiotic tobramycin of several *P. aeruginosa* strain, in a context relevant to their pathogenic *in vivo* mechanisms, these responses were evaluated in a relatively short time span, where the bacteria were exposed to the antibiotic for only 24 h. To emulate chronic levels of infection and understand, for instance, adaptability, a more extended timeframe of 3 days to weeks could be explored. Tweaking the delivery of mucin by coating the surface of the well could yield a more homogeneous and uniform biofilm that could be used to probe antibiotic susceptibility response.

In addition, all the genes studied are severely lacking information about their expression or regulation under anaerobic or polymicrobial conditions and no molecular mechanisms were examined. Gene expression assays could help fill some of these knowledge gaps. Furthermore, the responses of the three other bacterial species were not investigated. Indeed, it is possible that upon tobramycin treatment, a seemingly minor observation on a *P. aeruginosa* mutant represented a substantial shift in antibiotic susceptibility for a different species. Lastly, the co-incubation of two or more *P. aeruginosa* strains could not be assessed using this CF polymicrobial assay because the readout using CFU on selective media could

not differentiate between strains of the same species. Shifting to a readout based on fluorescence rather than CFU could help mitigate this limitation.

Notwithstanding these limitations, the CF polymicrobial assay provides valuable insights into *P. aeruginosa* responses to antibiotics in a context relevant to its pathogenicity. This enhances our understanding of potential target genes such as *tctED*, and more broadly, marks a significant step forward in the fight against antibiotic resistance.

3.7. Supplementary materials

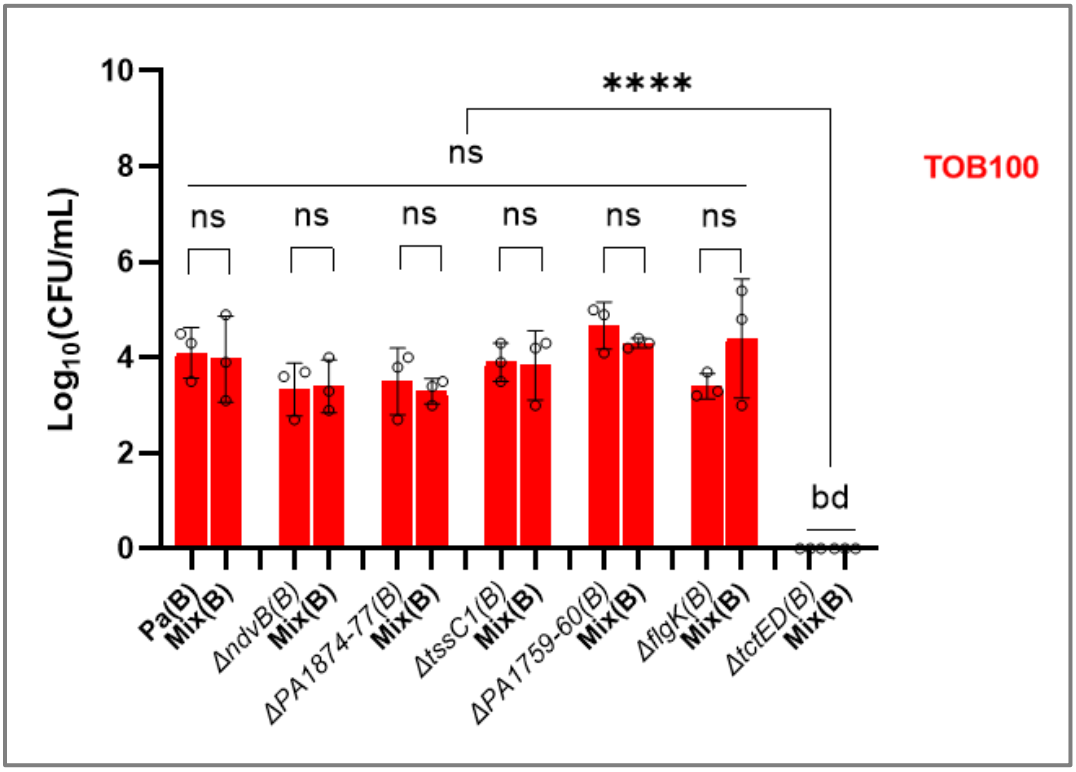

Figure S3.1: Comparison of tobramycin susceptibility of Δ*tctED* relative to PA14 WT (Pa) and the other mutant strains in a monoculture and a mixed culture (Mix) for biofilm cultures (B). The graph summarizes the CFU results of **Figures 3.4 – 3.9** for 100 µg/mL of tobramycin (TOB100). Statistical analysis was performed using ordinary one-way ANOVA and Tukey's multiple comparisons post-test with ****$p < 0.0001$, ns = non-significant and bd = below detection. Error bars represent SD.

Chapter 4: Spatial distribution of *P. aeruginosa* biofilms in mono- and mixed-cultures

4.1. Preface

All experiments and analyses presented in this chapter were performed by me, except where otherwise noted. I put together all the figures and designed all the experiments, including those involving plasmid construction, stabilization assay, and flow cytometry. These specific experiments were carried out by Olivier Chagnon-St-Amour, an undergraduate student whom I trained and directly supervised. Under my guidance, Olivier constructed the plasmids, conducted the plate reader-based stabilization assay, and collected the flow cytometry data. I ensured the experimental design was implemented correctly and maintained rigorous oversight of data quality. I am also grateful to France Manigat, who taught me how to analyze flow cytometry data, a skill I applied throughout this study.

4.2. Introduction

In **Chapter 2**, several plasmids were built for the purpose of labelling and imaging *P. aeruginosa* under anaerobic conditions. The plasmids were maintained in the bacteria by antibiotic selection (ampicillin and carbenicillin). However, for these tools to be amenable to a multi-species system, ensuring the plasmids are stably maintained without any antibiotic selection is essential. One method for maintaining plasmids in bacteria without using antibiotics is through toxin-antitoxin (TA) systems. A TA system consists of two genes in an operon, where one encodes a stable toxin and the other produces its labile antitoxin to ensure a specific equilibrium of the two within the bacterial cell [185, 336]. Beyond plasmid stabilization, TA systems play crucial roles in bacterial physiology, adaptation to environmental stresses, and virulence [162]. Regarding plasmid maintenance, there is a selective pressure for a bacterium to keep the plasmid encoding the TA. Indeed, in plasmid-free cells, the antitoxin is rapidly degraded due to its instability, resulting in the killing of the cell by the toxin—a phenomenon called post-segregational killing [164, 185, 337].

Among TA systems, I have selected three with reported evidence of plasmid stability in Gram-negative bacteria: CcdAB, VapBC and PumAB. The CcdAB system is based on the *E. coli* F-

plasmid and is known to be involved in plasmid maintenance [165]. VapBC is a TA system found in *S. flexneri,* which is vital in maintaining its virulence plasmid [177, 178]. A report on the TA system PumAB has demonstrated its ability to stabilize the plasmid pUM505 of *P. aeruginosa* in *E. coli* [180]. A key advantage of employing a *P. aeruginosa* reporter strain that doesn't depend on antibiotic selection is its versatility across different settings, including multi-species environments, to analyze its biofilm spatial distribution.

Investigating the spatial distribution of biofilms is important, as the organization of cells within these communities directly impacts their exposure to antimicrobial agents and nutrient availability, thereby shaping both treatment efficacy and bacterial behaviour [237–239]—an aspect that forms a central focus of my research. For instance, cells in deeper biofilm layers often experience hypoxia, reducing their metabolic activity and making them less susceptible to antibiotics [51]. The spatial structure of biofilms also shields inner bacterial populations from immune responses. For example, the extracellular polymeric matrix and outer cell layers act as physical barriers, limiting penetration by immune cells like neutrophils and reducing phagocytosis [82]. Furthermore, the spatial arrangement of cells within biofilms affects quorum sensing. Indeed, high-density regions within biofilms could enhance quorum-sensing signals, which may lead to increased virulence [338]. Altogether, these studies underscore that understanding how cells are spatially distributed within a biofilm is essential for managing biofilm-related infections like CF.

The objectives in this chapter are twofold: 1) Construct a plasmid that can be stably maintained in *P. aeruginosa* without antibiotic selection, and 2) Use this plasmid to transform *P. aeruginosa* into a reporter strain for studying its biofilm spatial distribution in the CF polymicrobial assay using microscopy. The spatial distribution in this instance entails the characterization of both the number and size of biofilm aggregates in mono- compared to mixed-species communities. It also encompasses the analysis of potential clustering patterns in the presence of other bacterial species—for instance, whether *P. aeruginosa* biofilms are uniformly distributed or exhibit spatial segregation. The findings in this chapter aim to characterize *P. aeruginosa* biofilms in the CF polymicrobial assay and to contrast the distribution of *P. aeruginosa* biofilm in mono- versus mixed-species communities. A long-

term goal is to provide spatially informed therapeutic strategies essential for the treatment of CF.

4.3. Materials and Methods

4.3.1. Construction of plasmids

The plasmids harbouring the TA systems (VapBC, CcdAB and PumAB) were constructed using the same methodology described in **Chapter 2 — Section 2.4.1**. Briefly, the expression vector pCFT4.2 encoding the fluorescent protein phiLOV2.1 [144] was used to clone each of the TA systems downstream of the ampicillin gene and using the *arcA* transcription terminator **(Figure 4.2)**. The *vapBC* and *ccdAB* genes were directly amplified from the virulence plasmid pINV of *Shigella flexneri* M90T by PCR with the high-fidelity Phusion DNA polymerase (ThermoFisher). The *pumAB* genes were synthesized (Integrated DNA Technologies, IA). The amplified *vapBC* and *ccdAB* genes and the synthetic *pumAB* were cloned into the pCFT4.2 vector using the NEB Gibson assembly master mix (NEB, #E2611). Sanger sequencing (Génome Québec) confirmed the cloned fragments in each plasmid. **Table 4.1** and **Supplementary Table S4.1** list the plasmids and primers used in this study, respectively.

4.3.2. Bacterial strains and Growth conditions

For plasmid construction, the strains and growth conditions are identical to **Chapter 2 — Section 2.4.2**, except that only planktonic cultures were assayed. Briefly, *E. coli* strain DH10B was used for plasmid propagation, and PA14 WT was used in the fluorescence experiments. The culture medium was LB supplemented with ampicillin (100 µg/mL) or carbenicillin (100 or 200 µg/mL) for DH10B and PA14 transformants, respectively. All incubations were performed at 37°C in a shaker incubator set at 250 rpm in an aerobic atmosphere.

All the assays requiring anaerobic incubation were performed at 37°C in a BactronEZ chamber (Sheldon Manufacturing, Inc., Cornelius, OR) under an anaerobic atmosphere of 5% H_2, 5% CO_2, 90% N_2 that contained fewer than 4.7 parts per million O_2 per the

manufacturer's specifications. The bacterial strains for each assay and specific culture conditions are listed in their respective sections.

4.3.3. Plasmid stability assays

4.3.3.1. Fluorescence plate reader assay

PA14 harbouring each of the plasmids encoding the TA systems (VapBC, CcdAB and PumAB) was grown aerobically at 37ºC with shaking (250 rpm), and the cultures were subsequently subcultured in LB ± carbenicillin 100 µg/mL every 24 h to an OD600 of 0.3. The fluorescence was recorded over five days on a Hybrid Synergy H4 Hybrid plate reader (BioTeK). The data were normalized according to the OD600 and correlated to the loss or maintenance of the plasmid in the absence of antibiotic selection. Controls were also assayed, including the expression vector pCFT4.2/phiLOV2.1 and an empty plasmid with no fluorescent protein (pUdO4a/EV). Three biological replicates were assessed.

4.3.3.2. Flow cytometry experiments

The PA14 cultures mentioned above that were used for the fluorescence plate reader assay were simultaneously used for the flow cytometry experiment, but only during the first three days of the experiment. Thus, for each of the three days of the experiments, the cell culture was diluted 1/4 in 1mL PBS. These dilutions were centrifuged at 2,500×g for 3 min and resuspended in 1mL PBS. This cell resuspension was washed three more times using 1mL PBS at the same centrifugation settings. The last resuspension was further diluted to 1/50 in 1mL PBS in flow cytometer tubes. The fluorescence intensities of the samples were measured with a Gallios Flow cytometer (Beckman Coulter): BFP, excitation: 405nm, emission:450±40nm; and analyzed with the software KALUZA (v.2.1). Graphs were prepared with GraphPad Prism 8 (GraphPad Software, La Jolla, CA).

4.3.4. PA14 carrying pCFT4.2.1 in the CF polymicrobial assay

Since the goal of stabilizing the plasmid pCFT4.2.1 in PA14 in the absence of antibiotic selection was to use it in the CF polymicrobial assay, I performed a colony forming units (CFU) assay as described in the previous chapter **(Chapter 3 – Section 3.3.2)**. In brief, PA14 harbouring pCFT4.2.1/phiLOV2.1+VapBC was cultivated in a 96-well plate as a mono- and

mixed-culture along with *S. aureus, S. sanguinis* and *P. melaninogenica* in the artificial sputum media containing 5 mg/mL of mucin (ASM+) designed to mimic a CF-like environment [293, 294]. The plate was then incubated anaerobically at 37°C, with each sample assayed in triplicate. The following day, the culture media were refreshed, and the incubation continued for another 24 h under the same conditions.

At the end of the incubation, the planktonic and biofilm fractions were separately collected, 10-fold serially diluted and plated on solid agar media selective for each bacterial species **(**see **Chapter 3 - Table 3.2)**. The respective agar plates were incubated under their optimal conditions to allow the formation of colonies. Finally, colony counting was conducted, and the CFU/mL was determined for each bacterial strain. At least three biological replicates were performed. The results were tabulated and plotted, and statistical analyses were computed with GraphPad Prism 8 (GraphPad Software, La Jolla, CA). Data are presented as mean ± standard deviation, with a 95% confidence level ($p < 0.05$).

4.3.5. Biofilm biomass quantification with the Crystal Violet staining assay

Biofilm biomass was characterized using a crystal violet assay [97, 339, 340]. The different *P. aeruginosa* strains previously introduced in **Chapter 3**, namely PA14 WT, Δ*ndvB*, Δ*PA1874-77*, Δ*tssC1*, Δ*tctED*, Δ*PA1759-60*, Δ*flgK* and PA14/pCFT4.2, were incubated at 37°C in either ASM+ media under aerobic conditions or ASM+ media and M63 minimal media supplemented with 1 mM $MgSO_4$, 0.4% L-arginine and 100 mM KNO_3 (M63N) under anaerobic conditions. The cells were incubated for 24 h in a 96-well microtiter plate, and the culture media were refreshed the following day. The incubation was pursued for another 24 h.

After a total of 48 h of incubation time, all the unattached cells were removed, and the plate was washed three times with distilled water. The adherent cells, which represent the biofilm cells, were stained with a 0.1 % crystal violet solution for 15 minutes. The excess crystal violet was subsequently removed and washed away with water three times. At this step, only the bound dye remained on the plate. After air-drying the plate for at least 16 h, pictures of the plate were taken, and the crystal violet was resolubilized with acetic acid

30%. The absorbance at 595 nm was then recorded and correlated with the biofilm biomass. Graphs were prepared with GraphPad Prism 8 (GraphPad Software, La Jolla, CA).

4.3.6. Live fluorescence imaging by microscopy

4.3.6.1. Microscopy aerobic

PA14 WT carrying no plasmid was used as a negative control. PA14 WT and PA14/pCFT4.2.1 were grown overnight in 5 mL LB and LB supplemented with 100 µg/mL carbenicillin, respectively. This incubation was performed at 37°C with shaking (250 rpm) under aerobic conditions. The following day, 500 µL of bacterial culture was centrifuged (2400×g; 10min). The M63N media was used to wash and resuspend the pellet to maintain cell viability during imaging. The dye SynaptoRed C2 (FM 4-64, Biotium, Fremont, CA) was used as a membrane probe. The pellets were washed once in M63N and resuspended in 1mL M63N ± 10 µM SynaptoRed C2. The samples were then put back in the incubator at 37°C for another 15 min to allow the dye to penetrate the cell membrane.

Afterwards, 200 µL of each cell suspension were loaded in a 35 mm glass-bottom dish (Cellvis, #D35-20-1.5H). To immobilize the cells during fluorescence imaging, the cell suspensions were each covered with a 2% agarose pad. The glass-bottom dish was then covered with a 35 mm glass-top cover (Cellvis, #D35-20-0-TOP) for differential interference contrast (DIC) imaging. Micrographs were acquired on a Zeiss LSM 880 AxioObserverZ1 confocal microscope equipped with an EC Plan-Neofluar 100×/1.3 oil M27 objective. Fluorescence was captured using the argon laser at 458 nm for phiLOV2.1 [excitation: 458 nm; emission: 466–537 nm] and at 514 nm for SynaptoRed C2 [excitation: 514 nm; emission: 591–722 nm]. All micrographs were collected with the ZEN software (Zeiss) and prepared with Zen Blue (Zeiss).

4.3.6.2. Microscopy anaerobic

4.3.6.2.1. Mono-Dual-Tri-Tetra biofilm imaging

After imaging PA14/pCFT4.2.1 in a simpler optimal system, the next step was to image anaerobic monocultures and gradually increase the complexity by incubating co-cultures of 2, 3 and 4 species. Biofilm monocultures of PA14/pCFT4.2.1 were prepared as in the CF

polymicrobial assay with a few modifications. Instead of a 96-well plate, 2 mL of the inoculum at an OD600 of 0.01 in ASM+ media was loaded into a 35 mm glass-bottom dish (Cellvis, #D35-20-1.5H) and incubated anaerobically for 24 h at 37°C. The media was then refreshed, and the incubation was pursued for another 24 h. Following the 48 h incubation, the spent supernatant was discarded and the plate was washed once with 1mL PBS. A volume of 200 µL of ASM without mucin (ASM) was added on top of the attached cells to preserve viability during imaging. Subsequently, a 2% agarose pad was layered on top of the cells, and the plate was covered with a 35 mm glass-top cover (Cellvis, #D35-20-0-TOP) for differential interference contrast (DIC) imaging, then processed for imaging using the same settings as in **Section 4.3.6.1.**

Because this initial imaging of PA14/pCFT4.2.1 revealed artifacts of residual mucin fluorescing at the same wavelength as phiLOV2.1, I made some alterations to the mucin preparation. Instead of the usual 10 mg/mL mucin stock, I prepared a 40 mg/mL solution that was centrifuged at 4900 rpm for 5 h at a 1 h interval to remove any solid residue. The clear supernatant was then collected, autoclaved, and used as a 2X mucin solution that was later combined with ASM to be used as culture medium. After a CFU count to verify that the relative counts of each bacterial species in the CF polymicrobial assay were not significantly affected by this change in mucin preparation, I proceeded by using this new formulation to culture bacteria for microscopy experiments.

Using this ASM media prepared with centrifuged mucin, I prepared monocultures of PA14/pCFT4.2.1 and equivalent ratios of dual cultures of PA14/pCFT4.2.1 and *S. aureus*, tri-cultures of the previous two species plus *S. sanguinis* and finally a tetra-culture of the last three species plus *P. melaninogenica*. The incubation and sample preparation were executed as mentioned at the beginning of this section. In addition, the dye SynaptoRed C2 at 10 µM was added to 200 µL of ASM and layered on top of the biofilm cells. The imaging setting was identical to the one in **Section 4.3.6.1**.

4.3.6.2.2. Anaerobic surface-attached biofilm in ASM+ media

Noticing another issue with PA14/pCFT4.2 and the ASM media prepared with centrifuged mucin—no biofilm in 48h and no fluorescence in mixed cultures—I reverted to the original/ regular mucin preparation in ASM+ media. To mitigate artifacts of mucin during imaging, special attention was paid to the washing step after the incubation. Two washes and delicate swirling and pipetting were performed to maximize the removal of sedimented mucin unattached to biofilm cells. The attached biofilm of PA14/pCFT4.2.1 monocultures and the four-species mixed-culture of PA14/pCFT4.2.1, *S. aureus*, *S. sanguinis* and *P. melaninogenica* were assayed. The sample preparation, processing, and imaging were performed as previously described, except Z-stacks across a depth of 4 µm were collected. All micrographs were collected with the ZEN software (Zeiss), and the volume and numbers of biofilm aggregates were calculated and collected using the ImageJ software [256]. These numbers, collected from three separate experiments, were plotted with GraphPad Prism 8 (GraphPad Software, La Jolla, CA).

4.3.6.2.3. Anaerobic Biofilm-like structure (BLS) in ASM+ media

Using ASM+ media and following the identical incubation and sample preparation protocol as in the first paragraph of **Section 4.3.6.2.1**, instead of discarding the supernatant after the incubation, I pipetted 100 µL and loaded it on a new 35 mm microscope dish. A 2% agarose pad was blanketed on top, and confocal imaging ensued at the setting previously listed.

To facilitate the comprehension of the methodology for anaerobic microscopy described in **Section 4.3.6.2**, a flowchart outlining all steps, troubleshooting, and final solution is presented below in **Figure 4.1**.

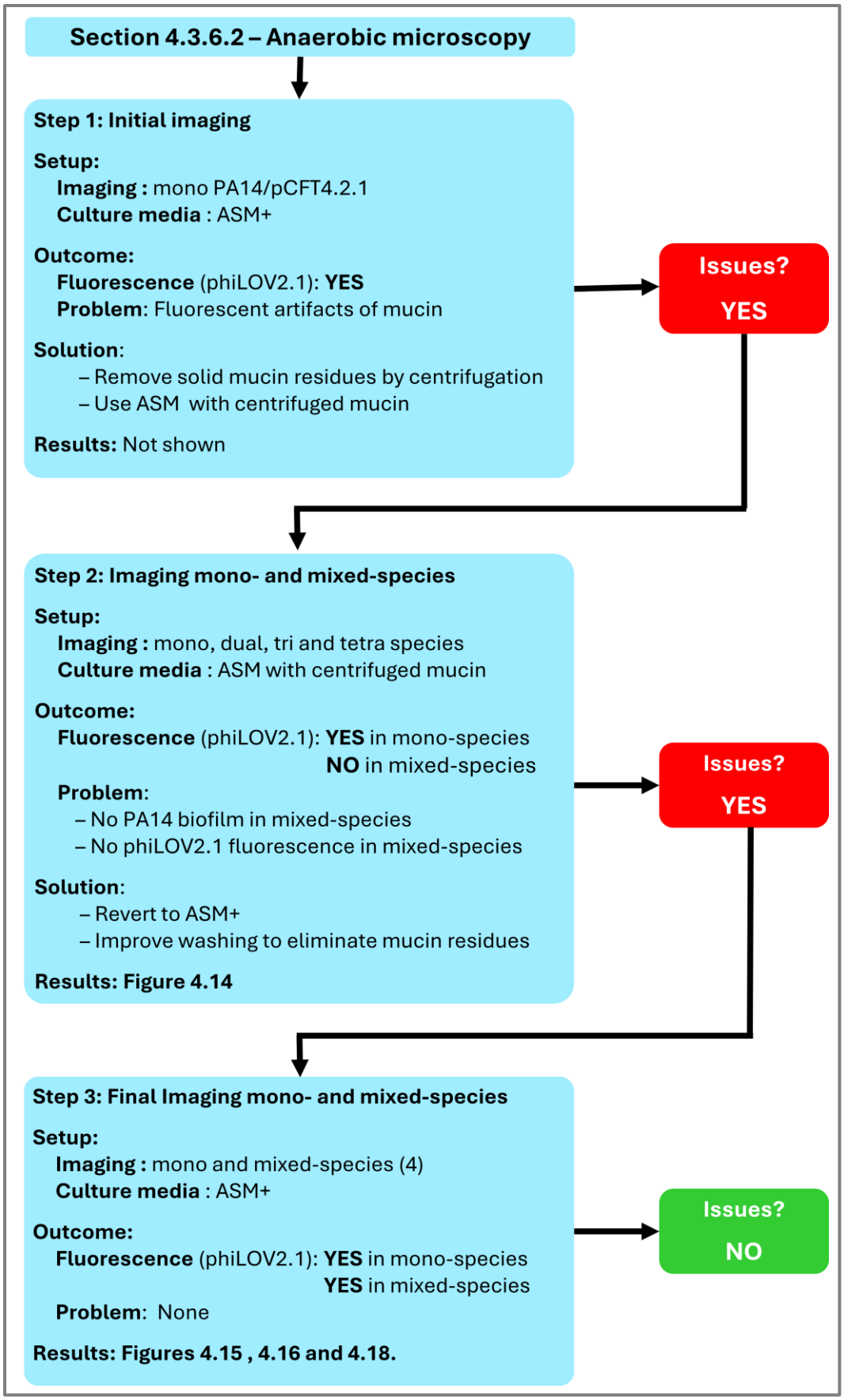
Section 4.3.6.2 – Anaerobic microscopy
Step 1: Initial imaging
Setup:
Imaging : mono PA14/pCFT4.2.1
Culture media : ASM+
Outcome:
Fluorescence (phiLOV2.1): YES
Problem: Fluorescent artifacts of mucin
Solution:
– Remove solid mucin residues by centrifugation
– Use ASM with centrifuged mucin
Results: Not shown
Issues?
YES
Step 2: Imaging mono- and mixed-species
Setup:
Imaging : mono, dual, tri and tetra species
Culture media : ASM with centrifuged mucin
Outcome:
Fluorescence (phiLOV2.1): YES in mono-species
NO in mixed-species
Problem:
– No PA14 biofilm in mixed-species
– No phiLOV2.1 fluorescence in mixed-species
Solution:
– Revert to ASM+
– Improve washing to eliminate mucin residues
Results: Figure 4.14
Issues?
YES
Step 3: Final Imaging mono- and mixed-species
Setup:
Imaging : mono and mixed-species (4)
Culture media : ASM+
Outcome:
Fluorescence (phiLOV2.1): YES in mono-species
YES in mixed-species
Problem: None
Results: Figures 4.15 , 4.16 and 4.18.
Issues?
NO

Figure 4.1: Flowchart summarizing the stepwise optimization of anaerobic microscopy using phiLOV2.1 fluorescence. Initial mono-species imaging in ASM+ revealed mucin-related artifacts, leading to the use of centrifuged mucin. Mixed-species imaging failed to show fluorescence and PA14 biofilm, prompting a return to ASM+ and improved washing steps. Final imaging in ASM+ yielded successful fluorescence without issues.

4.4. Results

4.4.1. Construction of plasmids carrying toxin-antitoxin (TA) systems

In order to use *P. aeruginosa* as a reporter strain in a CF polymicrobial assay, the anaerobic fluorescent reporter pCFT4.2 from **Chapter 2** was used to construct three plasmids carrying different toxin-antitoxin (TA) systems. The goal was to maintain the expression of the fluorescent protein phiLOV2.1 in the absence of antibiotic selection. The open reading frames of the TA systems VapBC, CcdAB and PumAB were selected and cloned into the vector pCFT4.2 to generate pCFT4.2.1, pCFT4.2.2 and pCFT4.2.3 **(Table 4.1** and **Figure 4.2)**. The plasmid map in **Figure 4.2** shows that the different TA systems were introduced downstream of the ampicillin coding sequence.

Table 4.1: Plasmids used and generated in this study

Plasmid name	Fluorescent protein	Toxin-Antitoxin	Antibiotic resistance	Reference
pUdO4a	Empty Vector (EV)	None	Ap, Cb	[250]
pCFT4.2	phiLOV2.1	None	Ap, Cb	[144]
pCFT4.2.1	phiLOV2.1	VapBC	Ap, Cb	This study
pCFT4.2.2	phiLOV2.1	CcdAB	Ap, Cb	This study
pCFT4.2.3	phiLOV2.1	PumAB	Ap, Cb	This study

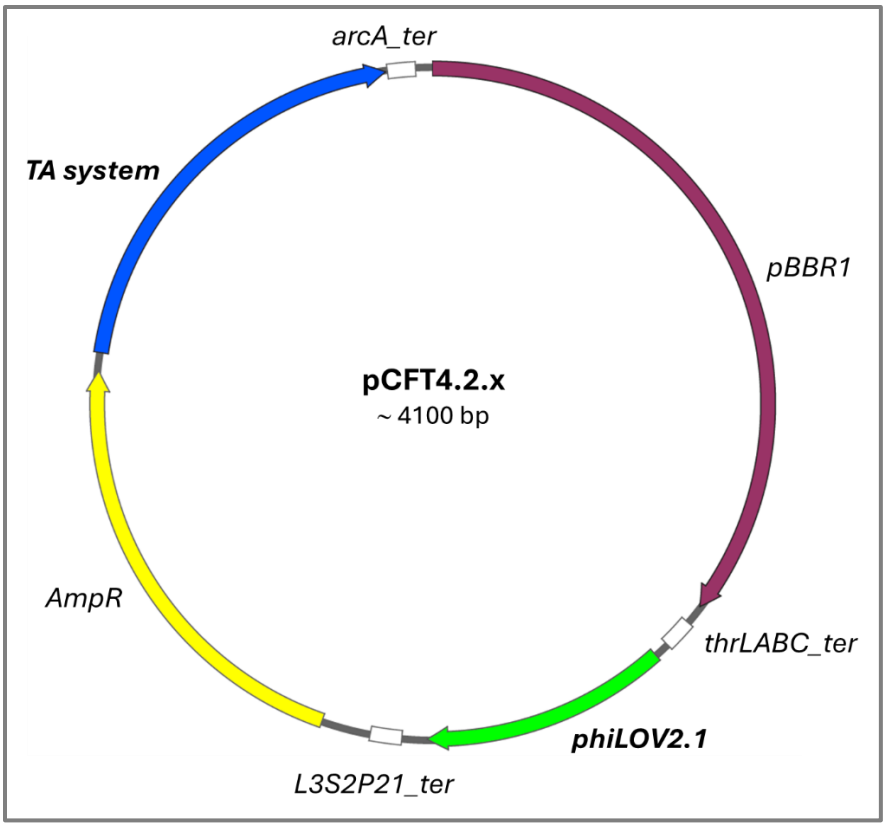

Figure 4.2: Plasmid map of pCFT4.2.x. pCFT4.2.x are derived from pCFT4.2, where different toxin-antitoxin (TA) systems – VapBC, CcdAB, and PumAB were introduced downstream of the *AmpR* coding sequence, yielding three distinct plasmids. *pBBR1* is the origin of replication. *thrLABC_ter, L3S2P21_ter,* and *arcA_ter* are the transcription terminators. The map is to scale, except for the TA systems, which vary slightly in length, and was created using SnapGene v.8.1.1.

4.4.2. Only pCFT4.2.1 is effectively stabilized in the absence of antibiotic selection

To assess whether, in the absence of antibiotic selection, the different TA systems (VapBC, CcdAB, and PumAB) stabilize the plasmids pCFT4.2.x in *P. aeruginosa* while expressing phiLOV2.1, a fluorescence assay with a plate reader was performed over five consecutive days using pCFT4.2/phiLOV2.1 as a negative control. The cultures were subcultured every 24 h to an OD600 of 0.3. The results showed that, in the presence of antibiotic selection, the fluorescence for all the strains was detectable and remained high and relatively constant over time **(Figure 4.3,** left panel**)**. By contrast, without the antibiotic,

the fluorescence declined abruptly for all strains and was abrogated by day 3, except for the strain carrying pCFT4.2.1 that harbours phiLOV2.1 and VapBC (**Figure 4.3,** right panel). This suggests that only the VapBC TA system effectively stabilized the plasmid in PA14 when there was no antibiotic selection.

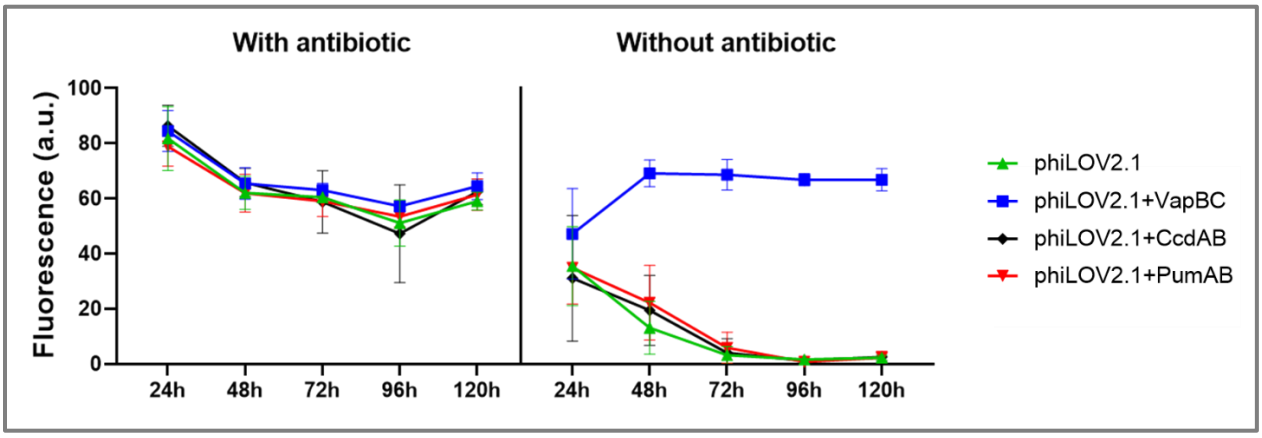

Figure 4.3: Fluorescence of *P. aeruginosa* PA14 expressing phiLOV2.1 with or without the toxin-antitoxin system VapBC (blue), CcdAB (black) and PumAB (red). The control strain (green) lacked a cloned toxin-antitoxin system. The cultures were grown aerobically with and without the antibiotic carbenicillin 100 µg/mL for five consecutive days, with daily subcultures to an OD600 of 0.3. The fluorescence was recorded every 24 h at 450 nm of excitation and 495±20 nm of emission. Error bars represent SD (n=3).

4.4.3. Over 90% of PA14 cells keep pCFT4.2.1 after 3 days without antibiotic selection

While the fluorescence assessment with the plate reader yielded the total fluorescence in the bacterial culture, it was also essential to evaluate quantitatively which percentage of PA14/pCFT4.2.1 cells was fluorescent versus which one was not, especially in the absence of antibiotics. For this experiment, flow cytometry was used to measure the percentage of cells that expressed fluorescence in the presence or absence of antibiotics. The empty vector pUdO4a (EV) with no fluorescence and no VapBC was used as a negative control for both parameters **(Figure 4.4)**. PA14/pCFT4.2 expressing phiLOV2.1 and no VapBC was used as a control for the proportion of fluorescent cells lost in the absence of VapBC and antibiotic selection.

The results show that in the absence of both VapBC and antibiotic selection, only 4% of the total bacterial population maintained their fluorescence, while 97% of cells still expressed phiLOV2.1 after 3 days in the presence of the antibiotic **(Figure 4.5)**. By contrast, when VapBC is present, 93% of cells expressed phiLOV2.1 even with no antibiotic in the media on day 3, compared to 98% in the presence of antibiotic **(Figure 4.6)**. This unequivocally indicates that not only does VapBC effectively stabilize the plasmid pCFT4.2.1, but also, a substantial 93% of the total cell population retains the plasmid and sustains phiLOV2.1 expression over at least 3 days. A summary graph of **Figures 4.4 – 6**, presented as **Figure 4.7**, explicitly substantiates those observations. It displays the percentage of fluorescent cells across all strains over three days, emphasizing VapBC as a highly effective plasmid stabilizer that does not require antibiotics for plasmid maintenance.

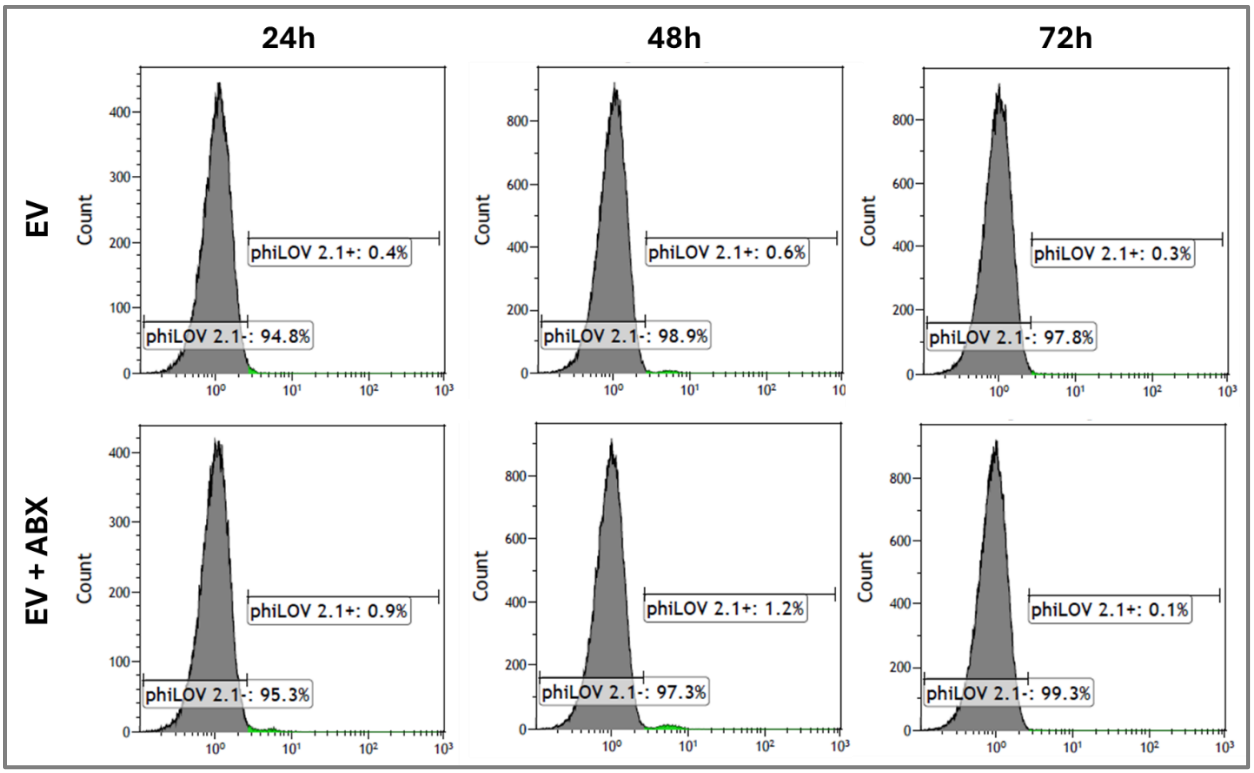

Figure 4.4: Flow cytometry analysis of *P. aeruginosa* PA14 carrying the pUdO4a empty vector (EV) used as a negative control. The graphs show the percentage of cells expressing (phiLOV2.1+; green) or not (phiLOV2.1-; gray) the fluorescent protein phiLOV2.1 at different times without (top) and with (bottom) the antibiotic carbenicillin (ABX). Cultures were grown aerobically for three consecutive days either with or without ABX. Fluorescence was

recorded every 24 h with a constant voltage at the excitation wavelength of 405 nm and the emission wavelength of 450±50nm.

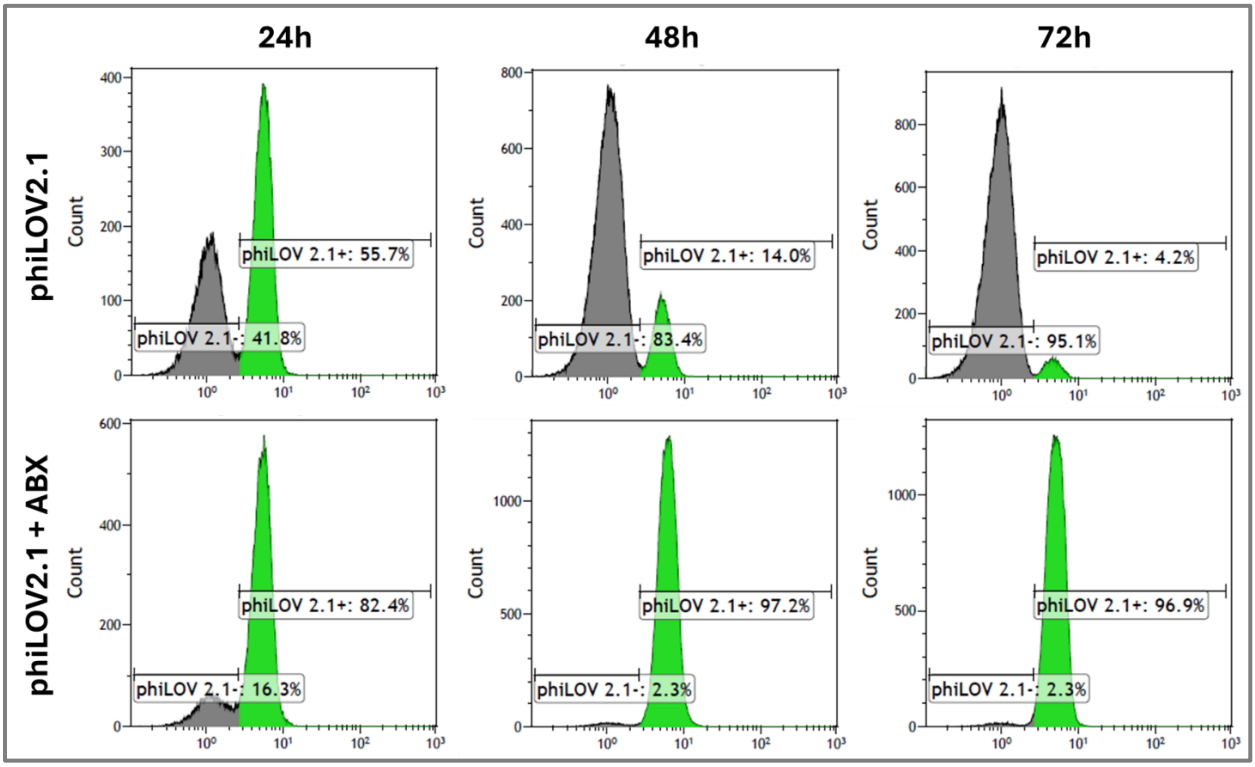

Figure 4.5: Flow cytometry analysis of *P. aeruginosa* PA14 carrying the pCFT4.2/phiLOV2.1. The graphs show the percentage of cells expressing (phiLOV2.1+, green) or not (phiLOV2.1-, grey) the fluorescent protein phiLOV2.1 at different times without (top) and with (bottom) the antibiotic carbenicillin (ABX). Cultures were grown aerobically for three consecutive days either with or without ABX. Fluorescence was recorded every 24 h with a constant voltage at the excitation wavelength of 405 nm and the emission wavelength of 450±50 nm.

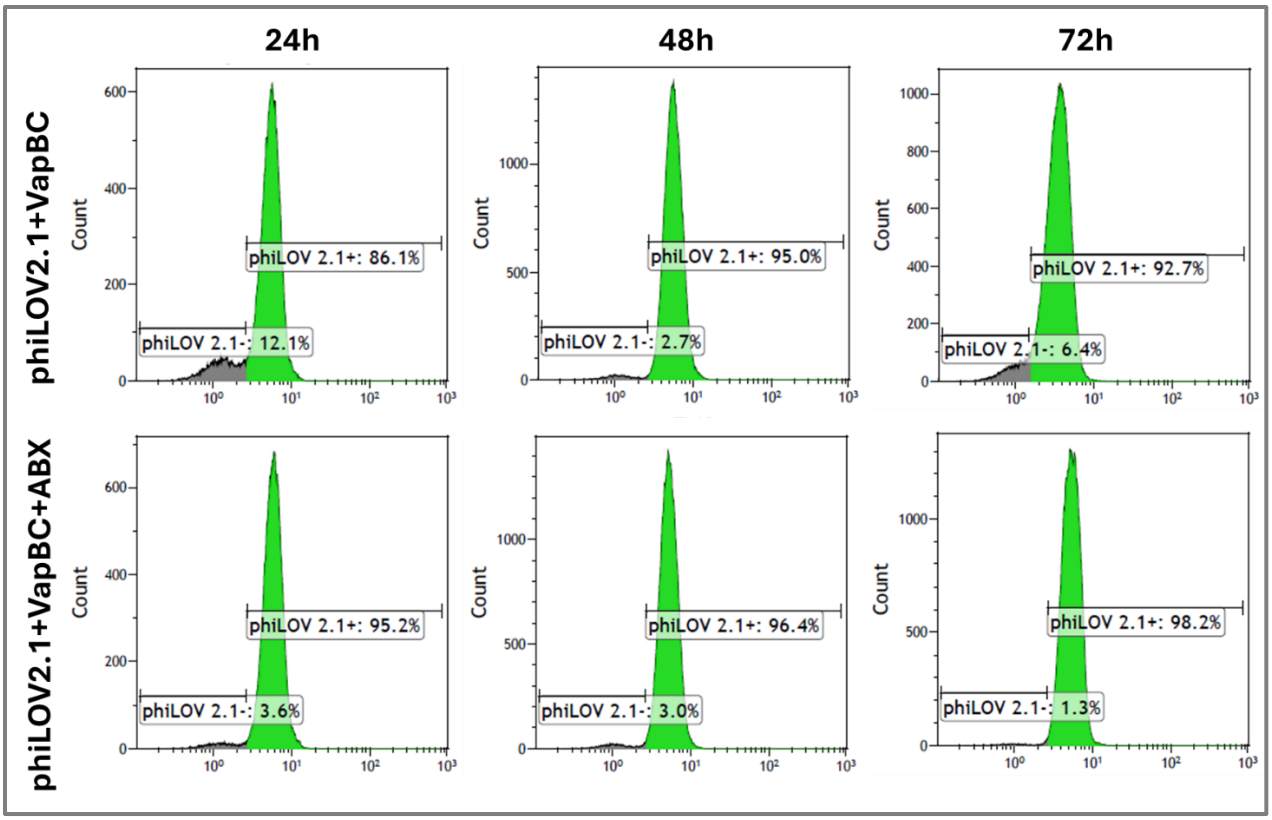

Figure 4.6: Flow cytometry analysis of *P. aeruginosa* PA14 carrying the pCFT4.2.1/phiLOV2.1+VapBC. The graphs show the percentage of cells expressing (phiLOV2.1+, green) or not (phiLOV2.1-, grey) the fluorescent protein phiLOV2.1 at different times without (top) and with (bottom) the antibiotic carbenicillin (ABX). Cultures were grown aerobically for three consecutive days either with or without ABX. Fluorescence was recorded every 24 h with a constant voltage at the excitation wavelength of 405 nm and the emission wavelength of 450±50 nm.

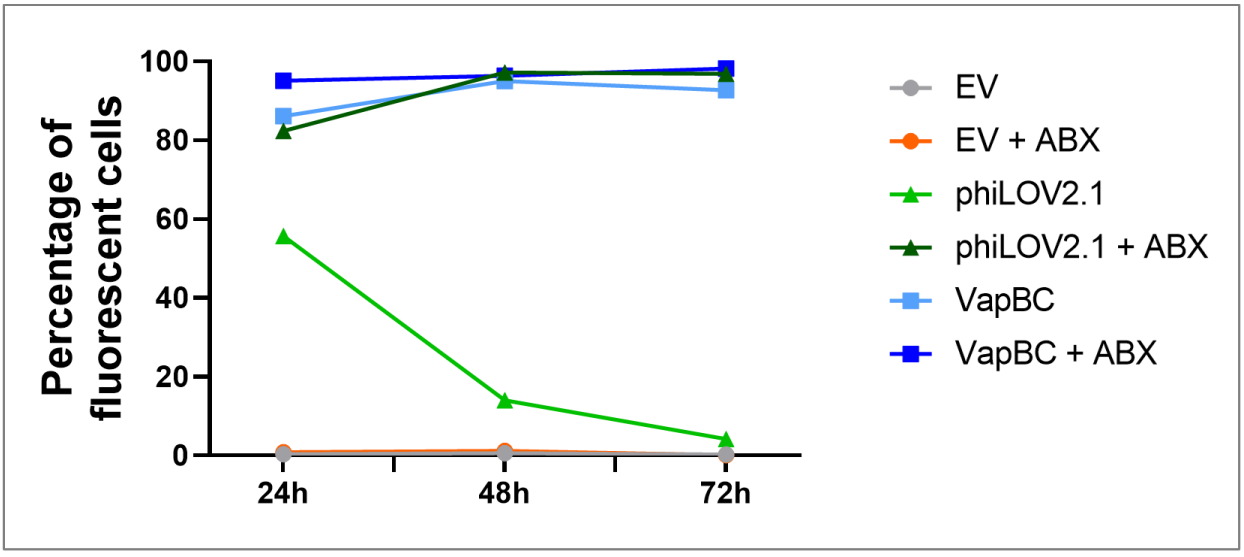

Figure 4.7: Summary of the flow cytometry analysis results of Figures 4.4 – 6. The graph represents the percentage of cells expressing phiLOV2.1 over 3 days in the presence or absence of the antibiotic carbenicillin (ABX). EV represents the empty vector pUdO4a. phiLOV2.1 represents pCFT4.2, which lacks the VapBC toxin-antitoxin system. VapBC represents pCFT4.2.1, which carries both phiLOV2.1 and the VapBC toxin-antitoxin system.

4.4.4. *P. aeruginosa* PA14 carrying pCFT4.2.1 is stably maintained in the CF polymicrobial assay

The goal of antibiotic-free maintenance of the plasmid pCFT4.2.1 in PA14 is to use this strain as a fluorescent reporter for tracking *P. aeruginosa* in the CF polymicrobial assay. The plasmid pCFT4.2.1 carries an ampicillin cassette, which confers resistance to β-lactam antibiotics such as ampicillin and carbenicillin to *P. aeruginosa*. To verify that this resistance gene does not confer any advantage or, on the contrary, a disadvantage to *P. aeruginosa* carrying this plasmid, it was crucial to assess the persistence of PA14/pCFT4.2.1 in the mixed culture composed of *S. aureus, S. sanguinis,* and *P. melaninogenica*.

Interestingly, when growing strain PA14/pCFT4.2.1 (referred to as VapBC) in the CF polymicrobial assay, the CFU counts for both biofilm and planktonic fractions in mono- or mixed-culture reached similar levels **(Figure 4.8)**. Moreover, the CFU count of PA14/pCFT4.2.1 is comparable to that of PA14 WT carrying no plasmid **(Chapter 3 – Section 3.4 – Figure 3.1)**. This suggests that carrying the plasmid does not alter *P. aeruginosa* behaviour in the presence of other bacteria in the assay, at least regarding CFU counts. Consequently, it was reasonable to use this fluorescent strain for downstream microscopy experiments. Because of the focus on *P. aeruginosa*, the CFU values for the other three species were not presented in this figure. However, they follow the same pattern as in the experiment featuring PA14 WT **(Chapter 3 – Section 3.4 – Figure 3.1)**.

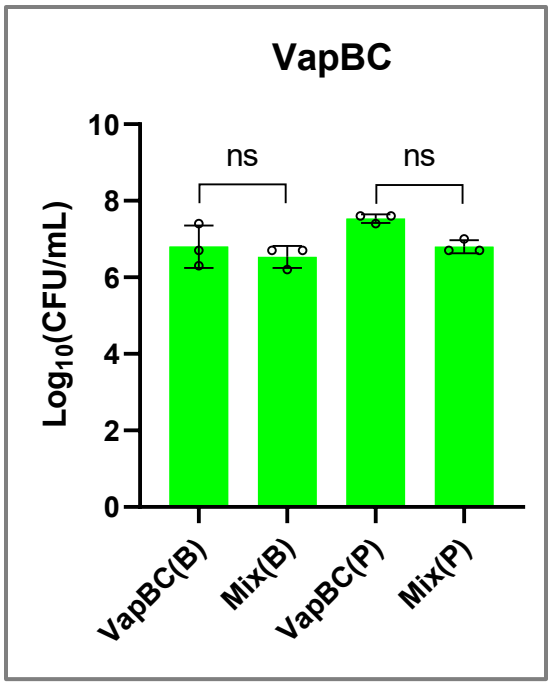

Figure 4.8: Colony forming units (CFU) counts of PA14 carrying pCFT4.2.1 (VapBC) grown anaerobically as a monoculture and in a mixed culture (Mix) for biofilm (B) and planktonic (P) fractions. The histogram represents the average of three biological replicates, and each data point represents the average of three technical replicates. Statistical analysis was performed using ordinary one-way ANOVA and Tukey's multiple comparisons post-test, with ns = non-significant. Error bars represent SD (n = 3).

4.4.5. Biofilm biomass quantification with the crystal violet staining assay

To characterize the nature of biofilms formed by *P. aeruginosa* under anaerobic conditions in ASM+ media, biofilm biomass was quantified using the crystal violet assay, a well-established and standard method for assessing biofilm formation [97, 339, 340]. Indeed, due to its alkaline nature, crystal violet typically binds to negatively charged surface molecules and polysaccharides in the extracellular matrix, including DNA, proteins, sugars, lipids, etc. [341, 342]. I used this assay to assess the biofilm biomass of eight *P. aeruginosa* strains (PA14 WT, Δ*ndvB*, Δ*PA1874-77*, Δ*tssC1*, Δ*tctED*, Δ*PA1759-60*, Δ*flgK,* and PA14/pCFT4.2.1 (VapBC)). All the deletion mutant strains were previously introduced in **Chapter 3**. Although PA14 WT and PA14/pCFT4.2.1 (VapBC) are the main focus of this experiment, the deletion mutant strains were introduced as an initial step towards the long-term objective of studying the biofilm formation of these strains as well. I performed a

qualitative and quantitative assessment of the biofilm biomass at 48 h incubation under aerobic and anaerobic conditions in mono- and mixed-cultures using ASM+ media. Δ*flgK* was used as a negative control for aerobic experiments because it does not form biofilm at the air-liquid interface due to its flagellar motility deficiency.

As expected, under aerobic conditions and for mono- and mixed-cultures, all *P. aeruginosa* strains except the Δ*flgK* control formed a biofilm at the air-liquid interface in ASM+ media as demonstrated by the presence of a purple ring with varying intensity on the side of the microplate wells **(Figure 4.9**, plate at the top**)**. In contrast, under anaerobic conditions, no purple coloration was visible, which suggested that no biofilm or an undetectable amount was formed for all the strains **(Figure 4.9**, plate at the bottom**)**. A quantification of the data presented in **Figure 4.9** revealed the amount of biofilm formed. Unsurprisingly, the quantification is on par with the qualitative observations of the crystal violet staining. Indeed, while detectable biomass levels were recorded for all aerobic cultures except for Δ*flgK,* as expected, no substantial record of biomass was noted for anaerobic cultures **(Figure 4.10)**.

Collectively, **Figures 4.9 and 4.10** indicate that under anaerobic conditions in ASM+ media, *P. aeruginosa* does not form the traditional surface-attached biofilm, which points to a different type of biofilm, likely the biofilm-like structure (BLS) previously reported by other groups [56, 343]. It is noteworthy that the polymicrobial context did not significantly influence the quantity of biomass formed aerobically, as there was no statistical difference in mono- versus mixed-cultures.

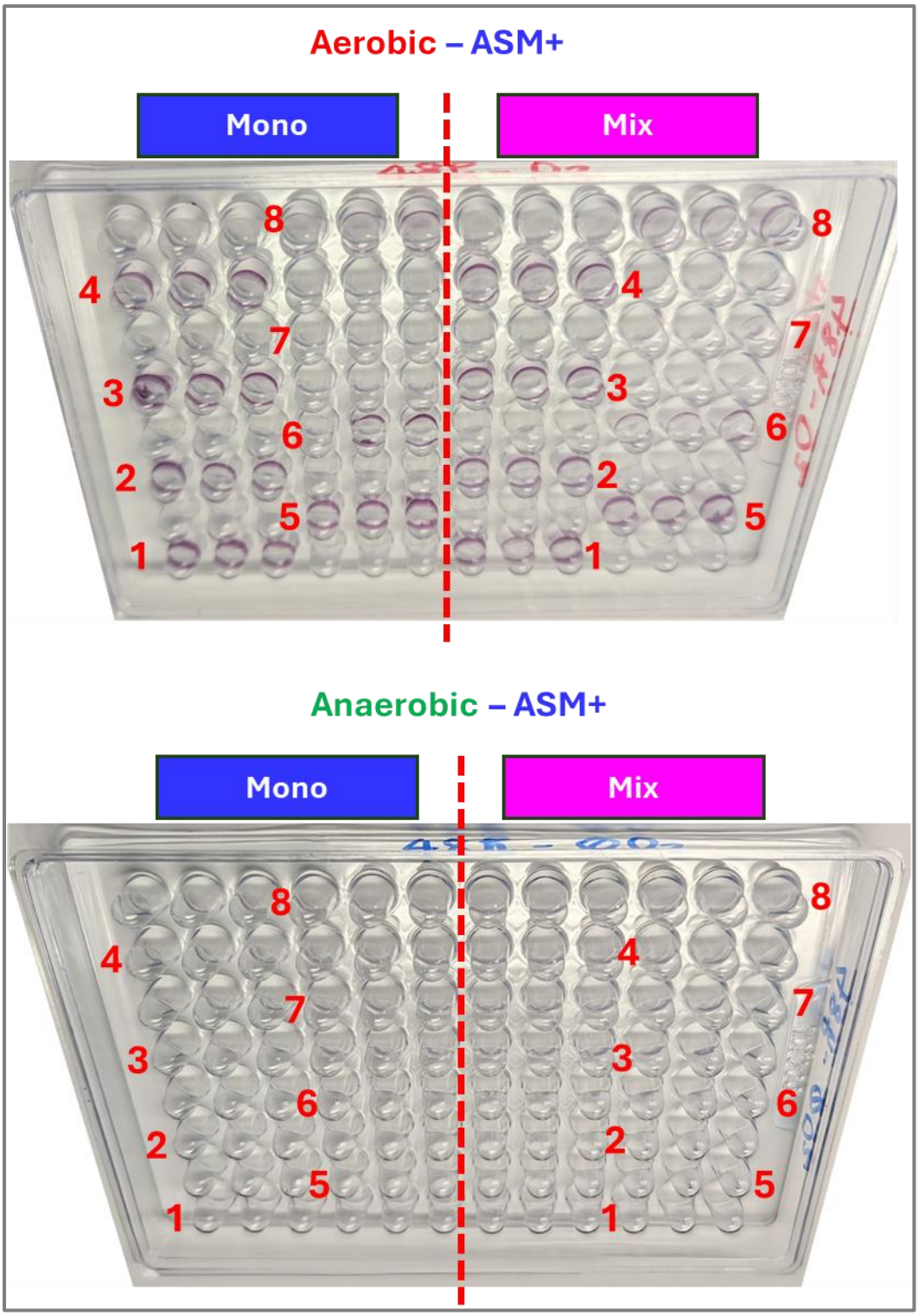

Figure 4.9: Crystal violet staining of bacterial biofilms grown aerobically (plate at the top) and anaerobically (plate at the bottom) for 48 h at 37°C in ASM+ media. The different bacterial strains (#1 – 8) were grown as monoculture (Mono) and mixed-culture (Mix) composed of *S. aureus, S. sanguinis and P. melaninogenica*. The crystal violet ring is

observable with variable intensity on all the various strains on the aerobic plate, except the control Δ*flgK*. The purple ring is characteristic of biofilm formed at the air-liquid interface. The absence of crystal violet staining is noticeable for all the strains on the anaerobic plate. Annotations for all plates are as follows: 1; PA14 WT, 2; Δ*ndvB*, 3; Δ*PA1874-77*, 4; Δ*tssC1*, 5; Δ*tctED*, 6; Δ*PA1759-60*, 7; Δ*flgK* and 8; PA14/pCFT4.2.1 (VapBC).

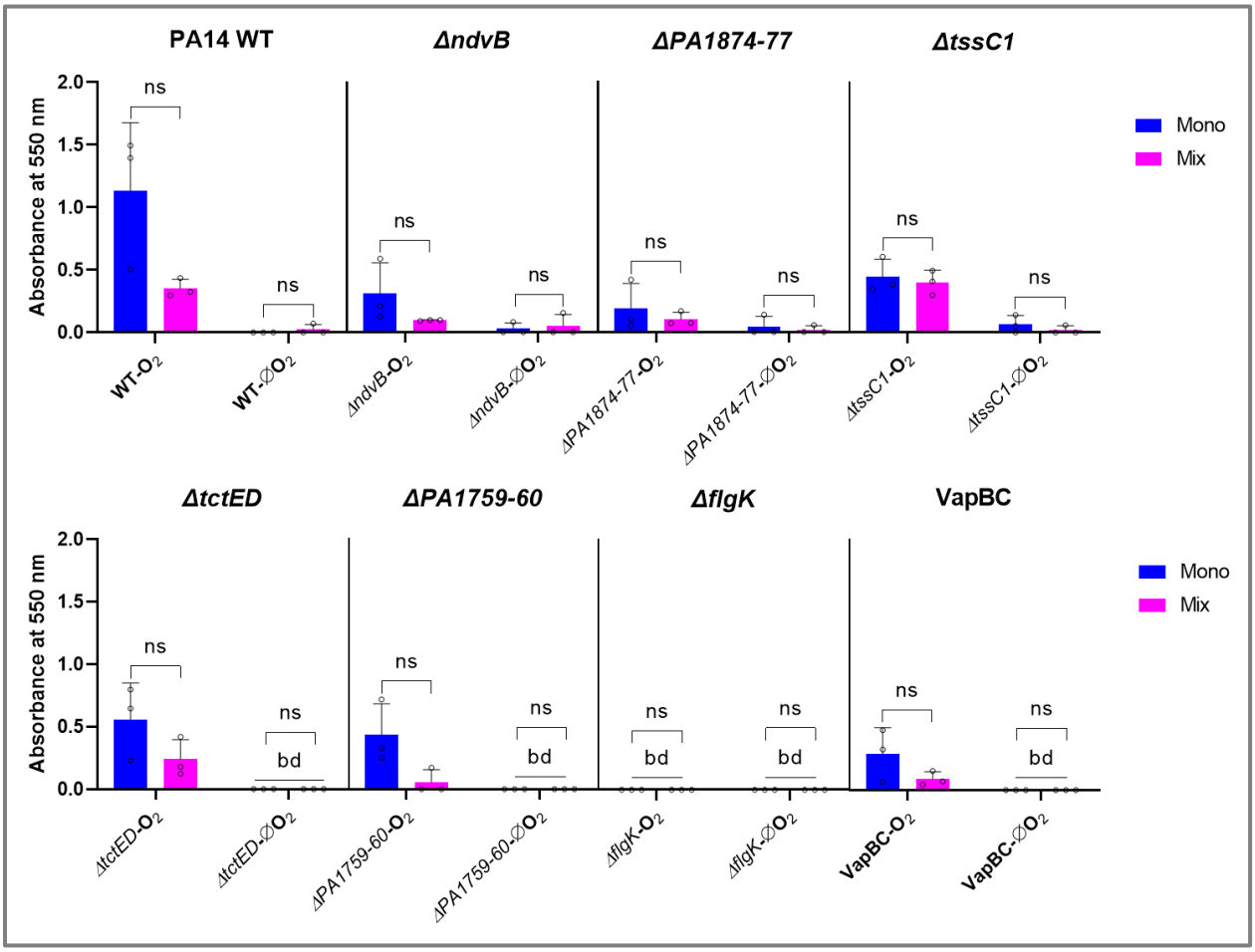

Figure 4.10: Biofilm quantification of the crystal violet assay from Figure 4.9. The biofilm of different bacterial strains was grown under aerobic (O_2) and anaerobic ($ØO_2$) conditions and as monoculture (Mono, blue bars) and mixed-culture (Mix, pink bars) composed of *S. aureus, S. sanguinis and P. melaninogenica*. VapBC is PA14/pCFT4.2.1. Biofilms were visualized by crystal violet staining and quantified by solubilizing the crystal violet with 30% acetic acid. The histogram represents the average of three replicates. Statistical analysis was performed using Two-way ANOVA and Sidak's multiple comparisons post-test, with ns = non-significant, bd = below detection. Error bars represent SD (n=3).

To decipher whether the inability of *P. aeruginosa* to form quantifiable surface-attached biofilm was due to ASM+ media or the anaerobic conditions, the M63 minimal media supplemented with nitrate (M63N) was used alongside ASM+. Only monocultures of the eight *P. aeruginosa* strains were assayed for 48 h using crystal violet for biofilm biomass qualitative and quantitative analysis.

Interestingly, under anaerobic conditions, a distinctive purple crystal violet coloration appeared in M63N media, contrasting with the lack of noticeable colour in ASM+ media **(Figure 4.11)**. This reinforces the notion that *P. aeruginosa* may form unconventional biofilms akin to BLS in ASM+ media under anaerobic conditions, as previously observed in **Figure 4.9**. The visible layer of crystal violet coloration at the bottom and on the side of the well with M63N suggests that the biofilm is attached to those surfaces and not solely at the air-liquid interface, as seen under aerobic conditions **(Figure 4.9)**. This outcome was expected because, under anaerobic conditions, *P. aeruginosa* does not need to swim to the air-liquid interface for respiration. Instead, it can directly utilize nitrate in the media as an alternative electron acceptor [4, 5].

The quantitative analysis supports the findings that the biomass collected for *P. aeruginosa* cultures in M63N was substantially greater than that of ASM+ **(Figure 4.12)**. A notable exception was for strain Δ*PA1759-60*, which had no measurable biomass regardless of the media. The inability of this strain to form detectable biofilm in M63N media after 48 h of incubation was previously reported by a colleague in our laboratory [96]. Taken together, the results from **Figures 4.9 – 12** suggest that *P. aeruginosa* does not form a traditional surface-attached biofilm in ASM+ under anaerobic conditions on a microtiter plate.

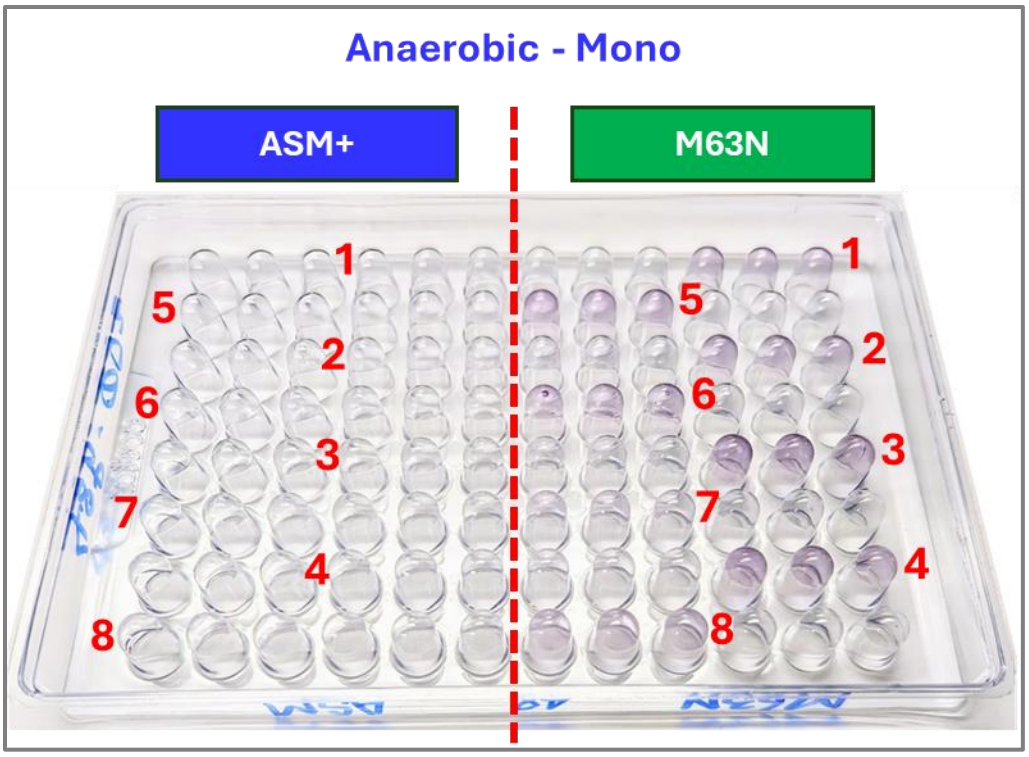

Figure 4.11: Crystal violet staining of bacterial biofilms grown anaerobically for 48 h at 37°C in ASM+ media (left) and M63N media (right). The different bacterial strains (#1 – 8) were grown as monocultures (Mono). The crystal violet coloration is observable with variable intensity for all the various strains on the M63N side of the plate except for Δ*PA1759-60*. The purple coloration is characteristic of biofilm attached to the well surface. The absence of crystal violet staining is noticeable for all the strains on the ASM+ side of the plate. Annotations for all plates are as follows: 1; PA14 WT, 2; Δ*ndvB*, 3; Δ*PA1874-77*, 4; Δ*tssC1*, 5; Δ*tctED*, 6; Δ*flgK* , 7; Δ*PA1759-60* and 8; PA14/pCFT4.2.1 (VapBC).

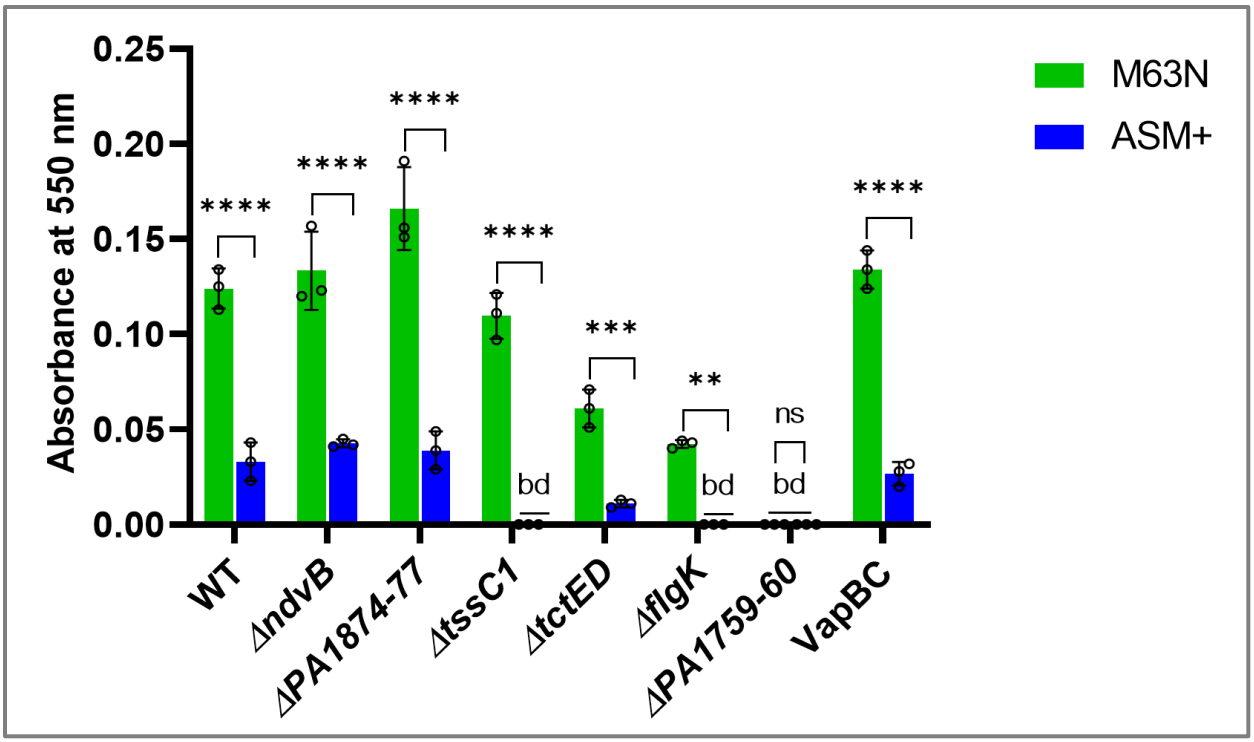

Figure 4.12: Biofilm quantification of the crystal violet assay from Figure 4.11. The biofilm of different bacterial strains was grown as monocultures under anaerobic conditions in M63N media (green bars) and ASM+ media (blue bars) for 48 h at 37°C. VapBC is PA14/pCFT4.2.1. Biofilms were visualized by crystal violet staining and quantified by solubilizing the crystal violet with 30% acetic acid. The histogram represents the average of three replicates. Statistical analysis was performed using Two-way ANOVA and Sidak's multiple comparisons post-test, with ns = non-significant, bd = below detection. Error bars represent SD (n=3).

4.4.6. Microscopy and Spatial distribution of PA14 WT biofilm in mono- vs mixed-culture

4.4.6.1. Aerobic Mono-species

The initial assessment of fluorescence by microscopy was performed using planktonic cells in LB medium grown under aerobic conditions. The goal was to evaluate the cells under simple, optimal and straightforward growth conditions for *P. aeruginosa*. The results of **Figure 4.13** revealed that PA14/pCFT4.2.1 expressing phiLOV2.1 was distinctly visible under the microscope. The WT strain served as the negative control and gave the expected result

of no phiLOV2.1 fluorescence. Furthermore, the red dye Synaptored C2, used as an indicator of bacterial cells, was identifiable in the membrane of each cell.

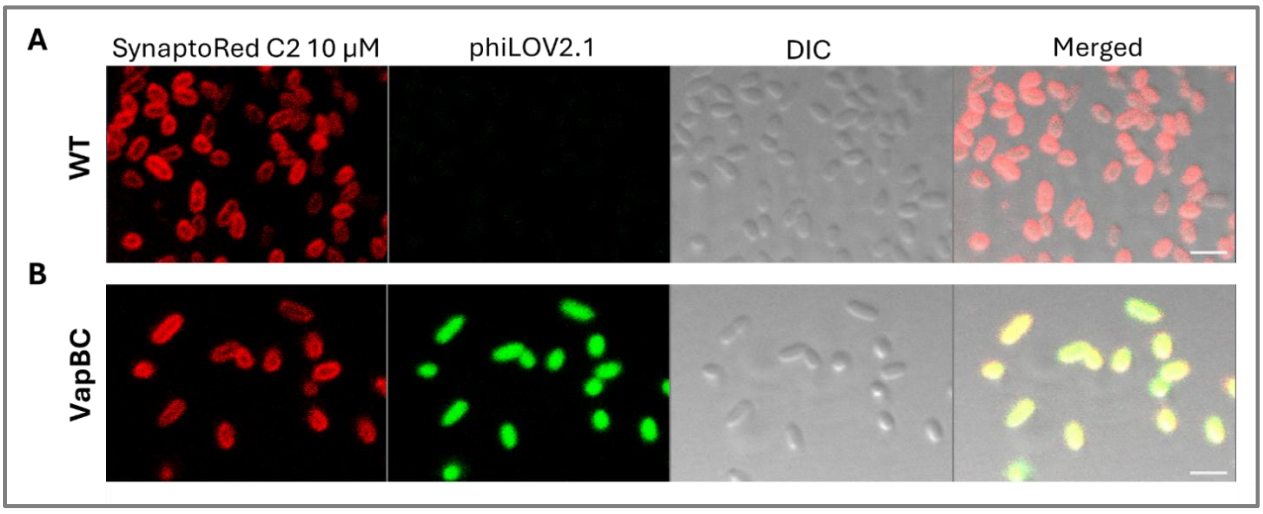

Figure 4.13: Fluorescence imaging of planktonic PA14 expressing phiLOV2.1 under aerobic conditions (Zoom factor: 2X). (A) Micrograph of PA14 WT (WT) stained with SynaptoRed C2 10 µM. (B) Micrograph of PA14/pCFT4.2.1 (VapBC) expressing phiLOV2.1 and the toxin-antitoxin system VapBC stained with SynaptoRed C2 10 µM. From left to right: red channel fluorescence showing cells membrane stained with SynaptoRed C2 10 µM (614 nm, 591-722 nm); green channel fluorescence showing cells expressing phiLOV2.1 (458 nm, 466-537 nm); differential interference contrast (DIC) and merged images (scale bar = 5 µm).

4.4.6.2. Anaerobic Mono-Dual-Tri-Tetra species imaging

Following this successful initial assessment, PA14/pCFT4.2.1 was exposed to a slightly more complex environment, and the fluorescence microscopy was performed once again. The growth conditions consisted of anaerobic incubation in ASM supplemented with centrifuged mucin, in contrast to the standard preparation method using non-centrifuged mucin. As noted in **Section 4.3.6.2.1** and in the flowchart for anaerobic microscopy presented in **Figure 4.1**, based on preliminary imaging experiments with PA14/pCFT4.2.1 in ASM+, I found artifacts of residual mucin that fluoresced at the same wavelengths as phiLOV2.1. To address this interference, the mucin was centrifuged to remove solid residues. The results for the mono- and mixed-cultures imaging are presented in **Figure 4.14**.

In monoculture of PA14 harbouring pCFT4.2.1 (VapBC), the fluorescence of phiLOV2.1 was observable in all the cells **(Figure 4.14A)**. The fluorescence seems to be substantially lower than that of the aerobic monoculture in LB media presented in **Figure 4.13B**. This is likely due to the increased stress on PA14 cells from the changes in culture media and oxygen levels. A dual-culture of PA14/pCFT4.2.1 (VapBC) and *S. aureus* failed to yield any phiLOV2.1 fluorescence **(Figure 4.14B**). It is possible that the low fluorescence observed in anaerobic monoculture **(Figure 4.13B)** is exacerbated by the lesser amount of VapBC inoculum in the mixed cultures, or that the change in culture media, particularly with the ASM prepared with centrifuged mucin, played a role in this outcome. It is worth adding that the distinct morphology of cocci, mostly diplococci and a few grape-like clusters associated with *S. aureus,* helped visualize these cells with the differential interference contrast (DIC) modality **(Figure 4.14B)**. However, the rod-shaped *P. aeruginosa* could not be visualized in this field of view, likely because, contrary to *S. aureus*, it may not form surface-attached biofilms in this experimental setting.

The three- and four-species cultures yielded similar observations to the dual-culture. Indeed, no phiLOV2.1 fluorescence was visible for VapBC in **Figures 4.14C and D**, respectively. The reasons mentioned previously to justify this observation could be extended here as well, notably, the low fluorescence of phiLOV2.1 in tandem with the change in culture media under anaerobic conditions. As a side note, *S. sanguinis* was identifiable in **Figure 4.14C** because of its distinctive cocci chain morphology visible on the DIC panel. Lastly, the morphology of non-fluorescent bacilli is distinguishable more easily in the far-left panel of the SynaptoRed C2 coloration, which could be attributed to *P. melaninogenica* **(Figure 4.14D)**.

Taken together, the phenotype of different bacterial morphologies was identifiable for each strain in the assay. However, the lack of phiLOV2.1 fluorescence in VapBC suggests that some optimizations of culture conditions are required for reliable and sustainable microscopy imaging.

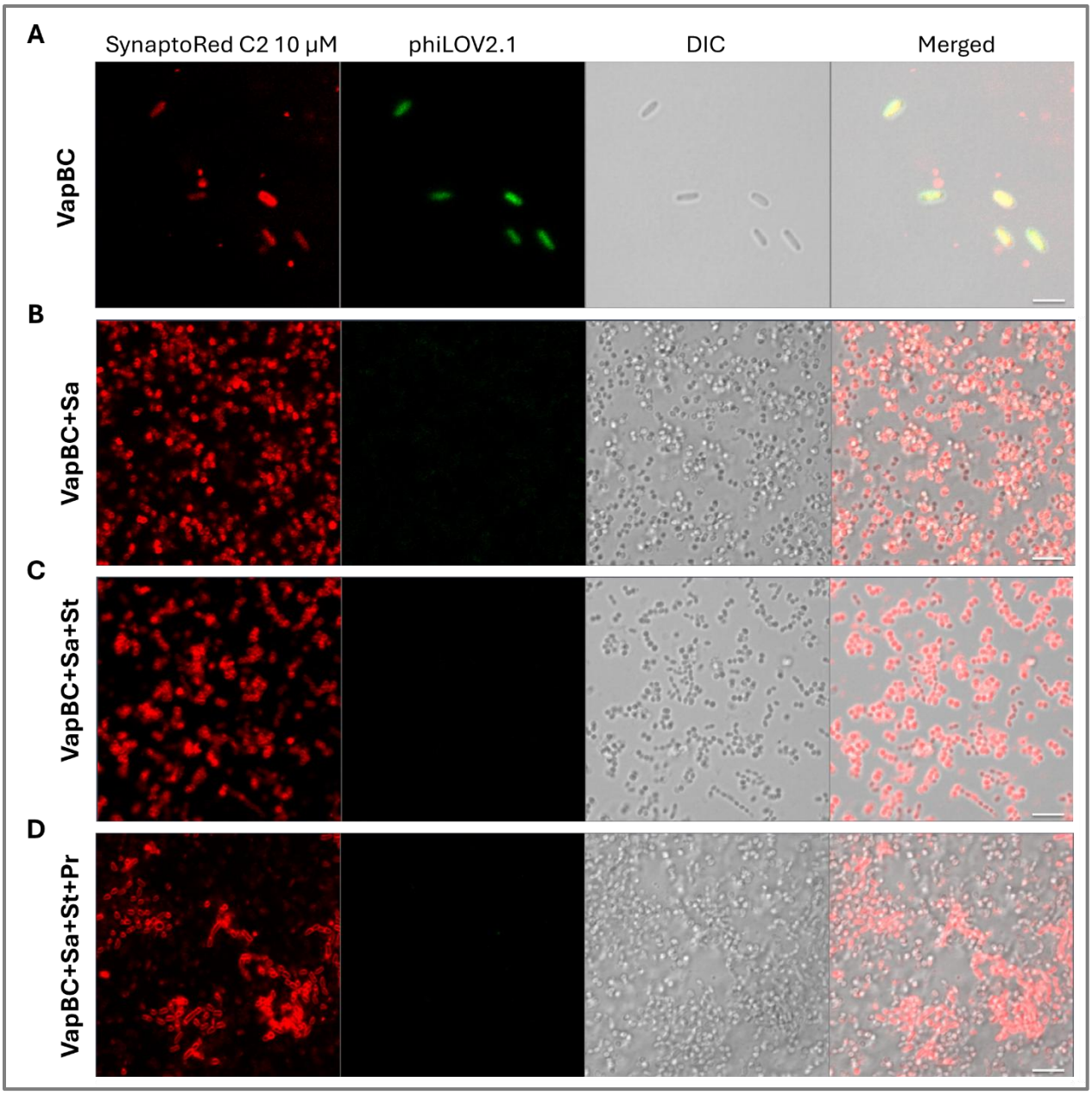

Figure 4.14: Fluorescence imaging of mono- and mixed-cultures of PA14/pCFT4.2.1 (VapBC) expressing phiLOV2.1 alongside other bacteria under anaerobic conditions (Zoom factor: 2X). (A) Micrograph of monoculture PA14/pCFT4.2 (VapBC) expressing phiLOV2.1 and the toxin-antitoxin system VapBC. (B) Micrograph of a co-culture of PA14/pCFT4.2.1 (VapBC) expressing philOV2.1 and *S. aureus* (1:1 inoculation ratio). (C) Micrograph of a co-culture of PA14/pCFT4.2.1 (VapBC) expressing philOV2.1, *S. aureus* (Sa) and *S. sanguinis* (St) (1:1:1) inoculation ratio. (D) Micrograph of a co-culture of PA14/pCFT4.2.1 (VapBC) expressing philOV2.1, *S. aureus* (Sa), *S. sanguinis* (St) and *P. melaninogenica* (Pr) (1:1:1:1) inoculation ratio. From left to right: red channel fluorescence showing cells membrane stained with SynaptoRed C2 10 µM (614 nm, 591-722 nm); green

channel fluorescence showing cells expressing phiLOV2.1 (458 nm, 466-537 nm); differential interference contrast (DIC) and merged images (scale bar = 5 µm).

4.4.7. *P. aeruginosa* surface-attached biofilms in artificial sputum media with mucin (ASM+) under anaerobic conditions

To optimize the culture conditions and ensure successful and reliable imaging of phiLOV2.1 in mono- and mixed-culture, the centrifuged mucin described in **Section 4.3.6.2.1** was substituted for the regular mucin in the ASM+ media preparation **(Figure 4.1)**. In addition, thorough washing steps post-incubation were followed to eliminate residual mucin that might interfere with imaging **(Figure 4.1)**. The washing also ensures the removal of any unattached cells or aggregates.

This strategy worked because **Figures 4.15 and 16** show micrographs depicting PA14/pCFT4.2.1 biofilms in mono- **(Figures 4.15A and 16A)** and mixed-cultures **(Figures 4.15B and 16B)** at a zoom factor of 2X and 0.6X, respectively. In **Figure 4.15**, there seem to be fewer and bigger biofilms for mono- than in the mixed-cultures. **Figure 4.16** also shows that the mixed culture had more biofilms. By compiling data from three biological replicates and quantifying the volumes and the number of biofilms, I found that overall, *P. aeruginosa* formed significantly more and larger biofilms when cultured in a mixed-culture environment compared to monoculture **(Figure 4.17)**. To properly perform this analysis, however, the Synaptored C2 dye was removed as it became unnecessary after the culture conditions and imaging were optimized.

These observations on the spatial distribution of PA14 biofilms are insightful and valuable; however, they only paint a partial picture. It is important to remember that the results of **Figures 4.15 and 16** reflect surface-attached biofilm cells, as unattached or poorly attached cells were thoroughly removed during the washing steps. Therefore, these results do not take into consideration the BLS previously reported under anaerobic conditions [343] and in synthetic mucus medium [56]. Using microscopy provided an opportunity to see if I could also observe these BLS in my experiments.

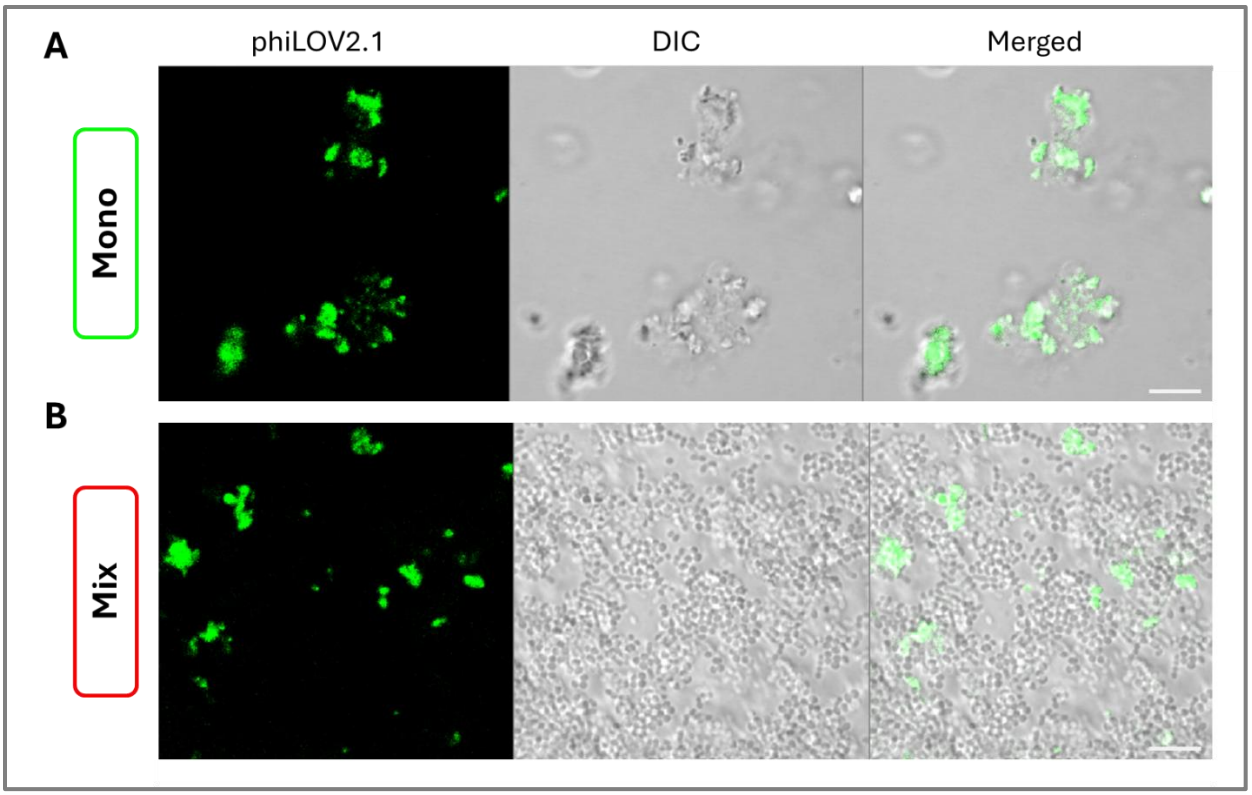

Figure 4.15: Fluorescence imaging of anaerobic biofilm cultures of PA14/pCFT4.2.1 expressing phiLOV2.1 in mono- and mixed-biofilm cultures (Zoom factor: 2X). (A) Micrographs of monocultures (Mono). (B) Micrographs of mixed cultures composed of *S. aureus*, *S. sanguinis*, and *P. melaninogenica* (Mix). Imaging was performed after 48 h of incubation. From left to right: green channel fluorescence showing cells expressing phiLOV2.1 (458 nm, 466-537 nm); differential interference contrast (DIC) and merged images (scale bar = 5 µm).

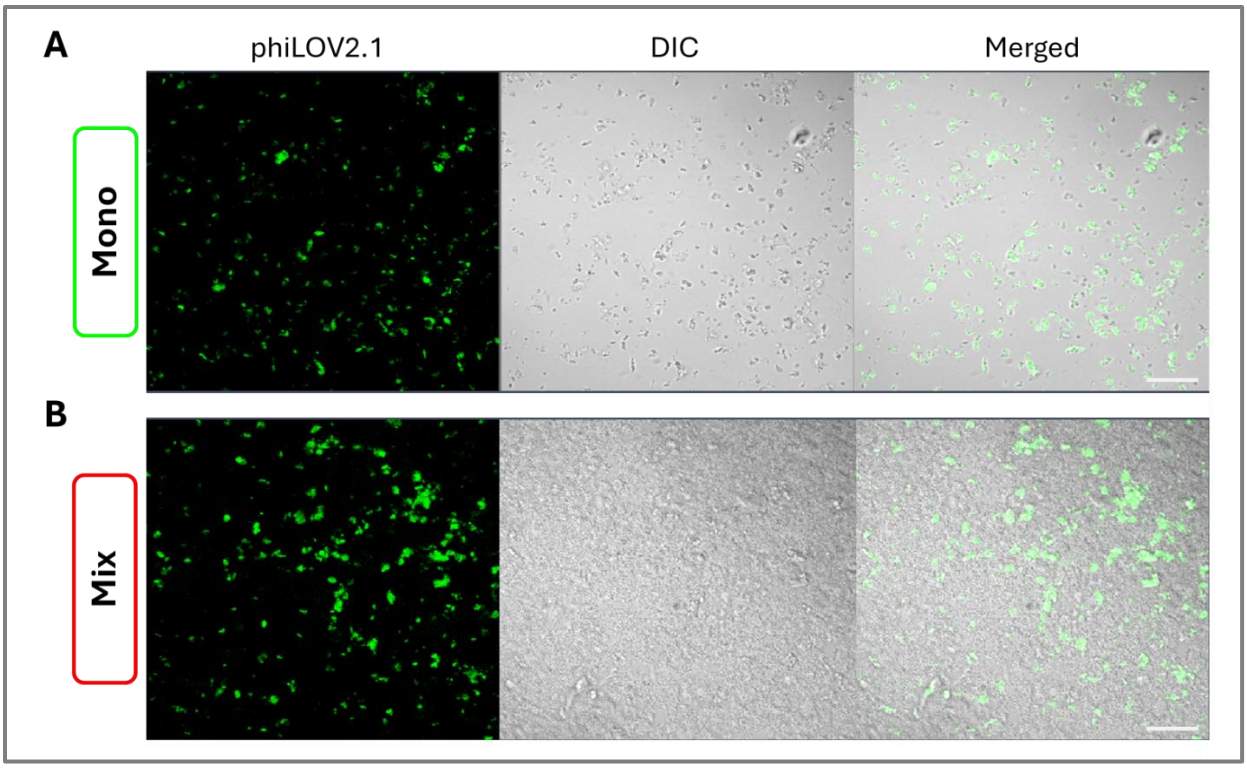

Figure 4.16: Fluorescence imaging of anaerobic biofilm cultures of PA14/pCFT4.2.1 expressing phiLOV2.1 in mono- and mixed-biofilm cultures (Zoom factor: 0.6X). (A) Micrographs of monocultures (Mono). (B) Micrographs of mixed cultures composed of *S. aureus*, *S. sanguinis*, and *P. melaninogenica* (Mix). Imaging was performed after 48 h of incubation. From left to right: green channel fluorescence showing cells expressing phiLOV2.1 (458 nm, 466-537 nm); differential interference contrast (DIC) and merged images (scale bar = 5 µm).

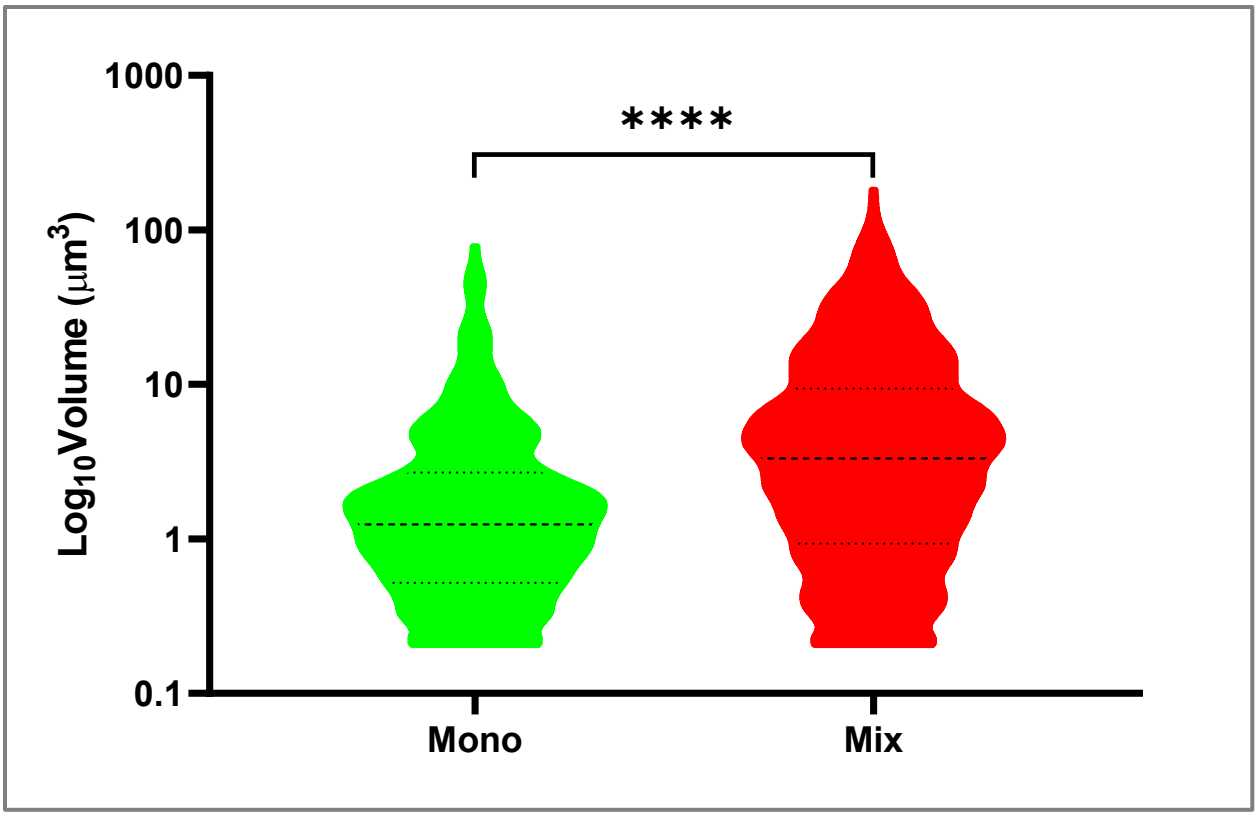

Figure 4.17: Distribution analysis of anaerobic PA14/pCFT4.2.1 biofilm sizes in monocultures (Mono, green violin) vs mixed cultures (Mix, red violin). The violins represent single-aggregate fluorescence quantification of phiLOV2.1. Statistical analysis was performed using an unpaired Student's and Mann-Whitney test (****$p < 0.001$; $n = 3$). The mixed community comprises *S. aureus*, *S. sanguinis*, and *P. melaninogenica*.

4.4.8. *P. aeruginosa* biofilm-like structures (BLS) in artificial sputum media with mucin (ASM+) under anaerobic conditions

Unlike traditional biofilms, BLS are not attached to surfaces; therefore, they are most likely to be found as suspended aggregates in the supernatant. An analysis of the bacterial culture supernatant revealed the presence of cell aggregates resembling biofilms that I identified as BLS **(Figure 4.18)**. In addition, the BLS encountered in the mixed culture appeared larger than the ones in the monoculture. This finding is consistent with the observations on biofilms from **Figures 4.15 – 17**. Importantly, this is a significant and crucial finding in the broader context of the entire culture.

Indeed, this study on *P. aeruginosa* biofilm spatial distribution demonstrates that *P. aeruginosa* has a dual capacity to form not only surface-attached biofilms but also floating BLS in a CF-like environment. This information should be considered when treating *P. aeruginosa* biofilm CF infections.

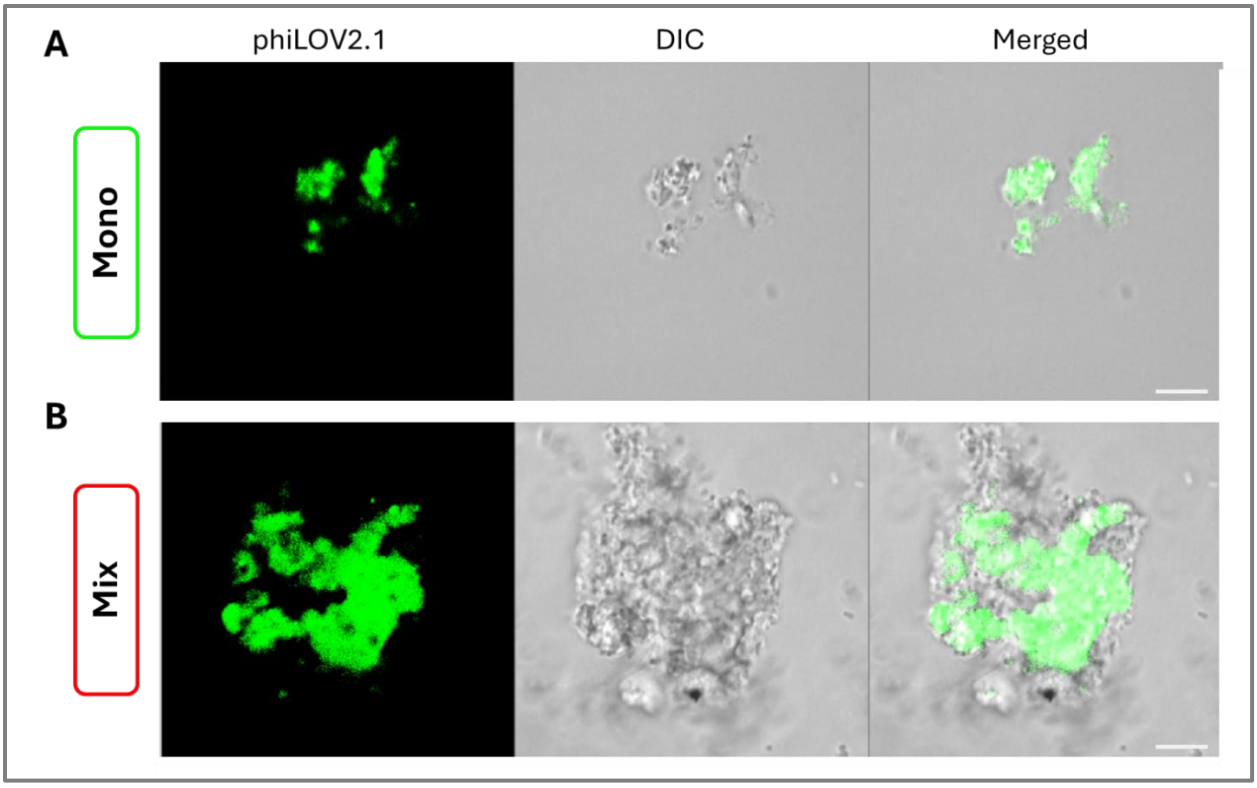

Figure 4.18: Fluorescence imaging of anaerobic biofilm-like structures (BLS) of PA14/pCFT4.2.1 expressing phiLOV2.1 in mono- and mixed-cultures (Zoom factor: 2X). Micrographs were acquired at a zoom factor of 2X. (A) Micrographs of monocultures (Mono). (B) Micrographs of mixed cultures composed of *S. aureus*, *S. sanguinis*, and *P. melaninogenica* (Mix). Imaging was performed after 48 h of incubation. From left to right: green channel fluorescence showing cells expressing phiLOV2.1 (458 nm, 466-537 nm); differential interference contrast (DIC) and merged images (scale bar = 5 µm).

4.5. Discussion

Plasmid construction and stabilization

In this chapter, I demonstrated that the newly engineered plasmid pCFT4.2.1—encoding the fluorescent protein phiLOV2.1 and the toxin-antitoxin system VapBC **(Figure 4.2)**—was stably maintained in PA14 WT for at least five days without antibiotic selection **(Figure 4.3)**. Notably, over 90% of the bacterial population retained the plasmid and exhibited detectable fluorescence for at least three days under non-selective conditions **(Figures 4.4 – 7)**.

To efficiently stabilize the plasmid pCFT4.2 that expresses phiLOV2.1 in PA14 without using antibiotic selection, three toxin-antitoxin (TA) systems previously untested in this organism—VapBC, CcdAB, and PumAB—were examined. VapBC was the sole successful TA system in this endeavour. As a reminder, a TA system is generally encoded by an operon and consists of a stable toxin and a labile antitoxin that counteracts the effects of the toxin. VapC toxins typically exhibit endoribonuclease activity against tRNA or mRNA, leading to translation inhibition and growth arrest [172]. VapB antitoxin binds to VapC, forming a stable complex that inhibits VapC ribonuclease activity [172]. CcdB toxin targets DNA gyrase by binding to its GyrA subunit, stabilizing a cleavage complex that leads to double-stranded DNA breaks, thus inhibiting DNA replication and transcription [166, 167]. CcdA antitoxin, on the other hand, stably binds to CcdB to prevent its interaction with DNA gyrase [168]. Lastly, PumA toxin functions as an endoribonuclease that cleaves mRNA, inhibiting translation and leading to growth arrest [180]. PumB forms a PumA-PumB complex that inhibits PumA endoribonuclease activity [181].

Arguably, the three TA systems mechanisms of action may impact *P. aeruginosa* physiology differently. The success of VapBC in stabilizing pCFT4.2 in *P. aeruginosa* compared to CcdAB and PumAB may stem from its ribonuclease-based toxin mechanism, which is less disruptive and more compatible with *P. aeruginosa* physiology. Indeed, the specificity of VapBC DNA targets may align well with *P. aeruginosa* translation machinery, ensuring effective plasmid stabilization [344]. Hence, VapBC may provide a balanced level

of toxicity that effectively kills plasmid-free cells without overwhelming the *P. aeruginosa* stress response systems.

In contrast, the CcdB DNA-damaging mechanism may be too lethal or poorly suited to *P. aeruginosa* gyrase. Indeed, CcdB, causing double-stranded DNA breaks, may be overly toxic to *P. aeruginosa* or trigger a repair mechanism that interferes with plasmid stabilization. Moreover, CcdAB is native to *E. coli* and structural differences between *E. coli* and *P. aeruginosa* gyrases—approximately 67% amino acid similarity [345]—may lead to less specificity, therefore less efficiency. Although PumAB is encoded on the plasmid pUM505, which is native to a *P. aeruginosa* isolate [180] and possesses endoribonuclease activity similar to VapBC, its regulation is tightly linked to *P. aeruginosa* quorum sensing (QS) systems and specific promoter elements [181, 186]. Therefore, PumA is possibly less effective on a non-native plasmid like pCFT4.2.1 in different genetic backgrounds or environmental conditions because these regulatory elements may not function correctly. Furthermore, overexpression of PumA increases *P. aeruginosa* virulence [180], which may divert its function from plasmid stabilization.

In essence, pCFT4.2.1 harbouring phiLOV2.1 and VapBC is maintained in *P. aeruginosa* for at least five days, with more than 90% of cells keeping the plasmid for at least three days. Although this time frame is reasonable, it would be interesting to pursue the experiment for several more days or weeks to demonstrate the applicability of this plasmid in long-term studies. Furthermore, a library with other fluorescent proteins like GFP could be created to diversify applications. Indeed, although phiLOV2.1 is renowned for its photostability in microscopy experiments, it is also flawed with low brightness [131, 144]. Lastly, the expression level of each TA system was not directly measured but was inferred from sequencing data. A Western blot analysis would have helped clarify this.

Plasmid pCFT4.2.1 was stably maintained in PA14 in the CF polymicrobial assay

Using the PA14/pCFT4.2.1 strain, I further established that it remained stable in the CF polymicrobial assay and achieved comparable colony forming unit (CFU) counts whether

grown as a monoculture or as a mixed culture alongside *S. aureus, S. sanguinis,* and *P. melaninogenica* **(Figure 4.8)**.

The ability of PA14/pCFT4.2.1 to thrive in the CF polymicrobial assay under anaerobic conditions at levels equivalent to PA14 WT carrying no plasmid underscores the fact that the plasmid plays no role or at least an insignificant one in the overall fitness of the strain. Indeed, the standard plasmid pCFT4.2.1 contains several genetic elements essential for its reporter function, including a pBBR1 origin of replication, an antibiotic resistance cassette conferring ampicillin resistance (AmpR), a gene of interest encoding the fluorescent protein phiLOV2.1, and an additional selectable marker encoding the VapBC toxin-antitoxin (TA) system **(Figure 4.2)**. Arguably, none of these elements influences *P. aeruginosa* metabolism, survival, or interactions with other species in a manner that confers an advantage or disadvantage to its persistence. Indeed, *P. aeruginosa* ability to survive in an anaerobic environment depends on its capacity to utilize alternative electron acceptors like nitrate or nitrite for anaerobic respiration [4, 5, 346]. These metabolic capabilities allow both plasmid-carrying and plasmid-free strains to persist effectively under anaerobic conditions, as the core metabolic machinery is chromosomally encoded and not dependent on plasmids. Similarly, *P. aeruginosa* competitiveness in a mixed community is mainly based on QS-regulated virulence factors [347, 348], which are not plasmid-dependent. Lastly, in the experimental conditions described here, the absence of antibiotic selection makes the antibiotic resistance gene irrelevant. The plasmid pCFT4.2.1, with a size of 4,055 bp, imposes a metabolic burden that may offset any potential benefits it confers, resulting in comparable fitness between plasmid-carrying and plasmid-free strains.

In short, the ability of PA14/pCFT4.2.1 to thrive in the CF polymicrobial assay is exclusively dependent on chromosomally encoded genes rather than the plasmid, which may explain why this strain reached CFU counts identical to PA14 WT.

Biofilm biomass characterization and Spatial distribution

To investigate the nature of *P. aeruginosa* anaerobic biofilms, I used crystal violet staining in a microtiter plate-based assay and the artificial sputum media supplemented with mucin

(ASM+), which is a medium specifically designed to approximate the nutritional content of the CF lung [293, 294]. In this experimental setup, *P. aeruginosa* did not form, or formed an undetectable/unquantifiable amount of surface-attached biofilms **(Figures 4.9 – 12)**. However, microscopy revealed that in anaerobic ASM+, *P. aeruginosa* formed surface-attached biofilms. Furthermore, these biofilms appeared more extensive in mixed cultures compared to monocultures in the CF polymicrobial assay **(Figures 4.15 – 17)**. In this same context, both surface-attached biofilms and biofilm-like structures (BLS)—structures resembling floating aggregates—were observed simultaneously **(Figure 4.18)**.

The proclivity for *P. aeruginosa* to form surface-attached biofilm on a microscope dish versus a microtiter plate in the experimental setup described here could partly be explained from a geometry and hydrodynamic standpoint. Indeed, microtiter plates have small, confined wells (about 6 mm bottom diameter versus 35 mm for a microscope dish), with limited medium volume (100 µL versus 2 mL). These differences lead to static conditions in a microtiter plate that may trap bacteria in the ASM+ viscous matrix, preventing surface contact, especially under anaerobic conditions where bacteria do not need to swim to the air-liquid interface for respiration. The entrapment of *P. aeruginosa* cells in close proximity within a gel-like environment, caused by mucin serving as a nucleation point, could indeed lead to the formation of cell aggregates [65, 349]. Furthermore, the extracellular matrix of non-attached *P. aeruginosa* aggregates is remarkably similar to that of surface-attached biofilms [57]. This observation supports the notion that, within the 48 h incubation period, *P. aeruginosa* does not form detectable surface-attached biofilms in microtiter plates under anaerobic ASM+ conditions, but rather predominantly develops suspended cell aggregates consistent with BLS [56]. Potentially, a more extended incubation period may produce a different outcome where surface-attached biofilms also become detectable in microtiter plates. In microscope dishes, the larger surface areas can enable bacteria to settle and stick to the surface or sedimented mucin residues present at the surface bottom, resulting in the surface-attached phenotype observed in my experiments.

The observation that *P. aeruginosa* forms more and larger biofilm aggregates in anaerobic ASM+ in a mixed culture with *S. aureus*, *S. sanguinis*, and *P. melaninogenica* compared to a

monoculture suggests that interspecies interactions significantly influence biofilm dynamics. Research indicates that *P. aeruginosa* and *S. aureus* develop mixed biofilms in CF lung models, where *S. aureus* promotes *P. aeruginosa* biofilm growth via co-aggregation and interactions within the matrix [350]. Additionally, certain compounds within the biofilm matrix—such as staphylococcal protein A (SpA) from *S. aureus* and Psl exopolysaccharide from *P. aeruginosa*—facilitate the development of large, dense biofilm aggregates [351–354]. Metabolic interactions in CF lung models show that *P. melaninogenica* produces short-chain fatty acids that enhance *P. aeruginosa* growth and biofilm formation under anaerobic conditions [310]. Thus, the growth of larger *P. aeruginosa* biofilms in mixed cultures may be fueled by metabolic influxes and cross-feeding interactions among the four bacterial species [355], which significantly benefits *P. aeruginosa* biofilm architecture and size.

Using microscopy, I also found that in anaerobic ASM+, *P. aeruginosa* forms both surface-attached biofilms and BLS. A study by Haley et al. reported that in a synthetic mucus medium, which contains mucin and extracellular DNA, *P. aeruginosa* forms BLS that are not surface-attached but suspended within the gelatinous medium [56]. Noticeably, the synthetic mucus medium in the Haley et al. study is also referred to as ASM+, although it differs in composition from the ASM+ media used in this study. For example, diethylene triamine pentaacetic acid, egg yolk emulsion, and casamino acids are not present in my ASM+ preparation, while present in theirs. Nonetheless, the components mucin and DNA found in both media formulations may be the common denominators driving BLS formation [98].

My study's novelty lies in providing evidence of this duality—observing both surface-attached biofilm and BLS simultaneously under identical conditions and experimental setup. Many studies focus on either surface-attached biofilms or non-attached aggregates, and only note the potential for both to coexist in specific setups [56, 57, 356, 357]. However, direct quantification of both structures co-occurring has not, to my knowledge, been demonstrated, as experimental designs often optimize for one phenotype.

The co-occurrence of both phenotypes in the CF polymicrobial assay suggests that physiological and regulatory factors might affect how *P. aeruginosa* develops different biofilm structures. *P. aeruginosa* may produce multiple extracellular polymeric substances (EPS), including alginate, Psl, and Pel polysaccharides, which are differentially regulated under anaerobic conditions. In anaerobic ASM+, *P. aeruginosa* produces BLS with high alginate content [358], contributing to its suspended, gelatinous structure [56]. In contrast, Psl and Type IV pili are critical for surface-attached biofilms, particularly on glass or plastic surfaces, as shown in studies using flow chambers or microscope dishes [97, 359, 360]. In addition, Psl is essential for initial attachment [361, 362], while alginate enhances aggregate stability in anaerobic environments [363], suggesting that *P. aeruginosa* can switch between these EPS types based on environmental cues. Lastly, *P. aeruginosa* biofilms are regulated by several factors, with a major one being the QS system [119, 364]. QS is critical for BLS formation under anaerobic conditions, with Las and Rhl systems regulating alginate and Pel production [56, 365–367]. Lee and Yoon noted that QS-driven heterogeneity allows *P. aeruginosa* to adapt to diverse niches, with surface-attached biofilms requiring Psl and pili [364].

In summary, the ability of *P. aeruginosa* to form both surface-attached biofilms and BLS in anaerobic ASM+ likely results from differential regulation of EPS components, QS systems and surface-specific adhesion. These dual strategies reflect *P. aeruginosa* adaptability to the complex CF lung environment, allowing it to exploit both surface and suspended niches.

Limits and Future Directions

While the findings presented in this chapter offer valuable insights and underscore the intricate interplay between anaerobic conditions, multi-species interactions, and the spatial organization of *P. aeruginosa* biofilms—thereby enhancing our understanding of its behaviour in a CF-like environment—a few limitations must be acknowledged, and numerous questions remain open for future investigation. First, while the crystal violet assay remains a gold standard for quantifying surface-attached biofilms [97, 339, 340], it primarily captures attached biomass and does not detect BLS present as suspended aggregates

under anaerobic conditions in ASM+. The complementary application of confocal microscopy therefore enriched the analysis, offering a more comprehensive view of *P. aeruginosa* biofilm architecture.

Second, the polystyrene microtiter plate or the glass surface of a microscopy dish may not fully mimic the physiological surfaces (e.g., mucus or epithelial cells) encountered in CF lungs, potentially affecting biofilm formation. Indeed, surface chemistry and material properties can influence bacterial attachment and biofilm development [368]. In this case, a mucin-coated surface, as proposed by Landry and colleagues, could enhance the relevance of the findings to *in vivo* infections [98]. In my experimental setup, for example, I could prime the bottom of the microscopy dish with a layer of mucin and add the bacterial culture on top, as I already suggested in the discussion of **Chapter 3**.

Third, while the multi-species context revealed enhanced biofilm formation, I did not explore any mechanistic insight. For instance, what are the main drivers of this phenotype? Are BLS simply surface-attached biofilms that have detached, or can BLS form spontaneously? Are BLS and biofilms structurally similar or different in this context? What is the contribution of each species or specific interactions at play in terms of metabolite exchange or quorum sensing? To address these questions, I could employ a time-lapse microscopy experiment to monitor the formation or appearance of BLS and use computational tools such as Comstat2 and Agent-Based Modelling (ABM). For instance, the structure of BLS could be characterized from 3D imaging data using Comstat2 [100, 369], and the resulting parameters could inform ABM to simulate and interpret the growth dynamics [111, 370].

In addition, I could also use metabolomics or transcriptomics to investigate molecular mechanisms (e.g., quorum sensing, siderophore production) to convey diverse interactions. For metabolomics, mass spectrometry could profile specific classes of metabolites, such as quorum sensing molecules (e.g. acyl-homoserine lactones) and their relative abundance [371]. Initial transcriptomic investigations by Kesthely and colleagues found that the transcriptional profile of *P. aeruginosa* remains relatively unaffected by the presence of other

members of this CF polymicrobial assay [372]. Conversely, the transcriptional profiles of the other community members are affected by one another and by environmental disturbances [372]. Building on these findings, mass spectrometry can zero in on profile-specific proteins expressed in the biofilm, such as those involved in adhesion or EPS synthesis (e.g. alginate synthase).

Lastly, I primarily focused on visual observations, such as the size and volume of the biofilm / BLS biomass. However, functional outcomes like changes in *P. aeruginosa* gene expression, virulence factor production, or antibiotic resistance in anaerobic or multi-species conditions were not investigated. Techniques such as qPCR targeting specific genes of interest could provide insights into these functional changes. In addition, the use of a flow-cell system to simulate the dynamic conditions of the CF lung (e.g., shear stress, nutrient gradients) and longer incubation time to approximate the chronic nature of a CF infection could be implemented. Collectively, these systems can support more complex biofilm structures and provide a better and more comprehensive model for studying anaerobic biofilms and their spatial distribution over time. Finally, *P. aeruginosa* mutants prevalent in CF could also be investigated.

4.6. Conclusions

The newly engineered plasmid pCFT4.2.1, harbouring the fluorescent protein phiLOV2.1 and the VapBC toxin-antitoxin system, was efficiently stabilized in PA14 with more than 90% retention among cells and strong fluorescence over 3 days in non-selective conditions. Moreover, PA14/pCFT4.2.1 is stably maintained in the CF polymicrobial assay and successfully allows the investigation of *P. aeruginosa* biofilm nature and spatial distribution. Interestingly, confocal microscopy imaging revealed that *P. aeruginosa* formed more and larger biofilms in the presence of other bacteria in the assay, namely *S. aureus, S. sanguinis,* and *P. melaninogenica*, than it did in monoculture. Most notably, I demonstrated through microscopy that in anaerobic ASM+, *P. aeruginosa* concurrently forms surface-attached biofilms and BLS.

While this study provides strong evidence of the spatial distribution of *P. aeruginosa* biofilms in mono- versus mixed-cultures and underscores the dual nature of *P. aeruginosa* biofilms in anaerobic ASM+, it is worth acknowledging that these observations are notably phenotypic in nature and no structural, functional or molecular mechanisms were investigated. Instead, my study aimed to serve as a building block for these future investigations. I highlighted how integrating computational methods like transcriptomics, metabolomics, Comstat2, and ABM can further our understanding of *P. aeruginosa* biofilm dynamics and distribution in the CF polymicrobial assay. Additionally, as outlined in **Chapter 3 – Section 3.5**, I proposed modifying mucin delivery by priming the culture surface prior to adding the cell suspension. This approach is intended to enhance experimental uniformity and consistency, and, more importantly, to better replicate the physiological surfaces encountered *in vivo* in CF airways. Finally, I proposed implementing a flow-cell system coupled with an extended incubation period to simulate the dynamic and chronic nature of CF infections more accurately.

To sum up, the findings in this chapter not only deepen our current understanding of *P. aeruginosa* biofilm behaviour but also lay the groundwork for more structural, molecular and functional investigations that could ultimately inform improved therapeutic strategies for CF infections.

4.7. Supplementary materials

Table S4.1: List of primers used in this study

Long name	Primers sequences
Vecteur_TA_fwd	CGCCTACCACCGTCAAAAAAAAC
Vecteur_TA_rev	CGCCTCAATTAGTTACCCTATAGTG
vapBC_fwd	TAGGGTAACTAATTGAGGCGTTCAGCCCCCTGGCCGGC
vapBC_rev	TTTTTTGACGGTGGTAGGCGTCAGCTCCAGTCTTCAGTTCTCAGGCC
pumAB_fwd	TAGGGTAACTAATTGAGGCGTTGAGGCCCCCTTTGATGATG
pumAB_rev	TTTTTTGACGGTGGTAGGCGTCACTGAGCATGCGGGCG
ccdAB_fwd	TAGGGTAACTAATTGAGGCGTGATACCTGCCGTCAGGTG
ccdAB_rev	TTTTTTGACGGTGGTAGGCGTTATATTCCCCAGAACATCAGGTTAATG

Chapter 5: General Conclusion

5.1. Overview

The studies presented in this thesis aimed to fill important gaps in the tools and models used to investigate *P. aeruginosa* under oxygen-limited and polymicrobial conditions, such as those found in cystic fibrosis (CF) airways. By developing new fluorescent reporters, characterizing *P. aeruginosa* deletion mutants and their antibiotic responses in a CF polymicrobial assay and engineering a stable plasmid to examine *P. aeruginosa* biofilm spatial distribution within this same assay, this work offers new tools and insights into *P. aeruginosa* behaviour in a complex CF-relevant environment. This chapter summarises the key findings from **Chapters 2 – 4**, emphasizes their novelty and contributions to the field, and outlines potential directions for future research.

5.2. Integration of Key Findings

The research presented in this thesis integrates three interconnected contributions: 1) the development of fluorescent reporters for monitoring *P. aeruginosa* under low-oxygen conditions, 2) the application of a validated anaerobic, polymicrobial CF model system to investigate the persistence and antibiotic response of *P. aeruginosa* deletion mutants, and 3) the construction and validation of a stable, antibiotic-independent plasmid system enabling fluorescent microscopy investigation of *P. aeruginosa* biofilm spatial distribution in a CF polymicrobial context.

Chapter 2 addressed the need for suitable fluorescent tools capable of functioning in hypoxic environments, which *P. aeruginosa* commonly encounters in biofilms and *in vivo* during chronic infections. The toolbox comprises eleven plasmids encoding eight different fluorescent proteins; six of which were previously shown to function under anaerobic conditions in other cellular systems. My work has specifically demonstrated the suitability of these fluorescent proteins to track *P. aeruginosa*. Furthermore, the implementation of phiLOV2.1 and FAST-based reporters offers a solution for dual-imaging of *P. aeruginosa* subpopulations in fluorescence microscopy. Importantly, these reporters were incorporated into a broad-host-range vector, facilitating their potential application across multiple Gram-negative species inhabiting similar ecological niches. This represents a significant technical

advancement, enabling more accurate investigations of bacterial activity in low-oxygen environments such as the CF airway.

Chapter 3 implemented a CF polymicrobial assay developed by Jean-Pierre et al. [199], composed of *P. aeruginosa*, *Staphylococcus aureus*, *Streptococcus sanguinis*, and *Prevotella melaninogenica,* cultured under anaerobic conditions. I successfully validated the assay with PA14 WT and used it to assess the persistence and tobramycin susceptibility under anaerobic conditions of six *P. aeruginosa* deletion mutant strains—Δ*ndvB,* Δ*PA1874-77,* Δ*tssC1,* Δ*tctED,* Δ*PA1759-60* and Δ*flgK*. These mutants have been previously associated with antibiotic resistance in *P. aeruginosa* in aerobic monoculture studies, and Δ*flgK* mutants are prevalent in CF lung infections. The results revealed that all the mutants evaluated could persist in the polymicrobial community. In addition, their susceptibility profiles to tobramycin mirrored that of the wild type strain when grown as biofilms, with more divergent profiles in planktonic cultures. Notably, the Δ*tctED* mutant emerged as a distinct outlier, exhibiting a markedly enhanced susceptibility to tobramycin relative to the wild type in biofilm cultures. Although the other deletion mutants did not reproduce the susceptibility phenotypes reported in aerobic monoculture studies, their roles in antibiotic resistance remain relevant given the diversity of CF infection environments. The pronounced susceptibility of Δ*tctED* under a broader array of experimental conditions reinforces the role of *tctED* as a biofilm-specific antibiotic resistance gene, warranting further investigation. Overall, the findings in this chapter underscore the importance of studying antimicrobial responses within a clinically relevant model, as interspecies interactions and environmental conditions can significantly influence bacterial behaviour.

Chapter 4 brings together the previous two chapters by expanding the fluorescent reporter repertoire with an engineered stable, antibiotic-independent plasmid and using it to investigate the nature and distribution of *P. aeruginosa* biofilm in the CF polymicrobial assay. The new plasmid pCT4.2.1, which encodes the oxygen-independent fluorescent protein phiLOV2.1 and the toxin-antitoxin system VapBC, was shown to be stably maintained in PA14 under non-selective conditions for at least five days, with high levels of fluorescence detectable for at least three days. The PA14/pCFT4.2.1 reporter strain remained stable in the

CF polymicrobial assay, achieving comparable colony forming units (CFU) counts in mono- and mixed-cultures. Notably, in this assay, *P. aeruginosa* formed more extensive surface-attached biofilms in mixed- compared to mono-cultures in the artificial sputum medium prepared with mucin (ASM+) under anaerobic conditions. More importantly, both surface-attached biofilms and biofilm-like structures (BLS) were simultaneously observed in this experimental setting. These findings highlight the complexity of *P. aeruginosa* biofilms and the role of interspecies interactions in modulating biofilm architecture, offering new insights into the dynamics of polymicrobial infections in low-oxygen conditions. Additionally, the plasmid pCFT4.2.1 enables numerous innovative research opportunities in *P. aeruginosa* and other bacterial species.

5.3. Contribution to the Field

This thesis provides several novel contributions to the study of *P. aeruginosa* and polymicrobial infections in CF. The development and validation of oxygen-independent fluorescent tools represent a valuable contribution to the field, addressing a major limitation in studying gene expression and localization in anaerobic or hypoxic environments. These tools have broad applicability, not only to *P. aeruginosa* research but also to other Gram-negative pathogens inhabiting oxygen-limited niches. The plasmids generated in **Chapter 2** were deposited in Addgene's repository, attracting interest from scientists in the USA, the UK, Belgium and Japan, who subsequently ordered them **(Supplementary Table S5.1)**. Moreover, among these plasmids, pCFT4.2 was further engineered to derive pCFT4.2.1. The pCFT4.2.1 plasmid, with its phiLOV2.1 and VapBC components, achieves stability in *P. aeruginosa* without antibiotic pressure in a polymicrobial community. This addresses the challenge in genetic manipulation in bacteria for studies aiming to mimic natural infection settings more closely, where constant antibiotic selection pressure is unrealistic.

The successful adaptation of an anaerobic CF polymicrobial assay provides a standardized, reproducible model for studying *P. aeruginosa* in a CF-relevant context. The assessment of mutant strains and their tobramycin susceptibility profiles in this setting offers new data on how polymicrobial interactions influence antibiotic efficacy. This work adds to a growing body of literature demonstrating that bacterial behaviour in monoculture

does not necessarily predict outcomes in complex microbial communities. By integrating fitness and antibiotic susceptibility assays into this model, I have shown that polymicrobial contexts can significantly modulate antibiotic response and biofilm dynamics.

Lastly, the dual advantages of fluorescence and stability offered by pCFT4.2.1 allow the observation of enhanced biofilm formation in mixed cultures, along with the coexistence of surface-attached biofilms and BLS in the same CF polymicrobial assay. This provides novel evidence of how interspecies interactions shape *P. aeruginosa* biofilm architecture in CF-like conditions. Ultimately, this has implications for understanding chronic infection persistence and designing targeted therapies.

Collectively, these contributions advance the methodological and conceptual frameworks for studying *P. aeruginosa* in polymicrobial, low-oxygen settings, with direct relevance to CF and other chronic infections.

5.4. Limitations of the Study and Future Directions

While this study offers various fluorescent proteins as an alternative to GFP and provides compelling evidence of their functionality in *P. aeruginosa* under hypoxic and anoxic conditions, their low brightness remains a conundrum. Brighter oxygen-independent fluorescent proteins are a matter of active investigation [277, 278] and will undoubtedly leverage the ability to track *P. aeruginosa* in increasingly complex experimental settings. Moreover, the stable antibiotic-independent plasmid pCFT4.2.1 could be further engineered to also be stable in other bacterial hosts to broaden its applicability.

In this study, the CF polymicrobial assay designed by Jean-Pierre et al. [199] was implemented to examine the growth dynamics of *P. aeruginosa* in anaerobic ASM+, both as a mono- and as a mixed-culture composed of *S. aureus*, *S. sanguinis* and *P. melaninogenica*. In this assay, the CFU counts are expected to remain relatively stable across culture conditions for all species, except *P. melaninogenica*, which is expected to exhibit reduced CF counts in the mixed culture compared to other species, and notably, no CFU count as a monoculture. However, working with mucin has represented a challenge on its own. The first obstacle I encountered was the spontaneous growth of *P. melaninogenica* as a monoculture

in ASM+, whereas multiple studies reported the opposite [199, 310, 311]. Two potential explanations for this discrepancy were proposed. First, the variability in the composition of mucin powder sourced from different suppliers may influence growth outcomes. Second, the current sterilization protocol, which relies exclusively on autoclaving, may require revision to better preserve or control the properties of mucin relevant to *P. melaninogenica* growth.

Another difficulty I found with mucin was the inconsistency in my tobramycin susceptibility assay, likely attributable to a batch effect. As a mitigating solution, meticulous attention to preparation protocols, strict consistency across batches and multiple biological replicates were employed to ensure reproducible results. As I progressed through the experiments, I also found fluorescent artifacts of mucin during microscopy experiments. This issue was addressed by optimizing cleaning steps to eliminate mucin residues before imaging. An alternative strategy in using mucin, proposed by Landry and colleagues [98], involves coating the culture surface with mucin before introducing the cell culture. Interestingly, this method is a promising approach to enhance experimental uniformity and consistency of *P. aeruginosa* observations in ASM+. In addition, this may mimic more closely the coating of lung tissue by mucins that are characteristic of CF airways *in vivo* [373–375].

Although the *in vitro* CF polymicrobial assay mimics several features of the CF airway environment, it does not incorporate host immune factors or tissue structures, which play critical roles in bacterial responses to antibiotics. Therefore, future iterations of this assay could incorporate these essential components. In addition, the studies conducted with the CF polymicrobial assay described in this thesis do not support simultaneous tracking of different *P. aeruginosa* strains, which is a common occurrence in the CF airways [330–335]. In this aspect, switching the current readout from CFU to fluorescence and using the fluorescent reporters from **Chapter 2** could address this limitation. Lastly, continually improving the experimental model to approximate the dynamic and chronic nature of CF infections by integrating a flow-cell system with an extended incubation period would further enhance the clinical relevance of prospective findings.

Overall, the work presented in this thesis is foundational to future investigations. For instance, the emergence of *tctED* as a potential target in combating antibiotic resistance in *P. aeruginosa* opens avenues for exploring its regulatory pathways and specific molecular mechanisms under anaerobic conditions and within a polymicrobial context. Similarly, the characterization of *P. aeruginosa* biofilm spatial distribution under these conditions could be expanded through transcriptomics, proteomics, metabolomics and their combination with targeted studies on the functional and molecular determinants underlying biofilm/BLS formation, structural organization, and associated interspecies interactions. In particular, elucidating the role of BLS in infection persistence could provide valuable insights for the development of novel therapeutic strategies. Furthermore, the observation of *P. aeruginosa* enhanced biofilm formation in mixed cultures warrants deeper investigations into the molecular mechanisms involved, including quorum sensing, metabolic cooperation, or physical co-aggregation. The enhanced biofilm observed also suggests that interspecies interactions may reduce antibiotic efficacy. Consequently, future studies could assess combination therapies targeting multiple species or disrupting biofilm architecture, using the CF polymicrobial assay as a screening platform.

5.5. Conclusion

This thesis has developed and applied novel tools to study *P. aeruginosa* in low-oxygen, polymicrobial environments, providing new insights into its behaviour in CF-like conditions. The constructed fluorescent reporters supplemented with an engineered stable plasmid system, the validated and implemented CF polymicrobial assay, in addition to examining *P. aeruginosa* deletion mutants fitness and antibiotic susceptibility, and the observations made of biofilm dynamics, collectively enhance our understanding of chronic infections and offer a foundation for future research. By addressing methodological challenges and uncovering the impact of interspecies interactions, this work contributes to advancing our ability to model, track, and understand the behaviour of *P. aeruginosa* within the challenging environments of chronic polymicrobial infections like CF. The proposed future directions will further leverage these advancements to deepen our understanding of microbial

pathogenesis and antibiotic resistance, ultimately benefiting patients with chronic respiratory infections.

5.6. Supplementary materials

Table S5.1: List of Addgene requests for the plasmids generated in Chapter 2

Addgene ID	Material	Requesting Principal Investigator	Requesting Organization	Requesting Country	Date Ordered
208807	pCFT4.2	Feng Zhang	Broad Institute	UNITED STATES	07/11/2025
208807	pCFT4.2	Evangelos Giampazolias	University of Manchester	UNITED KINGDOM	04/28/2025
208807	pCFT4.2	Sean Nair	University College London	UNITED KINGDOM	08/07/2024
208807	pCFT4.2	Sander Govers	Katholieke Universiteit Leuven	BELGIUM	05/07/2024
208807	pCFT4.2	Martin Robert	Kyoto University, Graduate School of Pharmaceutical Sciences	JAPAN	01/13/2024
208808	pCFT7.2	Martin Robert	Kyoto University, Graduate School of Pharmaceutical Sciences	JAPAN	01/13/2024

References

1. **Greenberg EP**. Pump up the versatility. *Nature* 2000;406:947–948.

2. **McCarthy M**. *Pseudomonas* genome reveals a formidable foe. *The Lancet* 2000;356:918.

3. **Arai H**. Regulation and Function of Versatile Aerobic and Anaerobic Respiratory Metabolism in *Pseudomonas aeruginosa*. *Front Microbiol* 2011;2:103.

4. **Zumft WG**. Cell biology and molecular basis of denitrification. *Microbiol Mol Biol Rev* 1997;61:533–616.

5. **Shapleigh JP**. Denitrifying Prokaryotes. In: Rosenberg E, DeLong EF, Lory S, Stackebrandt E, Thompson F (editors). *The Prokaryotes: Prokaryotic Physiology and Biochemistry*. Berlin, Heidelberg: Springer. pp. 405–425.

6. **Eschbach M, Schreiber K, Trunk K, Buer J, Jahn D, *et al.*** Long-Term Anaerobic Survival of the Opportunistic Pathogen *Pseudomonas aeruginosa* via Pyruvate Fermentation. *J Bacteriol* 2004;186:4596–4604.

7. **LaBauve AE, Wargo MJ**. Growth and Laboratory Maintenance of *Pseudomonas aeruginosa*. *Curr Protoc Microbiol* 2012;0 6:Unit-6E.1.

8. **Chauhan M, Kimothi A, Sharma A, Pandey A**. Cold adapted *Pseudomonas*: ecology to biotechnology. *Front Microbiol* 2023;14. DOI: 10.3389/fmicb.2023.1218708.

9. **Bodey GP, Bolivar R, Fainstein V, Jadeja L**. Infections Caused by *Pseudomonas aeruginosa*. *Clinical Infectious Diseases* 1983;5:279–313.

10. **Qin S, Xiao W, Zhou C, Pu Q, Deng X, *et al.*** *Pseudomonas aeruginosa*: pathogenesis, virulence factors, antibiotic resistance, interaction with host, technology advances and emerging therapeutics. *Signal Transduct Target Ther* 2022;7:199.

11. **Reynolds D, Kollef M**. The Epidemiology and Pathogenesis and Treatment of *Pseudomonas aeruginosa* Infections: An Update. *Drugs* 2021;81:2117–2131.

12. **Pang Z, Raudonis R, Glick BR, Lin T-J, Cheng Z**. Antibiotic resistance in *Pseudomonas aeruginosa*: mechanisms and alternative therapeutic strategies. *Biotechnology Advances* 2019;37:177–192.

13. **Lyczak JB, Cannon CL, Pier GB**. Lung infections associated with cystic fibrosis. *Clinical microbiology reviews* 2002;15:194–222.

14. **Lyczak JB, Cannon CL, Pier GB**. Establishment of *Pseudomonas aeruginosa* infection: lessons from a versatile opportunist1. *Microbes and Infection* 2000;2:1051–1060.

15. **Elmassry MM, Mudaliar NS, Colmer-Hamood JA, San Francisco MJ, Griswold JA, *et al.*** New markers for sepsis caused by *Pseudomonas aeruginosa* during burn infection. *Metabolomics* 2020;16:40.

16. **Mohan MS, Salim SA, Forgia N, Busi S**. *Pseudomonas aeruginosa* Virulence Factors and Biofilm Components: Synthesis, Structure, Function and Inhibitors. In: Busi S, Prasad R (editors). *ESKAPE Pathogens: Detection, Mechanisms and Treatment Strategies*. Singapore: *Springer Nature*. 2024. pp. 317–347.

17. **Zhang X, Zhang D, Zhou D, Zheng S, Li S, *et al.*** A comprehensive review of the pathogenic mechanisms of *Pseudomonas aeruginosa*: synergistic effects of virulence factors, quorum sensing, and biofilm formation. *Front Microbiol* 2025;16. DOI: 10.3389/fmicb.2025.1619626.

18. **Jurado-Martín I, Sainz-Mejías M, McClean S**. *Pseudomonas aeruginosa*: An audacious pathogen with an adaptable arsenal of virulence factors. *International Journal of Molecular Sciences* 2021;22:1–37.

19. **Azam MW, Khan AU**. Updates on the pathogenicity status of *Pseudomonas aeruginosa*. *Drug Discovery Today* 2019;24:350–359.

20. **Perraud Q, Kuhn L, Fritsch S, Graulier G, Gasser V, *et al.*** Opportunistic use of catecholamine neurotransmitters as siderophores to access iron by *Pseudomonas aeruginosa*. *Environmental Microbiology* 2022;24:878–893.

21. **Cornelis GR**. The type III secretion injectisome, a complex nanomachine for intracellular 'toxin' delivery. *Biol Chem* 2010;391:745–751.

22. **Sato H, Frank DW, Hillard CJ, Feix JB, Pankhaniya RR, *et al.*** The mechanism of action of the *Pseudomonas aeruginosa*-encoded type III cytotoxin, ExoU. *EMBO J* 2003;22:2959–2969.

23. **Liao C, Huang X, Wang Q, Yao D, Lu W**. Virulence Factors of *Pseudomonas aeruginosa* and Antivirulence Strategies to Combat Its Drug Resistance. *Front Cell Infect Microbiol* 2022;12. DOI: 10.3389/fcimb.2022.926758.

24. **Hauser AR**. The type III secretion system of *Pseudomonas aeruginosa*: infection by injection. *Nat Rev Microbiol* 2009;7:654–665.

25. **Jurado-Martín I, Sainz-Mejías M, McClean S**. *Pseudomonas aeruginosa*: An audacious pathogen with an adaptable arsenal of virulence factors. *International Journal of Molecular Sciences* 2021;22:1–37.

26. **Tuon FF, Dantas LR, Suss PH, Tasca Ribeiro VS**. Pathogenesis of the *Pseudomonas aeruginosa* Biofilm: A Review. *Pathogens* 2022;11:300.

27. **Lee J, Zhang L**. The hierarchy quorum sensing network in *Pseudomonas aeruginosa*. *Protein Cell* 2015;6:26–41.

28. **Stacey SD, Williams DA, Pritchett CL**. The *Pseudomonas aeruginosa* Two-Component Regulator AlgR Directly Activates rsmA Expression in a Phosphorylation-Independent Manner. *J Bacteriol* 2017;199:e00048-17.

29. **Sultan M, Arya R, Kim KK**. Roles of Two-Component Systems in *Pseudomonas aeruginosa* Virulence. *Int J Mol Sci* 2021;22:12152.

30. **Gooderham WJ, Hancock REW**. Regulation of virulence and antibiotic resistance by two-component regulatory systems in *Pseudomonas aeruginosa*. *FEMS Microbiol Rev* 2009;33:279–294.

31. **Francis VI, Stevenson EC, Porter SL**. Two-component systems required for virulence in *Pseudomonas aeruginosa*. *FEMS Microbiol Lett* 2017;364:fnx104.

32. **Roy R, Tiwari M, Donelli G, Tiwari V**. Strategies for combating bacterial biofilms: A focus on anti-biofilm agents and their mechanisms of action. *Virulence* 2017;9:522–554.

33. **Shree P, Singh CK, Sodhi KK, Surya JN, Singh DK**. Biofilms: Understanding the structure and contribution towards bacterial resistance in antibiotics. *Medicine in Microecology* 2023;16:100084.

34. **Bais HP, Fall R, Vivanco JM**. Biocontrol of Bacillus subtilis against Infection of Arabidopsis Roots by *Pseudomonas* syringae Is Facilitated by Biofilm Formation and Surfactin Production. *Plant Physiol* 2004;134:307–319.

35. **Buret AG, Allain T**. Gut microbiota biofilms: From regulatory mechanisms to therapeutic targets. *J Exp Med* 2023;220:e20221743.

36. **Saini S, Tewari S, Dwivedi J, Sharma V**. Biofilm-mediated wastewater treatment: a comprehensive review. *Mater Adv* 2023;4:1415–1443.

37. **O'Toole GA, Kaplan HB, Kolter R**. Biofilm Formation as Microbial Development. *Annual Review of Microbiology* 2000;54:49–79.

38. **Fernández-Billón M, Llambías-Cabot AE, Jordana-Lluch E, Oliver A, Macià MD**. Mechanisms of antibiotic resistance in *Pseudomonas aeruginosa* biofilms. *Biofilm* 2023;5:100129.

39. **Mah T-F**. Biofilm-specific antibiotic resistance. *Future Microbiology* 2012;7:1061–1072.

40. **Mah T-F, Pitts B, Pellock B, Walker GC, Stewart PS, *et al.*** A genetic basis for *Pseudomonas aeruginosa* biofilm antibiotic resistance. *Letters to Nature* 2003;426:1–5.

41. **Behzadi P, Gajdács M, Pallós P, Ónodi B, Stájer A, *et al.*** Relationship between Biofilm-Formation, Phenotypic Virulence Factors and Antibiotic Resistance in Environmental *Pseudomonas aeruginosa*. *Pathogens* 2022;11:1015.

42. **Ramesh R, Rekha ND, Gopal S**. *Pseudomonas aeruginosa* biofilm: treatment strategies to combat infection. *Arch Microbiol* 2025;207:141.

43. **Vohra M, Kamath N, Dubey R, Sharma S, Sharma S**. Complex Interplay between Biofilm Formation, Antibiotic Resistance, and Virulence in *Pseudomonas aeruginosa*: A Phenotypic and Genotypic Study. *Mol Genet Microbiol Virol* 2025;40:61–74.

44. **Haidar A, Muazzam A, Nadeem A, Atique R, Saeed HA, *et al.*** Biofilm formation and antibiotic resistance in *Pseudomonas aeruginosa*. *The Microbe* 2024;3:100078.

45. **Sauer K, Camper AK, Ehrlich GD, Costerton JW, Davies DG**. *Pseudomonas aeruginosa* Displays Multiple Phenotypes during Development as a Biofilm. *J Bacteriol* 2002;184:1140–1154.

46. **Valentini M, Filloux A**. Biofilms and Cyclic di-GMP (c-di-GMP) Signaling: Lessons from *Pseudomonas aeruginosa* and Other Bacteria. *J Biol Chem* 2016;291:12547–12555.

47. **Römling U, Galperin MY, Gomelsky M**. Cyclic di-GMP: the first 25 years of a universal bacterial second messenger. *Microbiol Mol Biol Rev* 2013;77:1–52.

48. **Petrova OE, Sauer K**. A Novel Signaling Network Essential for Regulating *Pseudomonas aeruginosa* Biofilm Development. *PLOS Pathogens* 2009;5:e1000668.

49. **Petrova OE, Gupta K, Liao J, Goodwine JS, Sauer K**. Divide and conquer: The *Pseudomonas aeruginosa* two-component hybrid SagS enables biofilm formation and recalcitrance of biofilm cells to antimicrobial agents via distinct regulatory circuits. *Environ Microbiol* 2017;19:2005–2024.

50. **Yoon MY, Lee KM, Park Y, Yoon SS**. Contribution of cell elongation to the biofilm formation of *Pseudomonas aeruginosa* during anaerobic respiration. *PLoS ONE* 2011;6. DOI: 10.1371/JOURNAL.PONE.0016105.

51. **Walters MC, Roe F, Bugnicourt A, Franklin MJ, Stewart PS**. Contributions of antibiotic penetration, oxygen limitation, and low metabolic activity to tolerance of *Pseudomonas aeruginosa* biofilms to ciprofloxacin and tobramycin. *Antimicrob Agents Chemother* 2003;47:317–323.

52. **Høiby N, Bjarnsholt T, Givskov M, Molin S, Ciofu O**. Antibiotic resistance of bacterial biofilms. *Int J Antimicrob Agents* 2010;35:322–332.

53. **Sionov RV, Steinberg D**. Targeting the Holy Triangle of Quorum Sensing, Biofilm Formation, and Antibiotic Resistance in Pathogenic Bacteria. *Microorganisms* 2022;10:1239.

54. **Schaible B, Rodriguez J, Garcia A, von Kriegsheim A, McClean S, *et al*.** Hypoxia Reduces the Pathogenicity of *Pseudomonas aeruginosa* by Decreasing the Expression of Multiple Virulence Factors. *The Journal of Infectious Diseases* 2017;215:1459–1467.

55. **Chung JCS, Rzhepishevska O, Ramstedt M, Welch M**. Type III secretion system expression in oxygen-limited *Pseudomonas aeruginosa* cultures is stimulated by isocitrate lyase activity. *Open Biol* 2013;3:120131.

56. **Haley CL, Colmer-Hamood JA, Hamood AN**. Characterization of biofilm-like structures formed by *Pseudomonas aeruginosa* in a synthetic mucus medium. *BMC microbiology* 2012;12:181.

57. **Alhede M, Kragh KN, Qvortrup K, Allesen-Holm M, Gennip M van, *et al*.** Phenotypes of Non-Attached *Pseudomonas aeruginosa* Aggregates Resemble Surface Attached Biofilm. *PLOS ONE* 2011;6:e27943.

58. **Passow U**. Transparent exopolymer particles (TEP) in aquatic environments. *Progress in Oceanography* 2002;55:287–333.

59. **Busch K, Endres S, Iversen MH, Michels J, Nöthig E-M, *et al*.** Bacterial Colonization and Vertical Distribution of Marine Gel Particles (TEP and CSP) in the Arctic Fram Strait. *Front Mar Sci* 2017;4. DOI: 10.3389/fmars.2017.00166.

60. **Zäncker B, Engel A, Cunliffe M**. Bacterial communities associated with individual transparent exopolymer particles (TEP). *Journal of Plankton Research* 2019;41:561–565.

61. **Cai YM**. Non-surface Attached Bacterial Aggregates: A Ubiquitous Third Lifestyle. *Frontiers in Microbiology* 2020;11:3106.

62. **Bjarnsholt T, Jensen PØ, Fiandaca MJ, Pedersen J, Hansen CR, *et al*.** *Pseudomonas aeruginosa* biofilms in the respiratory tract of cystic fibrosis patients. *Pediatric Pulmonology* 2009;44:547–558.

63. **Bjarnsholt T, Alhede M, Alhede M, Eickhardt-Sørensen SR, Moser C, *et al*.** The *in vivo* biofilm. *Trends Microbiol* 2013;21:466–474.

64. **Secor PR, Michaels LA, Ratjen A, Jennings LK, Singh PK**. Entropically driven aggregation of bacteria by host polymers promotes antibiotic tolerance in *Pseudomonas aeruginosa*. *Proceedings of the National Academy of Sciences* 2018;115:10780–10785.

65. **Kragh KN, Tolker-Nielsen T, Lichtenberg M**. The non-attached biofilm aggregate. *Commun Biol* 2023;6:898.

66. **Sauer K, Stoodley P, Goeres DM, Hall-Stoodley L, Burmølle M, *et al*.** The biofilm life cycle: expanding the conceptual model of biofilm formation. *Nat Rev Microbiol* 2022;20:608–620.

67. **Møller SA, Jensen PØ, Høiby N, Ciofu O, Kragh KN, *et al*.** Hyperbaric oxygen treatment increases killing of aggregating *Pseudomonas aeruginosa* isolates from cystic fibrosis patients. *Journal of Cystic Fibrosis* 2019;18:657–664.

68. **Reyne N, McCarron A, Cmielewski P, Parsons D, Donnelley M**. To bead or not to bead: A review of *Pseudomonas aeruginosa* lung infection models for cystic fibrosis. *Frontiers in Physiology* 2023;14. DOI: 10.3389/fphys.2023.1104856.

69. **D'Costa VM, McGrann KM, Hughes DW, Wright GD**. Sampling the Antibiotic Resistome. *Science* 2006;311:374–377.

70. **Giovagnorio F, De Vito A, Madeddu G, Parisi SG, Geremia N**. Resistance in *Pseudomonas aeruginosa*: A Narrative Review of Antibiogram Interpretation and Emerging Treatments. *Antibiotics* 2023;12:1621.

71. **Lorusso AB, Carrara JA, Barroso CDN, Tuon FF, Faoro H**. Role of Efflux Pumps on Antimicrobial Resistance in *Pseudomonas aeruginosa*. *Int J Mol Sci* 2022;23:15779.

72. **Li X-Z, Plésiat P**. Antimicrobial Drug Efflux Pumps in *Pseudomonas aeruginosa*. In: Li X-Z, Elkins CA, Zgurskaya HI (editors). *Efflux-Mediated Antimicrobial Resistance in Bacteria: Mechanisms, Regulation and Clinical Implications*. Cham: Springer International Publishing. 2016. pp. 359–400.

73. **Yu X-Q, Yang H, Feng H-Z, Hou J, Tian J-Q, *et al*.** Targeting efflux pumps prevents the multi-step evolution of high-level resistance to fluoroquinolone in *Pseudomonas aeruginosa*. *Microbiology Spectrum* 2025;0:e02981-24.

74. **Elfadadny A, Ragab RF, AlHarbi M, Badshah F, Ibáñez-Arancibia E, *et al*.** Antimicrobial resistance of *Pseudomonas aeruginosa*: navigating clinical impacts, current resistance trends, and innovations in breaking therapies. *Front Microbiol* 2024;15. DOI: 10.3389/fmicb.2024.1374466.

75. **Wagner VE, Iglewski BH**. *P. aeruginosa* Biofilms in CF Infection. *Clinical Reviews in Allergy & Immunology* 2008;35:124–134.

76. **Zhang L, Mah TF**. Involvement of a novel efflux system in biofilm-specific resistance to antibiotics. *Journal of Bacteriology* 2008;190:4447–4452.

77. **Zhang L, Hinz AJ, Nadeau JP, Mah T-F**. *Pseudomonas aeruginosa tssC1* links type VI secretion and biofilm-specific antibiotic resistance. *Journal of Bacteriology* 2011;193:5510–5513.

78. **Zhang L, Fritsch M, Hammond L, Landreville R, Slatculescu C, *et al*.** Identification of Genes Involved in *Pseudomonas aeruginosa* Biofilm-Specific Resistance to Antibiotics. *PLoS ONE* 2013;8:2–9.

79. **de la Fuente-Núñez C, Reffuveille F, Fernández L, Hancock RE**. Bacterial biofilm development as a multicellular adaptation: antibiotic resistance and new therapeutic strategies. *Current Opinion in Microbiology* 2013;16:580–589.

80. **Hoyle BD, Costerton JW**. Bacterial resistance to antibiotics: the role of biofilms. *Prog Drug Res* 1991;37:91–105.

81. **Tseng BS, Zhang W, Harrison JJ, Quach TP, Song JL, *et al*.** The extracellular matrix protects *Pseudomonas aeruginosa* biofilms by limiting the penetration of tobramycin. *Environ Microbiol* 2013;15:2865–2878.

82. **Leid JG, Willson CJ, Shirtliff ME, Hassett DJ, Parsek MR, *et al*.** The Exopolysaccharide Alginate Protects *Pseudomonas aeruginosa* Biofilm Bacteria from IFN-γ-Mediated Macrophage Killing. *The Journal of Immunology* 2005;175:7512–7518.

83. **Flemming H-C, Wingender J**. The biofilm matrix. *Nat Rev Microbiol* 2010;8:623–633.

84. **Costerton JW, Stewart PS, Greenberg EP**. Bacterial biofilms: a common cause of persistent infections. *Science* 1999;284:1318–1322.

85. **Soares A, Alexandre K, Etienne M**. Tolerance and Persistence of *Pseudomonas aeruginosa* in Biofilms Exposed to Antibiotics: Molecular Mechanisms, Antibiotic Strategies and Therapeutic Perspectives. *Front Microbiol* 2020;11. DOI: 10.3389/fmicb.2020.02057.

86. **Fernández-Billón M, Llambías-Cabot AE, Jordana-Lluch E, Oliver A, Macià MD**. Mechanisms of antibiotic resistance in *Pseudomonas aeruginosa* biofilms. *Biofilm* 2023;5:100129.

87. **Olsen I**. Biofilm-specific antibiotic tolerance and resistance. *Eur J Clin Microbiol Infect Dis* 2015;34:877–886.

88. **Liao J, Schurr MJ, Sauer K**. The MerR-like regulator BrlR confers biofilm tolerance by activating multidrug efflux pumps in *Pseudomonas aeruginosa* biofilms. *J Bacteriol* 2013;195:3352–3363.

89. **Taylor PK, Zhang L, Mah T-F**. Loss of the Two-Component System TctD-TctE in *Pseudomonas aeruginosa* Affects Biofilm Formation and Aminoglycoside Susceptibility in Response to Citric Acid. *mSphere* 2019;4. DOI: 10.1128/mSphere.00102-19.

90. **Hall CW, Mah T-F**. Molecular mechanisms of biofilm-based antibiotic resistance and tolerance in pathogenic bacteria. *FEMS Microbiology Reviews* 2017;41:276–301.

91. **Beaudoin T, Zhang L, Hinz AJ, Parr CJ, Mah T-F**. The biofilm-specific antibiotic resistance gene ndvB is important for expression of ethanol oxidation genes in *Pseudomonas aeruginosa* biofilms. *Journal of Bacteriology* 2012;194:3128–3136.

92. **Van Acker H, Coenye T**. The Role of Reactive Oxygen Species in Antibiotic-Mediated Killing of Bacteria. *Trends Microbiol* 2017;25:456–466.

93. **Dötsch A, Eckweiler D, Schniederjans M, Zimmermann A, Jensen V, *et al*.** The *Pseudomonas aeruginosa* Transcriptome in Planktonic Cultures and Static Biofilms Using RNA Sequencing. *PLoS ONE* 2012;7:e31092.

94. **Poudyal B, Sauer K**. The ABC of Biofilm Drug Tolerance: the MerR-Like Regulator BrlR Is an Activator of ABC Transport Systems, with PA1874-77 Contributing to the Tolerance of *Pseudomonas aeruginosa* Biofilms to Tobramycin. *Antimicrob Agents Chemother* 2018;62:e01981-17.

95. **Allsopp LP, Bernal P**. Killing in the name of: T6SS structure and effector diversity. *Microbiology* 2023;169:001367.

96. **Burian H**. *Characterization of Anaerobic Growth and Biofilm Formation in Pseudomonas aeruginosa Mutant Strain Lacking Genes PA1759 and PA1760*. Université d'Ottawa / University of Ottawa. http://hdl.handle.net/10393/50097 (2025, accessed 29 July 2025).

97. **O'Toole GA, Kolter R**. Flagellar and twitching motility are necessary for *Pseudomonas aeruginosa* biofilm development. *Molecular Microbiology* 1998;30:295–304.

98. **Landry RM, Dingding A, Hupp JT, Singh PK, Parsek MR**. Mucin-*Pseudomonas aeruginosa* interactions promote biofilm formation and antibiotic resistance. *Molecular Microbiology* 2006;59:142–151.

99. **Valentin JDP, Straub H, Pietsch F, Lemare M, Ahrens CH, *et al*.** Role of the flagellar hook in the structural development and antibiotic tolerance of *Pseudomonas aeruginosa* biofilms. *The ISME Journal 2021* 2021;1–11.

100. **Cleaver L, Garnett JA**. How to study biofilms: technological advancements in clinical biofilm research. *Front Cell Infect Microbiol* 2023;13:1335389.

101. **Yang Z, Khan SA, Walsh LJ, Ziora ZM, Seneviratne CJ**. Classical and Modern Models for Biofilm Studies: A Comprehensive Review. *Antibiotics* 2024;13:1228.

102. **Mir DH, Rather MA**. Advantages and Limitations of the Biofilm Study Methods. *Appl Biochem Microbiol* 2024;60:264–279.

103. **Davey ME, O'Toole GA**. Microbial Biofilms: from Ecology to Molecular Genetics. *Microbiol Mol Biol Rev* 2000;64:847–867.

104. **Madsen JS, Burmølle M, Hansen LH, Sørensen SJ**. The interconnection between biofilm formation and horizontal gene transfer. *FEMS Immunology & Medical Microbiology* 2012;65:183–195.

105. **Joo H-S, Otto M**. Molecular Basis of *In vivo* Biofilm Formation by Bacterial Pathogens. *Chemistry & Biology* 2012;19:1503–1513.

106. **Pantanella F, Valenti P, Natalizi T, Passeri D, Berlutti F**. Analytical techniques to study microbial biofilm on abiotic surfaces: pros and cons of the main techniques currently in use. *Ann Ig* 2013;25:31–42.

107. **Abushahba F, Algahawi A, Areid N, Vallittu PK, Närhi T**. Efficacy of biofilm decontamination methods of dental implant surfaces: A systematic review of in vitro studies. *Eur J Oral Sci* 2025;e70005.

108. **Li C, Xin W**. Different Disinfection Strategies in Bacterial and Biofilm Contamination on Dental Unit Waterlines: A Systematic Review. *Int J Dent Hyg* 2025. DOI: 10.1111/idh.12899.

109. **Grobas I, Bazzoli DG, Asally M**. Biofilm and swarming emergent behaviours controlled through the aid of biophysical understanding and tools. *Biochem Soc Trans* 2020;48:2903–2913.

110. **Seneviratne CJ, Suriyanarayanan T, Widyarman AS, Lee LS, Lau M, *et al*.** Multi-omics tools for studying microbial biofilms: current perspectives and future directions. *Crit Rev Microbiol* 2020;46:759–778.

111. **Koshy-Chenthittayil S, Archambault L, Senthilkumar D, Laubenbacher R, Mendes P, *et al*.** Agent Based Models of Polymicrobial Biofilms and the Microbiome—A Review. *Microorganisms* 2021;9:417.

112. **Lee JW, Jeong S-Y, Kim TG**. Epifluorescence Microscopy with Image Analysis as a Promising Method for Multispecies Biofilm Quantification. *J Microbiol Biotechnol* 2023;33:348–355.

113. **Sugimoto S, Okuda K, Miyakawa R, Sato M, Arita-Morioka K, *et al.*** Imaging of bacterial multicellular behaviour in biofilms in liquid by atmospheric scanning electron microscopy. *Sci Rep* 2016;6:25889.

114. **Chalfie M, Tu Y, Euskirchen G, Ward WW, Prasher DC**. Green fluorescent protein as a marker for gene expression. *Science* 1994;263:802–805.

115. **Chalfie M**. Green fluorescent protein. *Photochem Photobiol* 1995;62:651–656.

116. **Prasher DC**. Using GFP to see the light. *Trends Genet* 1995;11:320–323.

117. **Kain SR, Adams M, Kondepudi A, Yang TT, Ward WW, *et al.*** Green fluorescent protein as a reporter of gene expression and protein localization. *Biotechniques* 1995;19:650–655.

118. **Tsien RY**. The Green Fluorescent Protein. *Annual Review of Biochemistry* 1998;67:509–544.

119. **Davies DG, Parsek MR, Pearson JP, Iglewski BH, Costerton JW, *et al.*** The involvement of cell-to-cell signals in the development of a bacterial biofilm. *Science* 1998;280:295–298.

120. **Bloemberg GV, O'Toole GA, Lugtenberg BJ, Kolter R**. Green fluorescent protein as a marker for *Pseudomonas* spp. *Applied and environmental microbiology* 1997;63:4543–51.

121. **Bjarnsholt T, Jensen PØ, Rasmussen TB, Christophersen L, Calum H, *et al.*** Garlic blocks quorum sensing and promotes rapid clearing of pulmonary *Pseudomonas aeruginosa* infections. *Microbiology* 2005;151:3873–3880.

122. **Patterson GH, Lippincott-Schwartz J**. A Photoactivatable GFP for Selective Photolabeling of Proteins and Cells. *Science* 2002;297:1873–1877.

123. **Lippincott-Schwartz J, Snapp E, Kenworthy A**. Studying protein dynamics in living cells. *Nat Rev Mol Cell Biol* 2001;2:444–456.

124. **Cormack BP, Valdivia RH, Falkow S**. FACS-optimized mutants of the green fluorescent protein (GFP). *Gene* 1996;173:33–38.

125. **Yang T-T, Cheng L, Kain SR**. Optimized Codon Usage and Chromophore Mutations Provide Enhanced Sensitivity with the Green Fluorescent Protein. *Nucleic Acids Research* 1996;24:4592–4593.

126. **Iizuka R, Yamagishi-Shirasaki M, Funatsu T**. Kinetic study of de novo chromophore maturation of fluorescent proteins. *Analytical Biochemistry* 2011;414:173–178.

127. **Cubitt AB, Heim R, Adams SR, Boyd AE, Gross LA, *et al.*** Understanding, improving and using green fluorescent proteins. *Trends in Biochemical Sciences* 1995;20:448–455.

128. **Ellenberg J, Lippincott-Schwartz J, Presley JF**. Two-color green fluorescent protein time-lapse imaging. *Biotechniques* 1998;25:838–842, 844–846.

129. **Auldridge ME, Cao H, Sen S, Franz LP, Bingman CA, *et al.*** LucY: A Versatile New Fluorescent Reporter Protein. *PLoS One* 2015;10:e0124272.

130. **Prasher DC, Eckenrode VK, Ward WW, Prendergast FG, Cormier MJ**. Primary structure of the *Aequorea victoria* green-fluorescent protein. *Gene* 1992;111:229–233.

131. **Christie JM, Hitomi K, Arvai AS, Hartfield KA, Mettlen M, *et al.*** Structural tuning of the fluorescent protein iLOV for improved photostability. *The Journal of biological chemistry* 2012;287:22295–304.

132. **Monmeyran A, Thomen P, Jonquière H, Sureau F, Li C, *et al.*** The inducible chemical-genetic fluorescent marker FAST outperforms classical fluorescent proteins in the quantitative reporting of bacterial biofilm dynamics. *Scientific Reports* 2018;8:1–11.

133. **Wall MA, Socolich M, Ranganathan R**. The structural basis for red fluorescence in the tetrameric GFP homolog DsRed. *Nat Struct Mol Biol* 2000;7:1133–1138.

134. **Bhutani G, Verma P, Paul S, Dhamija S, Chattopadhyay K, *et al.*** Elucidating photocycle in large Stokes shift red fluorescent proteins: Focus on mKeima. *Photochemistry and Photobiology* 2024;100:897–909.

135. **Gross LA, Baird GS, Hoffman RC, Baldridge KK, Tsien RY**. The structure of the chromophore within DsRed, a red fluorescent protein from coral. *Proceedings of the National Academy of Sciences* 2000;97:11990–11995.

136. **Lagendijk EL, Validov S, Lamers GEM, De Weert S, Bloemberg GV**. Genetic tools for tagging Gram-negative bacteria with mCherry for visualization in vitro and in natural habitats, biofilm and pathogenicity studies: mCherry visualization of bacteria. *FEMS Microbiology Letters* 2010;305:81–90.

137. **Pavlou A, Cinquemani E, Geiselmann J, de Jong H**. Maturation models of fluorescent proteins are necessary for unbiased estimates of promoter activity. *Biophys J* 2022;121:4179–4188.

138. **Balleza E, Kim JM, Cluzel P**. Systematic characterization of maturation time of fluorescent proteins in living cells. *Nat Methods* 2018;15:47–51.

139. **Moore MM, Oteng-Pabi SK, Pandelieva AT, Mayo SL, Chica RA**. Recovery of Red Fluorescent Protein Chromophore Maturation Deficiency through Rational Design. *PLoS One* 2012;7:e52463.

140. **Drepper T, Eggert T, Circolone F, Heck A, Krauß U, *et al.*** Reporter proteins for *in vivo* fluorescence without oxygen. *Nature Biotechnology* 2007;25:443–445.

141. **Chapman S, Faulkner C, Kaiserli E, Garcia-Mata C, Savenkov EI, *et al.*** The photoreversible fluorescent protein iLOV outperforms GFP as a reporter of plant virus infection. *Proceedings of the National Academy of Sciences* 2008;105:20038–20043.

142. **Fischer M, Bacher A**. Biosynthesis of flavocoenzymes. *Nat Prod Rep* 2005;22:324–350.

143. **Kumagai A, Ando R, Miyatake H, Greimel P, Kobayashi T, *et al.*** A bilirubin-inducible fluorescent protein from eel muscle. *Cell* 2013;153:1602–1611.

144. **Tchagang CF, Mah T-F, Campbell-Valois F-X**. Anaerobic fluorescent reporters for live imaging of *Pseudomonas aeruginosa*. *Front Microbiol* 2023;14. DOI: 10.3389/fmicb.2023.1245755.

145. **Buckley AM, Petersen J, Roe AJ, Douce GR, Christie JM**. LOV-based reporters for fluorescence imaging. *Current Opinion in Chemical Biology* 2015;27:39–45.

146. **Plamont M-A, Billon-Denis E, Maurin S, Gauron C, Pimenta FM, *et al.*** Small fluorescence-activating and absorption-shifting tag for tunable protein imaging *in vivo*. *Proceedings of the National Academy of Sciences* 2016;113:497–502.

147. **Sun X, Zhang A, Baker B, Sun L, Howard A, *et al.*** Development of SNAP-Tag Fluorogenic Probes for Wash-Free Fluorescence Imaging. *Chembiochem* 2011;12:2217–2226.

148. **Filonov GS, Piatkevich KD, Ting L-M, Zhang J, Kim K, *et al.*** Bright and stable near infra-red fluorescent protein for *in vivo* imaging. *Nat Biotechnol* 2011;29:757–761.

149. **Fischer AJ, Lagarias JC**. Harnessing phytochrome's glowing potential. *Proc Natl Acad Sci U S A* 2004;101:17334–17339.

150. **Sharrock RA**. The phytochrome red/far-red photoreceptor superfamily. *Genome Biol* 2008;9:230.

151. **Rumyantsev KA, Shcherbakova DM, Zakharova NI, Emelyanov AV, Turoverov KK, *et al.*** Minimal domain of bacterial phytochrome required for chromophore binding and fluorescence. *Scientific Reports* 2015;5. DOI: 10.1038/srep18348.

152. **Shcherbakova DM, Baloban M, Verkhusha VV**. Near-infrared fluorescent proteins engineered from bacterial phytochromes. *Current Opinion in Chemical Biology* 2015;27:52–63.

153. **Lederberg J**. Cell Genetics and Hereditary Symbiosis. *Physiological Reviews* 1952;32:403–430.

154. **Hülter N, Ilhan J, Wein T, Kadibalban AS, Hammerschmidt K, *et al*.** An evolutionary perspective on plasmid lifestyle modes. *Current Opinion in Microbiology* 2017;38:74–80.

155. **Skippington E, Ragan MA**. Lateral genetic transfer and the construction of genetic exchange communities. *FEMS Microbiology Reviews* 2011;35:707–735.

156. **Wiedenbeck J, Cohan FM**. Origins of bacterial diversity through horizontal genetic transfer and adaptation to new ecological niches. *FEMS Microbiology Reviews* 2011;35:957–976.

157. **Austin S, Ziese M, Sternberg N**. A novel role for site-specific recombination in maintenance of bacterial replicons. *Cell* 1981;25:729–736.

158. **Ebersbach G, Gerdes K**. Plasmid segregation mechanisms. *Annu Rev Genet* 2005;39:453–479.

159. **Yarmolinsky MB**. Programmed cell death in bacterial populations. *Science* 1995;267:836–837.

160. **Melderen LV, Bast MSD**. Bacterial Toxin–Antitoxin Systems: More Than Selfish Entities? *PLOS Genetics* 2009;5:e1000437.

161. **Ogura T, Hiraga S**. Mini-F plasmid genes that couple host cell division to plasmid proliferation. *Proc Natl Acad Sci U S A* 1983;80:4784–4788.

162. **Singh G, Yadav M, Ghosh C, Rathore JS**. Bacterial toxin-antitoxin modules: classification, functions, and association with persistence. *Curr Res Microb Sci* 2021;2:100047.

163. **Jurėnas D, Fraikin N, Goormaghtigh F, Van Melderen L**. Biology and evolution of bacterial toxin–antitoxin systems. *Nat Rev Microbiol* 2022;20:335–350.

164. **Goeders N, Van Melderen L**. Toxin-Antitoxin Systems as Multilevel Interaction Systems. *Toxins* 2014;6:304–324.

165. **Gupta K, Tripathi A, Sahu A, Varadarajan R**. Contribution of the Chromosomal ccdAB Operon to Bacterial Drug Tolerance. *Journal of Bacteriology* 2017;199:10.1128/jb.00397-17.

166. **Bahassi EM, O'Dea MH, Allali N, Messens J, Gellert M, *et al.*** Interactions of CcdB with DNA Gyrase: Inactivation of GyrA, poisoning of the gyrase-DNA complex, and the antidote action of CcdA. *Journal of Biological Chemistry* 1999;274:10936–10944.

167. **Bernard P, Couturier M**. Cell killing by the F plasmid CcdB protein involves poisoning of DNA-topoisomerase II complexes. *J Mol Biol* 1992;226:735–745.

168. **Van Melderen L, Bernard P, Couturier M**. Lon-dependent proteolysis of CcdA is the key control for activation of CcdB in plasmid-free segregant bacteria. *Mol Microbiol* 1994;11:1151–1157.

169. **Pandey DP, Gerdes K**. Toxin–antitoxin loci are highly abundant in free-living but lost from host-associated prokaryotes. *Nucleic Acids Res* 2005;33:966–976.

170. **McKenzie JL, Robson J, Berney M, Smith TC, Ruthe A, *et al.*** A VapBC Toxin-Antitoxin Module Is a Posttranscriptional Regulator of Metabolic Flux in Mycobacteria. *J Bacteriol* 2012;194:2189–2204.

171. **Jeon H, Choi E, Hwang J**. Identification and characterization of VapBC toxin-antitoxin system in *Bosea* sp. PAMC 26642 isolated from Arctic lichens. *RNA* 2021;27:1374–1389.

172. **Winther KS, Gerdes K**. Enteric virulence associated protein VapC inhibits translation by cleavage of initiator tRNA. *Proc Natl Acad Sci U S A* 2011;108:7403–7407.

173. **Winther KS, Brodersen DE, Brown AK, Gerdes K**. VapC20 of *Mycobacterium tuberculosis* cleaves the sarcin-ricin loop of 23S rRNA. *Nat Commun* 2013;4:2796.

174. **Winther K, Tree JJ, Tollervey D, Gerdes K**. VapCs of *Mycobacterium tuberculosis* cleave RNAs essential for translation. *Nucleic Acids Res* 2016;44:9860–9871.

175. **Gerdes K, Christensen SK, Løbner-Olesen A**. Prokaryotic toxin–antitoxin stress response loci. *Nat Rev Microbiol* 2005;3:371–382.

176. **Robson J, McKenzie JL, Cursons R, Cook GM, Arcus VL**. The vapBC operon from *Mycobacterium smegmatis* is an autoregulated toxin-antitoxin module that controls growth via inhibition of translation. *J Mol Biol* 2009;390:353–367.

177. **Pilla G, Tang CM**. Going around in circles: virulence plasmids in enteric pathogens. *Nat Rev Microbiol* 2018;16:484–495.

178. **McVicker G, Hollingshead S, Pilla G, Tang CM**. Maintenance of the virulence plasmid in *Shigella flexneri* is influenced by Lon and two functional partitioning systems. *Mol Microbiol* 2019;111:1355–1366.

179. **Sayeed S, Reaves L, Radnedge L, Austin S**. The stability region of the large virulence plasmid of *Shigella flexneri* encodes an efficient postsegregational killing system. *J Bacteriol* 2000;182:2416–2421.

180. **Hernández-Ramírez KC, Chávez-Jacobo VM, Valle-Maldonado MI, Patiño-Medina JA, Díaz-Pérez SP, *et al.*** Plasmid pUM505 encodes a Toxin–Antitoxin system conferring plasmid stability and increased *Pseudomonas aeruginosa* virulence. *Microbial Pathogenesis* 2017;112:259–268.

181. **Hernández-Ramírez KC, Valle-Maldonado MI, Patiño-Medina JA, Calo S, Jácome-Galarza IE, *et al.*** Role of PumB antitoxin as a transcriptional regulator of the PumAB type-II toxin–antitoxin system and its endoribonuclease activity on the PumA (toxin) transcript. *Mol Genet Genomics* 2023;298:455–472.

182. **Yang QE, Walsh TR**. Toxin–antitoxin systems and their role in disseminating and maintaining antimicrobial resistance. *FEMS Microbiol Rev* 2017;41:343–353.

183. **Harms A, Brodersen DE, Mitarai N, Gerdes K**. Toxins, Targets, and Triggers: An Overview of Toxin-Antitoxin Biology. *Molecular Cell* 2018;70:768–784.

184. **Cooper CR, Daugherty AJ, Tachdjian S, Blum PH, Kelly RM**. Role of vapBC toxin–antitoxin loci in the thermal stress response of Sulfolobus solfataricus. *Biochemical Society transactions* 2009;37:123.

185. **Kamruzzaman M, Wu AY, Iredell JR**. Biological Functions of Type II Toxin-Antitoxin Systems in Bacteria. *Microorganisms* 2021;9:1276.

186. **Hernández-Ramírez KC, Valerio-Arellano B, Valle-Maldonado MI, Ruíz-Herrera LF, Meza-Carmen V, *et al.*** Virulence Conferred by PumA Toxin from the Plasmid-Encoded PumAB Toxin-Antitoxin System is Regulated by Quorum System. *Curr Microbiol* 2020;77:2535–2543.

187. **Stieber D, Gabant P, Szpirer CY**. The Art of Selective Killing: Plasmid Toxin/Antitoxin Systems and their Technological Applications. *BioTechniques* 2008;45:344–346.

188. The Canadian Cystic Fibrosis Registry - 2023 Annual Data Report. https://cystic-fibrosis.cdn.prismic.io/cystic-fibrosis/Z9sI9jiBA97GirFZ_2023-Annual-Data-ReportWEB-2-.pdf (accessed 9 April 2025).

189. **Chmiel JF, Davis PB**. State of the art: Why do the lungs of patients with cystic fibrosis become infected and why can't they clear the infection? *Respiratory Research* 2003;4:1–12.

190. **Stanford GE, Dave K, Simmonds NJ**. Pulmonary Exacerbations in Adults With Cystic Fibrosis. *Chest* 2021;159:93–102.

191. **Lopes SP, Azevedo NF, Pereira MO**. Microbiome in cystic fibrosis: Shaping polymicrobial interactions for advances in antibiotic therapy. *Critical Reviews in Microbiology* 2015;41:353–365.

192. **Magalhães AP, Azevedo NF, Pereira MO, Lopes SP**. The cystic fibrosis microbiome in an ecological perspective and its impact in antibiotic therapy. *Applied Microbiology and Biotechnology* 2016;100:1163–1181.

193. **Burgener EB, Sweere JM, Bach MS, Secor PR, Haddock N, *et al.*** Filamentous bacteriophages are associated with chronic *Pseudomonas* lung infections and antibiotic resistance in cystic fibrosis. *Sci Transl Med* 2019;11:eaau9748.

194. **Zemanick ET, Wagner BD, Robertson CE, Ahrens RC, Chmiel JF, *et al.*** Airway microbiota across age and disease spectrum in cystic fibrosis. *European Respiratory Journal* 2017;50. DOI: 10.1183/13993003.00832-2017.

195. **Coburn B, Wang PW, Diaz Caballero J, Clark ST, Brahma V, *et al.*** Lung microbiota across age and disease stage in cystic fibrosis. *Sci Rep* 2015;5:10241.

196. **Bragonzi A, Farulla I, Paroni M, Twomey KB, Pirone L, *et al.*** Modelling Co-Infection of the Cystic Fibrosis Lung by *Pseudomonas aeruginosa* and *Burkholderia cenocepacia* Reveals Influences on Biofilm Formation and Host Response. *PLoS ONE* 2012;7:e52330.

197. **Chattoraj SS, Murthy R, Ganesan S, Goldberg JB, Zhao Y, *et al.*** *Pseudomonas aeruginosa* alginate promotes *Burkholderia cenocepacia* persistence in cystic fibrosis transmembrane conductance regulator knockout mice. *Infection and immunity* 2010;78:984–93.

198. **Thornton CS, Acosta N, Surette MG, Parkins MD**. Exploring the Cystic Fibrosis Lung Microbiome: Making the Most of a Sticky Situation. *J Pediatric Infect Dis Soc* 2022;11:S13–S22.

199. **Jean-Pierre F, Hampton TH, Schultz D, Hogan DA, Groleau M-C, *et al.*** Community composition shapes microbial-specific phenotypes in a cystic fibrosis polymicrobial model system. *eLife* 2023;12:1–23.

200. **Pressler T, Bohmova C, Conway S, Dumcius S, Hjelte L, *et al.*** Chronic *Pseudomonas aeruginosa* infection definition: EuroCareCF Working Group report. *Journal of Cystic Fibrosis* 2011;10:S75–S78.

201. **Winstanley C, O'Brien S, Brockhurst MA**. *Pseudomonas aeruginosa* Evolutionary Adaptation and Diversification in Cystic Fibrosis Chronic Lung Infections. *Trends in Microbiology* 2016;24:327–337.

202. **O'Brien S, Fothergill JL**. The role of multispecies social interactions in shaping *Pseudomonas aeruginosa* pathogenicity in the cystic fibrosis lung. *FEMS Microbiology Letters* 2017;364:1–10.

203. Eradication of Initial *P. aeruginosa* Clinical Care Guidelines | Cystic Fibrosis Foundation. https://www.cff.org/medical-professionals/eradication-initial-p-aeruginosa-clinical-care-guidelines (accessed 10 January 2026).

204. **Hurley MN, Cámara M, Smyth AR**. Novel approaches to the treatment of *Pseudomonas aeruginosa* infections in cystic fibrosis. *European Respiratory Journal* 2012;40:1014–1023.

205. **Ehsan Z, Clancy JP**. Management of *Pseudomonas aeruginosa* infection in cystic fibrosis patients using inhaled antibiotics with a focus on nebulized liposomal amikacin. *Future Microbiol* 2015;10:1901–1912.

206. **Jackson L, Waters V**. Factors influencing the acquisition and eradication of early *Pseudomonas aeruginosa* infection in cystic fibrosis. *Journal of Cystic Fibrosis* 2021;20:8–16.

207. **Morello E, Saussereau E, Maura D, Huerre M, Touqui L, *et al*.** Pulmonary Bacteriophage Therapy on *Pseudomonas aeruginosa* Cystic Fibrosis Strains: First Steps Towards Treatment and Prevention. *PLOS ONE* 2011;6:e16963.

208. **Sagel SD, Gibson RL, Emerson J, McNamara S, Burns JL, *et al*.** Impact of *Pseudomonas* and Staphylococcus Infection on Inflammation and Clinical Status in Young Children with Cystic Fibrosis. *The Journal of Pediatrics* 2009;154:183-188.e3.

209. **Gangell C, Gard S, Douglas T, Park J, de Klerk N, *et al*.** Inflammatory Responses to Individual Microorganisms in the Lungs of Children With Cystic Fibrosis. *Clinical Infectious Diseases* 2011;53:425–432.

210. **Goss CH, Muhlebach MS**. Review: *Staphylococcus aureus* and MRSA in cystic fibrosis. *Journal of Cystic Fibrosis* 2011;10:298–306.

211. **Rumpf C, Lange J, Schwartbeck B, Kahl BC**. *Staphylococcus aureus* and Cystic Fibrosis—A Close Relationship. What Can We Learn from Sequencing Studies? *Pathogens* 2021;10:1177.

212. **Armstrong DS, Hook SM, Jamsen KM, Nixon GM, Carzino R, *et al*.** Lower Airway Inflammation in Infants with Cystic Fibrosis Detected by Newborn Screening. *Pediatric Pulmonology* 2005;40:500–510.

213. **Donlan RM, Costerton JW**. Biofilms: Survival Mechanisms of Clinically Relevant Microorganisms. *Clinical Microbiology Reviews*. 2002. DOI: 10.1128/cmr.15.2.167-193.2002.

214. **McKenney D, Pouliot KL, Wang Y, Murthy V, Ulrich M, *et al*.** Broadly Protective Vaccine for *Staphylococcus aureus* Based on an *in vivo*-Expressed Antigen. *Science* 1999;284:1523–1527.

215. **Melles DC, Gorkink RFJ, Boelens HAM, Snijders SV, Peeters JK, *et al*.** Natural population dynamics and expansion of pathogenic clones of *Staphylococcus aureus*. *J Clin Invest* 2004;114:1732–1740.

216. **Ren CL, Morgan WJ, Konstan MW, Schechter MS, Wagener JS, *et al*.** Presence of methicillin resistant *Staphylococcus aureus* in respiratory cultures from cystic fibrosis patients is associated with lower lung function. *Pediatric Pulmonology* 2007;42:513–518.

217. **Esposito S, Pennoni G, Mencarini V, Palladino N, Peccini L, *et al*.** Antimicrobial Treatment of *Staphylococcus aureus* in Patients With Cystic Fibrosis. *Front Pharmacol* 2019;10. DOI: 10.3389/fphar.2019.00849.

218. **Hill EM**. The Emergence of *Streptococcus anginosus* Group as a Cystic Fibrosis Pathogen. *Clinical Microbiology Newsletter* 2017;39:143–147.

219. **Harris JK, De Groote MA, Sagel SD, Zemanick ET, Kapsner R, *et al*.** Molecular identification of bacteria in bronchoalveolar lavage fluid from children with cystic fibrosis. *Proceedings of the National Academy of Sciences* 2007;104:20529–20533.

220. **Muhlebach MS, Hatch JE, Einarsson GG, McGrath SJ, Gilipin DF, *et al*.** Anaerobic bacteria cultured from cystic fibrosis airways correlate to milder disease: A multisite study. *European Respiratory Journal* 2018;52. DOI: 10.1183/13993003.00242-2018.

221. **Lamoureux C, Guilloux C-A, Beauruelle C, Gouriou S, Ramel S, *et al*.** An observational study of anaerobic bacteria in cystic fibrosis lung using culture dependant and independent approaches. *Sci Rep* 2021;11:6845.

222. **Grassi L, Asfahl KL, Van den Bossche S, Maenhout I, Sass A, *et al*.** Antibiofilm activity of *Prevotella* species from the cystic fibrosis lung microbiota against *Pseudomonas aeruginosa*. *Biofilm* 2024;7:100206.

223. **Tunney MM, Field TR, Moriarty TF, Patrick S, Doering G, *et al*.** Detection of anaerobic bacteria in high numbers in sputum from patients with cystic fibrosis. *American Journal of Respiratory and Critical Care Medicine* 2008;177:995–1001.

224. **Field TR, Sibley CD, Parkins MD, Rabin HR, Surette MG**. The genus *Prevotella* in cystic fibrosis airways. *Anaerobe* 2010;16:337–344.

225. **Lamoureux C, Guilloux CA, Beauruelle C, Jolivet-Gougeon A, Héry-Arnaud G**. Anaerobes in cystic fibrosis patients' airways. *Critical Reviews in Microbiology* 2019;45:103–117.

226. **Caverly LJ, LiPuma JJ**. Good cop, bad cop: Anaerobes in cystic fibrosis airways. *European Respiratory Journal* 2018;52:19–22.

227. **Flynn JM, Niccum D, Dunitz JM, Hunter RC**. Evidence and Role for Bacterial Mucin Degradation in Cystic Fibrosis Airway Disease. *PLoS Pathog* 2016;12:e1005846.

228. **Venkataraman A, Rosenbaum MA, Werner JJ, Winans SC, Angenent LT**. Metabolite transfer with the fermentation product 2,3-butanediol enhances virulence by *Pseudomonas aeruginosa*. *ISME J* 2014;8:1210–1220.

229. **Scott JE, O'Toole GA**. The Yin and Yang of *Streptococcus* Lung Infections in Cystic Fibrosis: a Model for Studying Polymicrobial Interactions. *J Bacteriol* 2019;201:e00115-19.

230. **Filkins LM, Hampton TH, Gifford AH, Gross MJ, Hogan DA, *et al*.** Prevalence of streptococci and increased polymicrobial diversity associated with cystic fibrosis patient stability. *Journal of Bacteriology* 2012;194:4709–4717.

231. **Lamoureux C, Guilloux C-A, Courteboeuf E, Gouriou S, Beauruelle C, *et al*.** *Prevotella melaninogenica*, a Sentinel Species of Antibiotic Resistance in Cystic Fibrosis Respiratory Niche? *Microorganisms* 2021;9:1275.

232. **Rosen BH, Chanson M, Gawenis LR, Liu J, Sofoluwe A, *et al*.** Animal and Model Systems for Studying Cystic Fibrosis. *J Cyst Fibros* 2018;17:S28–S34.

233. **Heirali A, Thornton C, Acosta N, Somayaji R, Laforest Lapointe I, *et al*.** Sputum microbiota in adults with CF associates with response to inhaled tobramycin. *Thorax* 2020;75:1058–1064.

234. **Heirali AA, Workentine ML, Acosta N, Poonja A, Storey DG, *et al*.** The effects of inhaled aztreonam on the cystic fibrosis lung microbiome. *Microbiome* 2017;5:51.

235. **Nelson MT, Wolter DJ, Eng A, Weiss EJ, Vo AT, *et al*.** Maintenance tobramycin primarily affects untargeted bacteria in the CF sputum microbiome. *Thorax* 2020;75:780–790.

236. **Vandeplassche E, Sass A, Ostyn L, Burmølle M, Kragh KN, *et al*.** Antibiotic susceptibility of cystic fibrosis lung microbiome members in a multispecies biofilm. *Biofilm* 2020;2:100031.

237. **Elias S, Banin E**. Multi-species biofilms: living with friendly neighbors. *FEMS Microbiology Reviews* 2012;36:990–1004.

238. **Fernandes S, Gomes IB, Sousa SF, Simões M**. Antimicrobial Susceptibility of Persister Biofilm Cells of *Bacillus cereus* and *Pseudomonas fluorescens*. *Microorganisms* 2022;10:160.

239. **Dayton H, Kiss J, Wei M, Chauhan S, LaMarre E, *et al*.** Cellular arrangement impacts metabolic activity and antibiotic tolerance in *Pseudomonas aeruginosa* biofilms. *PLOS Biology* 2024;22:e3002205.

240. **Høiby N, Ciofu O, Bjarnsholt T**. *Pseudomonas aeruginosa* biofilms in cystic fibrosis. *Future Microbiology* 2010;5:1663–1674.

241. **Stutts MJ, Knowles MR, Gatzy JT, Boucher RC**. Oxygen Consumption and Ouabain Binding Sites in Cystic Fibrosis Nasal Epithelium. *Pediatr Res* 1986;20:1316–1320.

242. **Worlitzsch D, Herberth G, Ulrich M, Doring G**. Catalase, myeloperoxidase and hydrogen peroxide in cystic fibrosis. *European Respiratory Journal* 1998;11:377–383.

243. **Worlitzsch D, Tarran R, Ulrich M, Schwab U, Cekici A, *et al*.** Effects of reduced mucus oxygen concentration in airway *Pseudomonas* infections of cystic fibrosis patients. *The Journal of clinical investigation* 2002;109:317–25.

244. **Yoon SS, Hennigan RF, Hilliard GM, Ochsner UA, Parvatiyar K, *et al*.** *Pseudomonas aeruginosa* Anaerobic Respiration in Biofilms: Relationships to Cystic Fibrosis Pathogenesis. *Developmental Cell* 2002;3:593–603.

245. **Campbell-Valois FX, Schnupf P, Nigro G, Sachse M, Sansonetti PJ, *et al*.** A fluorescent reporter reveals on/off regulation of the *Shigella* type III secretion apparatus during entry and cell-to-cell spread. *Cell Host and Microbe* 2014;15:177–189.

246. **Bajunaid W, Haidar-Ahmad N, Kottarampatel AH, Ourida Manigat F, Silué N, *et al*.** The T3SS of *Shigella*: Expression, Structure, Function, and Role in Vacuole Escape. *Microorganisms* 2020;8:1933.

247. **Shcherbakova DM, Verkhusha VV**. Near-infrared fluorescent proteins for multicolor *in vivo* imaging. *Nature Methods* 2013;10:751–754.

248. **Ma J, Campbell A, Karlin S**. Correlations between Shine-Dalgarno Sequences and Gene Features Such as Predicted Expression Levels and Operon Structures. *J Bacteriol* 2002;184:5733–5745.

249. **Ringquist S, Shinedling S, Barrick D, Green L, Binkley J, *et al*.** Translation initiation in *Escherichia coli*: sequences within the ribosome-binding site. *Molecular Microbiology* 1992;6:1219–1229.

250. **Manigat FO, Connell LB, Stewart BN, LePabic A-R, Tessier CJG, *et al*.** pUdOs: Concise Plasmids for Bacterial and Mammalian Cells. *ACS Synth Biol* 2024;13:485–497.

251. **Antoine R, Locht C**. Isolation and molecular characterization of a novel broad-host-range plasmid from *Bordetella bronchiseptica* with sequence similarities to plasmids from Gram-positive organisms. *Molecular Microbiology* 1992;6:1785–1799.

252. **Rahme LG, Stevens EJ, Wolfort SF, Shao J, Tompkins RG, *et al.*** Common Virulence Factors for Bacterial Pathogenicity in Plants and Animals. *Science* 1995;268:1899–1902.

253. **Lam KL, Lin S, Liu C, Wu X, Tang S, *et al.*** Low-Cost Method Generating in Situ Anaerobic Conditions on a 96-Well Plate for Microbial Fermentation in Food Research. *Journal of Agricultural and Food Chemistry* 2018;66:11839–11845.

254. **Li C, Plamont M-A, Sladitschek HL, Rodrigues V, Aujard I, *et al.*** Dynamic multicolor protein labeling in living cells. *Chem Sci* 2017;8:5598–5605.

255. **Streett HE, Kalis KM, Papoutsakis ET**. A Strongly Fluorescing Anaerobic Reporter and Protein-Tagging System for *Clostridium* Organisms Based on the Fluorescence-Activating and Absorption-Shifting Tag Protein (FAST). *Applied and Environmental Microbiology* 2019;85:1–15.

256. **Schneider CA, Rasband WS, Eliceiri KW**. NIH Image to ImageJ: 25 years of image analysis. 2012. DOI: 10.1038/nmeth.2089.

257. **Nigro G, Arena ET, Sachse M, Moya-Nilges M, Marteyn BS, *et al.*** Mapping of *Shigella flexneri*'s tissue distribution and type III secretion apparatus activity during infection of the large intestine of guinea pigs. *Pathogens and disease* 2019;77:1–9.

258. **Ponka P**. Cell Biology of Heme. *The American Journal of the Medical Sciences* 1999;318:241–256.

259. **Schmitt MP**. Utilization of host iron sources by *Corynebacterium diphtheriae*: identification of a gene whose product is homologous to eukaryotic heme oxygenases and is required for acquisition of iron from heme and hemoglobin. *Journal of Bacteriology* 1997;179:838–845.

260. **Wilks A, Schmitt MP**. Expression and Characterization of a Heme Oxygenase (Hmu O) from *Corynebacterium diphtheriae*. *Journal of Biological Chemistry* 1998;273:837–841.

261. **Zhu W, Hunt DJ, Richardson AR, Stojiljkovic I**. Use of Heme Compounds as Iron Sources by Pathogenic *Neisseriae* Requires the Product of the hemO Gene. *Journal of Bacteriology* 2000;182:439–447.

262. **Ratliff M, Zhu W, Deshmukh R, Wilks A, Stojiljkovic I**. Homologues of neisserial heme oxygenase in gram-negative bacteria: degradation of heme by the product of the pigA gene of *Pseudomonas aeruginosa*. *Journal of bacteriology* 2001;183:6394–6403.

263. **Skaar EP, Gaspar AH, Schneewind O**. IsdG and IsdI, Heme-degrading Enzymes in the Cytoplasm of *Staphylococcus aureus*. *Journal of Biological Chemistry* 2004;279:436–443.

264. **Wegele R, Tasler R, Zeng Y, Rivera M, Frankeinberg-Dinkel N**. The heme oxygenase(s)-phytochrome system of *Pseudomonas aeruginosa*. *Journal of Biological Chemistry* 2004;279:45791–45802.

265. **Chia HE, Zuo T, Koropatkin NM, Marsh ENG, Biteen JS**. Imaging living obligate anaerobic bacteria with bilin-binding fluorescent proteins. *Current Research in Microbial Sciences* 2020;1:1–6.

266. **Chia HE, Koebke KJ, Rangarajan AA, Koropatkin NM, Marsh ENG, *et al.*** New Orange Ligand-Dependent Fluorescent Reporter for Anaerobic Imaging. *ACS Chem Biol* 2021;16:2109–2115.

267. **Hancock REW, Woodruff WA**. Roles of porin and beta-lactamase in beta-lactam resistance of *Pseudomonas aeruginosa*. *Reviews of infectious diseases* 1988;10:770–775.

268. **Michea Hamzehpour M, Pechere J, Plesiat P**. OprK and OprM Define Two Genetically Distinct Multidrug Efflux Systems in *Pseudomonas aeruginosa*. *Antimicrobial Agents and Chemotherapy* 1995;39:2392–2396.

269. **Plesiat P, Aires JR, Godard C, Köhler T**. Use of steroids to monitor alterations in the outer membrane of *Pseudomonas aeruginosa*. *Journal of Bacteriology* 1997;179:7004–7010.

270. **Mordaka PM, Heap JT**. Stringency of Synthetic Promoter Sequences in *Clostridium* Revealed and Circumvented by Tuning Promoter Library Mutation Rates. *ACS Synth Biol* 2018;7:672–681.

271. **Streett H, Charubin K, Papoutsakis ET**. Anaerobic fluorescent reporters for cell identification, microbial cell biology and high-throughput screening of microbiota and genomic libraries. *Current Opinion in Biotechnology* 2021;71:151–163.

272. **Buckley AM, Jukes C, Candlish D, Irvine JJ, Spencer J, *et al.*** Lighting Up *Clostridium Difficile*: Reporting Gene Expression Using Fluorescent Lov Domains. *Scientific Reports 2016 6:1* 2016;6:1–11.

273. **Peron-Cane C, Fernandez J-C, Leblanc J, Wingertsmann L, Gautier A, *et al.*** Fluorescent secreted bacterial effectors reveal active intravacuolar proliferation of *Listeria monocytogenes* in epithelial cells. *PLOS Pathogens* 2020;16:e1009001.

274. **Hernandez E, Costa KC**. The Fluorescence-Activating and Absorption-Shifting Tag (FAST) Enables Live-Cell Fluorescence Imaging of Methanococcus maripaludis. *Journal of Bacteriology* 2022;204:e00120-22.

275. **Cowan SE, Gilbert E, Khlebnikov A, Keasling JD**. Dual Labeling with Green Fluorescent Proteins for Confocal Microscopy. *Appl Environ Microbiol* 2000;66:413–418.

276. **Davey ME, Caiazza NC, O'Toole GA**. Rhamnolipid surfactant production affects biofilm architecture in *Pseudomonas aeruginosa* PAO1. *J Bacteriol* 2003;185:1027–1036.

277. **Babakhanova S, Jung EE, Namikawa K, Zhang H, Wang Y, *et al.*** Rapid directed molecular evolution of fluorescent proteins in mammalian cells. *Protein Science* 2022;31:728–751.

278. **Liang GT, Lai C, Yue Z, Zhang H, Li D, *et al.*** Enhanced small green fluorescent proteins as a multisensing platform for biosensor development. *Frontiers in Bioengineering and Biotechnology* 2022;10:1–16.

279. **Tebo AG, Pimenta FM, Zhang Y, Gautier A**. Improved Chemical-Genetic Fluorescent Markers for Live Cell Microscopy. *Biochemistry* 2018;57:5648–5653.

280. **Li C, Tebo AG, Thauvin M, Plamont M-A, Volovitch M, *et al.*** A Far-Red Emitting Fluorescent Chemogenetic Reporter for *In vivo* Molecular Imaging. *Angewandte Chemie* 2020;132:18073–18079.

281. **Los GV, Encell LP, McDougall MG, Hartzell DD, Karassina N, *et al.*** HaloTag: A Novel Protein Labeling Technology for Cell Imaging and Protein Analysis. *ACS Chem Biol* 2008;3:373–382.

282. **Ramsey BW, Pepe MS, Quan JM, Otto KL, Montgomery AB, *et al.*** Intermittent Administration of Inhaled Tobramycin in Patients with Cystic Fibrosis. *New England Journal of Medicine* 1999;340:23–30.

283. **Malhotra S, Hayes Jr. D, Wozniak DJ**. Cystic Fibrosis and *Pseudomonas aeruginosa*: the Host-Microbe Interface. *Clinical Microbiology Reviews* 2019;32. DOI: 10.1128/cmr.00138-18.

284. **Thornton CS, Caverly LJ, LiPuma JJ**. Coming Up for Air: The Role of Anaerobes in Cystic Fibrosis. *Annals ATS* 2022;19:713–716.

285. **Ulrich M, Beer I, Braitmaier P, Dierkes M, Kummer F, *et al.*** Relative contribution of *Prevotella* intermedia and *Pseudomonas aeruginosa* to lung pathology in airways of patients with cystic fibrosis. 2010. DOI: 10.1136/thx.2010.137745.

286. **Waters VJ, LiPuma JJ**. Bacterial Infections and the Respiratory Microbiome. In: Davis SD, Rosenfeld M, Chmiel J (editors). *Cystic Fibrosis: A Multi-Organ System Approach*. Cham: Springer International Publishing. pp. 73–92.

287. **Zemanick ET, Harris JK, Wagner BD, Robertson CE, Sagel SD, *et al.*** Inflammation and Airway Microbiota during Cystic Fibrosis Pulmonary Exacerbations. *PLoS ONE* 2012;8. DOI: 10.1371/journal.pone.0062917.

288. **Sibley CD, Parkins MD, Rabin HR, Duan K, Norgaard JC, *et al.*** A polymicrobial perspective of pulmonary infections exposes an enigmatic pathogen in cystic fibrosis patients. *Proceedings of the National Academy of Sciences* 2008;105:15070–15075.

289. **Bonincontro G, Scuderi SA, Marino A, Simonetti G**. Synergistic Effect of Plant Compounds in Combination with Conventional Antimicrobials against Biofilm of *Staphylococcus aureus*, *Pseudomonas aeruginosa*, and Candida spp. *Pharmaceuticals (Basel)* 2023;16:1531.

290. **Walker TS, Bais HP, Déziel E, Schweizer HP, Rahme LG, *et al.*** *Pseudomonas aeruginosa*-plant root interactions. Pathogenicity, biofilm formation, and root exudation. *Plant Physiol* 2004;134:320–331.

291. **Poole K**. *Pseudomonas aeruginosa*: resistance to the max. *Front Microbiol* 2011;2:65.

292. **Mah TF, O'Toole GA**. Mechanisms of biofilm resistance to antimicrobial agents. *Trends Microbiol* 2001;9:34–39.

293. **Palmer KL, Mashburn LM, Singh PK, Whiteley M**. Cystic Fibrosis Sputum Supports Growth and Cues Key Aspects of *Pseudomonas aeruginosa* Physiology Cystic Fibrosis Sputum Supports Growth and Cues Key Aspects of *Pseudomonas aeruginosa* Physiology. *Journal of Bacteriology* 2005;187:5267–5277.

294. **Turner KH, Wessel AK, Palmer GC, Murray JL, Whiteley M**. Essential genome of *Pseudomonas aeruginosa* in cystic fibrosis sputum. *Proceedings of the National Academy of Sciences* 2015;112:4110–4115.

295. **Duthie ES**. Variation in the antigenic composition of staphylococcal coagulase. *J Gen Microbiol* 1952;7:320–326.

296. **Kilian M, Holmgren K**. Ecology and nature of immunoglobulin A1 protease-producing streptococci in the human oral cavity and pharynx. *Infect Immun* 1981;31:868–873.

297. **Shah HN, Collins DM**. *Prevotella*, a new genus to include *Bacteroides melaninogenicus* and related species formerly classified in the genus Bacteroides. *Int J Syst Bacteriol* 1990;40:205–208.

298. **Anderson GG, Moreau-Marquis S, Stanton BA, O'Toole GA**. In vitro analysis of tobramycin-treated *Pseudomonas aeruginosa* biofilms on cystic fibrosis-derived airway epithelial cells. *Infect Immun* 2008;76:1423–1433.

299. **Coleman SR, Blimkie T, Falsafi R, Hancock REW**. Multidrug Adaptive Resistance of *Pseudomonas aeruginosa* Swarming Cells. *Antimicrobial Agents and Chemotherapy* 2020;64:10.1128/aac.01999-19.

300. **Mah T-F**. Establishing the Minimal Bactericidal Concentration of an Antimicrobial Agent for Planktonic Cells (MBC-P) and Biofilm Cells (MBC-B). *Journal of Visualized Experiments*. 2014. DOI: 10.3791/50854.

301. **Ruddy J, Emerson J, Moss R, Genatossio A, McNamara S, *et al.*** Sputum Tobramycin Concentrations in Cystic Fibrosis Patients with Repeated Administration of Inhaled Tobramycin. *J Aerosol Med Pulm Drug Deliv* 2013;26:69–75.

302. **Eisenberg J, Pepe M, Williams-Warren J, Vasiliev M, Montgomery AB, *et al.*** A comparison of peak sputum tobramycin concentration in patients with cystic fibrosis using jet and ultrasonic nebulizer systems. Aerosolized Tobramycin Study Group. *Chest* 1997;111:955–962.

303. **Preston CA, Khoury AE, Reid G, Bruce AW, Costerton JW**. *Pseudomonas aeruginosa* biofilms are more susceptible to ciprofloxacin than to tobramycin. *Int J Antimicrob Agents* 1996;7:251–256.

304. **Lister PD, Wolter DJ, Hanson ND**. Antibacterial-Resistant *Pseudomonas aeruginosa*: Clinical Impact and Complex Regulation of Chromosomally Encoded Resistance Mechanisms. *Clin Microbiol Rev* 2009;22:582–610.

305. **Ahmed OB**. Detection of Antibiotic Resistance Genes in *Pseudomonas aeruginosa* by Whole Genome Sequencing. *Infect Drug Resist* 2022;15:6703–6709.

306. **Hall CW, Zhang L, Mah T-F**. PA3225 is a Transcriptional Repressor of Antibiotic Resistance Mechanisms in *Pseudomonas aeruginosa*. *Antimicrobial Agents and Chemotherapy* 2017;61:1–20.

307. **Augustin J-C, Bergis H, Midelet-Bourdin G, Cornu M, Couvert O, *et al.*** Design of challenge testing experiments to assess the variability of *Listeria monocytogenes* growth in foods. *Food Microbiology* 2011;28:746–754.

308. **Khan A ul M, Torelli A, Wolf I, Gretz N**. AutoCellSeg: robust automatic colony forming unit (CFU)/cell analysis using adaptive image segmentation and easy-to-use post-editing techniques. *Sci Rep* 2018;8:7302.

309. Standard Practice for Automated Colony Forming Unit (CFU) Assays—Image Acquisition and Analysis Method for Enumerating and Characterizing Cells and Colonies in Culture. https://store.astm.org/f2944-20.html (accessed 29 May 2025).

310. **El Hafi B, Jean-Pierre F, O'Toole GA**. *Pseudomonas aeruginosa* supports the survival of *Prevotella melaninogenica* in a cystic fibrosis lung polymicrobial community through metabolic cross-feeding. *bioRxiv* 2024;2024.10.21.619475.

311. **Henson MA, Orazi G, Phalak P, O'Toole GA**. Metabolic Modeling of Cystic Fibrosis Airway Communities Predicts Mechanisms of Pathogen Dominance. *mSystems* 2019;4. DOI: 10.1128/msystems.00026-19.

312. **Tailford LE, Crost EH, Kavanaugh D, Juge N**. Mucin glycan foraging in the human gut microbiome. *Front Genet* 2015;6. DOI: 10.3389/fgene.2015.00081.

313. **Na SW, Chun BH, Beak S-H, Khan SA, Haque MN, *et al.*** *Pseudoprevotella muciniphila* gen. nov., sp. nov., a mucin-degrading bacterium attached to the bovine rumen epithelium. *PLOS ONE* 2021;16:e0251791.

314. **Lallemand EA, Lacroix MZ, Toutain P-L, Boullier S, Ferran AA, *et al.*** *In vitro* Degradation of Antimicrobials during Use of Broth Microdilution Method Can Increase the Measured Minimal Inhibitory and Minimal Bactericidal Concentrations. *Front Microbiol* 2016;7. DOI: 10.3389/fmicb.2016.02051.

315. **Forey F, Coulet M, Brun Y, Fleurette J**. Influence of technical factors in the determination of minimal inhibitory concentration by microdilution. *Pathologie-biologie* 1985;33. https://pubmed.ncbi.nlm.nih.gov/3162138/ (1985, accessed 27 May 2025).

316. **Thabaut A, Meyran M**. Determination of the minimum bactericidal concentration. Influence of various technical factors. *Pathol Biol (Paris)* 1984;32:351–354.

317. **Rodríguez-Melcón C, Alonso-Calleja C, García-Fernández C, Carballo J, Capita R**. Minimum Inhibitory Concentration (MIC) and Minimum Bactericidal Concentration (MBC) for Twelve Antimicrobials (Biocides and Antibiotics) in Eight Strains of *Listeria monocytogenes*. *Biology (Basel)* 2021;11:46.

318. **Wu M, Guina T, Brittnacher M, Nguyen H, Eng J, *et al.*** The *Pseudomonas aeruginosa* Proteome during Anaerobic Growth. *J Bacteriol* 2005;187:8185–8190.

319. **Schobert M, Jahn D**. Anaerobic physiology of *Pseudomonas aeruginosa* in the cystic fibrosis lung. *International Journal of Medical Microbiology* 2010;300:549–556.

320. **Tribelli PM, Lujan AM, Pardo A, Ibarra JG, Fernández Do Porto D, *et al.*** Core regulon of the global anaerobic regulator Anr targets central metabolism functions in *Pseudomonas* species. *Sci Rep* 2019;9:9065.

321. **Filiatrault MJ, Picardo KF, Ngai H, Passador L, Iglewski BH**. Identification of *Pseudomonas aeruginosa* genes involved in virulence and anaerobic growth. *Infection and Immunity* 2006;74:4237–4245.

322. **Filiatrault MJ, Wagner VE, Bushnell D, Haidaris CG, Iglewski BH, *et al.*** Effect of anaerobiosis and nitrate on gene expression in *Pseudomonas aeruginosa*. *Infection and Immunity* 2005;73:3764–3772.

323. **Crespo A, Pedraz L, Astola J, Torrents E**. *Pseudomonas aeruginosa* exhibits deficient biofilm formation in the absence of class II and III ribonucleotide reductases due to hindered anaerobic growth. *Frontiers in Microbiology* 2016;7:688.

324. **Wolff JA, MacGregor CH, Eisenberg RC, Phibbs PV**. Isolation and characterization of catabolite repression control mutants of *Pseudomonas aeruginosa* PAO. *J Bacteriol* 1991;173:4700–4706.

325. **Hylemon PB, Phibbs PV**. Independant regulation of hexose catabolizing enzymes and glucose transport activity in *Pseudomonas aeruginosa*. *Biochemical and Biophysical Research Communications* 1972;48:1041–1048.

326. **Collier DN, Hager PW, Phibbs PV**. Catabolite repression control in the Pseudomonads. *Research in Microbiology* 1996;147:551–561.

327. **Mould DL, Finger CE, Conaway A, Botelho N, Stuut SE, *et al.*** Citrate cross-feeding by *Pseudomonas aeruginosa* supports lasR mutant fitness. *mBio* 2024;15:e0127823.

328. **Sasnow SS, Wei H, Aristilde L**. Bypasses in intracellular glucose metabolism in iron-limited *Pseudomonas putida*. *MicrobiologyOpen* 2016;5:3–20.

329. **Bielecki P, Jensen V, Schulze W, Gödeke J, Strehmel J, *et al.*** Cross talk between the response regulators PhoB and TctD allows for the integration of diverse environmental signals in *Pseudomonas aeruginosa*. *Nucleic Acids Res* 2015;43:6413–6425.

330. **Folkesson A, Jelsbak L, Yang L, Johansen HK, Ciofu O, *et al.*** Adaptation of *Pseudomonas aeruginosa* to the cystic fibrosis airway: an evolutionary perspective. *Nat Rev Microbiol* 2012;10:841–851.

331. **Goerke C, Wolz C**. Adaptation of *Staphylococcus aureus* to the cystic fibrosis lung. *Int J Med Microbiol* 2010;300:520–525.

332. **Workentine ML, Sibley CD, Glezerson B, Purighalla S, Norgaard-Gron JC, *et al.*** Phenotypic Heterogeneity of *Pseudomonas aeruginosa* Populations in a Cystic Fibrosis Patient. *PLOS ONE* 2013;8:e60225.

333. **Jorth P, Staudinger BJ, Wu X, Hisert KB, Hayden H, *et al*.** Regional Isolation Drives Bacterial Diversification within Cystic Fibrosis Lungs. *Cell Host Microbe* 2015;18:307–319.

334. **Cramer N, Klockgether J, Wrasman K, Schmidt M, Davenport CF, *et al*.** Microevolution of the major common *Pseudomonas aeruginosa* clones C and PA14 in cystic fibrosis lungs. *Environ Microbiol* 2011;13:1690–1704.

335. **Klockgether J, Cramer N, Fischer S, Wiehlmann L, Tümmler B**. Long-term microevolution of *Pseudomonas aeruginosa* differs between mildly and severely affected cystic fibrosis lungs. *American Journal of Respiratory Cell and Molecular Biology* 2018;59:246–256.

336. **Hayes F**. Toxins-antitoxins: plasmid maintenance, programmed cell death, and cell cycle arrest. *Science* 2003;301:1496–1499.

337. **Rawlings DE**. Proteic toxin-antitoxin, bacterial plasmid addiction systems and their evolution with special reference to the pas system of pTF-FC2. *FEMS Microbiology Letters* 1999;176:269–277.

338. **Davies DG, Parsek MR, Pearson JP, Iglewski BH, Costerton JW, *et al*.** The Involvement of Cell-to-Cell Signals in the Development of a Bacterial Biofilm. *Science* 1998;280:295–298.

339. **Christensen GD, Simpson WA, Younger JJ, Baddour LM, Barrett FF, *et al*.** Adherence of coagulase-negative staphylococci to plastic tissue culture plates: a quantitative model for the adherence of staphylococci to medical devices. *Journal of Clinical Microbiology* 1985;22:996–1006.

340. **Stepanović S, Vuković D, Dakić I, Savić B, Švabić-Vlahović M**. A modified microtiter-plate test for quantification of staphylococcal biofilm formation. *Journal of Microbiological Methods* 2000;40:175–179.

341. **Li X, Yan Z, Xu J**. Quantitative variation of biofilms among strains in natural populations of *Candida albicans*. *Microbiology* 2003;149:353–362.

342. **Das S, Takahashi S, Ohyama T, Bhowmik S, Sugimoto N**. Theranostic approach to specifically targeting the interloop region of BCL2 i-motif DNA by crystal violet. *Sci Rep* 2023;13:14338.

343. **O'May CY, Reid DW, Kirov SM**. Anaerobic culture conditions favor biofilm-like phenotypes in *Pseudomonas aeruginosa* isolates from patients with cystic fibrosis. *FEMS Immunology and Medical Microbiology* 2006;48:373–380.

344. **Ramage HR, Connolly LE, Cox JS**. Comprehensive Functional Analysis of *Mycobacterium tuberculosis* Toxin-Antitoxin Systems: Implications for Pathogenesis, Stress Responses, and Evolution. *PLOS Genetics* 2009;5:e1000767.

345. **Kureishi A, Diver JM, Beckthold B, Schollaardt T, Bryan LE**. Cloning and nucleotide sequence of *Pseudomonas aeruginosa* DNA gyrase gyrA gene from strain PAO1 and quinolone-resistant clinical isolates. *Antimicrob Agents Chemother* 1994;38:1944–1952.

346. **Diggle SP, Whiteley M**. Microbe Profile: *Pseudomonas aeruginosa*: opportunistic pathogen and lab rat. *Microbiology (Reading)* 2020;166:30–33.

347. **Pallett R, Leslie LJ, Lambert PA, Milic I, Devitt A, *et al.*** Anaerobiosis influences virulence properties of *Pseudomonas aeruginosa* cystic fibrosis isolates and the interaction with *Staphylococcus aureus*. *Sci Rep* 2019;9:6748.

348. **Tognon M, Köhler T, Gdaniec BG, Hao Y, Lam JS, *et al.*** Co-evolution with *Staphylococcus aureus* leads to lipopolysaccharide alterations in *Pseudomonas aeruginosa*. *ISME J* 2017;11:2233–2243.

349. **Staudinger BJ, Muller JF, Halldórsson S, Boles B, Angermeyer A, *et al.*** Conditions Associated with the Cystic Fibrosis Defect Promote Chronic *Pseudomonas aeruginosa* Infection. *Am J Respir Crit Care Med* 2014;189:812–824.

350. **Magalhães AP, França A, Pereira MO, Cerca N**. Unveiling Co-Infection in Cystic Fibrosis Airways: Transcriptomic Analysis of *Pseudomonas aeruginosa* and *Staphylococcus aureus* Dual-Species Biofilms. *Frontiers in Genetics* 2022;13. https://www.frontiersin.org/articles/10.3389/fgene.2022.883199 (2022, accessed 7 July 2023).

351. **Nguyen HTT, Nguyen TH, Otto M**. The staphylococcal exopolysaccharide PIA – Biosynthesis and role in biofilm formation, colonization, and infection. *Comput Struct Biotechnol J* 2020;18:3324–3334.

352. **Vestweber PK, Wächter J, Planz V, Jung N, Windbergs M**. The interplay of *Pseudomonas aeruginosa* and *Staphylococcus aureus* in dual-species biofilms impacts development, antibiotic resistance and virulence of biofilms in in vitro wound infection models. *PLoS One* 2024;19:e0304491.

353. **Armbruster CR, Wolter DJ, Mishra M, Hayden HS, Radey MC, *et al.*** *Staphylococcus aureus* Protein A Mediates Interspecies Interactions at the Cell Surface of *Pseudomonas aeruginosa*. *mBio* 2016;7:e00538-16.

354. **Beaudoin T, Yau YCW, Stapleton PJ, Gong Y, Wang PW, *et al.*** *Staphylococcus aureus* interaction with *Pseudomonas aeruginosa* biofilm enhances tobramycin resistance. *NPJ Biofilms Microbiomes* 2017;3:25.

355. **Jean-Pierre F, Vyas A, Hampton TH, Henson MA, O'toole GA**. One versus many: Polymicrobial communities and the cystic fibrosis airway. *mBio* 2021;12:1–7.

356. **Harmsen M, Yang L, Pamp SJ, Tolker-Nielsen T**. An update on *Pseudomonas aeruginosa* biofilm formation, tolerance, and dispersal. *FEMS Immunology & Medical Microbiology* 2010;59:253–268.

357. **Wang L, Wong Y-C, Correira JM, Wancura M, Geiger CJ, *et al*.** The accumulation and growth of *Pseudomonas aeruginosa* on surfaces is modulated by surface mechanics via cyclic-di-GMP signaling. *npj Biofilms Microbiomes* 2023;9:78.

358. **Hassett DJ**. Anaerobic production of alginate by *Pseudomonas aeruginosa*: alginate restricts diffusion of oxygen. *Journal of Bacteriology* 1996;178:7322–7325.

359. **Klausen M, Aaes-Jørgensen A, Molin S, Tolker-Nielsen T**. Involvement of bacterial migration in the development of complex multicellular structures in *Pseudomonas aeruginosa* biofilms. *Molecular Microbiology* 2003;50:61–68.

360. **Déziel E, Comeau Y, Villemur R**. Initiation of Biofilm Formation by *Pseudomonas aeruginosa* 57RP Correlates with Emergence of Hyperpiliated and Highly Adherent Phenotypic Variants Deficient in Swimming, Swarming, and Twitching Motilities. *Journal of Bacteriology* 2001;183:1195–1204.

361. **Ma L, Conover M, Lu H, Parsek MR, Bayles K, *et al*.** Assembly and Development of the *Pseudomonas aeruginosa* Biofilm Matrix. *PLOS Pathogens* 2009;5:e1000354.

362. **Zhao K, Tseng BS, Beckerman B, Jin F, Gibiansky ML, *et al*.** Psl trails guide exploration and microcolony formation in *Pseudomonas aeruginosa* biofilms. *Nature* 2013;497:388–391.

363. **Sønderholm M, Kragh KN, Koren K, Jakobsen TH, Darch SE, *et al*.** *Pseudomonas aeruginosa* aggregate formation in an alginate bead model system exhibits *in vivo*-like characteristics. *Appl Environ Microbiol* 2017;83. DOI: 10.1128/AEM.00113-17.

364. **Lee K, Yoon SS**. *Pseudomonas aeruginosa* Biofilm, a Programmed Bacterial Life for Fitness. *Journal of Microbiology and Biotechnology* 2017;27:1053–1064.

365. **Hassett DJ, Cuppoletti J, Trapnell B, Lymar SV, Rowe JJ, *et al*.** Anaerobic metabolism and quorum sensing by *Pseudomonas aeruginosa* biofilms in chronically infected cystic fibrosis airways: rethinking antibiotic treatment strategies and drug targets. *Advanced Drug Delivery Reviews* 2002;54:1425–1443.

366. **Furiga A, Lajoie B, El Hage S, Baziard G, Roques C**. Impairment of *Pseudomonas aeruginosa* Biofilm Resistance to Antibiotics by Combining the Drugs with a New Quorum-Sensing Inhibitor. *Antimicrobial Agents and Chemotherapy* 2016;60:1676–1686.

367. **Lin J, Cheng J**. Quorum Sensing in *Pseudomonas aeruginosa* and Its Relationship to Biofilm Development. In: *Introduction to Biofilm Engineering*. American Chemical Society. 2019;1323 pp. 1–16.

368. **Krasowska A, Sigler K**. How microorganisms use hydrophobicity and what does this mean for human needs? *Front Cell Infect Microbiol* 2014;4. DOI: 10.3389/fcimb.2014.00112.

369. **Vorregaard M**. *Comstat2 - a modern 3D image analysis environment for biofilms*. Technical University of Denmark; 2008.

370. **Nagarajan K, Ni C, Lu T**. Agent-based Modeling of Microbial Communities. *ACS Synth Biol* 2022;11:3564–3574.

371. **Mielko KA, Jabłoński SJ, Milczewska J, Sands D, Łukaszewicz M, *et al*.** Metabolomic studies of *Pseudomonas aeruginosa*. *World J Microbiol Biotechnol* 2019;35:178.

372. **Kesthely CA, Rogers RR, El Hafi B, Jean-Pierre F, O'Toole GA**. Transcriptional profiling and genetic analysis of a cystic fibrosis airway-relevant model shows asymmetric responses to growth in a polymicrobial community. *Microbiol Spectr* 2023;11:e02201-23.

373. **Ostedgaard LS, Moninger TO, McMenimen JD, Sawin NM, Parker CP, *et al*.** Gel-forming mucins form distinct morphologic structures in airways. *Proceedings of the National Academy of Sciences* 2017;114:6842–6847.

374. **Xie Y, Ostedgaard L, Abou Alaiwa MH, Lu L, Fischer AJ, *et al*.** Mucociliary Transport in Healthy and Cystic Fibrosis Pig Airways. *Ann Am Thorac Soc* 2018;15:S171–S176.

375. **Ermund A, Meiss LN, Dolan B, Bähr A, Klymiuk N, *et al*.** The mucus bundles responsible for airway cleaning are retained in cystic fibrosis and by cholinergic stimulation. *European Respiratory Journal* 2018;52. DOI: 10.1183/13993003.00457-2018.